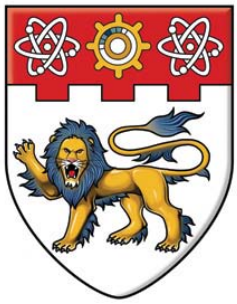

NANYANG TECHNOLOGICAL UNIVERSITY

COOPERATIVE COMMUNICATION: EFFICIENT SCHEMES AND PRACTICAL ASPECTS

Ernest Kurniawan
School of Computer Engineering

2009

COOPERATIVE COMMUNICATION: EFFICIENT SCHEMES AND PRACTICAL ASPECTS

ERNEST KURNIAWAN

School of Computer Engineering

A thesis submitted to the Nanyang Technological University
in fulfillment of the requirement for the degree of
Doctor of Philosophy

2009

Abstract

Cooperation has been considered as a key strategy to cater for the ever increasing demand for high data rate wireless communication. Over the past few years, researches in this area have seen a tremendous growth and advancement, where various cooperation strategies were proposed for different communication scenarios. The aim of this thesis is to illustrate the significance of cooperation in improving transmission quality, in which both cooperative broadcasting as well as cooperative relaying context are taken into consideration. An emphasis on the efficiency and practical aspects of different schemes are then given, and novel techniques to improve on both aspects are proposed.

In cooperative broadcast communication where each node is equipped with multiple antennas, it is shown that antenna selection can provide an effective solution for hardware complexity and space limitation issues inherent to multi antenna systems. A novel selection scheme for cooperative broadcast communication is then proposed. The scheme takes advantage of uplink-downlink duality to reduce computational requirement while still achieving most of the gain available. Starting from the single user system, a sub optimal selection strategy is proposed for multicarrier systems as well. Combining with the earlier method developed for cooperative broadcast scenario, effective antenna selection scheme for multicarrier broadcast systems is obtained. Complexity analysis is given to justify its practical aspect, and its performance when applied to Broadband Wireless Access system based on IEEE 802.16 is studied.

In cooperative relay communication, different issues are addressed. Starting from the simplest three node scenario, the fundamental question on whether the existence of relay node can improve end-to-end performance is addressed. The importance of power control is demonstrated, and it is shown that in some cases the problem of finding the optimal power distribution can be translated into finding the roots of polynomial equation; which can be solved using any available root finding algorithm. When message transmission to the destination node involves

multiple hops (relay stages), bandwidth efficiency penalty severely degrade the overall performance. A novel strategy to overcome this issue is proposed, which makes use of dirty paper concept of transmission in the presence of known interference. In practice, all nodes in the network have their own information to transmit and at the same time they are also potential destination. As such, network performance should be evaluated considering all possible source destination pairs, while the rest of the nodes act as potential helpers. In regular network where node locations are fixed, it is shown that a closed form outage probability expression can be derived. The effect of traffic pattern including traffic origins and locality is then studied. In random network where nodes can be located at any point in the network, an expression for the distance distribution is developed. By integrating the conditional performance with respect to the obtained distribution, network performance under different cooperative schemes are studied. Analysis on different types of gain achievable using different schemes and discussion on geometry specific issues including edge effects are presented. This serves as a framework for network analysis in generic cooperative communication systems.

Acknowledgement

I would like to express my sincere gratitude to my supervisor, Dr. A. S. Madhukumar for his guidance throughout my study as graduate student in NTU. I have benefited tremendously from his unique blend of passion, vision, and technical insights. Without his invaluable help, patience, and encouragement, this project would not have reached this stage. I would also like to thank Dr. Francois Chin for his continuous support and directions, which helped to improve my work and make this project a successful one.

I wish to thank Agency for Science Technology and Research (A*STAR) for granting the scholarship and for giving me wonderful inspirations, which strengthen my passion in research and lead me to the pursuit of PhD degree.

I would also like to thank the staff and technicians in Centre for Multimedia and Network Technology (CeMNet) for their kind assistance, as well as my friends for creating conducive environment to work and making my everyday research life an enjoyable one.

Finally, I would like to extend my thanks to my family for their love and support. It is them who always encourage me to persist in my dreams.

Table of Contents

List of Figures

List of Tables

List of Abbreviations

ACK	Acknowledgement
AMC	Adaptive Modulation and Coding
AnF	Amplify and Forward
ARQ	Automatic Repeat Request
AWGN	Additive White Gaussian Noise
BC	Broadcast Channel
BER	Bit Error Rate
BPSK	Binary Phase Shift Keying
BWA	Broadband Wireless Access
CDF	Cumulative Distribution Function
CDMA	Code Division Multiple Access
CSI	Channel State Information
D-AnF	Distributed Amplify and Forward
D-BLAST	Diagonal Bell Labs Layered Space Time Architecture
D-STBC	Distributed Space Time Block Coding
D-TxMRC	Distributed Transmitter Maximum Ratio Combining
DFE	Decision Feedback Equalisation
DMT	Diversity Multiplexing Tradeoff
DN	Destination Node
DnF	Decode and Forward
DPC	Dirty Paper Coding
FFT	Fast Fourier Transform
FUSC	Full Use of Sub Channels
GPS	Global Positioning System
ICI	Inter Carrier Interference
IFFT	Inverse Fast Fourier Transform
i.i.d.	Independent and Identically Distributed
ISI	Inter Symbol Interference
LAN	Local Area Network
LOS	Line of Sight
LST	Layered Space Time
MAC	Multiple Access Channel
MGF	Moment Generating Function

MIMO	Multiple Input Multiple Output
MISO	Multiple Input Single Output
ML	Maximum Likelihood
MMSE	Minimum Mean Square Error
MRC	Maximum Ratio Combining
MRRC	Maximum Receive Ratio Combining
NACK	Negative Acknowledgement
OFDM	Orthogonal Frequency Division Multiplexing
PDF	Probability Density Function
PUSC	Partial Use of Sub Channels
QAM	Quadrature Amplitude Modulation
QoS	Quality of Service
QPSK	Quadrature Phase Shift Keying
RF	Radio Frequency
RN	Relay Node
RS	Relay Stage
SDPC	Successive Dirty Paper Coding
SEP	Symbol Error Probability
SIC	Successive Interference Cancellation
SIMO	Single Input Multiple Output
SINR	Signal to Interference plus Noise Ratio
SN	Source Node
SNR	Signal to Noise Ratio
STBC	Space Time Block Coding
STC	Space Time Code
STTC	Space Time Trellis Coding
SVD	Singular Value Decomposition
TDMA	Time Division Multiple Access
TUSC	Tile Use of Sub Channels
UT	User Terminal
VAA	Virtual Antenna Array
ZF	Zero Forcing
ZMCSCG	Zero Mean Circularly Symmetric Complex Gaussian

Notations

x	Variable name of type constant
$\boldsymbol{x}$	Variable of type column vector
$\boldsymbol{H}$	Variable of type matrix
$\|x\|$	Absolute value of x
$\|\boldsymbol{x}\|_F^2$	Squared Frobenius norm of vector $\boldsymbol{x}$
$\|\boldsymbol{H}\|$	Determinant of matrix $\boldsymbol{H}$
$\|\boldsymbol{H}\|_F^2$	Squared Frobenius norm of matrix $\boldsymbol{H}$
$[\boldsymbol{H}]_{i,j}$	i^{th} row j^{th} column element of matrix $\boldsymbol{H}$
$Tr[.]$	Trace operation (sum of diagonal elements)
$Pr[.]$	Probability of the event specified in the argument
$E[.]$	Expectation (statistical average) operation
$[.]^*$	Conjugate operation
$[.]^T$	Transpose operation
$[.]^H$	Hermitian (conjugate transpose) operation
$\boldsymbol{I}_M$	Identity matrix of size $M \times M$
$f_X(x)$	Probability Density Function of random variable X evaluated at x
$F_X(x)$	Cumulative Distribution Function of random variable X evaluated at x
$diag(.)$	Diagonal matrix with its argument as the diagonal values

List of Publications

1. E. Kurniawan, A. S. Madhukumar, and Francois Chin, ”Performance Analysis of MIMO Enabled Broadband Wireless Access System for Mobile Multimedia Applications,” *Fifth International Conference on Information, Communications and Signal Processing*, pp. 941-945, December 2005

2. E. Kurniawan, A. S. Madhukumar, and Francois Chin, ”Comments on Enhanced Space Time Coded Diversity Feature of 802.16e,” *Asia-Pacific Conference on Communications*, pp. 1-5, August 2006

3. E. Kurniawan, A. S. Madhukumar, and Francois Chin, ”Performance Analysis of Broadband Wireless Access Systems with Antenna Selection,” *IEEE 17th International Symposium on Personal, Indoor and Mobile Radio Communications*, pp. 1-5, September 2006

4. E. Kurniawan, A. S. Madhukumar, and Francois Chin, ”Exploiting Antenna Selection Gain in IEEE 802.16 Broadband Wireless Access Systems,” *10th IEEE International Conference on Communication systems*, pp. 1-5, October 2006

5. E. Kurniawan, A. S. Madhukumar, and Francois Chin, ”Sub Optimal Antenna Selection Method for MIMO-OFDM Systems,” *IEEE Vehicular Technology Conference*, pp. 435-439, April 2007

6. E. Kurniawan, A. S. Madhukumar, and Francois Chin, ”Antenna selection technique for MIMO-OFDM systems over frequency selective Rayleigh fading channel,” *IET Communications*, vol. 1, pp. 458 - 463, June 2007

7. E. Kurniawan, A. S. Madhukumar, Francois Chin, and Y. C. Liang, ”Successive Dirty Paper Coding: New Relaying Scheme for Cooperative Networks,” *IEEE 18th International Symposium on Personal, Indoor and Mobile Radio Communications*, pp. 1-5, September 2007

8. E. Kurniawan, A. S. Madhukumar, and Francois Chin, ”Performance Analysis of Distributed Space Time Coding: A Geometric Approach,” *IEEE 18th International Symposium on Personal, Indoor and Mobile Radio Communications*, pp. 1-5, September 2007

9. E. Kurniawan, A. S. Madhukumar, and Francois Chin, ”Relaying and Power Control Strategy for 2-Hop Distributed Cooperative Communication,” *IEEE Vehicular Technology Conference*, pp. 98-102, May 2008

10. E. Kurniawan, A. S. Madhukumar, and Francois Chin, ”Exact Outage Probability Analysis of Distributed Cooperative Transmission,” *International Symposium on Information Theory and its Applications*, pp. 1-5, December 2008

11. E. Kurniawan, A. S. Madhukumar, and Francois Chin, ”Heuristic Antenna Selection Algorithm for Multiuser Multi-antenna Downlink,” *IEEE Vehicular Technology Conference*, To appear, April 2009

12. E. Kurniawan, A. S. Madhukumar, and Francois Chin, ”Low Complexity Antenna Selection Scheme for Multiuser MIMO Broadcast Systems,” *IEEE Conference on Communications*, To appear, June 2009

13. E. Kurniawan, A. S. Madhukumar, and Francois Chin, ”Performance Analysis of Distributed Transmission Schemes in Cooperative Random Networks,” *IEEE Transactions on Wireless Communications*, Under Review

14. E. Kurniawan, A. S. Madhukumar, and Francois Chin, ”A Systematic Analysis on Edge Effect for Cooperative Random Networks,” *IEEE Transactions on Wireless Communications*, Under Review

15. E. Kurniawan, A. S. Madhukumar, Francois Chin, and Fumiyuki Adachi, ”Network Outage Probability Analysis of Generic Cooperative Relay Networks,” *IEEE Transactions on Vehicular Technology*, Under Review

16. E. Kurniawan, A. S. Madhukumar, and Francois Chin, ”Low Complexity Antenna Selection Scheme for Multicarrier MIMO Broadcast Communication,” *Springer Journal of Signal Processing Systems*, To appear

Chapter 1

Introduction

1.1 Background

Cooperative communication describes a situation where transmission involving several users' data, each affecting one another's performance, considered collectively to achieve mutual benefit for all users. The term cooperation was first introduced by Cover and Bergmans in 1974 [1] mainly for broadcast communication. In their paper, two co-located radio transmitters (sharing total power and total bandwidth constraint) communicate with two spatially separated receivers, and cooperation represents the strategy to simultaneously transmit messages to both receivers in order to enlarge the overall rate region.

Without cooperation, data for different users are considered individually. Transmission is then performed via multiplexing, either through time or frequency. In time multiplexing, transmission is directed to only one user at any one time (using all available power and bandwidth). Whereby in frequency multiplexing, transmission to both users is performed simultaneously, with a certain portion of the bandwidth and power allocated to one user, while the remaining portion is allocated to the other. It is shown that in this scenario, cooperation can improve the overall performance by considering data from both users collectively instead of individually. With cooperation, encoding is performed in two stages. At the first stage, data for the first user

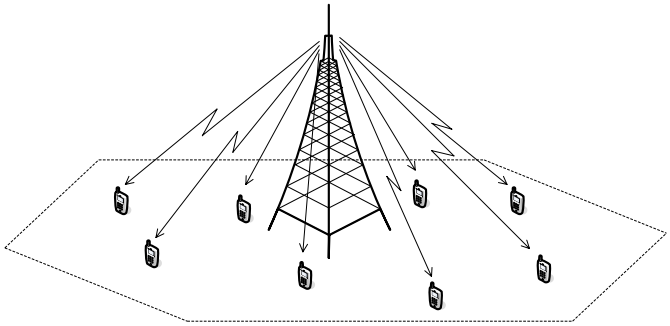

Figure 1.1: Cooperative Communication in Cellular Downlink Scenario

is encoded as usual. At the second stage, data for the second user is encoded using the knowledge of the encoded data for the first user. The resulting codewords are then added together and transmitted over the channel.

At the receiver, conventional decoding process is used. It can be seen that the first user experiences interference from the second user's codeword. However, due to the result in [2], transmission to the second user is as good as that in interference free channel. The resulting rate region using cooperation is shown to dominate both time as well as frequency multiplexing scheme, irrespective to the resource allocation method used. This simple example shows the role of cooperation in improving the performance of broadcast communication.

In practice, broadcast communication scenario fits well into cellular downlink communication as illustrated in Figure 1.1, where one base station with multiple information sources broadcasts messages to multiple users. Here, cooperation represents base station encoding strategy to consider messages for all users collectively in order to achieve the best possible outcome, such as increasing the overall throughput or improving transmission quality of service (QoS). Following the result of [1] for the two users case, this can potentially improve the current strategy which adopt Code Division Multiple Access (CDMA) technique to separate different channels and perform individual encoding of data for different users.

Together with the development of multiple antenna systems [3]-[4], a study on Multiple Input Multiple Output (MIMO) Broadcast Channel (BC) has attracted a lot of attention over the

past few years. The cooperative scenario in MIMO-BC is more complex with the introduction of multiple antennas, as new dimensions are added in the optimisation problem. As opposed to single antenna BC, MIMO-BC is in general non-degraded; hence the expression of capacity region is more complex. The capacity region for MIMO-BC is addressed using duality of broadcast and multiple-access channel (MAC) in [5], and it is shown to be equal to the capacity region achieved by dirty paper coding scheme (also known as dirty paper region). Despite its superiority compared to single antenna BC, as with conventional MIMO systems, there are several practical difficulties in implementing MIMO-BC. This includes channel condition (fading correlation between antenna pairs), hardware cost, as well as space limitation; each of which has to be addressed before the real implementation can be practically justified.

Recently, cooperative communication is proposed in different context known as cooperative relaying, where cooperation represents multiple users helping each other to transmit to their destinations [6]-[7]. The idea behind this technique is to make use of partner's antenna as a relay or virtual antenna, such that the effective channel to the destination emulates MIMO channel. By doing so, benefits of multi antenna systems can be exploited in distributed manner. For this reason, this type of cooperation is sometimes referred to as distributed MIMO.

In practice, this technique is applicable to ad-hoc network as well as cellular uplink communication. In ad-hoc network, there is no centralised controller. When a node wants to transmit a message to the destination which is located further away from its transmission range, cooperation with other nodes is necessary. Transmission is then performed via multiple hops transmission, as illustrated in Figure 1.2a. The number of hops or relay stages (RS) depends on the distance between source and destination, and cooperation here represents the forwarding strategy used at different nodes in every RS, which includes any space time processing techniques available for point to point MIMO systems. The main challenge associated with this relaying transmission, however, is the reduction in bandwidth efficiency. Since more transmission slots are required to transmit a message from source to destination, the end to end

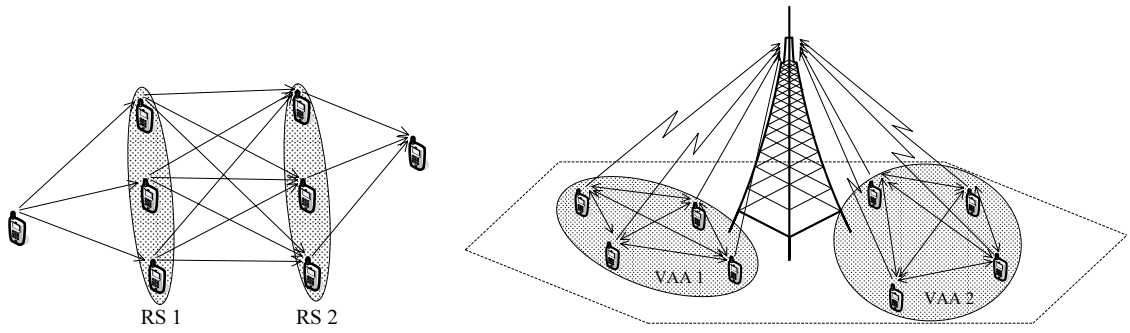

(a) Ad-hoc network (b) Cellular Uplink

Figure 1.2: Different Cooperative Relaying Scenarios

throughput decreases as the number of hops increases. Efficient cooperation scheme must ensure that the drawback caused by bandwidth efficiency penalty does not outweigh the benefit of cooperation.

In cellular uplink communication, the scenario is slightly different. Nodes which are relatively close to one another form a virtual antenna array (VAA) as illustrated in Figure 1.2b. All nodes in the same VAA group then cooperate with one another to communicate with base station. Here, cooperation represents the strategy on how different nodes in VAA group assist one another to improve transmission quality to the base station. The advantage of this kind of distributed cooperation is two-fold. First of all, since different antennas belong to different users, the channels are uncorrelated as the antennas are spatially well separated. Secondly, only one antenna is required for each user, therefore hardware cost and space limitation in user terminal is not an issue. Despite these advantages, the challenges associated with this cooperative scenario is in deciding the cooperation strategy. This includes deciding which node to cooperate with, what kind of cooperative transmission technique to use, and how to allocate resources among different nodes.

When cooperation is applied to ad-hoc network whereby every node has its own message to transmit and every other node is a potential destination, it is necessary to include all possible source destination pair into consideration when evaluating network performance. Due to

path loss, transmission quality is inversely proportional to the source destination distance. In addition, the number of nodes in the vicinity of source node also plays an important role in the overall performance. The difficulty here lies in determining the distance distribution between any two given nodes. Moreover, some geometry specific considerations such as proximity of source node towards network edge must be integrated in performance calculation, since it affects the number of helper nodes in its vicinity.

1.2 Motivation and Objectives

Given the potential of cooperative communication in providing high spectral efficiency for wireless transmission, it is deemed necessary to study its performance under different cooperative schemes. Additionally, limitations and practical considerations in implementing the system need to be identified and solutions to the problems to be proposed. This work is motivated to study cooperative communication strategies under both cooperative broadcast communication as well as cooperative relaying scenario. In particular, several issues discussed in the previous section for different cooperative scenarios are addressed.

In multiple antenna systems, antenna selection has been recognised as an effective method to overcome the problem of hardware cost and space limitation. By having less number of RF chains (consisting of amplifiers, analog to digital converters, etc.) compared to the number of available antennas, hardware cost can be reduced significantly. Moreover, when channel state information (CSI) is available, antenna subset which has the best gain and smallest mutual correlation can be selected to improve the overall performance. The motivation of this work is to extend the antenna selection concept into cooperative MIMO-BC scenario, with the objective of developing a selection algorithm which maximise the sum rate capacity of the system. Extension to multiple carrier case is also taken into consideration.

In multiple hop cooperative relay transmission, the simplest scenario is a three node line network, where one relay node is positioned in a straight line between source and destination

node. This work aims to answer a fundamental question on whether the existence of relay node can indeed improve the performance. In other words, given the same amount of total power and total bandwidth, the influence of relay node towards end to end performance is studied. The optimality conditions regarding relay position and power allocation are also addressed. In general, bandwidth efficiency penalty is incurred whenever a message requires more than one hop to reach destination. Although deploying more antennas can compensate this penalty to some extend, it is not always a viable alternative, especially when space and node's resources are limited. As such, in order to eliminate this penalty, the network should allow a new message to be transmitted at every transmission slot. However, this will introduce mutual interference between messages, which might bring down the overall performance. The motivation of this work in this area is to propose a novel strategy to allow simultaneous transmission of messages as it travels through different hops. The scheme is to cater for the interference cancellation property required so that it does not severely degrade the existing transmission in the network.

As far as cooperation in ad-hoc network is concerned, this work is motivated to quantify the amount of improvement different cooperation schemes can bring. Starting with an idealistic scenario where source and destination node locations are known a priori while all other relay node positions are fixed, the end to end performance is studied. Extending this further, when destination node is not known a priori, every other node can be the destination; while the remaining nodes are potential relay nodes. A network with fixed structure whereby nodes are placed at lattice points is considered. The motivation of this work is to analyse the average performance considering all possible destination node locations. The effect of traffic pattern towards average performance is also considered.

Finally, in the most generic case when the network does not have any particular structure (termed as random network), where every node in the network are potential source as well as destination node, the goal is to come out with a framework to analyse the average network performance. To do this, a distance distribution between any given two nodes is developed.

Then, a method to approximate the number as well as position of relay nodes that are needed is proposed, which consider different scenarios including the presence of source nodes near network edges. Different gains available using different cooperative scheme can then be quantified using the proposed framework, and the average performances under different network parameters are compared.

1.3 Thesis Organisation

The remaining part of this report is organised as follows:

Chapter 2 provides literature review on some of the existing cooperative transmission strategies, both in cooperative broadcasting as well as cooperative relaying scenario. In cooperative broadcast scenario, single antenna case and multiple antenna case are discussed separately, and optimal strategy known for each of the cases are explained. In cooperative relaying scenario, the single relay case and multiple relay case are discussed separately, and different forwarding strategies as well as their performances are highlighted. Discussion on some of the challenges and open problems in the area are also given.

Chapter 3 addresses the issues pertaining to cooperative broadcasting in MIMO-BC, in which an antenna selection scheme is proposed. The single carrier case is first considered, and the selection algorithm which maximises the sum rate capacity is given. Then, a sub optimal antenna selection scheme for multicarrier point to point MIMO system is developed as the basis to extend the earlier result into multiple carrier case. Combining the two algorithms together, a selection scheme for multi carrier MIMO-BC is proposed. Performance of antenna selection when applied to Broadband Wireless Access (BWA) systems based on IEEE 802.16 is analysed.

Chapter 4 focuses on cooperative relaying scenario, in which the significance of power control and interference cancellation in multi hop transmission is described. Considering three node line network, an optimal power control scheme is proposed based on the knowledge of

second order statistics of the channel. Then, a novel interference cancellation strategy for multi hop transmission to allow for new message transmission at each relay stage is proposed. The underlying theory behind this technique is explained, and its performance compared to the other cooperative relaying strategies is presented.

In Chapter 5, the analysis of cooperative relaying is extended for multiple relay case. First, an ideal scenario is considered, with all relay nodes located equidistant from source and destination. Derivation of closed form expression for the average outage probability is presented, and the gain achieved in relation to the number of relay nodes is quantified. Using similar technique, the analysis is extended for regular network where nodes are placed in lattice points. The effects of traffic pattern including traffic origins and traffic locality towards overall performance are also analysed.

The most generic case without any particular network structure is considered in Chapter 6. As highlighted earlier, since source and destination nodes can be located anywhere within the network boundaries, all possible distances need to be considered. For this purpose, a distance distribution of any given two nodes is developed. Similarly, since the network is random, the number of potential helper nodes is also random. A systematic method to approximate the number and position of relay nodes is then proposed, and average outage performance of random network under different cooperative schemes are analysed.

Finally, conclusions and contributions of this work are summarised in Chapter 7. In addition, some possible research areas which serve as future directions are also presented.

Chapter 2

Literature Review

2.1 Introduction

The use of cooperation in wireless communication context has been considered since more than three decades ago. Initially proposed for point to multi-point broadcast communication, it was shown that cooperation is capable of improving the overall rate region of the system. Cooperation in broadcast communication represents the encoding strategy, which requires a collective consideration of data streams from different users, and simultaneously transmit the information to all users. Along with the development of MIMO systems, research on cooperative broadcast communication has also been extended into multiple antenna case. However, the implementation of multi-antenna cooperative broadcast systems is faced with the problem of hardware cost and computational complexity. In point-to-point MIMO systems, antenna selection has been recognised as an effective solution to alleviate this problem. One of the motivations of this work is to extend the idea of antenna selection into cooperative MIMO broadcast communication.

In some cases, deploying multiple antennas into a single terminal is not a viable solution. To exploit the gain similar to those available in MIMO systems in such scenario, a concept of virtual antenna array (also known as VAA) is introduced. By establishing some form of

cooperation into several single-antenna terminals, it was shown that VAA systems can improve the overall system performance. This adds a new meaning into cooperative communication, whereby the term cooperation is used to represent the collective effort of several single-antenna terminals to improve transmission quality. Furthermore, due to the causality of message transmission, it is apparent that relaying forms an integral part of this type of cooperation. As such, it is sometimes referred to as cooperative relaying. In this work, several aspects of cooperative relay communication is studied. Starting from single relay case, the optimality condition pertaining to the resource allocation problem is studied. Extension to the case of multiple relay nodes is then considered, and the end to end performance is evaluated for different cooperative schemes. Applying cooperative relay communication into ad-hoc network, whereby nodes are located at a fixed regular pattern, the overall system performance is analysed in terms of network outage probability. The analysis is extended to the case when the network is random with no particular structure.

In this chapter, an overview of different types of cooperative communication is presented. Section 2.2 discusses in detail the cooperative broadcast communication. An overview on multiple antenna systems and the types of gain available are also given. The concept of antenna selection and several schemes available for point to point MIMO systems are then presented. Combining multiple antenna concept with cooperative broadcast communication, the system model for cooperative MIMO-BC is given, which is used for further analysis in this area. Discussion on cooperative relay network is presented in Section 2.3. Both single relay and multiple relay configuration are described, and various challenges associated with their practical implementations are explained. Finally, Section 2.4 ends this chapter with a summary.

2.2 Cooperative Broadcast Communication

A study on BC was first initiated by Cover in [8], where broadcast transmission in discrete memoryless channel is considered. In the paper, transmission is performed from one sender

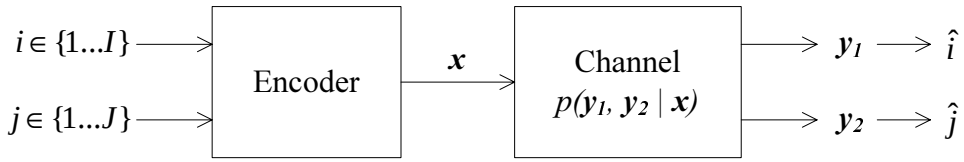

Figure 2.1: Broadcast Channel Block Diagram

to two separate receivers, and the idea of superimposing information intended to one receiver on top of those intended to the other is introduced. It is shown that such approach is better than time sharing scheme, which divides the transmission time into two slots (one slot for transmitting simultaneously to both receivers at the capacity equal to the minimum capacity between the two receivers, and the other slot for transmitting to only one receiver having the higher capacity). This technique is then named as superposition coding, and the proof of its optimality is presented in the ensuing work by Cover and Bergmans [1], in which it is shown that superposition coding not only outperforms time sharing scheme, but also any type of time and frequency multiplexing irrespective to the power allocation scheme used. Correspondingly, the transmission scenario is termed as cooperative broadcasting, to emphasise the encoding process which takes a collective consideration of information intended for different users.

Broadcast communication is a subset of multi user information theory [9], where one sender wanted to transmit information to multiple users. The block diagram of two user BC is depicted in Figure 2.1. To send a message $i \in \{1...I\}$ to the first user and message $j \in \{1...J\}$ to the second user, an encoding function takes both i and j to construct a length-n codeword $\boldsymbol{x} \in \mathcal{X}^n$ from input alphabet $\mathcal{X}$, and transmit it through the channel. The first and second receiver, upon receiving the transmitted codeword as $\boldsymbol{y_1} \in \mathcal{Y}_1^n$ and $\boldsymbol{y_2} \in \mathcal{Y}_2^n$, makes an estimate to their respective messages $\hat{i}$ and $\hat{j}$. The channel transition probability $p(\boldsymbol{y_1}, \boldsymbol{y_2}|\boldsymbol{x})$ determines the relationship between the transmitted and received codewords. For discrete memoryless channel, the transition probability can be written as:

$$p(\boldsymbol{y_1}, \boldsymbol{y_2}|\boldsymbol{x}) = \prod_{i=1}^{n} p(y_1^{(i)}, y_2^{(i)}|x^{(i)}) \tag{2.1}$$

A rate pair $(R_1, R_2) = (n^{-1}log_2(I), n^{-1}log_2(J))$ is said to be achievable if there exist a coding scheme of the form $((2^{nR_1}, 2^{nR_2}), n)$ which maps a message pair (i, j) into codeword $\boldsymbol{x}$ such that the decoding error probability $P_e = Pr\left[\hat{i} \neq i\right] + Pr\left[\hat{j} \neq j\right]$ goes to 0 as the block size n goes to infinity. The capacity region of BC is then defined as the convex closure of the set of achievable rates.

For several years, many efforts have been given for deriving the capacity region of BC. Solution for the capacity region of BC has been found for some special cases. For the case of degraded BC, superposition coding proposed in [1] and [8] is optimal, and achieves BC capacity. The proof of achievability is presented by Bergmans in [10], and its converse was established by Bergmans [11] and Gallager [12]. A broadcast channel is said to be degraded if one user's output is *more capable* than the other, such that the channel transition probability can be decomposed into $p(y_1, y_2|x) = p(y_1|x)p(y_2|y_1)$. The capacity region of a degraded BC is given as [13, Theorem 1]:

$$\begin{aligned} (R_1, R_2): \quad R_2 &\leq I(U; Y_2) \\ R_1 &\leq I(X; Y_1|U) \end{aligned} \tag{2.2}$$

for some joint distribution $p(u)p(x|u)p(y1, y2|x)$. The outline of the proof goes as follows. First, determine the *less capable* user, and construct an auxiliary random variable U which will be used to transmit a message to it at rate R_2. In order to do this, U has to be designed in such a way that it is distinguishable by the *less capable* user. Without loss of generality, let receiver 2 be the *less capable* user. Here, U serves as a cloud center, and since it is distinguishable by the *less capable* user, it is also distinguishable by the other user. Then for each cloud center, construct 2^{nR_1} codewords on $\mathcal{X}^n$. Decoding at receiver 2 is performed by looking at the closest cloud center to the received codeword $\boldsymbol{y_2}$, which can be done at negligible error rate as long as $R_2 \leq I(U; Y_2)$. At receiver 1, the same process is done. However, once the closest cloud center is found, decoding is performed by looking at the corresponding point within the cloud

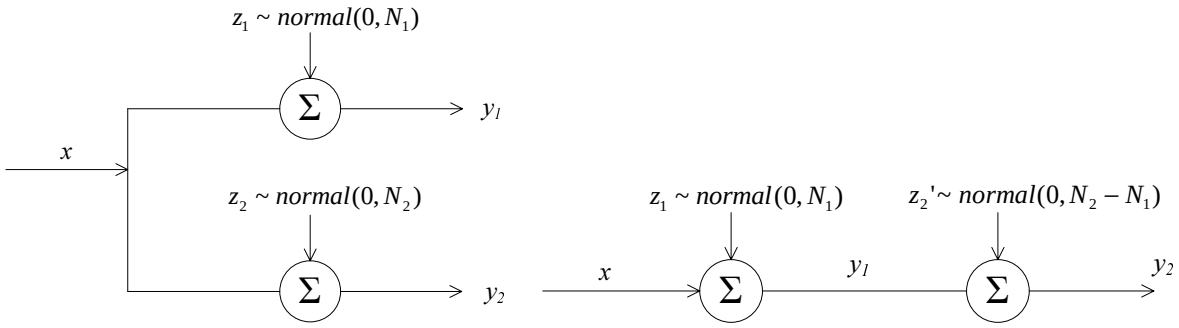

(a) Conventional Model (b) Equivalent (degraded) Model

Figure 2.2: Illustration of Gaussian Broadcast Communication Scenario

center that is closest to the received codeword $\boldsymbol{y_1}$. This can be done at negligible error rate as long as $R_1 \leq I(X;Y_1|U)$. Combining the constraints for both users, the capacity region as expressed in equation (2.2) is obtained. The more formal proof of the theorem is given in [13].

Another special case of broadcast channel is Gaussian BC (Figure 2.2a), where the received symbol at receiver 1 and 2 can be expressed as:

$$\begin{aligned} y_1 &= x + z_1 \\ y_2 &= x + z_2 \end{aligned} \tag{2.3}$$

Here, x is the transmitted symbol and satisfies the power constraint $E[|x|^2] \leq P$, z_1 and z_2 are Additive White Gaussian Noise (AWGN) distributed according to $\mathcal{N}(0, N_1)$ and $\mathcal{N}(0, N_2)$ respectively. It is apparent that Gaussian BC is always degraded. Without loss of generality, let the noise variance of receiver 1 be smaller than receiver 2 ($N_1 < N_2$). As illustrated in Figure 2.2b, the received signal in equation (2.3) can be rewritten into:

$$\begin{aligned} y_1 &= x + z_1 \\ y_2 &= y_1 + z_2' \end{aligned} \tag{2.4}$$

with z_2' distributed according to $\mathcal{N}(0, N_2 - N_1)$. In other words, the signal received at receiver

2 is a degraded version of that in receiver 1. As such, the capacity region can be found using the earlier result on degraded BC, and is given as [13, Theorem 2]:

$$\begin{aligned}(R_1, R_2): \quad R_2 &\leq I(U;Y_2) = \frac{1}{2}\log_2\left(1+\frac{(1-\alpha)P}{\alpha P+N_2}\right)\\ R_1 &\leq I(X;Y_1|U) = \frac{1}{2}\log_2\left(1+\frac{\alpha P}{N_1}\right)\end{aligned} \tag{2.5}$$

where α indicates the portion of power used for user 1. The above capacity region is achieved using two Gaussian codebooks (one for each receiver). The encoding process is similar to that in degraded BC. First, generate 2^{nR_2} Gaussian codewords independent and identically distributed (i.i.d.) according to $\mathcal{N}(0,(1-\alpha)P)$. For each codeword, generate 2^{nR_1} satellite Gaussian codewords according to $\mathcal{N}(0,\alpha P)$. To transmit message i and j to the first and second receiver, the j^{th} codeword from the first codebook and the i^{th} codeword from the second codebook is added and transmitted over the channel. Decoding at the second user is performed as usual, considering the codeword intended for the first user as additive interference. Meanwhile, decoding at the first user is performed by first detecting the second user's codeword (which is possible since the first user's channel is better), subtracting out the codeword from the received sequence, and continue decoding the desired message. Using the above scheme, decoding error probability can be made arbitrarily small as long as condition (2.5) is satisfied.

For the case when BC is deterministic (the channel transition probability matrix contains only ones and zeros), the capacity region has been fully characterised. Capacity region of Blackwell channel (one example of deterministic BC) is solved by Gelfand in [14]. Generalisation to the capacity region of any deterministic BC is then given by Marton [15] and Pinsker [16]. In deterministic BC, the channel output received by different user can be expressed as:

$$\begin{aligned}y_1 &= g_1(x)\\ y_2 &= g_2(x)\end{aligned} \tag{2.6}$$

In other words, the channel outputs are just a deterministic function of the channel input. It turns out that the capacity region of this kind of channel is very closely related to the problem of sending correlated information over noiseless channel, which was addressed by Slepian and Wolf in [17]. The result in [17] gives a minimum data rate required to send arbitrarily correlated information sources to a destination. Their scheme involves the idea of random binning, in which all codewords are randomly grouped into bins, and the bin index (instead of the actual codeword index) is used for message transmission. When this technique is applied to deterministic BC, the resulting capacity region can be shown to be [15], [16]:

$$\begin{aligned} (R_1, R_2): \quad R_1 &\leq H(Y_1) \\ R_2 &\leq H(Y_2) \\ R_1 + R_2 &\leq H(Y_1, Y_2) \end{aligned} \tag{2.7}$$

Although the capacity region of BC is known for the above special cases, the capacity region for the general BC is only known in terms of inner bound [13]. Attempts to characterise the general BC capacity inner bound include the work by van der Meulen [18] and Cover [19]. To date, the largest known achievable region for general BC is Marton's region [20], and it is expressed as follows:

$$\begin{aligned} (R_1, R_2): \quad R_1 &\leq I(U; Y_1) \\ R_2 &\leq I(V; Y_2) \\ R_1 + R_2 &\leq I(U; Y_1) + I(V; Y_2) - I(U; V) \end{aligned} \tag{2.8}$$

for some joint distribution $p(u, v, x)$.

With the introduction of MIMO systems by Teletar and Foschini in [3]-[4], the incorporation of multiple antennas into cooperative broadcast communication is inevitable. Given the ability of MIMO systems to achieve very high spectral efficiency, it is expected that the capacity

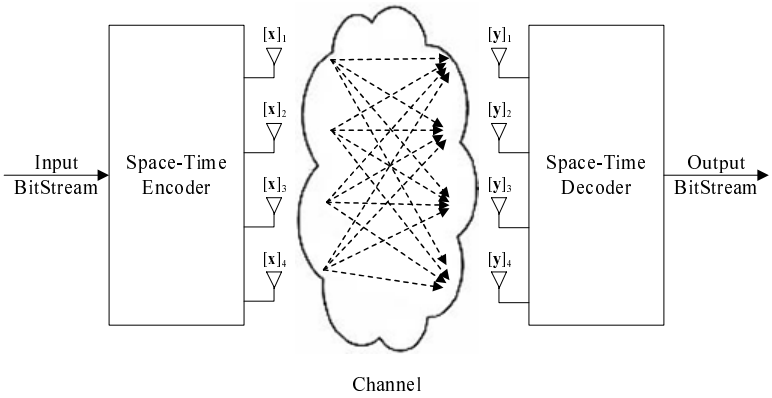

Figure 2.3: 4 by 4 Multiple Input Multiple Output System Diagram

region of MIMO-BC is significantly larger than its single antenna counterpart. The analysis of MIMO-BC, however, is more difficult since MIMO-BC is generally non-degraded (even for the Gaussian channel case). Before proceeding further into MIMO-BC capacity analysis, a brief overview on MIMO system is given in the following subsection.

2.2.1 Multiple Input Multiple Output Overview

The underlying idea of MIMO systems is to deploy more than one antenna at the transmitter or receiver or both, with the objective to create multiple spatial data streams between the two. An illustration of typical MIMO system is shown in Figure 2.3. The discrete time signal model can be expressed as:

$$\boldsymbol{y} = \boldsymbol{H}\,\boldsymbol{x} + \boldsymbol{n} \tag{2.9}$$

where $\boldsymbol{x}$ and $\boldsymbol{y}$ are the transmitted and received symbol vector of size $N_t \times 1$ and $N_r \times 1$ respectively (N_r being the number of receive antennas and N_t being the number of transmit antennas), $\boldsymbol{H}$ is the channel matrix of size $N_r \times N_t$, and $\boldsymbol{n}$ is the noise vector of size $N_r \times 1$ at the receiver. As long as sufficient scatterers exist around transmitter as well as receivers and sufficient antenna spacings is provided, the channel gain between different transmit-receive antenna pairs can be assumed to be mutually independent. Depending on how this channel independence is exploited, there are different types of gain associated with MIMO systems,

namely array gain, diversity gain, and multiplexing gain. The next subsections discuss these different types of gain in detail.

Array Gain

Array gain is characterised by the increase in average received signal to noise ratio (SNR) due to coherent combining effect of the transmitted symbol. To exploit this type of gain, channel state information (CSI) is required either at the transmitter or at the receiver, depending on where the scheme is applied. One technique that fully exploits array gain is known as maximum ratio combining (MRC). The idea of MRC originates from [21], where linear diversity combining is studied. Its application into MIMO context is then proposed by [22]. Array gain can be exploited either at the transmitter, or at the receiver, or both. In Single Input Multiple Output (SIMO) systems, the channel matrix $\boldsymbol{H}$ is a column matrix of size $N_r \times 1$. By multiplying the received symbol vector $\boldsymbol{y}$ with $\boldsymbol{H}^H$ (the superscript $[.]^H$ denotes a Hermitian or conjugate transpose operation), the average received signal SNR is enhanced by a factor of $E\left[\|\boldsymbol{H}\|_F^2\right]$, where $\|.\|_F^2$ denotes the squared Frobeius norm operation. Similarly, in Multiple Input Single Output (MISO) systems, where the channel matrix $\boldsymbol{H}$ is a row vector, the transmitted symbol vector can be constructed as $\boldsymbol{x} = \boldsymbol{H}^H x$. The average received signal SNR in this case is enhanced by the same factor of $E\left[\|\boldsymbol{H}\|_F^2\right]$. For the case of MIMO systems, the array gain can be achieved by a technique called Eigen Beamforming [23]-[24], where the transmit and receive symbol vectors are multiplied by the right and left channel eigenvector respectively corresponding to the largest eigenvalue. The increase in average receive SNR is then proportional to the largest eigenvalue of the channel matrix.

Diversity Gain

Diversity gain characterises the rate of decrease in average error probability with respect to an increase in SNR. It is achieved by transmitting the same symbol over several independently

faded channel, such that the receiver has multiple copies of the same message. In this way, since the possibility of all channels in deep fade at the same time is much smaller compared to the probability of only one channel in deep fade, the overall channel quality is improved and better decoding reliability is achieved. Mathematically, diversity gain is quantified as [25]:

$$G_D = \lim_{\rho\to\infty} \frac{-\log \overline{P_e}(\rho)}{\log \rho} \tag{2.10}$$

where ρ is the operating SNR and $\overline{P_e}(\rho)$ is the corresponding average error probability. Several schemes have been proposed to exploit diversity gain in MIMO systems. One prominent example is Alamouti scheme [26], which is designed for 2×1 MIMO systems. In order to transmit two symbols (denoted as s_1 and s_2) over two periods, Alamouti scheme transmits s_1 and s_2 through the first and second antennas at the first time slot, followed by $-s_2^*$ and s_1^* through the first and second antennas at the second time slot. This symbol structure makes it possible to exploit full diversity gain (of order 2) at the receiver without requiring any CSI at the transmitter. Other examples of transmission scheme that exploits diversity gain were developed by Tarokh, Javarkhani, Seshadari, and Calderbank, known as Space Time Block Codes (STBC) [27], as well as a more general Space Time Trellis Coding (STTC) [28]-[30]. These techniques can be applied for MIMO systems with larger number of antennas.

Multiplexing Gain

To enhance the transmission throughput over MIMO channel, a technique called spatial multiplexing is used. The idea of this technique is to transmit independent messages over all spatial data streams available in MIMO channel. The resulting gain is called multiplexing gain, which is characterised by a linear increase in the transmission throughput [25]:

$$G_M = \lim_{\rho\to\infty} \frac{R(\rho)}{\log \rho} \tag{2.11}$$

where $R(\rho)$ is the transmission rate at ρ operating SNR. In any MIMO systems, the multiplexing gain G_M is upper bounded by $G_M \leq \min(N_t, N_r)$. Different schemes have been proposed to exploit multiplexing gain in point to point MIMO systems, including a well known Layered Space Time (LST) architecture by Foschini [31] (also known as Diagonal Bell Labs Layered Space Time Architecture or D-BLAST). This scheme breaks each message block into sub blocks, and transmit them through different transmit antennas in a sequential manner. Sub blocks from different message blocks are transmitted concurrently using all available transmit antennas, hence the effective throughput is increased. A modification of D-BLAST scheme is proposed by the same author in [32], which allows all sub blocks from each message block to be transmitted in parallel (instead of sequentially) using all available transmit antennas. This scheme improves on the original D-BLAST scheme by removing the necessity of empty blocks in the initial transmission, and it is called V-BLAST respectively. However, its performance is slightly worse compared to the original D-BLAST due to the absence of time diversity. Subsequent modification on V-BLAST scheme is proposed in [33], which uses successive interference cancellation (SIC) technique to perform equalisation of different data streams at the receiver. Extending it further, the work in [34] proposed an iterative method to combine SIC technique and closed loop feedback, which uses the initial symbol estimate to subtract off its contribution as interference from the currently decoded data stream at every iteration. It is shown that this method is able to extract full diversity as well as multiplexing gain.

To date, the subject of point to point MIMO communication has been well understood, and a substantial amount of work can be found in the literature (see [35]-[38] and the references therein for an extensive summary on the subject). When perfect CSI is available at the transmitter, transmission can be performed at the channel capacity, which is quantified as [3]:

$$C = \max_{\boldsymbol{R}_{xx} \geq 0,\ Tr(\boldsymbol{R}_{xx}) \leq P_{tot}} \log_2 \left(\left| \boldsymbol{I}_{N_r} + \boldsymbol{H}\boldsymbol{R}_{xx}\boldsymbol{H}^H \right| \right) \tag{2.12}$$

where $|.|$ is a determinant operation, $\boldsymbol{I}_{N_r}$ is identity matrix of size $N_r \times N_r$, and $\boldsymbol{R}_{xx}$ is the

covariance matrix of the transmitted symbol vector $\boldsymbol{x}$. This can be done by multiplying the transmit and receive symbol vector with the right and left singular matrix of $\boldsymbol{H}$ respectively, followed by waterfilling power allocation strategy according to [39]. Let the singular value decomposition (SVD) of the channel matrix be expressed as follows:

$$\boldsymbol{H} = \boldsymbol{U}\,\boldsymbol{\lambda}\,\boldsymbol{V}^H \tag{2.13}$$

where $\boldsymbol{U}$ and $\boldsymbol{V}$ are the left and right singular matrix of $\boldsymbol{H}$ respectively, and the diagonal matrix $\boldsymbol{\lambda}$= diag$\{\lambda_1, \lambda_2, \cdots, \lambda_K\}$ represents channel singular values (K being the rank or available spatial data stream of the channel matrix, which has a maximum of min(N_t, N_r)). Multiplying the transmit symbol vector with $\boldsymbol{V}$ results in the following covariance matrix:

$$\boldsymbol{R}_{xx} = \boldsymbol{V}\,\boldsymbol{P}\,\boldsymbol{V}^H \tag{2.14}$$

where $\boldsymbol{P}$= diag$\{P_1, P_2, \cdots, P_{N_t}\}$ is the diagonal matrix representing power allocation across different transmit antennas. Using equations (2.13) and (2.14), given that the channel rank is $K = N_t$ (full rank channel matrix and $N_r \geq N_t$), the maximisation argument in equation (2.12) can be simplified as:

$$\begin{aligned}
\log_2\left(\left|\boldsymbol{I}_{N_r} + \boldsymbol{H}\boldsymbol{R}_{xx}\boldsymbol{H}^H\right|\right) &= \log_2\left(\left|\boldsymbol{I}_{N_r} + \boldsymbol{U}\boldsymbol{\lambda}\boldsymbol{V}^H\,\boldsymbol{V}\boldsymbol{P}\boldsymbol{V}^H\,\boldsymbol{V}\boldsymbol{\lambda}\boldsymbol{U}^H\right|\right) \\
&= \log_2\left(\left|\boldsymbol{I}_{N_r} + \boldsymbol{U}\boldsymbol{\lambda}\boldsymbol{P}\boldsymbol{\lambda}\boldsymbol{U}^H\right|\right) \\
&= \log_2\left(\left|\boldsymbol{I}_{N_r} + \boldsymbol{\lambda}\boldsymbol{P}\boldsymbol{\lambda}\right|\right) \\
&= \sum_{i=1}^{K} \log_2\left(1 + \lambda_i^2\,P_i\right)
\end{aligned} \tag{2.15}$$

and the maximisation condition can be translated into:

$$P_i \geq 0\ \ \forall i, \sum_i P_i \leq P_{tot} \tag{2.16}$$

According to [39], the solution for the above power allocation can be expressed as $P_i = \left(\psi - \lambda_i^{-2}\right)^+$; where ψ is the water level chosen in such a way that the total power constraint is satisfied, and $(s)^+ = max(0, s)$ is to make sure that all powers have positive values.

In practice, perfect CSI at the transmitter is either difficult to obtain or requires a large amount of feedback. Moreover, the algorithm for finding the optimal power allocation can be too complex for the receiver. As an alternative solution, a sub optimal approach can be used by distributing the total power equally across favourable substreams [40] (which is in general less than the total number of transmit antennas). It is shown that the threshold used in conventional waterfilling is good enough to determine the set of favourable substreams, and the capacity penalty incurred by this approach is only minimal.

As far as MIMO equalisation is concerned, different techniques have been proposed, and their performances have been evaluated. The optimal MIMO equalisation scheme is Maximum Likelihood (ML) detector, which makes symbol decision based on maximum likelihood probability $\hat{\boldsymbol{x}} = \arg\max p(\boldsymbol{y}|\hat{\boldsymbol{x}})$. Equivalently, this criterion can be translated into a minimum distance detector, which makes symbol decision based on minimum euclidean distance according to $\hat{\boldsymbol{x}} = \arg\min \|\boldsymbol{y} - \boldsymbol{H}\hat{\boldsymbol{x}}\|$. Performance of MIMO systems using ML receiver is analysed in [41]-[44].

Despite its optimality, ML receiver is not practical to implement due to its computational complexity (which grows exponentially with respect to the number of antennas and constellation size). A more practical MIMO equalisation scheme is to use linear receiver, such as Zero Forcing (ZF) and Minimum Mean Square Error (MMSE) method. Using ZF receiver, channel effect is completely eliminated, hence Inter-Symbol Interference (ISI) at the receive antenna is zero. This is done by multiplying the received symbol vector $\boldsymbol{y}$ with $(\boldsymbol{H}^{\boldsymbol{H}}\boldsymbol{H})^{-1}\ \boldsymbol{H}^{\boldsymbol{H}}$, a Moore-Penrose pseudo-inverse of the channel matrix [45, Section 5.5.4]. Although ISI is completely eliminated, the drawback of ZF receiver is noise enhancement during the channel inversion process. A better choice of linear receiver is to adopt MMSE technique. Instead

of eliminating ISI, MMSE receiver combines the effect of ISI and additive noise to minimise the mean squared error of the estimated symbol vector. This is achieved by multiplying the received symbol vector $\boldsymbol{y}$ with $(\boldsymbol{H}^{\boldsymbol{H}}\ \boldsymbol{H}+\rho^{-1}\ \boldsymbol{I}_{N_t})^{-1}\ \ \boldsymbol{H}^{\boldsymbol{H}}$, and it outperforms ZF receiver. In high SNR regime ($\rho \rightarrow \infty$), MMSE equaliser reduces to ZF, and both schemes result in the same performance. The error probability of ZF and MMSE receiver are analysed in [44].

The study on MIMO systems have also been extended to broadband frequency selective channel scenario, in which Orthogonal Frequency Division Multiplexing (OFDM) is used in conjunction with MIMO techniques [46]-[49]. Several issues pertaining to MIMO-OFDM systems have also been addressed. Reference [47] considers differential encoding strategy for MIMO-OFDM systems to eliminate the need of CSI. Transmit power allocation and subcarrier assignment are proposed in [48] and [49] respectively. The problem of Inter-Carrier Interference (ICI) inherent to OFDM systems when applied to highly mobile environment is addressed in [50], which extends the result of [51] into MIMO scenario.

Besides OFDM, there are also other techniques which can be used for MIMO communication over broadband frequency selective channel. For instance, [52] proposes a space time transmit diversity technique for wideband CDMA systems, while the work in [53] uses Decision Feedback Equalisation (DFE) technique at the transmitter to achieve diversity gain in frequency selective channel.

In general, the performance of MIMO systems largely depends on the channel condition. When the number of scatterers is insufficient or when the antenna is placed in high altitude, fading across different antenna pairs might be correlated. Since fading correlation reduces the rank (equivalently the number of spatial data stream) of MIMO channel, performance degradation is inevitable. The detrimental effect of fading correlation towards MIMO capacity and error performance is studied in [54] and [55] respectively. One simple strategy to effectively overcome this issue is to use only a subset of available antennas which has low mutual correlation. The advantage of this antenna selection strategy is two-fold. Firstly, since only part of

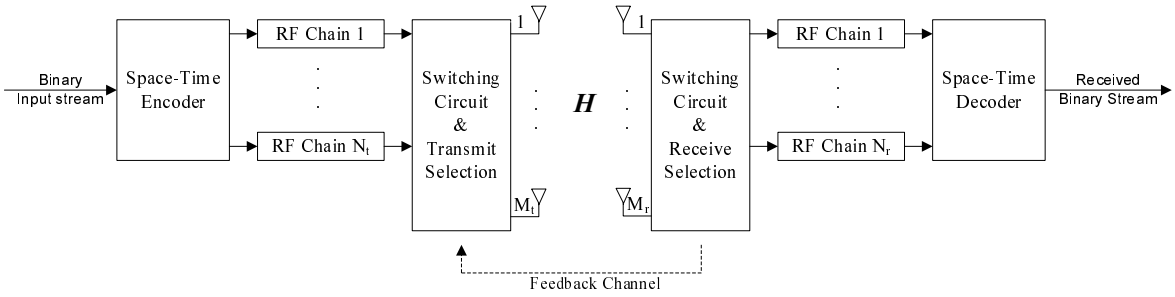

Figure 2.4: Block Diagram of Point to Point MIMO System with Antenna Selection

the available antennas are used at any one time, the number of RF-chain (a series of Radio Frequency devices consisting of amplifier, analog to digital converter, and filter banks) required is reduced. Using a low cost switching circuitry to connect the selected antenna subset to the available RF-chain, the overall hardware cost can be reduced. Secondly, using an appropriate selection scheme based on the information obtained through feedback, optimal antenna subset can be selected, hence the overall performance can be improved. The block diagram of typical MIMO systems with antenna selection is depicted in Figure 2.4. An overview on antenna selection schemes is given in the following subsection.

2.2.2 Overview on Antenna Selection

There are various selection schemes available in the literature, each catered for different MIMO settings such as the transmission method used (spatial multiplexing or space time coded transmission), location where the selection is performed (at the transmitter, receiver, or both), the available information (full CSI or only statistical CSI), receiver equalisation method used (ML, ZF, MMSE, or SIC), as well as the selection objectives (maximise the throughput capacity, minimise the instantaneous/average error probability, or maximise the effective SNR). A considerable amount of work has been done in the field of antenna selection, out of which one of the most notable contribution is by Paulraj together with his team and collaborators (Gore, Nabar, Heath, and Gorokhov) [56]-[62]. Below is a list of various selection criteria that have been proposed for different MIMO settings.

1. ***Maximise Frobenius norm of effective channel matrix or the determinant of correlation matrix:*** Antenna selection in space-time coded MIMO systems which minimises instantaneous and average error probability is proposed in [56]. When full CSI is available at the transmitter, it is shown that selecting antenna subset which maximises the effective channel's Frobenius norm is optimal. The argument follows from the fact that the effective SNR is proportional to the Frobenius norm of the effective channel matrix. Since instantaneous error probability is inversely proportional to the SNR, the selection condition is to choose a subset with the largest norm. When only statistical channel information is available, it is shown that selecting antenna subset which maximises the determinant of the effective correlation matrix is optimal. This follows from the derivation of average pairwise error probability, which is inversely proportional to the determinant of the covariance of vectorised effective channel matrix. Analysis on the performance of selection scheme (based on antenna subset which maximises the channel Frobenius norm) in terms of outage probability is presented in [57].

2. ***Maximise determinant or product of minimum singular values of transmit and receive correlation matrices:*** Antenna selection in spatial multiplexing MIMO systems which minimises average error probability is proposed in [58]. When ML receiver is used, it is shown that optimal receive antenna combination is the one that maximises the determinant of effective receive correlation matrix. Meanwhile, unlike the space-time coded MIMO systems, optimal transmit antenna combination can not be obtained directly by maximising the determinant of transmit correlation matrix. Instead, optimal transmit antenna combination is dependent on the characteristics of the error vectors, and should be searched by minimising the average pairwise error probability expression. It is shown that the optimal transmit and receive antenna subset are the ones that maximise the product of minimum singular values of effective transmit and receive channel correlation matrices for a ZF receiver.

3. ***Maximise the minimum column norm of effective channel matrix or the actual capacity expression:*** Capacity based receive antenna selection scheme for spatial multiplexing MIMO systems is proposed in [59]. When ordered SIC scheme is used at the receiver, the capacity is upper bounded by the number of transmit antenna multiplied by a monotonically increasing function of channel matrix column norm. Therefore, the receive selection criterion is to choose the antenna subset which maximises the minimum column norm of the effective channel matrix. On the other hand, the theoretical capacity can be expressed in a closed form for an MMSE receiver. For both cases, receive antenna selection can be performed by choosing the antenna subset which maximises the capacity expression.

4. ***Maximise the rank of right singular channel matrix with the largest determinant:*** Transmit antenna selection scheme for spatial multiplexing MIMO systems which maximises capacity using only statistical CSI at the transmitter is proposed in [60]. The work is motivated by the fact that end to end capacity is largely dependent on the effective channel rank. Therefore, selecting transmit antenna subset which has a full rank right singular matrix is optimal. Furthermore, when more than one combination satisfies this criterion, choosing the one that maximises the determinant of the right singular matrix is optimal, as it provides additional coding gain.

5. ***Minimise the trace or maximum diagonal value of inverse transmit correlation matrix:*** Another transmit antenna selection scheme for spatial multiplexing MIMO systems using only statistical CSI is proposed in [61]. Using ZF receiver, the statistics of effective SNR is derived and subsequently applied to find the expression of average error probability and average capacity. When the objective is to maximise the average throughput, the selection criterion is shown to be equivalent to selecting transmit antenna subset which minimises the trace of the inverse transmit correlation matrix. On the other hand, when the objective is to minimise the average error probability, it is shown that the selection

criterion is to choose transmit antenna subset which minimises the maximum diagonal value of inverse transmit correlation matrix.

6. ***Maximise minimum SNR, minimum singular values of effective channel matrix, and capacity expression:*** A slightly different variant of transmit antenna selection for spatial multiplexing MIMO systems is proposed in [62]. Here, instead of performing the selection at the transmitter using CSI available, selection is performed at the receiver using full CSI (which can be obtained by good channel estimation algorithm), and then the optimal antenna subset is sent back to the transmitter via low rate feedback. The selection objective considered is to maximise effective SNR. MMSE and ZF receiver are considered whereby the expression of effective SNR at different spatial data streams are obtained. Three schemes are proposed, choosing transmit antenna subset which directly maximise the minimum SNR across all data stream, choosing the one which maximises the minimum singular values, and choosing the one which result in largest capacity.

7. ***Maximise capacity through successive addition or removal of channel row/column:*** An information theoretic approach of joint antenna selection which maximises the capacity of spatial multiplexing MIMO systems is presented in [63]. It studies the effect of mutual information and channel power towards MIMO capacity and exploit them as antenna selection criteria. It also analyses the algorithm complexity. Another information theoretic approach of capacity maximising antenna selection scheme is proposed in [64]-[66], whereby iterative algorithm to successively add/remove channel row/column is developed. It is shown that this approach can significantly reduce the selection complexity. The performance of the scheme when applied to MIMO systems with MMSE and ordered SIC receiver is analysed. The capacity of MIMO systems with receive antenna selection is studied in [67]. It is shown that as long as the number of selected receive antennas is as large as the number of transmit antennas, a capacity close to a full complexity system can be achieved. An upper bound on capacity is developed for

the cases when receive antennas is less than and greater than the number of transmit antennas, and their performances are evaluated via simulation studies.

Similar to MIMO systems, the study on antenna selection has been applied to broadband frequency selective channel scenario as well [68]-[72]. Since channel conditions at different subcarriers are generally different, the selection process in this scenario has to take into consideration of all subcarriers jointly. The optimal antenna subset is the one that results into the best performance at all or most of the subcarriers. Receive antenna selection in MIMO-OFDM systems which minimises the error probability averaged over all subcarriers is considered in [68]. A similar technique is also used in [69] for transmit antenna selection case. Although efficient schemes have been developed for selecting optimal antenna subset in broadband frequency selective channel, the complexity of these schemes are often very high, especially when the number of subcarriers is large. Motivated by this fact, the work in [71] and [72] proposed a sub-optimal antenna selection strategy for MIMO-OFDM systems.

A different approach on antenna selection for broadband frequency selective channel is proposed in [73]-[76], where the problem of allocating subcarrier to the best antenna is considered. In terms of hardware cost, this scheme requires the same number of RF-chains as the total available antennas, hence no cost reduction is achieved. The advantage of this scheme, however, is the extra flexibility for resource allocation. Since each subcarrier is transmitted through only one antenna, power allocation and bit loading (using adaptive modulation and coding scheme) can be readily applied.

2.2.3 Multi-antenna Cooperative Broadcast Communication

Having seen the superiority of MIMO systems and its extensive study in point to point communication, it is natural that the application of multi antenna configuration is also considered in cooperative broadcast scenario. As pointed out earlier, the analysis of MIMO-BC is more challenging compared to single antenna BC due to its non-degraded nature. The capacity re-

gion of MIMO-BC is still an open problem to date. Attempt to characterise the achievable rate region of Gaussian MIMO-BC was made by Caire and Shamai in [77], in which the theorems from Costa's Dirty Paper Coding [2], Marton's region for generic scalar BC [20], and Sato's capacity outer bound [78] were used to find the achievable region of two user MIMO-BC (one transmitter with two antennas and two single antenna users). In their work, the MIMO-BC is first decomposed into a set of interference channel, after which Dirty Paper Coding scheme is applied at the transmitter, followed by successive encoding of different user's data. The resulting achievable region is then known as Dirty Paper region.

Capacity outer bound of MIMO-BC is obtained by assuming that all receivers fully co-operate with one another, such that the overall throughput/sum rate is equal to point to point MIMO capacity, in which the number of transmit antenna is equal to the number of broadcast transmitter's antenna, and the number of receive antennas is equal to the sum of all receivers' antennas [78]. However, since different receivers are disjoint, noise between different user's antenna can be arbitrarily correlated, and the capacity outer bound must consider the worst case noise correlation. Using conventional technique of MIMO capacity, the sum-rate capacity outer bound of MIMO-BC can be calculated. Dirty Paper region found in [77] is shown to achieve the same sum rate as this capacity outer bound, therefore it is said to achieve the sum-rate capacity of MIMO-BC.

The more general case of MIMO-BC with arbitrary number of users, transmit antennas, and receive antennas was considered by Yu and Cioffi. It is shown that the achievable rate region can be expressed as [79, Theorem 1]:

$$(R_1, \cdots, R_K) \; : \; R_i \leq \frac{1}{2} \log_2 \frac{\left| \sum_{k=i}^{K} \boldsymbol{H}_i \boldsymbol{S}_k \boldsymbol{H}_i^H + \boldsymbol{S}_{z_i z_i} \right|}{\left| \sum_{k=i+1}^{K} \boldsymbol{H}_i \boldsymbol{S}_k \boldsymbol{H}_i^H + \boldsymbol{S}_{z_i z_i} \right|} \tag{2.17}$$

where K is the total number of receivers, $\boldsymbol{S}_{z_i z_i}$ is the noise covariance matrix at receiver i, and $\boldsymbol{S}_k$ is a set of positive semi-definite matrices satisfying the total power constraint. It is

also shown that the above rate can be achieved using precoding strategy through Generalised Decision Feedback Equalisation at the transmitter. As far as sum capacity of MIMO-BC is concerned, [79] provides rigorous proof to show that sum capacity is a saddle point of the mutual information game in the form of min max operation, where maximisation is performed with respect to all transmit covariance matrices satisfying the total power constraint, while the minimisation is performed with respect to the least favorable noise covariances.

Using the duality theorem of BC and MAC proposed in [80], Vishwanath, Jindal, and Goldsmith gives an alternative expression for MIMO-BC sum rate capacity in [81] and [5]. The outline of the derivation is as follows. First, duality between Dirty Paper region and MIMO-MAC capacity region is proved by showing that for a given set of covariance matrices in Dirty Paper region, it is possible to obtain another set of covariance matrices in MIMO-MAC region having the same total power and resulting in the same sum rate. Then, it is shown that the maximum sum-rate in the dual MIMO-MAC capacity region intersects with Sato cooperative capacity outer bound for MIMO-BC. Hence, it is concluded that the sum capacity of MIMO-BC can be computed through the dual MIMO-MAC having the same total power constraint as follows:

$$C_{sum} = \max_{\boldsymbol{S}_k \geq 0,\ \sum_k Tr(\boldsymbol{S}_k) \leq P_{tot}} \frac{1}{2} \log_2 \left| \boldsymbol{I} + \sum_{k=1}^{K} \boldsymbol{H}_k^H \boldsymbol{S}_k \boldsymbol{H}_k \right| \tag{2.18}$$

which is much simpler and easier to analyse compared to the original expression of MIMO-BC sum capacity obtained through Dirty Paper region as follows [79]:

$$C_{sum} = \max_{\boldsymbol{Q}_{\varphi(i)} \geq 0,\ \sum_i Tr(\boldsymbol{Q}_{\varphi(i)}) \leq P_{tot}} \sum_{j=1}^{K} \frac{1}{2} \log_2 \frac{\left| \boldsymbol{I} + \sum_{i=j}^{K} \boldsymbol{H}_{\varphi(j)} \boldsymbol{Q}_{\varphi(i)} \boldsymbol{H}_{\varphi(j)}^H \right|}{\left| \boldsymbol{I} + \sum_{i=j+1}^{K} \boldsymbol{H}_{\varphi(j)} \boldsymbol{Q}_{\varphi(i)} \boldsymbol{H}_{\varphi(j)}^H \right|} \tag{2.19}$$

where the maximisation has to be done over all possible encoding order φ and all positive semi-definite transmit covariances $\boldsymbol{Q}_{\varphi(i)}$ that satisfy total power constraint. The relationship between MIMO-BC, MIMO-MAC, and Sato upper bound has also been pointed out through independent work by Viswanath and Tse in [82].

The analysis on MIMO-BC so far assumed that perfect CSI is available at the transmitter and all receivers. In practice, this requires a large amount of feedback from all receivers. A sub optimal approach to overcome this issue was proposed in [83], whereby the concept of one-shot scalable feedback for MIMO-BC is introduced. For the case when perfect CSI is not available, an alternative transmission scheme for MIMO-BC with only partial CSI is proposed in [84]. By sending a probe message to random directions following isotropic distribution, each receiver can measure the best beam having the largest Signal to Interference plus Noise Ratio (SINR) and send that information back to the transmitter via feedback channel. Transmission is then performed only to a subset of receiver having the best SINR. It is shown that this strategy can achieve sum rate throughput that scales as fast as the optimal MIMO-BC strategy.

Other sub-optimal broadcast transmission strategies have also been proposed in [85] and [86], in which TDMA and block diagonalisation scheme are considered, and their performance are compared to the optimal Dirty Paper strategy. In TDMA, only one user is served at any one time. While TDMA is sum rate optimal for single antenna BC, it is not the case for MIMO-BC. It is shown in [85] that the sum rate capacity achieved using Dirty Paper strategy is several times larger than TDMA sum rate, and the ratio can be up to the minimum between number of transmit antenna and total number of users. As for the block diagonalisation scheme, a precoding matrix is applied to different message vectors intended for different users. The objective here is to eliminate interuser interference so that receiver equalisation can be simplified. It is shown in [86] that under idealistic case where user's channel are mutually orthogonal, block diagonalisation scheme can achieve Dirty Paper performance. Otherwise the performance is somewhere in between TDMA sum rate and the optimal Dirty Paper sum rate capacity.

Since MIMO-BC is a multiple antenna system in nature, the problems inherent to MIMO systems (such as hardware cost, space limitation, channel correlation) persist in this system as well. Before the practical application of MIMO-BC can be justified, these problems need to be addressed. In the previous subsection, the role of antenna selection in providing an effective

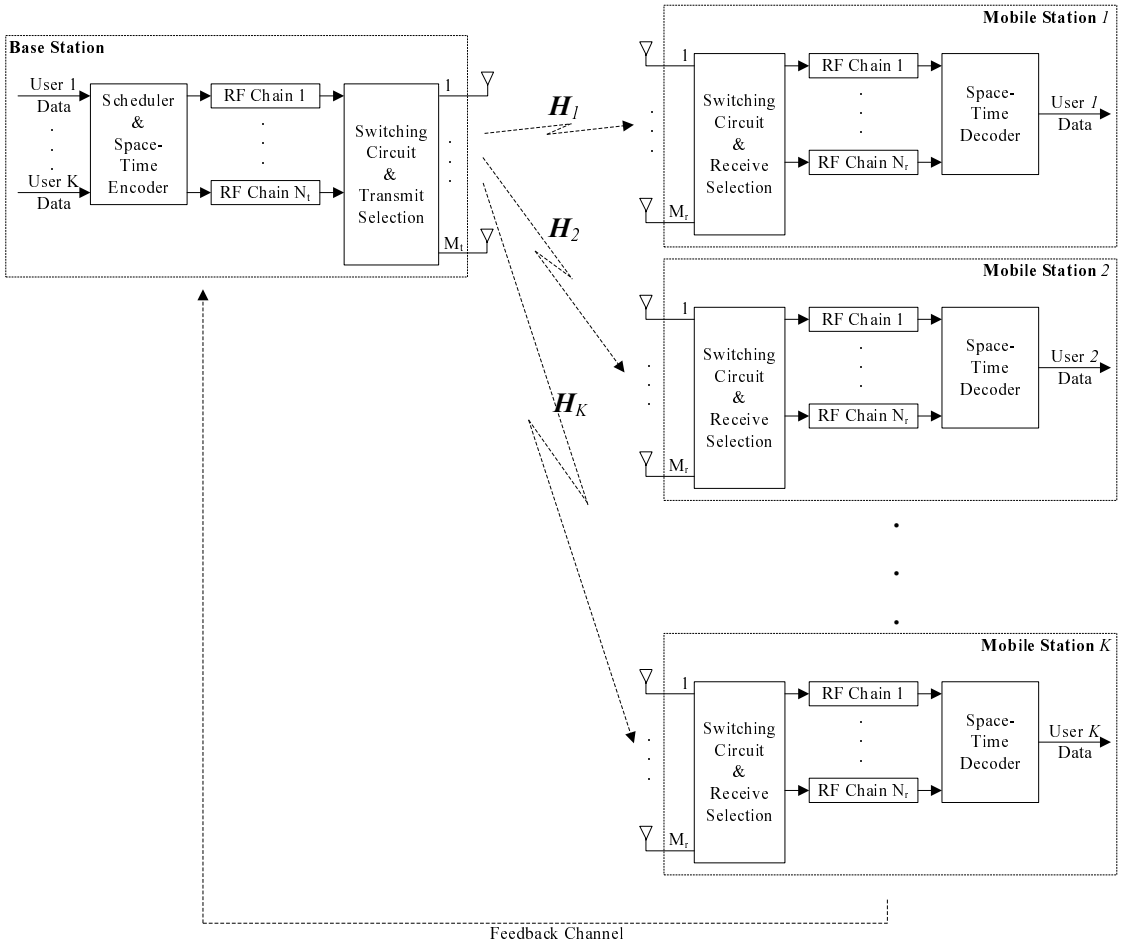

Figure 2.5: Block Diagram of MIMO-BC System with Antenna Selection

solution to these problems for point to point MIMO case has been demonstrated. One of the objectives of this work is to extend the antenna selection concept into MIMO-BC scenario.

Block diagram of a typical MIMO-BC system with antenna selection is depicted in Figure 2.5. The subscript index of the channel matrices above indicates the user index. As opposed to point to point MIMO system, applying antenna selection in MIMO-BC is more challenging. Selecting a particular antenna subset at the transmitter would affect the performance of all receivers, hence transmit antenna selection strategy must take into consideration of the collective effect to all users. At the same time, the selection algorithm complexity must be kept as low as possible. Antenna selection strategy for MIMO-BC is a subject of analysis in this thesis, and its detailed discussion is presented in Chapter 3.

2.3 Cooperative Relay Network

The cooperative scenario in relay network is fundamentally different from cooperative broadcast communication. As opposed to broadcast communication where messages are co-located in central location, each node in relay network carries their own information to transmit. Cooperation in this scenario represents joint effort of different nodes to improve decoding reliability at the destination. The underlying concept of cooperative relay network is to make use of partner's antenna in order to create multiple spatial data streams towards destination, hence any benefit of MIMO systems can be exploited, even though each node is equipped with only one antenna. In this regard, cooperative relaying can be viewed as a synergic fusion of relaying (where message must travel through several hops to reach destination) and multi antenna systems (where multiple spatial data streams are created, hence improving transmission quality).

Some of the pioneering works in cooperative relay network include the contribution by Sendonaris, Erkip, and Aazhang; in which cooperation is applied to two user system communicating with a common destination [6]-[7]. In that work, an achievable rate region of the system is developed, whereby an idea to split each user's message into three portions is introduced (one portion intended to send directly to destination, one portion for the partner node, and another portion to send cooperative message containing both its own and partner's message to destination). As far as practical implementation is concerned, a CDMA scheme is used to separate different portions of the message, and the resulting throughput and error performance are analysed.

Following [6] and [7], research on cooperative relay network has been extended into many directions, and several aspects of the subject have been considered. Different forwarding strategies have been proposed, including Amplify and Forward (AnF), Decode and Forward (DnF), Coded Cooperation, and many others. In the following two subsections, two different classes of cooperative relay networks (namely single relay configuration and multiple relay configuration) are addressed.

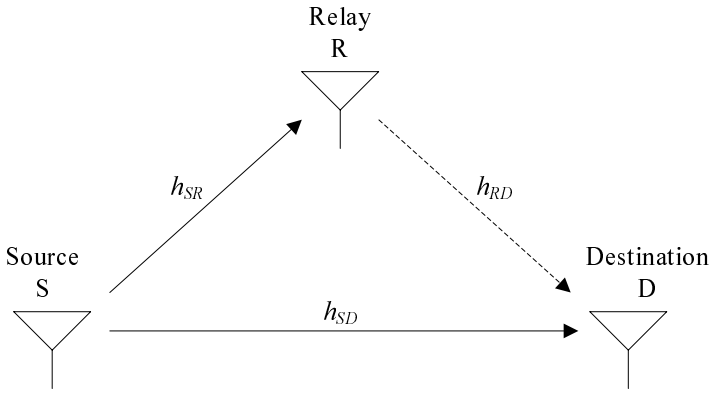

Figure 2.6: Illustration of a Three Node Network

2.3.1 Single Relay Configuration

The simplest configuration of cooperative relay network is a three node network (Figure 2.6), where one source node communicates to the destination node with the help of a single relay node located between the two. Interestingly, even in this most simplistic configuration, the number of possible cooperation strategies is seemingly infinite, and a plethora of works can be found in the literature discussing this particular cooperative setting ([87]-[107]).

Here, transmission of a message from source to destination involves two time slots. On the first slot, source node broadcasts the message to both source and destination, and the received signal can be expressed using the following discrete time signal model:

$$y_r = h_{sr}\, x + n_r \tag{2.20}$$

$$y^{(1)} = h_{sd}\, x + n^{(1)} \tag{2.21}$$

where h_{sr} and h_{sd} are the channel gain from source to relay and source to destination node respectively, x is the transmitted symbol satisfying power constraint $E[|x|^2] \leq P$, while n_r and $n^{(1)}$ are AWGN at relay and destination node during the first time slot respectively, and they are distributed with equal variance according to complex normal distribution $\mathcal{CN}(0, N_0)$. At the second time slot, relay node forwards the received information to destination. Depending on

how relay node process the signal prior to forwarding it to the destination, and how destination node makes use of that extra information from relay node to make better decoding reliability, various cooperative relaying schemes are defined.

Reference [87] provides a tutorial overview of three cooperative relaying strategies in three node network, namely AnF, DnF, and Coded Cooperation. In AnF scheme, relay node simply forwards a scaled version of whatever it received at the first time slot, and the received signal at the destination can be expressed as:

$$y^{(2)} = h_{rd}\, A\, y_r + n^{(2)} \tag{2.22}$$

where h_{rd} is the channel gain from relay to destination node, A is the scaling factor chosen to satisfy the power constraint at the relay, y_r is as expressed in equation (2.20), and $n^{(2)}$ is the AWGN at the destination during the second time slot. The destination, upon receiving the signal at both time slots, will then use $y^{(1)}$ and $y^{(2)}$ to decode the original message. It is apparent that extra diversity gain is available at the destination, hence better decoding reliability can be achieved.

In DnF scheme, the scenario is slightly different. Here, instead of just scaling the received signal, relay node tries to decode the message before forwarding it to the destination. The received signal at destination in this case can be expressed as:

$$y^{(2)} = h_{rd}\, \hat{x} + n^{(2)} \tag{2.23}$$

where $\hat{x}$ is the message estimate at the relay node. The advantage of such an approach is the non-propagation of channel distortion and additive noise to the subsequent stages, which results in the relaying of clean message to the destination. The drawback in such approach, however, is the additional complexity required at the relay node to perform message decoding. Error propagation is also a problem inherent to DnF scheme. When the decoded message at

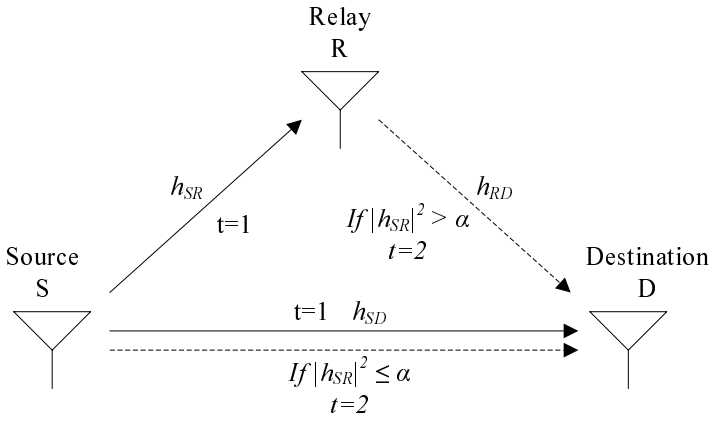

Figure 2.7: Illustration of Selection Cooperation in Three Node Network

relay node is incorrect, the forwarded message would be erroneous, which will in turn degrade the decoding reliability at the destination.

Coded cooperation is another type of cooperative scheme in three node network [88]-[91]. The main difference between this scheme and the previous two is that coded cooperation is always used in conjunction with channel coding. The idea is to let relay node transmit a certain portion of parity information to destination node. Hence, in the first time slot, the channel coded message is appropriately punctured at the source node and subsequently sent to both relay and destination. At the relay, message decoding is performed and different puncturing pattern is used to generate enhancement parity which is sent to destination at the second time slot. Code combining technique is then used at the destination to decode the original message with better reliability.

On top of the above three cooperative techniques, several variants of the scheme have been considered. In [92], Laneman, Tse, and Wornell introduced an adaptive scheme called selection relaying and incremental relaying for three node networks; and their performances in terms of outage probability are shown to outperform fixed relaying with either AnF or DnF. The underlying idea of these proposed schemes are described in the following two paragraphs.

In selection relaying (see Figure 2.7 for illustration), relay node measures the channel quality from the source node. If the channel gain is above a certain threshold, it will continue

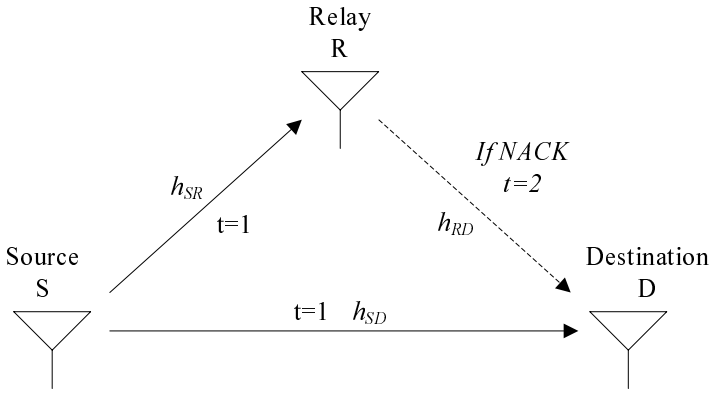

Figure 2.8: Illustration of Incremental Relaying in Three Node Network

to forward the message to destination node. Otherwise, it remain silent at the second time slot, and let the source node transmit instead (using repetition coding or other more powerful codes). The intuition behind this scheme is as follows. When the channel gain between source and relay is not sufficiently high, it is likely that the relay node receives an erroneous message. Therefore, letting the relay node forward the message under this condition will bring down the performance. This scheme tries to avoid this situation by having the source node retransmit instead. As far as the threshold is concerned, an outage condition can be used. In other words, given a target rate, the minimum channel gain required to achieve a certain outage probability can be calculated. Using that gain as the threshold is equivalent to letting relay node forward the message only when the source relay channel is not in outage as desired.

Incremental relaying provides an extension of hybrid-ARQ (Automatic Repeat Request) into relay scenario (see Figure 2.8 for illustration). Upon receiving a message at the first slot, the destination node tries to decode it. If the destination is able to decode the message correctly (as indicated by an error detection mechanism), then positive acknowledgement (ACK) is sent, and source node continues to transmit at the following time slot. Otherwise, negative acknowledgement (NACK) is sent, and relay node will forward the message it received during the first time slot to destination. The advantage of this scheme is that extra time slot is required only when destination is unable to decode the message from source node; as such, higher bandwidth

efficiency is attained. The drawback of this scheme is the necessity of feedback channel for the destination to send acknowledgement; however, this penalty is minimal compared to the bandwidth efficiency savings it provides.

The performance of cooperative communication in three node networks using AnF and DnF are analysed by the same authors using average error probability [93] and outage probability [94] as the performance metric, and it is demonstrated that cooperation outperforms direct transmission. In [95], Nabar, Bolcskei, and Kneubuhler presented an information theoretic analysis of AnF and DnF scheme in three node network. The technique used in the analysis is to arrange the received symbol at the destination into vector form, such that the effective channel can be represented by a matrix. Then, conventional mutual information calculation for MIMO systems can be applied directly. Three different scenarios are considered. In the first scenario, source node broadcasts its message at the first time slot to both relay and destination. Then, both source and relay transmit to the destination at the second time slot. In the second scenario, source node again broadcasts to both relay and destination at the first time slot. However, at the second time slot, only relay node forwards the message to destination. This scenario captures a situation where the source node is engaged in data reception from other terminal during second time slot. Finally, in the third scenario, source node transmits solely to the relay node at the first time slot (as destination node is engaged in data transmission to other node). While both source and relay node transmit to destination node at the second time slot.

In [96], Vishwanath, Jafar, and Sandhu analysed the achievable region of three node network, and subsequently gave the corresponding outer bound. It first breaks the transmission into two periods. In the first period, source node broadcasts to both relay and destination node, hence the transmission is limited by BC communication. At the second period, both source and relay transmit to destination, hence the transmission is limited by MAC communication. Maximum flow minimum cut theorem [97] is then applied to obtain the achievable region. Another constraint in three node network is that the information from relay node could not exceed the

information it received from the source. Incorporating this constraint into the earlier achievable region, the corresponding outer bound is developed, and a Gaussian channel example is given.

When conducting performance evaluation in cooperative three node networks, it is often necessary to characterise the effective SNR at the destination. When MRC technique is adopted to combine the signal from the first and second time slot, the effective SNR is simply the addition of the individual SNR at both slots ($\rho_{eff} = \rho^{(1)} + \rho^{(2)}$). The SNR characterisation at the first time slot is straightforward, as it is just a conventional point to point transmission. From equation (2.21), this SNR can be expressed as:

$$\rho^{(1)} = \frac{P}{N_0} |h_{sd}|^2 \tag{2.24}$$

The SNR characterisation at the second time slot, however, is more difficult, as the message undergoes fading twice before reaching destination. Assuming AnF, this SNR can be expressed as:

$$\rho^{(2)} = \frac{P}{N_0} \left(\frac{|h_{sr}|^2 |h_{rd}|^2}{|h_{sr}|^2 + |h_{rd}|^2 + \frac{N_0}{P}} \right) \tag{2.25}$$

In [98], a high-SNR characterisation for the second slot transmission is derived using the Probability Density Function (PDF) of a harmonic mean of two exponential random variables. Meanwhile, the Cumulative Distribution Function (CDF) of ρ_{eff} which is useful in analysing the outage probability of the system is derived in [99]-[100].

When applied to broadband frequency selective channel, ISI complicates the analysis. Reference [101] extends the analysis of cooperative three node network in frequency selective channel, in which three equalisation schemes are proposed. The first scheme applies Lindskog-Paulraj STBC technique [102] in distributed scenario, while the other two schemes use OFDM based equalisation to eliminate ISI.

Despite all the analysis that have been provided for cooperative three node network, most of them focused on the performance analysis in terms of capacity, average SNR, and average

probability of error at the destination. While it is true that the additional relay node can improve the overall performance, it does so with an additional time slot. In order to make a fair comparison with direct transmission, equal end to end throughput must be considered; hence modulation order (the number of bits per symbol) has to be doubled for the relay scenario, which will in turn bring down the performance.

Motivated by this fact, this thesis tried to address the above issue by answering a fundamental question on whether adding relay node can indeed improve the end to end performance. In other words, given the same amount of total power, total bandwidth constraint, and equal end to end throughput, the role of relay node in improving direct transmission performance is studied. The condition of optimality is also considered, which provides a connection to the subject of resource allocation. The significance of resource allocation in cooperative three node network has been recognised in the past. For example, reference [103] presented a power allocation scheme to minimise outage probability and to maximise the average SNR. Ergodic capacity maximising power allocation scheme is presented in [104], while reference [105] considered delay limited capacity as a criteria. Other ergodic capacity based power allocation scheme can be found in [106]-[107]. Considering the practical aspect of power allocation algorithm, the selection parameters must depend on relatively static values such as channel variance instead of its instantaneous values. A detailed discussion on the proposed power control strategy for cooperative relay network is given in the first half of Chapter 4.

2.3.2 Multiple Relay Configuration

A natural extension of cooperative three node network is to consider the case when there are more than one relay node present to help message transmission. Different schemes have been considered in this cooperative scenario, including repetition coding and distributed space time coding (sometimes referred to as space time coded cooperative diversity) which was introduced by Laneman and Wornell in [108] and [109]. A typical system setup of multiple relay

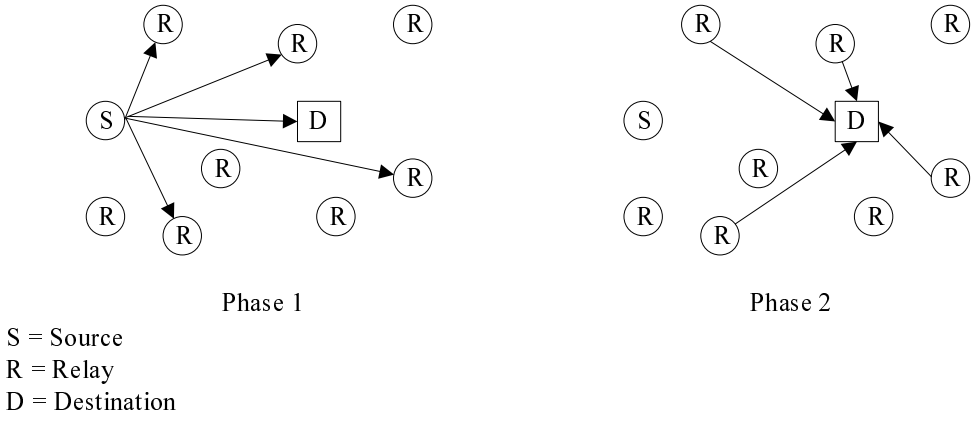

Figure 2.9: Multiple Relay Cooperative Network

cooperative network is depicted in Figure 2.9. Just as the three node network case, transmission is divided into two phases. On the first phase, source node broadcasts its message to all other nodes (including the destination node). Subsequently, on the second phase, some or all of the relay nodes forward the message they received to the destination. Depending on the cooperative scheme adopted, the way different relay nodes transmit are also different.

In repetition coding, all relay nodes who overheard message transmission during the first time slot will join the relay group. In the second phase, these nodes will take turns to repeat the message it received to destination node. Using this scheme, destination node would have multiple copies of the same message, providing extra diversity hence improving decoding reliability. However, the major drawback of this scheme is the extra time slot required for different relay nodes to repeat the message. The larger the number of nodes in the relay group, the more is the time slots required to transmit the message to destination, resulting in a severe bandwidth efficiency penalty.

In distributed space time coding, all nodes in relay group construct the corresponding space time code (STC) matrix based on the message it received during the first phase. Once they have the necessary information, each node will then transmit their respective row of the code matrix simultaneously to the destination. Since all relay nodes transmit at the same time, bandwidth efficiency penalty is not as severe as in the repetition coding. Meanwhile, the same diversity

benefit is still available due to the STC structure used.

In reference [110], performance comparison of repetition coding with AnF and DnF scheme are presented. In AnF scheme, all other nodes except the source and destination node are joined into the relay group; while in DnF scheme, only those nodes who are able to decode the message correctly are joined into the relay group. Both schemes are shown to achieve the same diversity, which is in the order of the number of nodes in the relay group. Therefore, given that all available relay nodes can decode correctly, the diversity order of both schemes are identical. When there are decoding errors at the relay nodes, DnF scheme generally has smaller diversity order than AnF scheme. This result is pointed out in [111], whereby a piecewise linear combining receiver is used to derive a closed form expression of average bit error rate (BER) in dual-hop relay transmission using coherent and non-coherent DnF scheme as well as coherent AnF scheme. Diversity analysis is then performed by taking a high SNR approximation to the average BER, which shows that there is a factor of 2 loss in diversity order when DnF scheme is used. Another difference between AnF and DnF scheme lies in the achieved coding gain, which are characterised in [110]. The same author also provides an outage probability analysis for repetition coding and parallel channel coding in [112].

Many other performance analysis in multiple relay cooperative networks can be found in the literature. Reference [113] introduces the concept of degradation factor to analyse BER in cooperative network, where relay nodes are equipped with multiple antennas. It is shown that channel correlation across different antennas at relay nodes contributes to the degradation factor, and potentially bring the performance down. Reference [114] also studied the BER performance of cooperative network where source and destination has single antenna, while multiple relay nodes with multiple antennas are deployed in the fixed location between source and destination. Symbol error probability (SEP) for general cooperative links with multiple relay and multiple hops is developed in [115]. First, it developed a theorem to characterise the SEP in single relay dual hop system. The general case of arbitrary number of relay nodes and

arbitrary number of hops is then obtained by applying the theorem several times as necessary, and it is demonstrated that the obtained SEP expression is very close to the experimental results. A slightly different multi-hop configuration is considered in [116], whereby relay node at each relay stage considers the transmission of nodes from all relay stages prior to itself. As opposed to the conventional setup where relay node only considers transmission from the relay stage just before itself, the BER and SEP analysis is more complicated. It is also highlighted that at high SNR regime, the resulting performance is independent to the number of preceding relay stages considered for message forwarding.

Cooperative communication using multiple relay nodes has also been termed differently. In his thesis [117], Dohler introduced a new term called Virtual Antenna Array (VAA), which is used to emphasise the connection with multi antenna systems. The term VAA was first used in [118] and [119], in which Dohler, Lefranc, and Aghvami studied a scenario where base station with two antennas communicates with a single antenna node using two single antenna relays. Alamouti code is used as the space time code, and two scenarios are considered; namely when the two relays are within a CDMA chip range and when they are separated more than one chip duration. Generalisation to the case of more than two relay nodes is also given, and their BER performances are analysed. The capacity analysis of VAA systems is provided in [120], whereby it is shown that the optimal configuration is to have relay nodes possess equal number of antenna as the base station. Space time code design for VAA systems is studied in [121]. It turns out that the rank and determinant criterion used for conventional MIMO systems (as proposed by Tarokh in [28]) is also applicable for VAA systems. Reference [122] presented various relaying scenarios possible in VAA system, while [123] analysed the BER performance of various VAA configuration using different modulation orders. Influence of channel distribution is studied in [124], where the effect of Rayleigh, Nakagami, and Rician fading towards BER performance in VAA systems is analysed.

An information theoretic analysis of multiple relay cooperative network in terms of diver-

sity multiplexing tradeoff (DMT), a framework developed by Zheng and Tse [25], is presented in [125], where repetition coding using AnF is considered. A DMT analysis for the case where nodes are equipped with multiple antennas and for the case when there are multiple source destination pairs are considered in [126]. As far as outage probability performance of multiple relay cooperative network is concerned, reference [127] and [128] gave an outage analysis for AnF and DnF scheme respectively.

As in single relay configuration, the analysis of multiple relay cooperative network has also been extended into broadband frequency selective case in [129]. In the following, several issues pertaining to multiple relay cooperative network are discussed, and the existing solution is explained.

Resource allocation

The discussion so far assumed equal power allocation across different relay nodes. When the system allows flexibility to allocate different power to different relay nodes, it is possible to optimise the allocation strategy to achieve better performance. Furthermore, when different relay nodes are allowed to use different fractional bandwidth to forward during the second phase, both power and bandwidth allocation can be optimised jointly. In [130], Dohler, Aghvami, Li, and Vucetic developed power and bandwidth allocation strategy to maximise the end to end throughput of cooperative relay network. Subsequently, joint optimisation is proposed in [131]-[133] using capacity as the criterion. It was shown that in order to maximise the end to end capacity, the fractional power and bandwidth should be allocated such that the capacity on each hop are equal. Extension to the analysis for non ergodic channel is given in [134], where outage throughput maximisation is used as the allocation criteria. When instantaneous CSI is not available, resource allocation algorithm must rely on the statistical CSI. Reference [135] proposed a power allocation strategy using only statistical CSI for AnF, DnF, and distributed space time coded systems; whereby outage minimisation is used as the criteria.

Relay node selection

In some cases, it is more beneficial to use only a subset of available relay nodes to forward the message to destination; such as to minimise total transmit power, to reduce the amount of interference towards other transmissions in the network, or to better utilise the available relay nodes so that the remaining relay node can serve other transmissions. When location information of the nodes are available (which can be obtained via global positioning system/GPS devices), the relay node that is closest to both source and destination can be selected as the best candidate [136]. However, location information it hardly available in practice. Without location information, relay nodes must use other metric such as receive signal strength to find the best candidate. In reference [137], three different relay selection methods are proposed, namely best average SNR, best instantaneous SNR, and random selection; and their performances are compared.

When applied to multi-hop relaying systems, reference [138] proposed to select a relay node having the largest geometric average of the mean channel gain to the nodes at the following relay stage as the best candidate. It is shown that such approach has a good end to end outage performance. A somewhat different approach of relay selection is considered in [139], where the problem of node pairing in a network with common destination is considered. Different schemes including maximum weight-matching, greedy matching, worst link first matching, and random matching are considered, and their performances are compared. As far as DMT performance, reference [140] shows that using only one best relay node achieves the same DMT performance as using all available relay nodes. Similar conclusion is also obtained in an independent work on opportunistic relaying with AnF and DnF schemes [141]. A scenario with multiple source nodes is considered in [142], in which relay selection problem translates into choosing an optimal set of source nodes for every relay. The tradeoff here lies on the fact that each relay node is power limited. When only one source is transmitting through a particular relay node, it can use all its power for forwarding. However, when there

are more than one source transmitting through it, the total power must be divided accordingly. The overall performance are then analysed in terms of outage probability.

Variable number of relay nodes issue

In repetition coding, the relay nodes repeat the source message to the destination. Message combining is then performed at the destination before the original message is decoded. Although the number of relay nodes is not known a-priori, this does not impose any practical issue, as message combining works for any number of relay nodes. In distributed space time coding, however, variable number of relay nodes imposes an implementation problem, as each relay node needs to know the actual number of relay nodes a-priori before constructing an appropriate STC matrix. This problem is considered in [143]-[145], where the concept of randomising the STC matrix is introduced. The outline of the scheme is as follows. During the first phase, relay nodes receive a message block from source node and decode it accordingly. Subsequently, relay nodes who are able to decode the message block correctly will construct the STC matrix based on the decoded message. At the second phase, instead of transmitting a certain row of the STC matrix (as in the conventional distributed space time coding systems), a relay node transmits a random linear combination of different rows in STC matrix. This is achieved by multiplying the STC matrix with a randomisation matrix. Doing so would ensure that the received message at destination node contains a linear combination of the entire original STC matrix, hence better decoding reliability can be achieved. Other techniques dealing with variable number of relay nodes issue is proposed in [146] and [147].

Synchronisation issue

In MIMO systems, transmission of space time codes from different transmit antennas are assumed to be synchronous. This is a reasonable assumption as different antennas are co-located at the same terminal. In distributed communication systems, different virtual transmit antennas

are represented by different relay nodes' antenna. As such, transmission towards destination are not necessarily synchronised. Conventional space time codes for point to point MIMO systems are designed for synchronous systems, hence it is inappropriate for distributed co-operative systems. Reference [148] provides a space time code construction to cater for the asynchronism issue. It is shown that as long as the amount of time lag between different transmit antennas are known at the destination, simple decoding is possible, and a performance close to the synchronous case can be achieved.

Multiplexing gain in cooperative network

When the objective is to increase the effective data rate, multiplexing gain is considered, and it has been shown that it is possible to achieve such gain in a distributed manner. In [149], a scenario where single antenna source node communicates to a multi-antenna base station with the help of several relay nodes is considered. The concept of cooperative spatial multiplexing is introduced, in which source node uses high order modulation to send a message to all relay nodes within its vicinity. Following that, each relay node is responsible to decode different portions of the message bits, and then forward them simultaneously to the destination at the second slot. Decoding at the destination is possible as multiple antennas are available to separate different data streams from all relay nodes. Different decoding schemes have also been proposed in [150], whereby SIC ordering based on substream SNR and log likelihood ratio metric is used to improve decoding performance. In reference [151], the study of cooperative spatial multiplexing is extended into multiple hops case. The analysis in this case is similar to the two-hop scenario, except that the message must travel through several relay stages (with multiple relay nodes at each stage) before it is finally decoded at the multi-antenna destination.

2.3.3 Generalisation of Cooperative Networks

As pointed out in the earlier sections, research on cooperative communication has been generalised to consider multiple hops case. However, the focus so far has been to improve end to end performance. In other words, given a fixed source and destination node, the objective is to decide what kind of forwarding strategy should relay nodes adopt in order to facilitate the transmission. Practically, every node in the network is identical, and each has its own message to transmit. Hence, no distinction should be made between source, relay, and destination node, as every node can take any role depending on the scenario. Due to half duplex constraint, when a node acts as a relay to facilitate message transmission, it must refrain from transmitting its own message. Therefore, as more relay nodes are required as the number of hops increases, the effective throughput of the network decreases. In order to alleviate this problem, relay node should be allowed to transmit its own information at every transmission slot, allowing new information to be infused through the network. However, doing so will introduce interference to any existing message transmission, hence an appropriate interference cancellation strategy must be employed. In this thesis, a new strategy to allow new message transmission on every slot while keeping the interference minimal is developed, and its detailed discussion is given in the second half of Chapter 4.

Cooperative communication is inherently a network solution. In order to generalise performance evaluation at network level, all possible source destination node pairs need to be considered. Most of the works found in the literature considered fixed source and destination node. Extending the result to consider all possible source destination pairs is one of the main topic addressed in this thesis. In Chapter 5, cooperative network with fixed regular structure is considered. Starting with the ideal case whereby all relay nodes are located in the middle between source and destination, a closed form solution for the average outage probability is developed. Generalising the result into planar network, a case where each node is located in lattice points is considered. The network outage probability is then analysed, considering all

other nodes are potential destination. The effect of traffic pattern such as traffic locality and source node location is studied. In the most general case of random network, where nodes can be located anywhere within the network boundaries are considered in Chapter 6. Three different cooperative schemes are considered, namely Distributed Amplify and Forward (D-AnF), Distributed Transmitter Maximum Ratio Combining (D-TxMRC), and Distributed Space Time Block Coding (D-STBC); each of which has different challenges or difficulties in evaluating its performance. In D-AnF scheme, the difficulty lies in determining the location of relay node. As the network is random, the number of node within a given area is also random. In addition, the performance analysis must consider all possible relay node locations as well. Meanwhile, for D-TxMRC and D-STBC scheme, the difficulty lies in characterising the pattern of relay nodes in the vicinity of the source node. Moreover, the bounded nature of the network complicates the analysis, as edge effect would change the shape and pattern of these relay nodes. A detailed analysis of the above problems and the proposed workarounds are the topic of discussion in Chapter 6.

2.4 Summary

In this chapter, a literature review on cooperative communication is presented. Starting with the cooperative broadcast communication, some special cases together with their respective capacity regions are discussed. The achievable rate region for a general cooperative broadcast channel is then given. An overview of multiple antenna systems and the inherent gain available are presented. This provides a motivation to the study on multi antenna cooperative broadcast communication. Several techniques and practical limitations of multiple antenna systems are then discussed, and overview on antenna selection techniques for point to point MIMO systems are presented. The system model of multi antenna cooperative broadcast communication and the respective achievable rate region, which provides a foundation for the subsequent analysis, is then given.

A scenario where each node is only equipped with single antenna is also considered. In this case, VAA concept is considered as a distributed way to exploit the gains available in MIMO systems through cooperation. An overview on cooperative relay communication is then given, and several schemes available for both single relay and multiple relay configurations are discussed. Some practical implementation challenges as well as their existing solutions are explained, and generalisation into cooperative ad-hoc network is presented. Several open problems associated with cooperative relay communication in generic ad-hoc network, which serves as the motivation to the subsequent development of this thesis, are explained.

Chapter 3

Antenna Selection for Cooperative Broadcast Communication

3.1 Introduction

This chapter focuses on cooperative broadcast communication scenario, where one multi-antenna BS communicates with several user terminals (UTs), each having multiple antennas. As single user MIMO systems are able to achieve higher bandwidth efficiency in point to point systems, the capacity of MIMO-BC is also larger than its single antenna counterpart, both in capacity region as well as in sum rate point of view. Together with the advantages, however, all the drawbacks associated with MIMO systems such as hardware cost, space limitation, and receiver complexity also persist in MIMO-BC. All these problems need to be addressed before any implementation of MIMO-BC can be practically justified.

The antenna selection algorithm for multiuser MIMO-BC is discussed in Section 3.2 of this chapter. It provides an extension of antenna selection concept, which has been recognised as a simple but effective strategy to overcome the inherent problems in MIMO systems mentioned above, into broadcast scenario. Its application to the case where MIMO-BC is used in broadband frequency selective channel is then considered in Section 3.3. Practical exam-

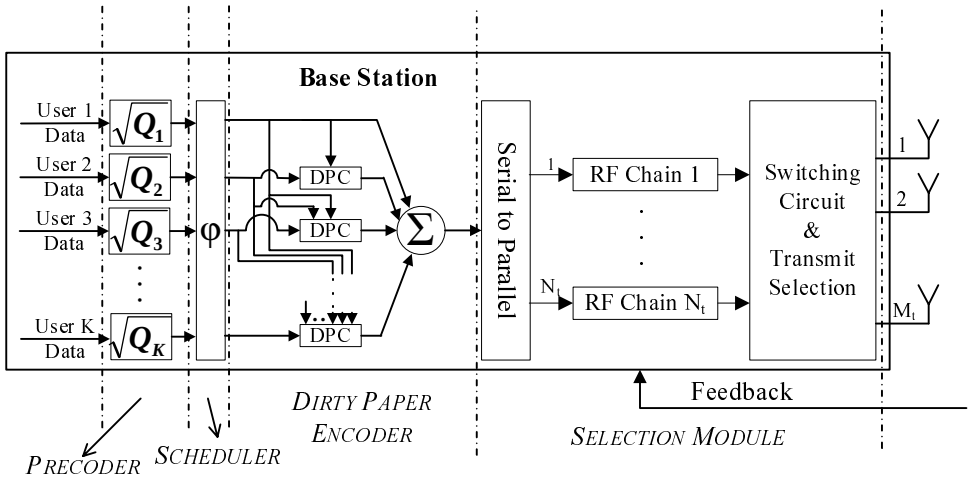

Figure 3.1: Transmitter Structure of MIMO-BC with Antenna Selection

ple of antenna selection in IEEE broadband wireless access 802.16 d/e standard for wireless metropolitan area network is also analysed as the case study of antenna selection in MIMO OFDM with STBC. Finally, Section 3.4 ends this chapter with a summary on the results and conclusions obtained throughout the exercise for MIMO-BC antenna selection.

3.2 Antenna Selection Scheme for Multiuser MIMO-BC

As explained earlier in Section 2.2.3 of Chapter 2, the sum rate capacity of MIMO-BC is achieved by dirty paper coding. The encoding process is as follows. First, a codeword for user 1 is selected. Then, the transmitter selects a codeword for user 2 with non-causal knowledge of user 1's codeword, such that user 2 will not get any interference from user 1. This can be done without increasing user 2's transmit power requirement [2]. This process continues for all users, therefore user k is interference free with respect to any preceding users $(1..k-1)$. Once the encoding for all K users are done, their codewords are added together, serial-to-parallel converted, and transmitted through multiple antennas.

Transmitter structure of MIMO-BC that achieves sum rate capacity is depicted in Figure 3.1. It can be seen that there are three main portions constructing the transmitter, namely

precoder, scheduler, and dirty paper encoder; whereas the last portion (selection module) is optional. When the total number of RF chains is equal to the number of available antennas, there is no antenna selection capability, and the selection module simply connects the output of each RF chain to its corresponding antenna. Meanwhile, the role of the three main portions of the transmitter can be described as follows. First, data streams intended for different users are processed in the precoder block. By multiplying each stream with its corresponding precoder $\sqrt{\boldsymbol{Q}_k}$ (where $\boldsymbol{Q}_k$ is the desired transmit covariance matrix of user k), the transmit covariance of each user's data can be steered to achieve the best performance. The output of precoder module is then passed to the scheduler, which selects the best encoding order φ for dirty paper coding. Once the encoding order is determined, the dirty paper encoder block performs the actual encoding, and the resulting codewords are added together; to be then serial to parallel converted and passed to the RF chains.

3.2.1 System Model

Let us consider a broadcast system where BS with M_t antennas communicates with K user terminals (UTs) each having M_r antennas. Although uniform setting where all users have the same number of antennas is assumed in this analysis, generalisation into cases where different UTs has different number of antennas is straightforward. Let N_t and N_r be the number of available RF-chains in BS and each UT respectively. Assuming that BS has the full knowledge of the channel (which can be obtained by permuting training symbols over all transmit/receive antennas using the available RF-chains and appropriate feedback), a selection algorithm determines which antenna subset is used in order to maximise certain objective function. When brute force method is used, BS needs to check all possible selections of N_t out of M_t antennas. Meanwhile, each of the UT needs to check all possible selections of N_r out of M_r antennas. The complexity of such approach is then in the order of $C_{N_t}^{M_t}\left(C_{N_r}^{M_r}\right)^K$, which very quickly becomes impractical as M_t, M_r, or K grows. The term C_n^m here is used to represent the com-

bination operation of choosing n out of m. Denoting the effective channel gain between BS and i^{th} UT after antenna selection as $\hat{\boldsymbol{H}}_i$, the received symbol vector at i^{th} user can be expressed as follows:

$$\boldsymbol{y}_i = \hat{\boldsymbol{H}}_i \, \boldsymbol{x} + \boldsymbol{n}_i \tag{3.1}$$

where $\boldsymbol{n}_i$ is the $N_r \times 1$ unit variance additive white Gaussian noise (AWGN) vector, $\hat{\boldsymbol{H}}_i \in \mathcal{C}^{N_r \times N_t}$ with its $[\hat{\boldsymbol{H}}_i]_{j,k}$ element represents channel gain between k^{th} selected transmit antenna to j^{th} selected receive antenna of i^{th} UT which is modeled as i.i.d. Rayleigh fading, and the transmit vector $\boldsymbol{x} \in \mathcal{C}^{N_t \times 1}$ satisfies total power constraint $Tr\left[E\left[\boldsymbol{x}\boldsymbol{x}^H\right]\right] \leq P_{tot}$ (with $Tr\left[.\right]$ as the trace operation, which is the sum of diagonal elements of its argument).

Here, instead of using capacity region which has not been fully characterised, sum rate capacity is considered as the performance criterion. The optimal antenna subset combination is the one that results in the largest sum rate capacity. Finding the optimal antenna subset in MIMO-BC configuration is difficult due to the broadcast nature of the transmission. From the sum-rate equation (2.19) shown in the previous chapter, it is apparent that the search for optimal transmit and receive antenna combination has to be done jointly considering all UTs. Meanwhile, in designing the selection algorithm for MIMO-BC, practical implementation is an important aspect to consider, and selection complexity must be kept as low as possible.

Expanding the sum-rate capacity in equation (2.19), the maximisation term can be expressed as:

$$C_{sum}^{BC} = \frac{1}{2}\log\frac{\left|\boldsymbol{I} + \boldsymbol{H}_{\varphi(1)} \sum_{i=1}^{K} \boldsymbol{Q}_{\varphi(i)} \boldsymbol{H}_{\varphi(1)}^H\right|}{\left|\boldsymbol{I} + \boldsymbol{H}_{\varphi(1)} \sum_{i=2}^{K} \boldsymbol{Q}_{\varphi(i)} \boldsymbol{H}_{\varphi(1)}^H\right|} + \frac{1}{2}\log\frac{\left|\boldsymbol{I} + \boldsymbol{H}_{\varphi(2)} \sum_{i=2}^{K} \boldsymbol{Q}_{\varphi(i)} \boldsymbol{H}_{\varphi(2)}^H\right|}{\left|\boldsymbol{I} + \boldsymbol{H}_{\varphi(2)} \sum_{i=3}^{K} \boldsymbol{Q}_{\varphi(i)} \boldsymbol{H}_{\varphi(2)}^H\right|} + \\ \ldots + \frac{1}{2}\log\left|\boldsymbol{I} + \boldsymbol{H}_{\varphi(K)} \boldsymbol{Q}_{\varphi(K)} \boldsymbol{H}_{\varphi(K)}^H\right| \tag{3.2}$$

The optimal encoding order is to set the best user to be encoded last, since it is free from interference and therefore capable of achieving high throughput.

The difficulty in finding antenna subset which maximises the above sum rate capacity lies in its dependence on the transmit covariance matrices. From equation (3.2), it appears that the dominating term is the last term, which is the best user capacity $\frac{1}{2}\log\left|\boldsymbol{I}+\boldsymbol{H}_{\varphi(K)}\boldsymbol{Q}_{\varphi(K)}\boldsymbol{H}_{\varphi(K)}^{H}\right|$. Hence by maximising this term over all possible antenna subsets, the total sum-rate is expected to be maximised. Unfortunately, this is not the case, because maximising best user's capacity involves selecting the right transmit covariance matrix $\boldsymbol{Q}_{\varphi(K)}$, and choosing $\boldsymbol{Q}_{\varphi(K)}$ solely to maximise best user's capacity will bring adverse effect to total sum-rate, as the term $\boldsymbol{Q}_{\varphi(K)}$ affects the interference of all other users.

3.2.2 Proposed Antenna Selection Method

To simplify the selection process, the proposed algorithm breaks the transmit and receive selection procedure into two disjoint processes. First, assuming that all receive antennas are used, transmit selection is performed by solving:

$$\hat{\boldsymbol{H}}_{opt}^{Tx}=\arg\max_{\hat{\boldsymbol{H}}}\left[\max_{\boldsymbol{R}_{xx}\geq 0,\,Tr(\boldsymbol{R}_{xx})\leq P_{tot}}\frac{1}{2}\log\left|\boldsymbol{I}+\hat{\boldsymbol{H}}\boldsymbol{R}_{xx}\hat{\boldsymbol{H}}^{H}\right|\right] \tag{3.3}$$

where $\boldsymbol{H}=[\boldsymbol{H}_1^T\boldsymbol{H}_2^T...\boldsymbol{H}_K^T]^T$ is the compound channel of all users (with superscript $[.]^T$ denotes transposition), and $\hat{\boldsymbol{H}}$ is the subset of $\boldsymbol{H}$ after removing M_t-N_t columns (with $\hat{\boldsymbol{H}}_{opt}^{Tx}$ as the optimal subset corresponding to the selected transmit antennas), and $\boldsymbol{R}_{xx}$ is any positive semidefinite transmit covariance matrix satisfying total power constraint. The above maximisation problem is equivalent to selecting a transmit antenna subset which maximises the capacity upper bound of the MIMO-BC [78]. This involves a search over $C_{N_t}^{M_t}$ combinations. In each combination, the complexity required involves finding the optimal transmit covariance matrix $\boldsymbol{R}_{xx}$. In general, $\boldsymbol{R}_{xx}$ is expressed as the multiplication of the right singular matrix of the compound channel and the power allocation obtained via water-filling strategy according to equation (2.14). Therefore, the complexity is equivalent to that of performing singular

value decomposition to the compound channel matrix $\hat{\boldsymbol{H}}$, followed by water filling operation across the available substreams. Noting that the dimension of the compound channel matrix is $KMr \times Nt$, the complexity of finding $\boldsymbol{R}_{xx}$ is in the order of min $(K^2M_r^2N_t, KM_rN_t^2)$.

For receive antenna selection, following BC-MAC duality principle, the receive antenna combination which maximises MIMO-MAC and MIMO-BC sum-rate capacity are identical. From equation (2.18), it is observed that given the transmit antenna combination obtained from the previous step, optimum receive antenna combination of user k can be found by solving:

$$\hat{\boldsymbol{H}}_{k,opt}^{Rx} = \arg\max_{\hat{\boldsymbol{H}}_k} \left[\max_{\hat{\boldsymbol{S}}_i \geq 0, \sum_i Tr(\hat{\boldsymbol{S}}_i) \leq P_{tot}} \frac{1}{2}\log\left| \boldsymbol{I} + \sum_{i=1}^{K} \hat{\boldsymbol{H}}_i{}^H \hat{\boldsymbol{S}}_i \hat{\boldsymbol{H}}_i \right| \right] \tag{3.4}$$

Similarly, $\hat{\boldsymbol{H}}_{k,opt}^{Rx}$ is the optimal channel sub matrix corresponding to selected receive antenna at user k. Expanding the summation term in the maximisation argument, equation (3.4) can be written as:

$$\hat{\boldsymbol{H}}_{k,opt}^{Rx} = \arg\max_{\hat{\boldsymbol{H}}_k} \left[\max_{\hat{\boldsymbol{S}}_i \geq 0, \sum_i Tr(\hat{\boldsymbol{S}}_i) \leq P_{tot}} \frac{1}{2}\log\left| \boldsymbol{I} + \hat{\boldsymbol{H}}_k{}^H \hat{\boldsymbol{S}}_k \hat{\boldsymbol{H}}_k + \sum_{i=1, i\neq k}^{K} \hat{\boldsymbol{H}}_i{}^H \hat{\boldsymbol{S}}_i \hat{\boldsymbol{H}}_i \right| \right] \tag{3.5}$$

where $\hat{\boldsymbol{H}}_k{}^H \hat{\boldsymbol{S}}_k \hat{\boldsymbol{H}}_k$ represents user k signal component, and $\sum_{i=1, i\neq k}^{K} \hat{\boldsymbol{H}}_i{}^H \hat{\boldsymbol{S}}_i \hat{\boldsymbol{H}}_i$ represents the interference from all other users with respect to k. Note that the interference component is constant from the point of view of user k, and it does not affect user k's receive selection. However, the functional constraint $\sum_i Tr(\hat{\boldsymbol{S}}_i) \leq P_{tot}$ of the inner maximisation prevents us from using $\arg\max_{\hat{\boldsymbol{H}}_k} \left[\max_{\hat{\boldsymbol{S}}_k \geq 0} \frac{1}{2}\log\left| \boldsymbol{I} + \hat{\boldsymbol{H}}_k{}^H \hat{\boldsymbol{S}}_k \hat{\boldsymbol{H}}_k \right| \right]$ to solve for optimal receive antenna subset.

To overcome this, two-step maximisation is proposed. First, using the obtained transmit antenna subset, optimal covariance matrices for all i are found using method in [152] by assuming no receive selection. Denote these matrices as $\boldsymbol{T}_i$ for $i \in \{1..K\}$. Substituting $\boldsymbol{S}_i$ with $\boldsymbol{T}_i$ for all i in equation (3.5), it is clear that the inner maximisation is satisfied, since $\boldsymbol{T}_i$ is the solution of MIMO-MAC sum-rate capacity with power constraint P_{tot}. Furthermore, since

$\sum_{i=1,i\neq k}^{K} \hat{\boldsymbol{H}}_i{}^H \hat{\boldsymbol{S}}_i \hat{\boldsymbol{H}}_i$ does not affect user k's receive selection, optimal receive antenna subset can be obtained by searching over $C_{N_r}^{M_r}$ possible combinations to solve:

$$\hat{\boldsymbol{H}}_{k,opt}^{Rx} = \arg\max_{\hat{\boldsymbol{H}}_k} \left[\frac{1}{2} \log \left| \boldsymbol{I} + \hat{\boldsymbol{H}}_k{}^H \hat{\boldsymbol{T}}_k \hat{\boldsymbol{H}}_k \right| \right] \tag{3.6}$$

Once optimal transmit and receive antenna subsets for all k are found, optimal covariance matrices $\hat{\boldsymbol{S}}_k$ which satisfy total power constraint is re-calculated. Transformation into optimal transmit covariance matrices $\hat{\boldsymbol{Q}}_k$ for MIMO-BC is then performed following the steps in [5, Sec. IV.B]. In summary, the proposed antenna selection algorithm can be described as follows:

1. Transmit antenna subset is obtained by solving equation (3.3).
2. With the obtained transmit antenna subset, calculate optimal covariance matrices of dual MIMO-MAC assuming no receive selection by following method in [152].
3. For each k, search for the best receive antenna subset using the obtained covariance matrices according to equation (3.6).
4. Recalculate transmit covariance matrices using the resulting transmit and receive antenna subset (which maximises the dual MIMO-MAC sum-capacity), followed by MAC to BC transformation according to [5].

The complexity of the above algorithm is in the order of $C_{N_t}^{M_t} + KC_{N_r}^{M_r}$, which is significantly smaller than the brute force complexity $C_{N_t}^{M_t} \left(C_{N_r}^{M_r}\right)^K$.

3.2.3 Sum Rate Capacity Upper Bound

It is not difficult to see that the cooperative upper bound of the system considered is equal to the capacity of point-to-point MIMO system with M_t transmit and $K\,M_r$ receive antennas, out of which only N_t and KN_r subset are used for transmission and reception respectively (a well established body of work can be found in this field [56], [67]).

Let $\boldsymbol{H}_o$ be the overall $KM_r \times M_t$ matrix, and $\hat{\boldsymbol{H}}_o$ be the submatrix of $\boldsymbol{H}_o$ obtained by removing $M_t - N_t$ columns and $K\,(M_r - N_r)$ rows corresponding to the unselected antennas. The capacity of this system can be calculated as:

$$C_{sum}^{UB} = \min_{\hat{\boldsymbol{R}}_{zz}} \max_{\hat{\boldsymbol{H}}_o \in \boldsymbol{\mathcal{H}}_o, \hat{\boldsymbol{R}}_{xx} \geq 0, Tr(\hat{\boldsymbol{R}}_{xx}) \leq P_{tot}} \frac{1}{2}\log \frac{\left|\hat{\boldsymbol{R}}_{zz} + \hat{\boldsymbol{H}}_o \hat{\boldsymbol{R}}_{xx} \hat{\boldsymbol{H}}_o{}^H\right|}{\left|\hat{\boldsymbol{R}}_{zz}\right|} \tag{3.7}$$

where $\boldsymbol{\mathcal{H}}_o$ is the set containing all possible $KN_r \times N_t$ submatrices of $\boldsymbol{H}_o$, and $\hat{\boldsymbol{R}}_{zz}$ is the noise covariance matrix having sub-unit diagonal value. Using minimax duality, it has been proven in [153, Sec. III.B] that the above calculation can be translated into a single maximisation problem as follows:

$$C_{sum}^{UB} = \max_{\hat{\boldsymbol{H}}_o \in \boldsymbol{\mathcal{H}}_o, \hat{\boldsymbol{\Sigma}} \in \boldsymbol{\mathcal{B}}_d, \hat{\boldsymbol{\Sigma}} \geq 0, Tr(\hat{\boldsymbol{\Sigma}}) \leq P_{tot}} \frac{1}{2}\log \left|\boldsymbol{I} + \hat{\boldsymbol{H}}_o{}^H \hat{\boldsymbol{\Sigma}} \hat{\boldsymbol{H}}_o\right| \tag{3.8}$$

where $\boldsymbol{\mathcal{B}}_d$ is a family of block diagonal matrices, and $\hat{\boldsymbol{\Sigma}}$ is the transmit covariance matrix of the flipped channel $\hat{\boldsymbol{H}}_o{}^H$. Denoting the sum capacity upper bound as C_{sum}^{UB}, the following series of inequality are obtained:

$$\begin{aligned}
C_{sum}^{UB} &\leq \max_{\hat{\boldsymbol{H}}_o \in \boldsymbol{\mathcal{H}}_o, \hat{\boldsymbol{\Sigma}} \geq 0, Tr(\hat{\boldsymbol{\Sigma}}) \leq P_{tot}} \frac{1}{2}\log \left|\boldsymbol{I} + \hat{\boldsymbol{H}}_o{}^H \hat{\boldsymbol{\Sigma}} \hat{\boldsymbol{H}}_o\right| && (3.9)\\
&\leq \max_{\hat{\boldsymbol{H}}_o \in \boldsymbol{\mathcal{H}}_o} \frac{1}{2}\log \left(\prod_{i=1}^{N_t} (1 + P_i\, \lambda_i^2)\right) && (3.10)\\
&\leq \max_{\hat{\boldsymbol{H}}_o \in \boldsymbol{\mathcal{H}}_o} \frac{1}{2}\log \left(\left(\frac{\sum_{i=1}^{N_t} (1 + P_i\, \lambda_i^2)}{N_t}\right)^{N_t}\right) && (3.11)\\
&\leq \max_{\hat{\boldsymbol{H}}_o \in \boldsymbol{\mathcal{H}}_o} \frac{N_t}{2}\log \left(1 + \frac{\sum_{i=1}^{N_t} P_i}{N_t} \lambda_{max}^2\right) && (3.12)\\
&\leq \frac{N_t}{2}\log \left(1 + \frac{P_t}{N_t} \max_{j, \hat{\boldsymbol{H}}_o \in \boldsymbol{\mathcal{H}}_o} \left[\hat{\boldsymbol{H}}_o \hat{\boldsymbol{H}}_o{}^H\right]_{jj}\right) && (3.13)
\end{aligned}$$

where inequality in equation (3.9) is due to the optimisation domain expansion, equation (3.10) follows from traditional MIMO waterfilling technique and full rank $\hat{\boldsymbol{H}}_o$ assumption (P_i and λ_i denotes the i^{th} substream power allocation and the i^{th} singular value of $\hat{\boldsymbol{H}}_o$ respectively), equation (3.11) is because the product of a sequence is always less than the product of their average, equation (3.12) is due to replacing λ_i with its maximum value, and finally equation (3.13) is because the highest eigenvalue of $\hat{\boldsymbol{H}}_o\hat{\boldsymbol{H}}_o^{\ H}$ majorises its highest diagonal term, which holds for any square hermitian matrix [154].

Given the selected submatrix $\hat{\boldsymbol{H}}_o$, each diagonal elements of $\left[\hat{\boldsymbol{H}}_o\hat{\boldsymbol{H}}_o^{\ H}\right]$ is random and distributed according to chi-squared distribution with $2N_t$ degree of freedom. The capacity upper bound can then be written as:

$$C_{sum}^{UB} \leq \frac{N_t}{2}\log\left(1+\frac{P_t}{N_t}\chi\right) \tag{3.14}$$

where χ is the maximum element of a set of $KM_rC_{N_t}^{M_t}$ independent and identically distributed random variables following chi-squared distribution with $2N_t$ degree of freedom. The probability density function $f_\chi(\chi)$ can be expressed as [155]:

$$f_\chi(\chi) = KM_rC_{N_t}^{M_t} \times \left(\frac{\int_0^\chi t^{N_t-1}e^{-t}dt}{(N_t-1)!}\right)^{KM_rC_{N_t}^{M_t}-1} \times \frac{\chi^{(N_t-1)}e^{-\chi}}{(N_t-1)!} \tag{3.15}$$

Finally, the ergodic capacity upper bound can be calculated by integrating equation (3.14) with respect to equation (3.15) as follows:

$$E\left[C_{sum}^{UB}\right] = \int_0^\infty C_{sum}^{UB} f_\chi(\chi)d\chi \tag{3.16}$$

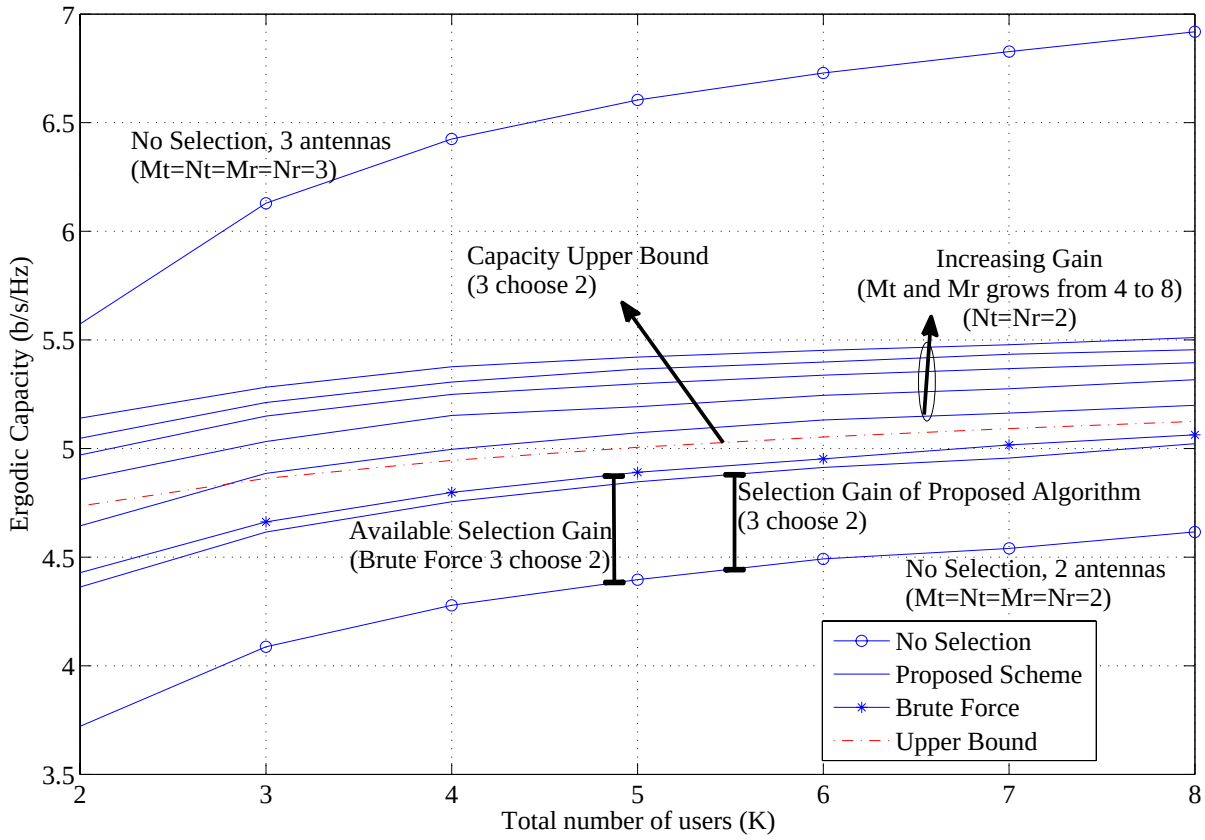

Figure 3.2: Antenna Selection Performance in MIMO-BC Systems with Different Number of Users

3.2.4 Numerical Results

The selection performance is analysed for $N_t = N_r = 2$. The channel from BS to UTs are modelled as Rayleigh i.i.d. flat fading which remains constant for one block, and changes to an independent realisation on the following block. The block duration is assumed to be sufficiently long that the notion of Shannon's definition of reliable communication over large block code can be used, and the number of blocks is sufficiently large such that the use of ergodic capacity as performance metric can be justified. In this work, the simulation is performed over 1000 Monte Carlo realisations at 10 dB operating SNR, and the sum rate capacity is calculated and averaged over all realisations to obtain the ergodic capacity.

Figure 3.2 shows the ergodic sum-rate capacity of the system under different configurations, which is calculated using equation (3.2) (with transmit and receive antenna subset found

according to (3.3) and (3.6) respectively). As a baseline comparison, the performance of the system without antenna selection (whereby the number of RF-chains is the same as the number of available antennas) is shown for 2 antennas and 3 antennas cases, and their performance curves are labeled as "No Selection, 2 antennas" and "No Selection, 3 antennas" in Figure 3.2 respectively.

From the figure, it is observed that there is a large gap of approximately 2 b/s/Hz between the capacity of "No Selection" with three available antennas and that of using antenna selection (three antennas and two RF chains). The main reason of this gap is due to the difference in the number of spatial data streams available. In 'No Selection' with three antennas, the number of available data streams is equal to three, as all of the antennas are always active. Meanwhile, in the system using antenna selection (three antennas and two RF chains), although the number of antennas is the same, the number of spatial data streams available is two; as only two of the antennas are active at any one time.

Figure 3.2 also shows that as the number of user K increases, the sum-rate capacity increases. This is due to the inherent multiuser diversity gain in MIMO-BC. It is also observed that the gain diminishes as K becomes too large, since the growth rate of the capacity (as shown in Figure 3.2) follows a $log\ log\ K$ scaling behaviour. Similar observation has also been reported in [156], whereby the capacity gain of transmit antenna selection is studied on the limit of large number of antennas. When there are 3 available antennas, selection gain up to 0.75 b/s/Hz in the sum rate capacity is achievable, and the proposed selection algorithm is able to attain $85-90\%$ of the gain. This is achieved at a complexity that is much lower than full-complexity scheme. Figure 3.2 also shows the increase in selection gain as the number of available antennas is increased from 4 to 8. This demonstrates the extra selection diversity of the system, which also has diminishing return as total number of antennas is too large. Finally, the capacity upper bound calculated using equation (3.16) via numerical integration is depicted for 3 available antennas case. It can be seen from the figure that the upper bound is

tight, especially when the number of users is large.

3.3 Extension to Multiple Carriers Case

As the data rate increases, the amount of bandwidth occupied by the signal will also be larger, and the channel behaves as a frequency selective channel, in which different frequency bands experience different amount of fading. In such channel, one transmitted symbol will arrive at the destination several times, each with different delay and attenuation depending on the multipath propagation profile. As such, the ISI issue will complicate the receiver equalisation process and degrade the decoding performance. OFDM has been recognised as an effective solution to overcome this problem. By using IFFT (Inverse Fast Fourier Transform) and FFT (Fast Fourier Transform) block at the transmitter and receiver respectively, the frequency selective channel can be converted into a series of frequency flat channels (called subcarriers), after which a single tap equalisation can be used.

In high rate MIMO-BC systems, the channel between different transmit-receive antenna pairs from different users exhibit frequency selective fading with different delay profiles. Although OFDM can be applied in this scenario, the fact that different subcarriers experience different fading complicates the antenna selection process. In this section, an antenna selection scheme for multicarrier MIMO-BC systems is developed. Starting with the single user case, the following subsection proposed a low complexity sub-optimal antenna selection scheme for MIMO-OFDM systems under frequency selective fading channel. The multiple user MIMO-BC scenario is then addressed by combining the MIMO-BC selection technique developed earlier with the antenna selection scheme for MIMO-OFDM. The selection performance and its complexity analysis for both single user and multi-user settings are also given to demonstrate the amount of gain achievable.

3.3.1 Antenna Selection for Single User MIMO-OFDM Systems

Using earlier convention, denote M_t and M_r the number of available antennas at the transmitter and receiver respectively. Due to the limitation on the available RF-chain, only N_t and N_r of those antennas are active at any one time. In frequency selective fading, the propagation channel between any transmit-receive antenna link is represented by l-ray model with impulse response:

$$h_{n,m}(t,\tau) = \sum_{l=0}^{L-1} \gamma_{n,m}^{l}(t)\ \delta(\tau - \tau_l) \tag{3.17}$$

where $\gamma_{n,m}^{l}(t)$ is the time varying complex path gain coefficient of the l^{th} path between n^{th} receive and m^{th} transmit antenna, and τ_l is the corresponding path delay. $\gamma_{n,m}^{l}(t)$ is modelled as random process whose sample is i.i.d. zero mean circularly symmetric complex Gaussian (ZMCSCG) random variable with no correlation between different paths and spaces. The frequency response of the channel is given by:

$$H_{n,m}(t,f) = \int_{-\infty}^{+\infty} h_{n,m}(t,\tau)\ e^{-j2\pi f\tau}\ d\tau \tag{3.18}$$

Assuming that the cyclic prefix is longer than the maximum path delay of the channel response in any transmit-receive pair, the channel frequency response can be written as [157]:

$$H_{n,m}[p,q] \ = \ H_{n,m}(pT_f, q\Delta f) = \sum_{l=0}^{L-1} h_{n,m}[p,l]\ F_N^{ql} \tag{3.19}$$

where N is the total number of FFT points, $F_N = e^{-j2\pi/N}$, $h_{n,m}[p,l] = h_{n,m}(pT_f, lT_s/N)$, T_f is the block length, Δf is the subcarrier spacing, and T_s is the symbol duration.

At the receiver side, signal observed at n^{th} antenna after cyclic prefix removal, serial to parallel conversion, and FFT operation, can be expressed as:

$$Y_n[p,q] = \sum_{m=1}^{N_t} H_{n,m}[p,q]X_m[p,q] \ + \ \eta_n[p,q] \tag{3.20}$$

where $X_m[p,q]$ is the modulated transmit signal at m^{th} antenna, over p^{th} OFDM symbol and q^{th} subcarrier. η is the additive white Gaussian noise (AWGN).

Analysing the system using frequency domain model in equation (3.20), MIMO-OFDM system can be interpreted as a parallel group of N frequency flat MIMO system [158]. It is necessary to note that although there are $(N \times M_t) \times (N \times M_r)$ frequency flat channels, the switching circuit is only able to perform selection for a group of N antennas in bulk. Therefore, effectively, there are only a total of $C_{N_t}^{M_t} C_{N_r}^{M_r}$ possible transmit receive antenna combinations. This is due to the fact that all data from N subcarriers in one RF chain have to be transmitted through their corresponding antenna once it is selected. Now let:

$$\boldsymbol{x}_m[p] = (X_m[p,1] \,..\, X_m[p,N])^T \quad , m = 1, \ldots, N_t \tag{3.21}$$

$$\boldsymbol{y}_n[p] = (Y_n[p,1] \,..\, Y_n[p,N])^T \quad , n = 1, \ldots, N_r \tag{3.22}$$

$$\boldsymbol{\eta}_n[p] = (\eta_n[p,1] \,..\, \eta_n[p,N])^T \quad , n = 1, \ldots, N_r \tag{3.23}$$

be $N \times 1$ vectors representing the transmitted symbols, received symbols, and additive noise on N subcarriers during p^{th} OFDM symbol at m^{th} transmit antenna and n^{th} receive antenna respectively. Stacking N_t transmit symbols and N_r receive symbols and noise arrays for different transmit and receive antennas, the following tall column matrices are defined:

$$\mathbf{x}[p] = (\boldsymbol{x}_1[p]^T \,..\, \boldsymbol{x}_{N_t}[p]^T)^T \tag{3.24}$$

$$\mathbf{y}[p] = (\boldsymbol{y}_1[p]^T \,..\, \boldsymbol{y}_{N_r}[p]^T)^T \tag{3.25}$$

$$\mathbf{n}[p] = (\boldsymbol{\eta}_1[p]^T \,..\, \boldsymbol{\eta}_{N_r}[p]^T)^T \tag{3.26}$$

Assuming that the channel is quasi-static over P OFDM symbol periods, an $(N \times N_t) \times P$ matrix $\mathbf{X} = (\mathbf{x}[1] \,..\, \mathbf{x}[P])$ is defined. Similarly for the receive symbols and noise vector, $\mathbf{Y} = (\mathbf{y}[1] \,..\, \mathbf{y}[P])$ and $\mathbf{N} = (\mathbf{n}[1] \,..\, \mathbf{n}[P])$. Now, channel matrix is rearranged accordingly by

defining a diagonal matrix:

$$\mathbf{H}_{n,m} = diag(H_{n,m}[1,1], H_{n,m}[1,2], \ .. \ , H_{n,m}[1,N]) \tag{3.27}$$

The overall full system response can then be represented as:

$$\mathbf{H} = \begin{bmatrix} \mathbf{H}_{1,1} & \mathbf{H}_{1,2} & \cdots & \mathbf{H}_{1,M_t} \\ \mathbf{H}_{2,1} & \mathbf{H}_{2,2} & \cdots & \vdots \\ \vdots & \vdots & \ddots & \vdots \\ \mathbf{H}_{M_r,1} & \cdots & \cdots & \mathbf{H}_{M_r,M_t} \end{bmatrix} \tag{3.28}$$

Effective channel response after antenna selection will be the sub-matrix of $\mathbf{H}$ having $(N \times N_t)$ columns and $(N \times N_r)$ rows corresponding to the selected transmit and receive antennas. Denoting the selected sub matrix channel response as $\widehat{\mathbf{H}}$, frequency domain system response can be simplified into the following expression:

$$\mathbf{Y} = \widehat{\mathbf{H}}\,\mathbf{X} \ + \ \mathbf{N} \tag{3.29}$$

The central problem of antenna selection is to choose the best sub-matrix $\widehat{\mathbf{H}}$ such that transmitted message $\mathbf{X}$ can be recovered from $\mathbf{Y}$ with minimum probability of error (or such that the rate is maximised from the capacity point of view).

Before discussing the proposed algorithm, let's first consider a brute force approach of antenna selection. This method basically checks every possible transmit-receive antenna combination, and selects the best out of them. Although optimality is guaranteed to be achieved using this method, computational load that it requires render it unsuitable for real system implementation. A detailed complexity analysis of brute force scheme and the proposed sub optimal algorithm will be discussed in Section 3.3.2.

Brute Force Selection Method

As opposed to single carrier case, the selection process needs to be conducted on each and every subcarrier separately. The best combination is the one that *collectively* optimise system performance, for this reason, the overall full system response in equation (3.28) needs to be broken down into individual subcarrier. Let:

$$\mathbf{H}[q] = \begin{bmatrix} \mathbf{H}_{1,1}[q] & \mathbf{H}_{1,2}[q] & \cdots & \mathbf{H}_{1,M_t}[q] \\ \mathbf{H}_{2,1}[q] & \mathbf{H}_{2,2}[q] & \cdots & \vdots \\ \vdots & \vdots & \ddots & \vdots \\ \mathbf{H}_{M_r,1}[q] & \cdots & \cdots & \mathbf{H}_{M_r,M_t}[q] \end{bmatrix} \tag{3.30}$$

be the channel response for subcarrier q. Here, block index p has been removed for ease of representation. Defining three column matrices:

$$\boldsymbol{x}[q] = (X_1[q] \,..\, X_{N_t}[q])^T \tag{3.31}$$

$$\boldsymbol{y}[q] = (Y_1[q] \,..\, Y_{N_r}[q])^T \tag{3.32}$$

$$\boldsymbol{\eta}[q] = (\eta_1[q] \,..\, \eta_{N_r}[q])^T \tag{3.33}$$

to be the transmitted symbol, received symbol, and AWGN at subcarrier q respectively, and $\widehat{\mathbf{H}}[q]$ to be the effective channel matrix for q^{th} subcarrier after antenna selection, the received signal at subcarrier q can then be expressed as:

$$\boldsymbol{y}[q] = \widehat{\mathbf{H}}[q]\, \boldsymbol{x}[q] \; + \; \boldsymbol{\eta}[q] \tag{3.34}$$

When MMSE linear receiver is used, the received symbol is multiplied by an equaliser matrix as follows:

$$\mathbf{G}[q] = \left[\widehat{\mathbf{H}}[q]^H \, \widehat{\mathbf{H}}[q] \; + \; N_0/\mathcal{E}_s \; \boldsymbol{I}_{N_t}\right]^{-1} \widehat{\mathbf{H}}[q]^H \tag{3.35}$$

where $\widehat{\overline{\mathbf{H}}}[q]$ is defined as the estimated channel response at the receiver. The equaliser output $\overline{\boldsymbol{x}}$[q] is expressed as:

$$\overline{\boldsymbol{x}}[q] \;=\; \mathbf{G}[q]\,\boldsymbol{y}[q] \;=\; \mathbf{G}[q]\widehat{\mathbf{H}}[q]\boldsymbol{x}[q] \;+\; \mathbf{G}[q]\boldsymbol{\eta}[q] \tag{3.36}$$

It has been shown in [62] and [69] that the best antenna subset is the one resulting in maximum of minimum sub-stream SNR. Denoting the s^{th} row of $\mathbf{G}[q]$ as $\boldsymbol{g_s}[q]$, and the s^{th} column of $\widehat{\mathbf{H}}[q]$ as $\hat{\boldsymbol{h}}_{\boldsymbol{s}}[q]$, the SNR at stream s of subcarrier q can be calculated as follows:

$$SNR_s[q] = \frac{\mathcal{E}_s \left|\boldsymbol{g_s}[q]\,\hat{\boldsymbol{h}}_{\boldsymbol{s}}[q]\right|^2}{N_t\,N_0\,\left\|\boldsymbol{g_s}[q]\right\|^2 \;+\; \mathcal{E}_s\,\sum_{j\neq s}\left|\boldsymbol{g_s}[q]\hat{\boldsymbol{h}}_{\boldsymbol{j}}[q]\right|^2} \tag{3.37}$$

where $\mathcal{E}_s$ and N_0 are as defined earlier which represent the average input signal energy and noise spectral density respectively.

Brute force algorithm will need to compute

$$\max \min_{s} SNR_s[q], \;\; \forall q \tag{3.38}$$

and the maximisation has to be performed over all possible transmit receive antenna combination, whose cardinality is $C_{N_t}^{M_t} C_{N_r}^{M_r}$.

In single carrier case, once the maximum of minimum sub-stream SNR is found, the optimal transmit receive antennas is obtained. However, this is not the case for multicarrier case, since each subcarrier has their own optimal transmit receive combination which might be different from the other subcarriers. In order to allow reduction in the number of transmit and receive antennas, additional step needs to be performed as explained in the following.

To make the concept clearer, a table with N columns and the number of rows equaling to the total cardinality of $C_{N_t}^{M_t} C_{N_r}^{M_r}$ is defined. This table is to store the minimum sub-stream SNR value found in equation (3.38). The problem is now translated into finding the row with the

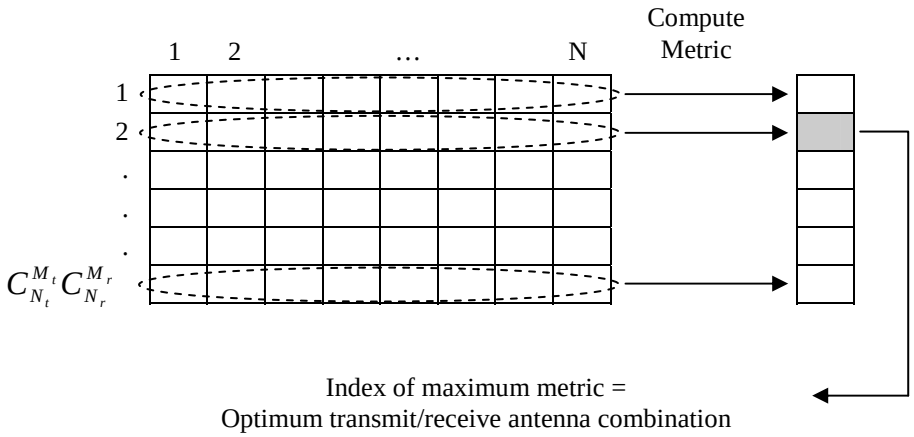

Figure 3.3: Flow Diagram of Brute Force Selection Approach

best metric. Two different metrics are evaluated, namely:

- Global minimum sub-stream SNR

  For each row, find the minimum entry and assign it as the score of that particular row. Optimum antenna combination is the one corresponding to the row with the largest score.

- Average minimum sub-stream SNR

  For each row, calculate the average value and use it as the score of that particular row. Optimum antenna combination is the one corresponding to the row with the largest score.

Once all the scores have been computed, the row with the largest score is selected, and it corresponds to the optimum transmit receive antenna configuration. The flow diagram of this selection process is depicted in Figure 3.3. The proposed selection algorithm is mainly to reduce the computational load of brute force approach, as described in the following.

Method I: By separating transmit and receive selection

Here, the basic idea to reduce complexity is to decouple selection process into transmit and receive selection. It serves as an extension to the method proposed in [159] into multicarrier case. In this method, table construction is broken into two steps. On the first step, only transmit selection is considered; therefore the table will have N columns and only $C_{N_t}^{M_t}$ rows. Then, the

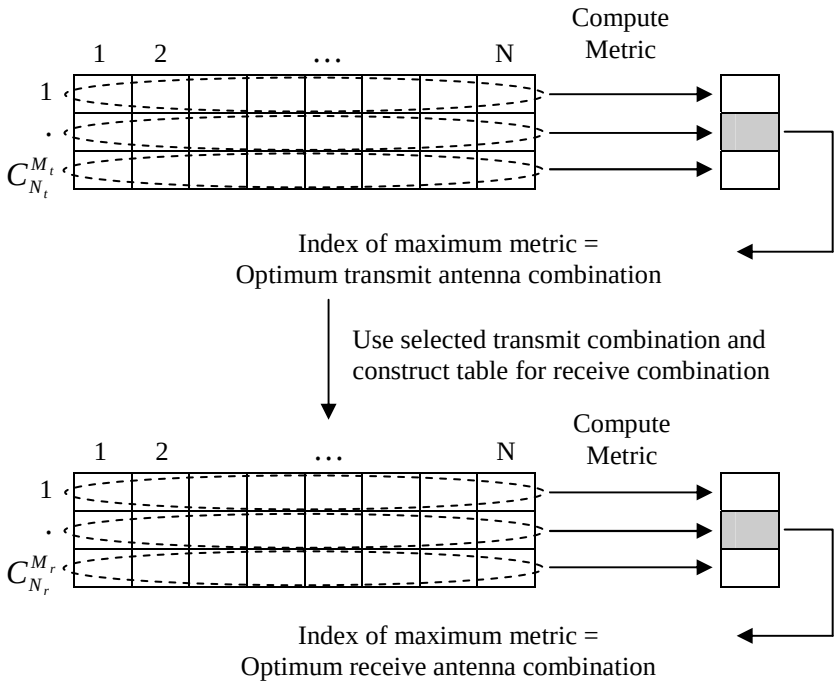

Figure 3.4: Flow Diagram of Selection Method I

metric calculation is performed as per normal, and a row with the best metric is selected. This selected row corresponds to transmit antenna combination. On the second step, the table will have N columns and only $C_{N_r}^{M_r}$ rows, each representing different receive antenna combination (with the selected transmit antenna combination obtained from the first step). Again, the metric calculation is then performed to obtain the final transmit/receive antennas combination. The flow diagram of this selection process is depicted in Figure 3.4.

Method II: By exploiting frequency correlation

The second method exploits frequency correlation to reduce the overall complexity. By considering those subcarriers that are sufficiently far apart, less computation is required to find the optimum transmit/receive antenna combination. One way to do this is to consider only subcarriers that are multiple of $N_s > 1$, such that the total number of columns in the constructed table is reduced to N/N_s. The flow diagram of this selection process is depicted in Figure 3.5.

Although this method is very effective in reducing the computational complexity, choice

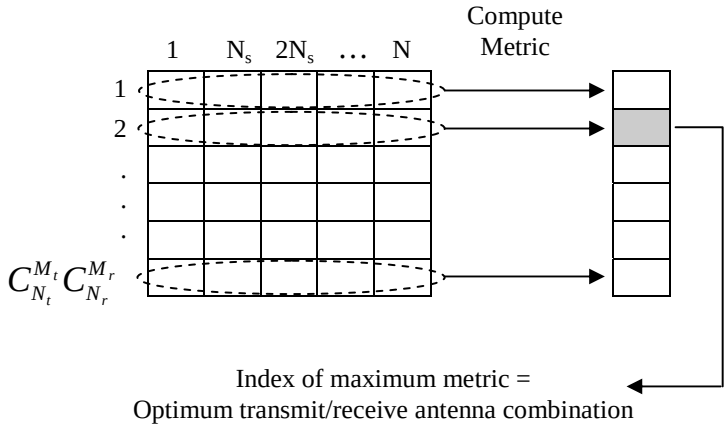

Figure 3.5: Flow Diagram of Selection Method II

of N_s has to be carefully performed. Ideal value of N_s would be proportional to the coherent bandwidth of the channel. If it is too large, the receiver performance will degrade. On the other hand, if it is too small, the complexity reduction it contributes will be compromised.

3.3.2 Complexity and Selection Performance Analysis

The complexity of the proposed algorithms are evaluated in terms of number of additions, multiplications, and comparisons. First, let's begin with SNR calculation expressed in equation (3.37). It can be shown that computing SNR requires $(N_t \times N_r)$ complex multiplications, $(N_t \times (N_r - 1))$ complex additions, $(2N_t + 2N_r + 5)$ real multiplications, and $(2N_t + 2N_r - 2)$ real additions. Using the fact that one complex multiplication is equal to four real multiplications and two real additions, and that one complex addition is equal to two real additions, the SNR calculation requires $(4N_tN_r + 2N_t + 2N_r + 5)$ real multiplications, and $(2N_tN_r + 2N_r - 2)$ real additions.

The minimum sub-stream SNR is found by calculating the SNR for N_t different streams, and find their minimum. Therefore, to find one minimum sub-stream SNR, the complexity is:

$$\begin{aligned} C_{minSNR} &= [N_t \times (4N_tN_r + 2N_t + 2N_r + 5) \text{ real multiplications}] \\ &\quad + [N_t \times (2N_tN_r + 2N_r - 2) \text{ real additions}] + [(N_t - 1) \text{ comparisons}] \end{aligned} \quad (3.39)$$

Now, let's consider the brute force approach. The decision table constructed in this approach has a total of $NC_{N_t}^{M_t}C_{N_r}^{M_r}$ elements, hence the complexity required is $NC_{N_t}^{M_t}C_{N_r}^{M_r}\ C_{minSNR}$ operations, where the complexity of C_{minSNR} is as expressed in equation (3.39). Then, on each one of $C_{N_t}^{M_t}C_{N_r}^{M_r}$ rows, metric computation is performed. Assuming that "Global minimum sub-stream SNR" criterion is used, one metric computation requires $N-1$ comparisons. Once all the metrics are found, the search for the maximum metric requires another $[C_{N_t}^{M_t}C_{N_r}^{M_r}]-1$ comparisons. Therefore, the overall complexity for brute force approach is:

$$\begin{aligned} C_{BF} &= NC_{N_t}^{M_t}C_{N_r}^{M_r}C_{minSNR} \text{ operations} \\ &\quad + C_{N_t}^{M_t}C_{N_r}^{M_r}(N-1) \text{ comparisons} \\ &\quad + [C_{N_t}^{M_t}C_{N_r}^{M_r}]-1 \text{ comparisons} \\ &\approx NC_{N_t}^{M_t}C_{N_r}^{M_r}(C_{minSNR} \text{ operations} + 1 \text{ comparison}) \end{aligned} \tag{3.40}$$

where C_{minSNR} is as expressed in equation (3.39). Using the selection method I, the first table constructed will have $NC_{N_t}^{M_t}$ elements. Therefore complexity for constructing the first table is $NC_{N_t}^{M_t}C_{minSNR}$ operations. Then, assuming that "Global minimum sub-stream SNR" criterion is used, $C_{N_t}^{M_t}(N-1)$ comparisons is required to compute the metrics. Finally, search for the first maximum metric requires another $C_{N_t}^{M_t}-1$ comparisons. Similarly, complexity for constructing the second table is $NC_{N_r}^{M_r}C_{minSNR}$ operations. Metric calculation will require $C_{N_r}^{M_r}(N-1)$ comparisons. And finally the search for second maximum metric requires another $C_{N_r}^{M_r}-1$ comparisons. In total, the complexity for the selection method I is:

$$\begin{aligned} C_{M1} &= N[C_{N_t}^{M_t}+C_{N_r}^{M_r}]C_{minSNR} \text{ operations} \\ &\quad + [C_{N_t}^{M_t}+C_{N_r}^{M_r}](N-1) \text{ comparisons} \\ &\quad + [C_{N_t}^{M_t}+C_{N_r}^{M_r}]-2 \text{ comparisons} \\ &\approx N[C_{N_t}^{M_t}+C_{N_r}^{M_r}](C_{minSNR} \text{ operations} + 1 \text{ comparison}) \end{aligned} \tag{3.41}$$

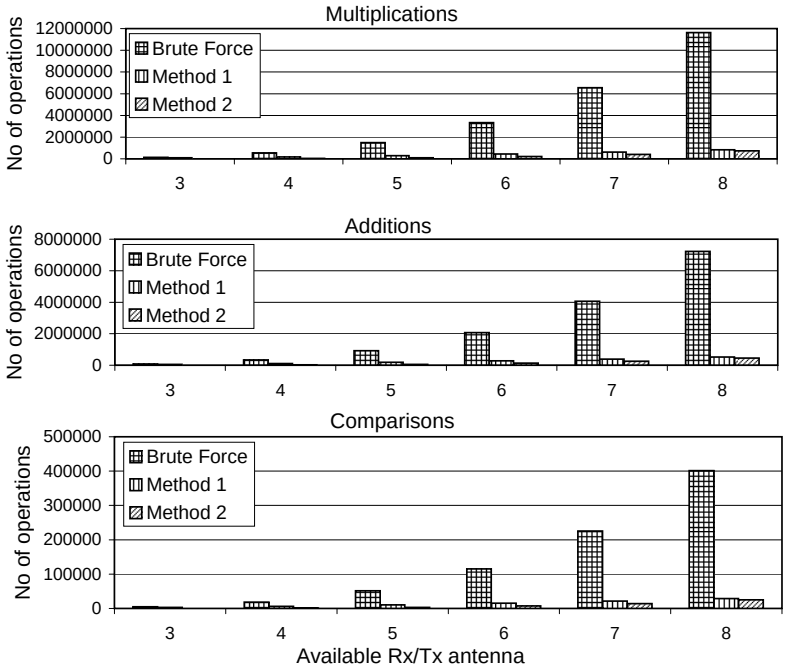

Figure 3.6: Complexity comparisson

For the second selection method, the table only contains $\left(\frac{N}{N_s}\right) C_{N_t}^{M_t} C_{N_r}^{M_r}$ elements. Therefore complexity for constructing the table is $\left(\frac{N}{N_s}\right) C_{N_t}^{M_t} C_{N_r}^{M_r} C_{minSNR}$ operations. Then, assuming that "Global minimum sub-stream SNR" criterion is used, $C_{N_t}^{M_t} C_{N_r}^{M_r} \left(\left(\frac{N}{N_s}\right) - 1\right)$ comparisons are required to compute the metrics. Finally, the search for maximum metric require $C_{N_t}^{M_t} C_{N_r}^{M_r} - 1$ comparisons. In total, the complexity for the selection method II is:

$$\begin{aligned} C_{M2} &= \left(\frac{N}{N_s}\right) C_{N_t}^{M_t} C_{N_r}^{M_r} C_{minSNR} \text{ operations} \\ &\quad + C_{N_t}^{M_t} C_{N_r}^{M_r} \left(\left(\frac{N}{N_s}\right) - 1\right) \text{ comparisons} \\ &\quad + C_{N_t}^{M_t} C_{N_r}^{M_r} - 1 \text{ comparisons} \\ &\approx \left(\frac{N}{N_s}\right) C_{N_t}^{M_t} C_{N_r}^{M_r} (C_{minSNR} \text{ operations} + 1 \text{ comparison}) \end{aligned} \tag{3.42}$$

Comparing equation (3.40), (3.41), and (3.42), it can be seen that selection method I cuts down computational complexity by transforming $C_{N_t}^{M_t} C_{N_r}^{M_r}$ into $C_{N_t}^{M_t} + C_{N_r}^{M_r}$; while selection method II cuts down computational complexity by a factor of N_s. Figure 3.6 shows the differences in the

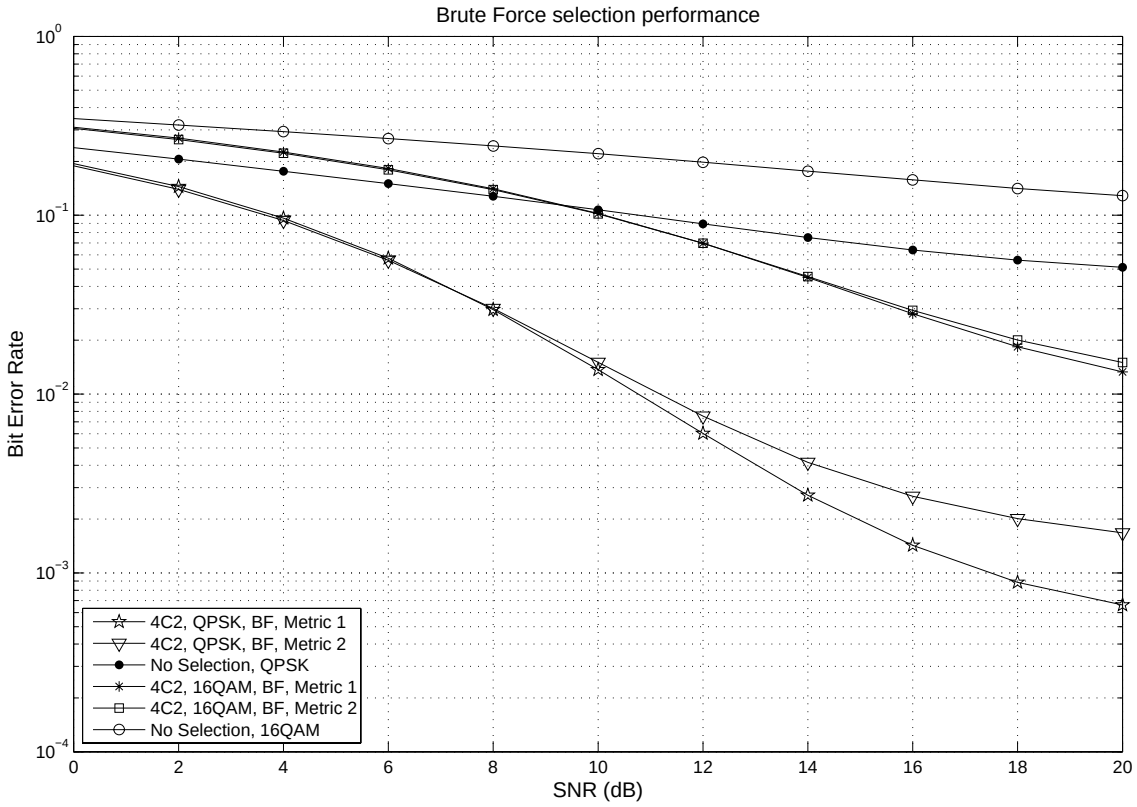

Figure 3.7: Brute Force selection performance

number of operations required under brute force method and the two sub optimal algorithms. Here, FFT points used is 256 and the number of RF chains available in both transmitter and receiver end is fixed to 2. Different settings of total available antenna ranging from 3 to 8 are evaluated.

As for the performance, the simulation system used in this study employs 256 points OFDM with $20\ MHz$ signal bandwidth operating at $2.6\ GHz$ carrier frequency, resulting in $78.125KHz$ subcarrier spacing and $12.8\mu sec$ OFDM symbol duration. Cyclic prefix used is $1/16^{th}$ of total FFT points, which is equal to 16 samples. The propagation channel in every transmit/receive pair is modeled using exponential power delay profile with $L = 5$ taps. These taps are generated as i.i.d. correlated in time with a correlation function according to Jakes' fading model [160]. Mobile speed assumed in this model is $125Km/hr$, which translate into maximum Doppler frequency of $300Hz$.

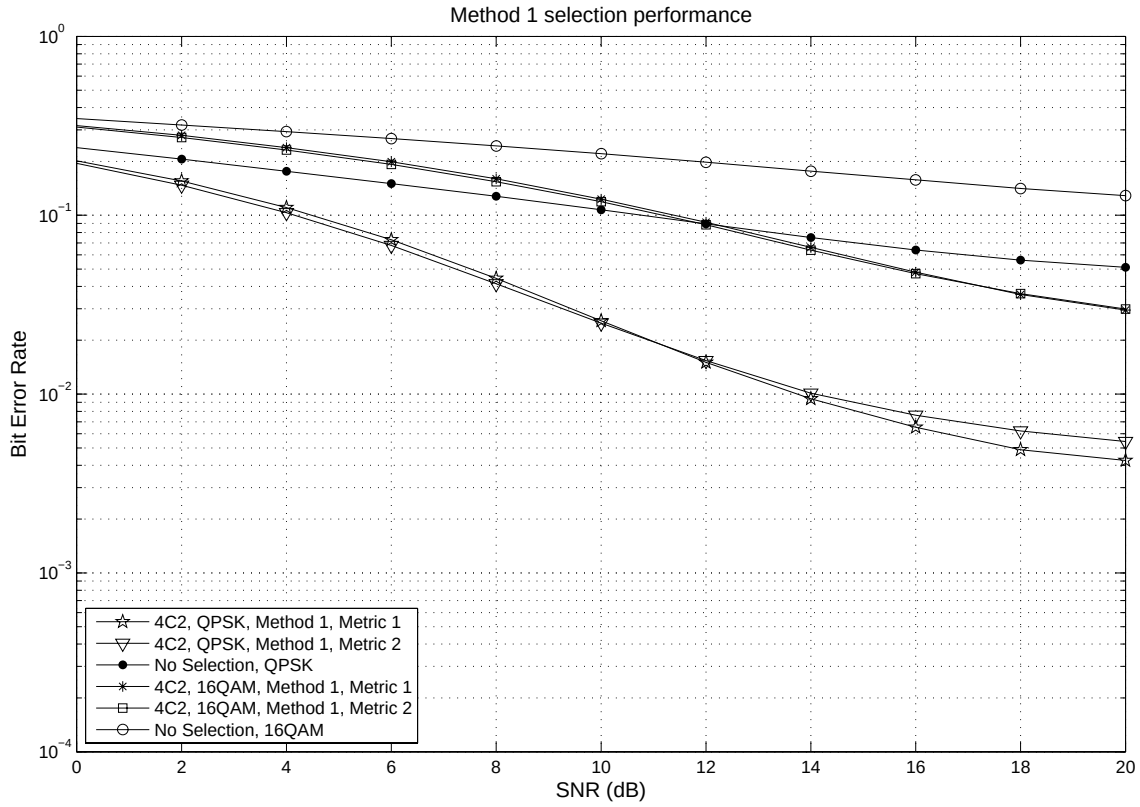

Figure 3.8: Method 1 selection performance

6.25% of subcarriers (16 uniformly spaced subcarriers) are dedicated for pilot symbols. These pilots are used during training period for channel estimation purpose. The receiver employs comb-type least square channel estimation with second order interpolation as described in [161]. This estimated channel is used as the base for antenna selection as well as equalisation purpose. 4 antennas and 2 RF chains are assumed available on both transmitter and receiver. The system is simulated under QPSK and 16QAM signaling, and the performance is measured in terms of BER.

Figure 3.7 shows the brute force selection performance which uses (3.38) to search for optimal antenna combination. It can be seen that the scheme can significantly improve system performance, and it is superior to the reduced complexity algorithm (both method 1 and 2 as depicted in Figure 3.8 and 3.9 respectively). It is also observed that the use of "Global minimum sub-stream SNR" (metric 1) as the selection metric delivers better performance compared to

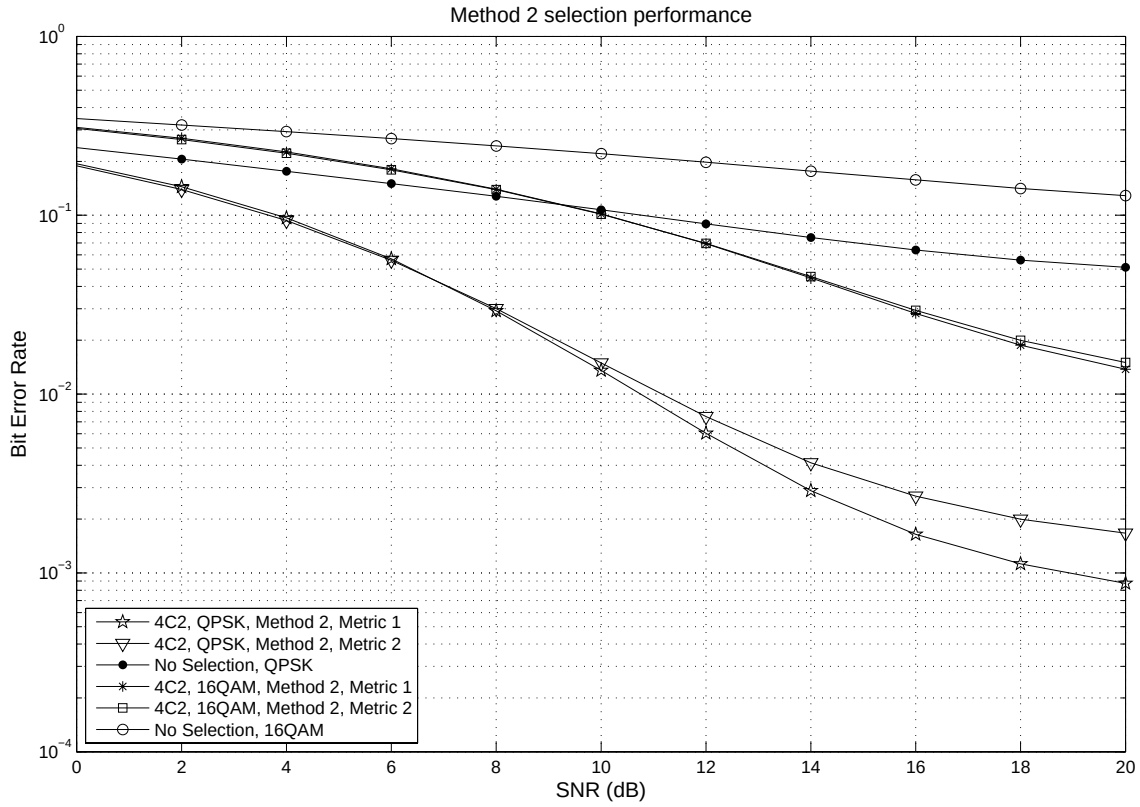

Figure 3.9: Method 2 selection performance

"Average minimum sub-stream SNR" (metric 2), especially in high SNR regime. However, the difference between the two becomes negligible when 16QAM modulation is used (as compared to the QPSK case). This signifies the role of minimum sub-stream SNR to system performance as highlighted in [62]. Under 16QAM modulation, receiver becomes more susceptible to noise as the distances between signal constellations are closer than that in QPSK modulation. This effect lowers the influence of antenna selection to system performance, hence decrease in the performance difference between metric 1 and metric 2 is evident.

Comparing method 1 and method 2 with respect to the brute force selection scheme using both QPSK and 16QAM modulation (as depicted in Figure 3.10), it is observed that selection method 1 suffers more penalty in the performance due to complexity reduction. It is worth noting that in this simulated environment, method 2 delivers more complexity reduction as compared to method 1, which does not agree with the intuition that larger complexity reduction

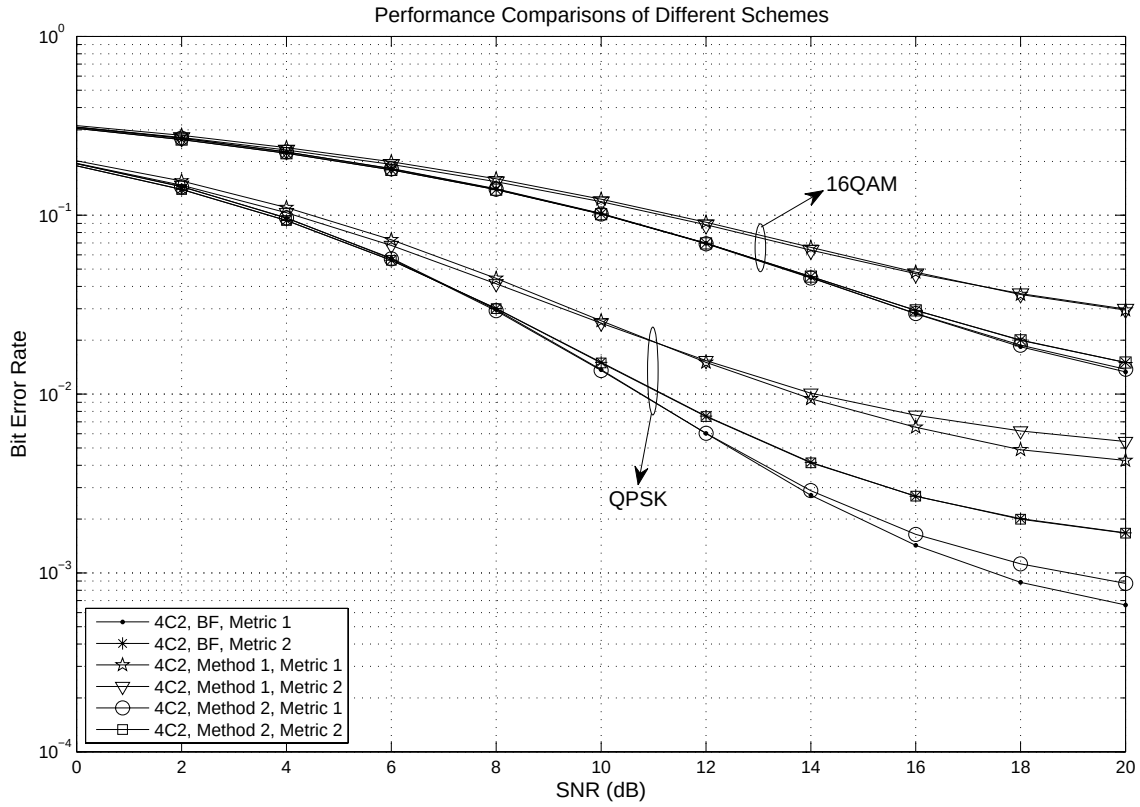

Figure 3.10: Performance comparisons between Method 1, Method 2, and Brute Force selection

will cause more severe performance penalty. This can be explained using the fact that method 2 exploit coherence frequency property of the channel, and in this simulation, it is designed that the reduction factor is equal to channel coherence bandwidth. Therefore, the information lost in method 2 is less significant than those in method 1. In real environment, it is not necessarily the case, because there is likely to be a mismatch between the reduction factor employed and channel coherence bandwidth.

Another interesting observation is that in all the performance curves presented, as the SNR increases, the BER does not continuously decrease; but instead, there are changes toward positive direction on the BER curve gradient in high SNR regime, creating an irreducible error floor. This is the effect caused by channel estimation error, which put a limit on the equaliser performance, regardless on how good the SNR is.

3.3.3 Antenna Selection for Multi-User MIMO-OFDM Systems

Comparing the selection Method I developed for single user MIMO-OFDM systems with the MIMO-BC antenna selection scheme developed earlier in Section 3.2, it is observed that they both adopt similar technique. First, transmit antenna combination is searched assuming no receive selection. Then, receive antenna selection is performed using the obtained transmit antenna combination. This suggests that it is possible to combine both schemes to arrive at the antenna selection strategy for multi-user MIMO-OFDMA systems. However, some modifications are required as more than one receiver is involved, and the selection algorithm needs to find the antenna combination that is jointly optimal for all users.

In multi-user MIMO-OFDM systems, the channel from one transmit antenna to one receive antenna at any one user is modelled as multipath l-ray frequency selective channel. Given one particular user, the derivation of channel model after appropriate IFFT and FFT operation is identical to that in single user MIMO-OFDM system presented in Section 3.3. Denoting the $M_r \times M_t$ channel matrix from the transmitter to user k at subcarrier q as $\mathbf{H}^{(k)}[q]$, the following relation is obtained:

$$\mathbf{H}^{(k)}[q] = \begin{bmatrix} \mathbf{H}^{(k)}_{1,1}[q] & \mathbf{H}^{(k)}_{1,2}[q] & \cdots & \mathbf{H}^{(k)}_{1,M_t}[q] \\ \mathbf{H}^{(k)}_{2,1}[q] & \mathbf{H}^{(k)}_{2,2}[q] & \cdots & \vdots \\ \vdots & \vdots & \ddots & \vdots \\ \mathbf{H}^{(k)}_{M_r,1}[q] & \cdots & \cdots & \mathbf{H}^{(k)}_{M_r,M_t}[q] \end{bmatrix} \tag{3.43}$$

where $\mathbf{H}^{(k)}_{i,j}[q]$ denotes the frequency domain channel from j^{th} transmit antenna to i^{th} receive antenna of user k at subcarrier q. Here, since one transmitter communicates with several receivers simultaneously, it is inherently a broadcast system, hence sum-rate capacity is used as the selection criteria. The central problem of antenna selection in this kind of system is to select the transmit antenna combination which is jointly optimal for all users in most or all subcarriers, as well as to select the receive antenna combination at each receiver such that the sum rate

capacity across all subcarriers are maximised. Using brute force method, this search involves checking all possible $C_{N_t}^{M_t}(C_{N_r}^{M_r})^K$ antenna combinations, each of which would require a calculation of N sum rate capacities at different subcarriers. In order to reduce the computational complexity, a sub optimal selection method is proposed, which combines the selection method in single carrier MIMO-BC systems and the selection method in single user MIMO-OFDM systems. Detailed discussion on the selection process is given in the next paragraph.

First, the selection process is broken into two parts, one for transmit antenna selection and another for receive antenna selection. For transmit antenna selection, the same strategy as in the single user MIMO-OFDM antenna selection can be used, whereby a table having $C_{N_t}^{M_t}$ rows and number of columns equals to the total number of subcarriers N is constructed. However, since sum rate capacity maximasation is used as the criteria, the values stored in the table have to be modified. Here, similar technique as in the single carrier MIMO-BC antenna selection is used. First, denote the $(KM_r) \times M_t$ compound frequency domain channel of all users at subcarrier q as $\mathbf{H_c}[q] = [\mathbf{H^{(1)}}[q]^T\ \mathbf{H^{(2)}}[q]^T\ ...\ \mathbf{H^{(K)}}[q]^T]^T$. Depending on the transmit antenna combination used (which is denoted by the row index of the decision table), the following value is computed:

$$\max_{\boldsymbol{R}_{xx}[q] \geq 0, \sum_q Tr(\boldsymbol{R}_{xx}[q]) \leq P_{tot}} \frac{1}{2}\log\left|\boldsymbol{I} + \widehat{\mathbf{H}}_c[q]\boldsymbol{R}_{xx}[q]\widehat{\mathbf{H}}_c[q]^H\right| \tag{3.44}$$

where $\widehat{\mathbf{H}}_c[q]$ is the subset of $\mathbf{H_c}[q]$ after removing $M_t - N_t$ columns corresponding to the unselected transmit antennas. Note that the above value corresponds to the capacity upper bound of the broadcast communication at subcarrier q, and it is used to populate the q^{th} column of the decision table. The next step is a metric computation to decide which row (transmit antenna combination) to be used. Since the selection objective is to maximise sum rate capacity, it is natural to use the sum of capacity upper bound across all subcarriers as the selection metric. In other words, for each row of the decision table, calculate the sum across all columns, and

use it as the score of that particular row. Optimum transmit antenna combination is the one corresponding to the row with the largest score.

Using the selected transmit antenna combination, the optimal transmit covariance matrices which achieves sum rate capacity at each subcarrier is calculated. The same technique proposed for single carrier system in [152] can be used on individual subcarrier. Denote the optimal transmit covariance matrix for user k at q^{th} subcarrier as $\boldsymbol{T}_k[q]$. The next step is to determine the optimal receive antenna combination for each receiver. In single carrier MIMO-BC antenna selection, it has been shown that using BC-MAC duality, the sum rate maximising receive antenna selection process can be performed independently at different receiver. This property also holds for multi user MIMO-OFDM systems, as the channel can be viewed as a series of single carrier MIMO-BC systems. In the following, receive antenna selection for user k is described. Note that the same technique is to be applied to all receivers.

First, as in the MIMO-OFDM antenna selection technique, another decision table is constructed having $C_{N_r}^{M_r}$ rows and N columns. Given the receive antenna combination corresponding to a particular row of the table, its q^{th} column is populated with the following value:

$$\frac{1}{2}\log\left|\boldsymbol{I} + \widehat{\mathbf{H}}^{(k)}[q]^H \widehat{\boldsymbol{T}}_k[q] \widehat{\mathbf{H}}^{(k)}[q]\right| \tag{3.45}$$

where $\widehat{\mathbf{H}}^{(k)}[q]$ is the frequency domain channel response of user k at subcarrier q after selection, and $\widehat{\boldsymbol{T}}_k[q]$ is the subset of transmit covariance matrix of user k at subcarrier q after removing $M_r - N_r$ columns and rows corresponding to the the unselected antennas. Once the decision table has been fully populated, the final step is to decide which row (receive antenna combination) is to be used. Similarly, since the objective is to maximise the sum rate capacity, the same metric is used as in the transmit antenna selection. Hence, for each row of the decision table, calculate the sum across all columns, and assign it as a score of that particular row. Optimum receive antenna combination for user k is the one corresponding to the row with the largest score.

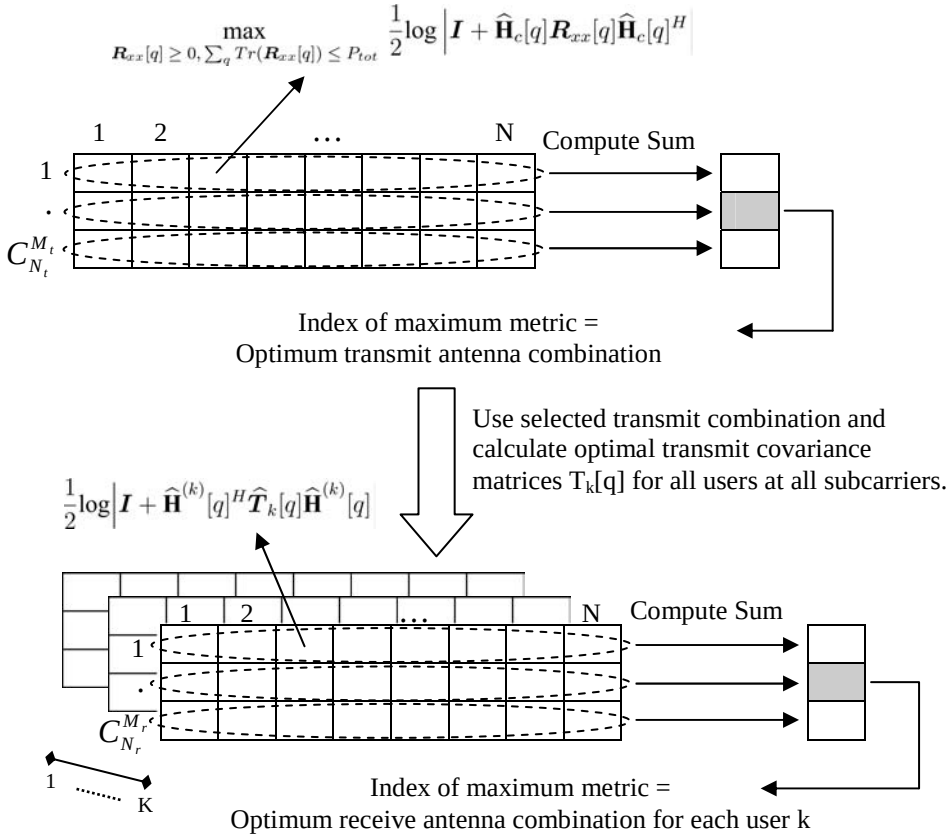

Figure 3.11: Flow Diagram of Multi User MIMO-OFDM Selection

The flow diagram of the selection process is depicted in Figure 3.11. To summarise, the selection algorithm can be described as follows:

1. Construct the first decision table having $C_{N_t}^{M_t}$ rows and N columns, and populate them with the capacity upper bound calculated according to equation (3.44).

2. Compute the metric for the first decision table and select the row with the best metric. The selected row corresponds to the selected transmit antenna combination.

3. With the obtained transmit antenna subset, calculate optimal covariance matrices of dual MIMO-MAC for each subcarrier assuming no receive selection using the method proposed in [152].

4. For each user k, construct the second decision table having $C_{N_r}^{M_r}$ rows and N columns,

and populate them with the single user capacity calculated using equation (3.45).

5. Compute the metric for the second decision table and select the row with the best metric. The selected row corresponds to the selected receive antenna combination for that particular user k.

6. Finally, the optimal sum rate maximising antenna subset is obtained by combining the transmit combination and the receive combination for all user $k \in \{1..K\}$.

3.3.4 Complexity and Selection Performance Analysis

In this subsection, the algorithm complexity and selection performance are analysed. As a baseline of comparison, the complexity of brute force approach is first studied. Then, the complexity of the proposed algorithm are analysed and compared to the brute force approach in order to signify the complexity reduction. Due to the non static behaviour of some of the functions involved (such as threshold based waterfilling process), the study on algorithm complexity is given in terms of its limiting behaviour using big-oh $\mathcal{O}(.)$ notation.

In brute force approach, the selection algorithm simply iterates through all possible antenna subset combinations in transmitter as well as all receivers. This involves $C_{N_t}^{M_t}(C_{N_r}^{M_r})^K$ number of possibilities. For each possibility, the algorithm needs to compute the sum rate capacity for each of N subcarriers. Calculating sum rate capacity involves a search for optimal covariance matrix. Using the algorithm proposed in [152], this process requires $(K^2 - K)$ matrix multiplication of size $N_t \times N_r$ and $N_r \times N_r$, $(K^2 - K)$ matrix multiplication of size $N_t \times N_r$ and $N_r \times N_t$, and a single Singular Value Decomposition (SVD) on a matrix of size $KN_r \times N_t$. To simplify the notations, define the following two functions:

$$K_{mult}(A, B, C) = \mathcal{O}\left(A\,C\,[B \text{ multiplications} + (B-1) \text{ additions}]\right) \quad (3.46)$$

$$K_{SVD}(A, B) = \mathcal{O}\left(\min(A^2\,B, A\,B^2)\,[\text{multiplications} + \text{additions}]\right) \quad (3.47)$$

where $K_{mult}(A, B, C)$ represents the complexity required to perform multiplication of a matrix of size $A \times B$ with another matrix of size $B \times C$, while $K_{SVD}(A, B)$ represents the complexity required to perform SVD operation on a $A \times B$ matrix. Using these notations, the complexity of finding the optimal covariance matrix according to [152] can be expressed as:

$$K_{cov} = (K^2-K)K_{mult}(N_t, N_r, N_r) + (K^2-K)K_{mult}(N_t, N_r, N_t) + K_{SVD}(KN_r, N_t) \quad (3.48)$$

Once the optimal covariance is obtained, sum rate capacity for a particular subcarrier can be calculated accordingly. This computation involves K matrix multiplication of size $N_t \times N_r$ and $N_r \times N_r$, K matrix multiplication of size $N_t \times N_r$ and $N_r \times N_t$, and determinant computation of a matrix of size $N_t \times N_t$. Note that the complexity of computing a determinant of an $A \times A$ matrix is in the order of $\mathcal{O}(A^3\ [\text{multiplications}+\text{additions}])$. Using the same notation as above, the complexity of calculating the sum rate capacity given the optimal covariance matrix can be calculated as:

$$K_{sum}=K(K_{mult}(N_t, N_r, N_r)+K_{mult}(N_t, N_r, N_t))+\mathcal{O}(N_t^3[\text{multiplications}+\text{additions}]) \quad (3.49)$$

To find the best antenna combination, sum rate capacity at different subcarriers are added, and the antenna combination which results in the largest sum is selected as the solution. This process requires $C_{N_t}^{M_t}(C_{N_r}^{M_r})^K\ (N-1)$ additions and $C_{N_t}^{M_t}(C_{N_r}^{M_r})^K - 1$ comparisons. In overall, it can be shown that the total complexity of brute force method is expressed as:

$$K_{tot}^{BF} = C_{N_t}^{M_t}(C_{N_r}^{M_r})^K N\ [(K^2)(K_{mult}(N_t, N_r, N_r)+K_{mult}(N_t, N_r, N_t)) + K_{SVD}(KN_r, N_t) + \mathcal{O}(N_t^3\ [\text{multiplications} + \text{additions}])] + \ (C_{N_t}^{M_t}(C_{N_r}^{M_r})^K\ (N-1))\ \text{additions}\ + (C_{N_t}^{M_t}(C_{N_r}^{M_r})^K - 1)\ \text{comparisons} \quad (3.50)$$

Now, consider the proposed selection algorithm. The first step is to construct a decision

table with $C_{N_t}^{M_t}$ rows and N columns, and fill it with the capacity upper bound. Calculating the capacity upper bound is equivalent to calculating MIMO capacity whose channel matrix has $K\ M_r$ rows and N_t columns. This involves calculating the SVD of channel matrix (which require a complexity of $K_{SVD}(K\,M_r, N_t)$) and a determinant computation of a $N_t \times N_t$ matrix (which require a complexity of $\mathcal{O}(N_t^3\ [\text{multiplications} + \text{additions}])$). Therefore, the overall complexity of constructing the first decision table is equal to:

$$K^{(1)} = C_{N_t}^{M_t}\ N\ (K_{SVD}(K\ M_r, N_t)\ +\ \mathcal{O}(N_t^3\ [\text{multiplications} + \text{additions}])) \tag{3.51}$$

Then, the metric is computed for the first decision table, and the best metric is selected which determine the optimal transmit antenna combination. The complexity required in this computation can be shown to be:

$$K_{met}^{(1)} = (C_{N_t}^{M_t}\ (N-1))\ \text{additions}\ +\ (C_{N_t}^{M_t} - 1)\ \text{comparisons} \tag{3.52}$$

With the selected transmit antenna combination, optimal covariance matrix is calculated for each subcarrier assuming all receiver's antennas are used. This requires $(K^2 - K)\ N$ matrix multiplication of size $N_t \times M_r$ and $M_r \times M_r$, $(K^2 - K)\,N$ matrix multiplication of size $N_t \times M_r$ and $M_r \times N_t$, and N SVD computation on a matrix of size $KM_r \times N_t$; the complexity of which can be calculated as:

$$K_{cov}^{(1)} = (K^2 - K)N(K_{mult}(N_t, M_r, M_r) + K_{mult}(N_t, M_r, N_t)) + NK_{SVD}(KM_r, N_t) \tag{3.53}$$

Using the obtained covariance matrix, each user k constructs the second decision table with $C_{N_r}^{M_r}$ rows and N columns, and fill it with the theoretical single user capacity. Calculating the theoretical capacity involves a single matrix multiplication of size $N_t \times N_r$ and $N_r \times N_r$, a single matrix multiplication of size $N_t \times N_r$ and $N_r \times N_t$, and a matrix determinant calculation

of size $N_t \times N_t$. The complexity for constructing the second decision table in all users can be expressed as:

$$K^{(2)} = KC_{N_r}^{M_r} N(K_{mult}(N_t, N_r, N_r) + K_{mult}(N_t, N_r, N_t) + \mathcal{O}(N_t^3 \text{ [multiplications+additions]})) \tag{3.54}$$

Once the second decision table is constructed, each user compute the corresponding metric and select the best metric to arrive at the optimal receive antenna combination. For each user, this would require $C_{N_r}^{M_r}\ (N-1)$ additions and $(C_{N_r}^{M_r} - 1)$ comparisons. Hence, the total complexity for this process is:

$$K_{met}^{(2)} = K\ (C_{N_r}^{M_r}\ (N-1) \text{ additions} + (C_{N_r}^{M_r} - 1) \text{ comparisons}) \tag{3.55}$$

Therefore, the overall complexity of the proposed algorithm can be calculated by adding the terms in equation (3.51), (3.52), (3.53), (3.54), and (3.55), which results in the following:

$$K_{tot}^{(sub)} = (K^2 - K)N(K_{mult}(N_t, M_r, M_r) + K_{mult}(N_t, M_r, N_t)) + KC_{N_r}^{M_r} N(K_{mult}(N_t, N_r, N_r) + K_{mult}(N_t, N_r, N_t)) \ +\ (C_{N_t}^{M_t} + KC_{N_r}^{M_r})(N\,\mathcal{O}(N_t^3) + (N-1) \text{ additions} + 1 \text{ comparisons}) \ +\ (C_{N_t}^{M_t} + 1)\ N\ K_{SVD}(KM_r, N_t) \ -\ (K+1) \text{ comparisons} \tag{3.56}$$

To signify the complexity reduction of the proposed selection algorithm with respect to the brute force approach, the overall complexity of the two schemes are compared, and expressed as a parameter called complexity ratio, defined as the ratio of the overall complexity of the brute force scheme (given in equation (3.50)) to the overall complexity of the proposed selection (given in equation (3.56)). The larger the ratio, the larger the complexity reduction achieved by the proposed selection method. The complexity ratios of different types of operations (namely multiplications, additions, and comparisons) for the case when there are different number of available antennas and different total number of users, while the number of selected antennas

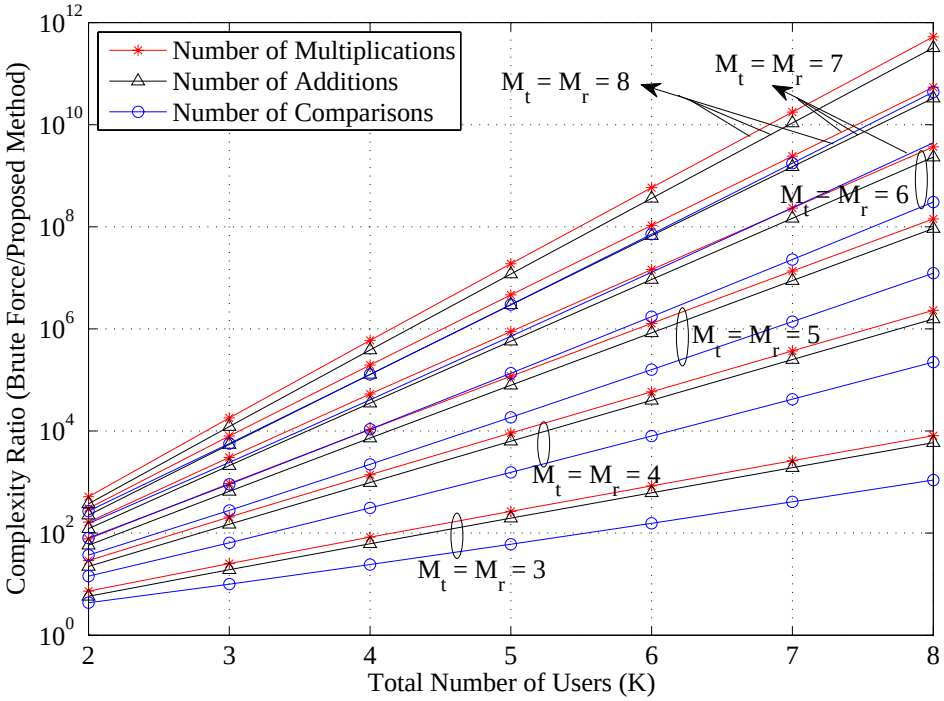

Figure 3.12: Complexity Ratio of Brute Force Scheme with respect to the Proposed Selection (Number of selected antennas or available RF chain is 2)

is fixed to 2, are depicted in Figure 3.12. The simulation system employs 256 FFT points, and each terminal is only equipped with 2 RF chains. It can be seen from the figure that the amount of complexity reduction is very significant, especially when the the number of users and/or the number of available antennas is large.

For the performance analysis, the same system parameters as in single user MIMO-OFDM are used; which is a 256 points OFDM system with 20 MHz signal bandwidth operating at 2.6 GHz carrier frequency. All users adopt the same cyclic prefix size, which is set to be $1/16^{th}$ of total FFT points (equivalent to 16 samples). As far as the channel model is concerned, multi tap power delay profile with number of taps equal to 5 is used. The profile of each individual tap varies in time according to Jake's fading model [160] with 300 Hz Doppler frequency.

Here, sum rate capacity is used as the performance metric, and error free feedback channel is assumed available for each receiver to tell transmitter the receive antenna combination used. At the receiver, the channel matrix is estimated using pilot symbols which are spread uniformly

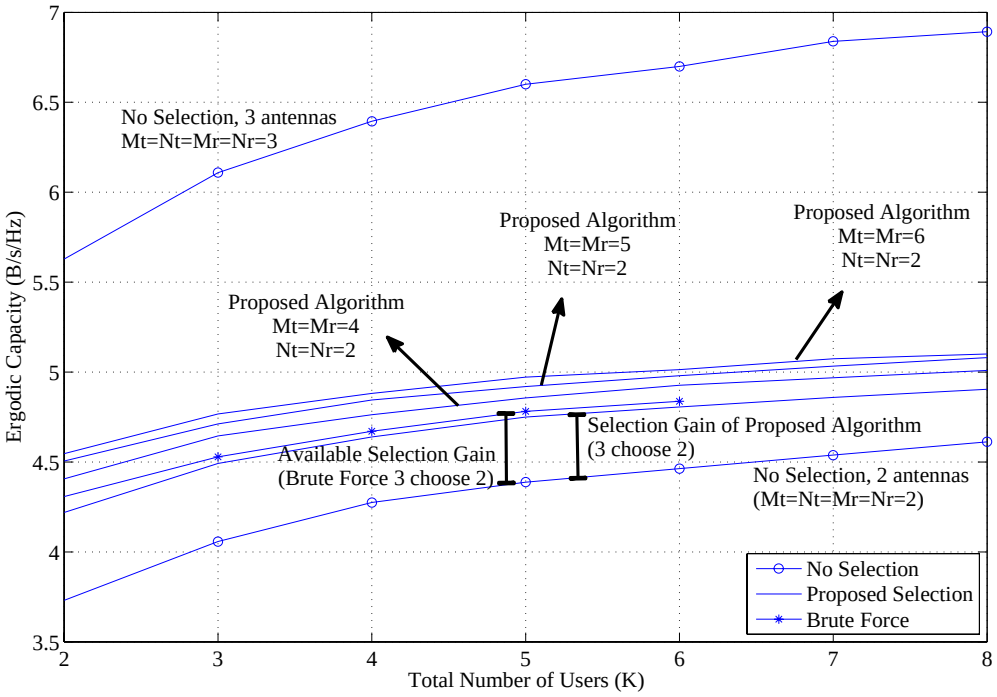

Figure 3.13: Multiuser MIMO-OFDM Selection Performance

across subcarriers. A total of 16 pilot subcarriers are used for this purpose, and comb-type least square channel estimation with second order interpolation is adopted at the receivers. Figure 3.13 shows the gain in sum rate capacity for varying number of available antennas at 10 dB operating SNR, which is calculated using equation (3.2) for all subcarriers with the selected antenna combination. As expected, the extra available antenna is able to increase the overall sum capacity even though the number of RF chains is fixed.

An approximately 0.5 b/s/Hz is attained for 3 available antennas with 2 RF chains, and the proposed selection algorithm is capable of achieving $80\% - 90\%$ of the gain. As the number of antennas increases, the gain increases. Similarly, due to multiuser diversity gain, the overall sum rate capacity increases with the number of users. Note that the same behaviour is observed in single carrier MIMO-BC systems. Therefore, it is apparent that multicarrier broadcast channel can be viewed as a series of single carrier MIMO-BC, in which the characteriscitcs of MIMO-BC is applicable on each subcarrier independently. However, the amount of gain achieved is lower than the single carrier case, due to averaging effect across subcarriers.

3.3.5 A Case Study of Antenna Selection for MIMO OFDM with STBC

Having shown the potential of antenna selection in improving system capacity, it is now time to see how antenna selection performs in a typical IEEE 802.16 based system. More details for a typical 802.16 based system parameters are given at appendix A, and the detailed specifications are given in [162]. In the standard, antenna selection is included as part of the optional feature. When base station has more than one antenna, spatial diversity can be used in conjunction with the antenna selection. Configurations for two, three, or four antennas are defined. The present work focuses on the rate-1 four antennas configuration, in which the standard defines three transmit diversity matrices for antenna selection process as shown in Figure 3.14:

$$A_1 = \begin{bmatrix} S_1 & -S^*_2 & 0 & 0 \\ S_2 & S^*_1 & 0 & 0 \\ 0 & 0 & S_3 & -S^*_4 \\ 0 & 0 & S_4 & S^*_3 \end{bmatrix} \quad A_2 = \begin{bmatrix} S_1 & -S^*_2 & 0 & 0 \\ 0 & 0 & S_3 & -S^*_4 \\ S_2 & S^*_1 & 0 & 0 \\ 0 & 0 & S_4 & S^*_3 \end{bmatrix} \quad A_3 = \begin{bmatrix} S_1 & -S^*_2 & 0 & 0 \\ 0 & 0 & S_3 & -S^*_4 \\ 0 & 0 & S_4 & S^*_3 \\ S_2 & S^*_1 & 0 & 0 \end{bmatrix}$$

Figure 3.14: Rate-1 four antenna transmit matrices

These transmit diversity matrices defines which subset of antennas to be used first at any one time. For example, when matrix A_1 is selected, four symbols are transmitted over four time slots as follows. At the first time slot, symbol S_1 and S_2 are transmitted through the first and second antenna respectively. At the second time slot, symbol $-S_2^*$ and S_1^* are transmitted through the same set of antennas. Following that, at the third time slot, symbol S_3 and S_4 are transmitted through the third and fourth antenna respectively. Finally, at the fourth time slot, symbol $-S_4^*$ and S_3^* are again transmitted through the third and fourth antenna respectively.

There are two different ways to select which transmit diversity matrix to be used. Firstly, base station can use the logical data subcarrier number of the first tone using the following formula:

$$k_m = \text{mod}(\text{subcarrier\_number\_of\_first\_tone}, 3) + 1$$

where k_m is the index of the transmit matrix to be used. Note that in this way, base station

does not take channel condition into consideration in choosing transmit matrix. This method is termed *Pure STBC*.

Secondly, base station can request the mobile station to feedback the best transmit matrix index to be used. In this case, mobile station is required to perform Carrier to Interference plus Noise Ratio (CINR) calculation using the available pilots on the received symbol. Transmit matrix index which maximise the CINR is then reported to the base station via Channel Quality Information Channel (CQICH), a data region in uplink allocated by base station. The transmit diversity matrix used is always updated every time the CQICH is received. This method is termed as *Enhanced STBC* consequently (section 8.4.8.3.5 of reference [163]).

Looking at the transmit diversity matrices in Figure 3.14, it is observed that all four transmit antennas are involved in the transmission, regardless of which matrix is used. The only difference is just the sequence of which antennas are being used. This prevents the scheme to fully capture the selection gain.

In order to illustrate this, consider a condition when the first and third antennas have very good channel gain, while the second and fourth antennas experience deep fading. In this case, regardless of transmit diversity matrix selected, some of the symbols will be allocated to second and fourth antenna, resulting in a performance degradation. Based on this observation, a modified enhanced transmit diversity scheme is proposed (termed as *Modified Enhanced STBC*).

The idea behind this scheme is to exploit selection diversity gain by assigning user symbols to only two antennas for the entire duration of the frame. The available transmit diversity matrices under this scheme is shown in Figure 3.15. Considering the same scenario as in the earlier example, when the first and third antennas have very good channel gain while the second and fourth antennas experience deep fading, this scheme will select transmit diversity matrix A_2. This will improve the performance, since only antennas with good channel gain are used, while the other two are left unused.

$$A_1 = \begin{bmatrix} S_1 & -S^*_2 & S_3 & -S^*_4 \\ S_2 & S^*_1 & S_4 & S^*_3 \\ 0 & 0 & 0 & 0 \\ 0 & 0 & 0 & 0 \end{bmatrix} \quad A_2 = \begin{bmatrix} S_1 & -S^*_2 & S_3 & -S^*_4 \\ 0 & 0 & 0 & 0 \\ S_2 & S^*_1 & S_4 & S^*_3 \\ 0 & 0 & 0 & 0 \end{bmatrix} \quad A_3 = \begin{bmatrix} S_1 & -S^*_2 & S_3 & -S^*_4 \\ 0 & 0 & 0 & 0 \\ 0 & 0 & 0 & 0 \\ S_2 & S^*_1 & S_4 & S^*_3 \end{bmatrix}$$

$$A_4 = \begin{bmatrix} 0 & 0 & 0 & 0 \\ S_1 & -S^*_2 & S_3 & -S^*_4 \\ S_2 & S^*_1 & S_4 & S^*_3 \\ 0 & 0 & 0 & 0 \end{bmatrix} \quad A_5 = \begin{bmatrix} 0 & 0 & 0 & 0 \\ S_1 & -S^*_2 & S_3 & -S^*_4 \\ 0 & 0 & 0 & 0 \\ S_2 & S^*_1 & S_4 & S^*_3 \end{bmatrix} \quad A_6 = \begin{bmatrix} 0 & 0 & 0 & 0 \\ 0 & 0 & 0 & 0 \\ S_1 & -S^*_2 & S_3 & -S^*_4 \\ S_2 & S^*_1 & S_4 & S^*_3 \end{bmatrix}$$

Figure 3.15: Rate-1 four antenna modified transmit matrices

It is worth noting that the decision on transmit diversity matrix is taken independently on per user basis. Therefore, since one frame contains data from multiple users, it is very likely that all base station antennas will be used. This is true even though each user's symbols are transmitted exclusively through two antennas during the transmission of a frame.

Despite the performance improvements by using the proposed scheme, it adds computational burden to the mobile station, since they need to find the maximum SINR out of six different configurations rather than three. Moreover, the number of bits required to indicate which matrix to use is increased by one. It is necessary to consider these aspects for the practical implementation of the system.

In the following, the performance of different antenna selection techniques are evaluated under different channel condition according to Stanford University Interim (SUI) standard [164]. There are six channel models defined within the reference, namely SUI type-1 to SUI type-6. Parameters related to each of these channel models are shown in Appendix B.

The signal bandwidth used in this simulation is $20MHz$, which is equal to $22,856KHz$ after factoring in the sampling frequency rate of $8/7$. This corresponds to $11.16KHz$ subcarrier spacing, and approximately $89.6\mu sec$ of OFDMA symbol duration. QPSK modulation is considered, and the performance are evaluated under SNR range of -10dB to 10dB. The system is simulated for pedestrian speed of $5Km/hr$, which corresponds to a maximum Doppler value of $12Hz$ at $2.6GHz$ operating frequency.

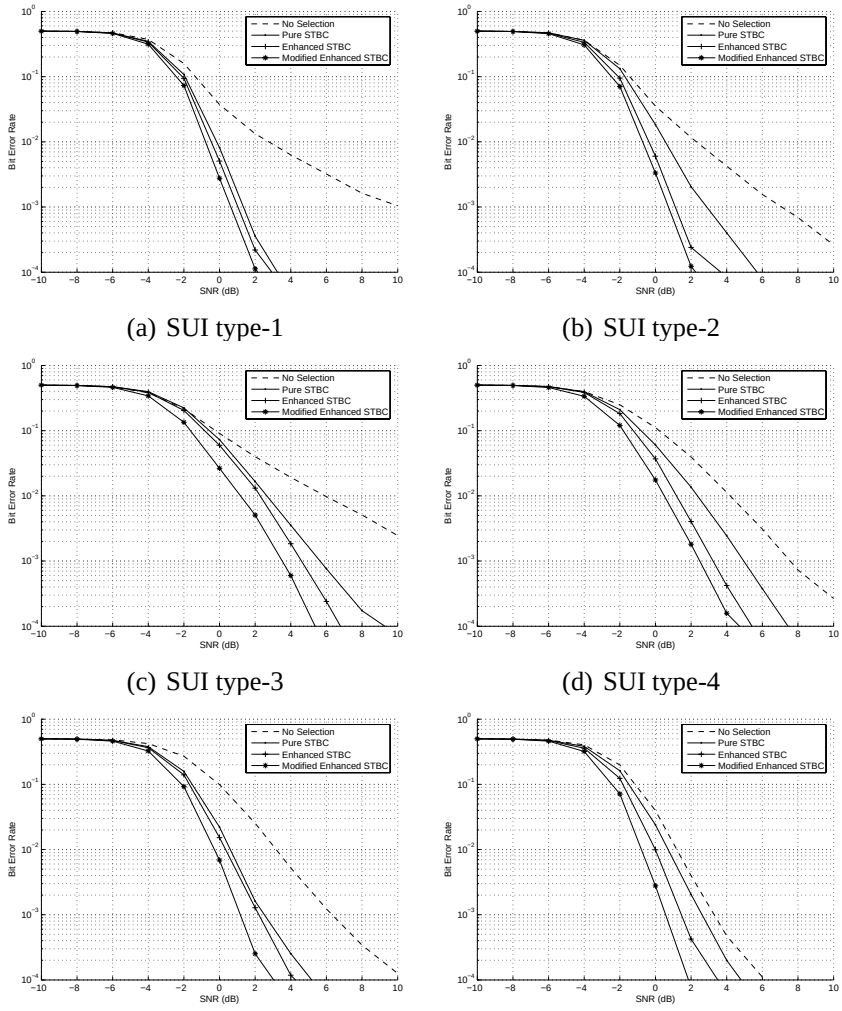

(a) SUI type-1 (b) SUI type-2

(c) SUI type-3 (d) SUI type-4

(e) SUI type-5 (f) SUI type-6

Figure 3.16: Bit error performance of different transmit diversity schemes under different channel conditions

Figure 3.16a to 3.16f shows bit error rate (BER) performances under SUI type-1 to SUI type-6 channel models obtained via simulation. From the figure, it is observed that transmit diversity of *Pure STBC* scheme are capable of achieving significant performance gain. At 10^{-3} BER level, improvement of up to 6.5dB is observed under SUI type-3 model. Furthermore, *Enhanced STBC* scheme can bring additional 0.5dB to 2dB gain with respect to *Pure STBC* schemes by making use of feedback information; while the proposed *Modified Enhanced STBC* scheme can bring additional 1dB to 2.5dB gain due to the extra selection gain exploited by the

Table 3.1: Achievable Gain of Different Transmit Diversity Schemes

	Pure STBC	**Enhanced STBC**	**Modified Enhanced STBC**
SUI type-1	6 dB	6.5 dB	7 dB
SUI type-2	4 dB	6 dB	6.5 dB
SUI type-3	6.5 dB	7.5 dB	8.5 dB
SUI type-4	2.5 dB	4.5 dB	5 dB
SUI type-5	4 dB	4.5 dB	5.5 dB
SUI type-6	0.5 dB	1.5 dB	2 dB

scheme (at the expense of one additional bit in the feedback information).

The improvement that transmit diversity brings to the system performance varies for different channel models used. This is due to different path loss magnitudes and the number of multipaths (which relates directly to the terrain types and tree densities) that the channel model simulates. It is evident from the figure that the proposed scheme outperforms other transmit diversity schemes in all six different channel models.

The amount of gain achieved by different transmit diversity schemes with respect to the single antenna (no selection) configuration under six different channel models are summarised in table 3.1. All measurements are taken at 10^{-3} BER level.

3.4 Summary

In this chapter, antenna selection scheme in cooperative broadcast systems is discussed. Motivated to address the practical issues of MIMO-BC systems, which promises large capacity at the expense of extra hardware cost, a sub optimal antenna selection strategy is proposed. By having less number of RF chains compared to the available antennas, hardware cost can be reduced significantly while still maintaining a certain amount of gain achievable. Moreover, the sub optimal selection algorithm is able to bring the computational complexity down into practical level, as compared to the otherwise unrealisable brute force method. Extra caution needs to be given when multiple carriers system is considered, however, as the selection complexity can be very high, especially when the number of subcarriers is large.

A sub optimal antenna selection algorithm for single carrier MIMO-BC system is proposed. The transmit antenna selection is performed using capacity upper bound maximisation of MIMO-BC, while BC-MAC duality is used for receive antenna selection. When there are 3 available antennas and only 2 RF chains, it is shown that approximately 0.75 b/s/Hz gain is available via brute force method. The proposed algorithm is then shown to be able to reduce the overall complexity from the order of $C_{N_t}^{M_t}(C_{N_r}^{M_r})^K$ into the order of $C_{N_t}^{M_t} + KC_{N_r}^{M_r}$ while maintaining up to 90% of the capacity gain.

The analysis is also extended for the case of broadband frequency selective channel. First, a sub optimal antenna selection for single user MIMO-OFDM systems is proposed. The concept of using decision table in performing antenna selection is introduced, whereby two performance metrics (namely global minimum sub-stream SNR and average minimum sub-stream SNR across subcarriers) are used. Two sub optimal selection methods are then proposed; one of which segregates the transmit and receive antenna selection into two disjoint processes, and the other one exploits the frequency correlation of the channel. It is demonstrated that both selection methods are able to bring performance improvement. The global minimum sub-stream SNR metric also achieves better performance. As for the complexity, the sub optimal method that segregates the transmit and receive selection process is able to reduce the overall complexity from the order of $C_{N_t}^{M_t}C_{N_r}^{M_r}$ into the order of $C_{N_t}^{M_t} + C_{N_r}^{M_r}$. Meanwhile, a complexity reduction by a factor of N_s (the number of subcarriers to be assumed correlated) is achieved by the second selection method.

Combining the selection algorithm proposed for single carrier MIMO-BC systems with the one for single user MIMO-OFDM systems, it is possible to develop a sub optimal antenna selection algorithm for multicarrier MIMO-BC system. By using the decision table concept together with the selection metrics for MIMO-BC systems, up to 0.45 b/s/Hz gain is attainable. This is achieved at the complexity that is considerably lower than the brute force method, which can only achieve up to 0.5 b/s/Hz gain. Complexity reduction of the proposed scheme is also

studied, and it is shown that as the number of users and/or available antennas is increased, the gain becomes more significant. The reduction in complexity is more prominent than in the single carrier case, as the improvement is achieved on all subcarriers compared to just on a single carrier.

Finally, the application of antenna selection in practical system is also analysed, whereby multiuser OFDMA based IEEE 802.16 standard for broadband wireless access systems is considered. It is shown that the incorporation of antenna selection can potentially improve the overall performance. An additional 2.5 dB gain can be achieved compared to the traditional STBC scheme without selection. Even when the channel condition is unfavourable, the selection scheme can still bring approximately 1 dB of SNR gain.

Chapter 4

Power Control and Interference Cancellation in Cooperative Ad-hoc Network

4.1 Introduction

In the previous chapter, the discussion mainly focuses on the cooperative broadcast scenario. Here, another class of cooperation known as cooperative relaying is considered, whereby multiple single antenna nodes cooperate with one another to improve transmission quality towards destination. In particular, this chapter tackles two most fundamental issues in cooperative relay network. Firstly, the basic question whether adding relay node can indeed improve transmission quality as compared to direct transmission is addressed. For this, the most basic setup of three node line network is used in the analysis. Although many works have been devoted to study this class of cooperative network as summarised in Section 2.3.1, none of them has considered this very basic albeit important question. Hence, this work complements the present results on three node cooperative network. Secondly, it has been well recognised that bandwidth

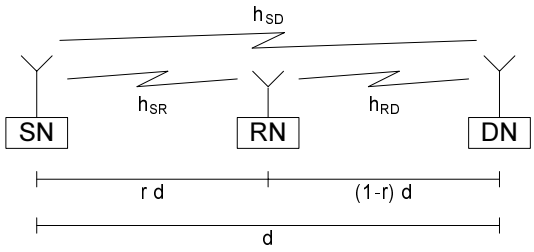

Figure 4.1: System Diagram of Three Node Line Network

efficiency is the major concern in multi-hop relay communication. As the message needs to go through several stages before reaching its destination, the end to end throughput is severely compromised as the number of hops increases. In this work, a novel interference cancellation technique is proposed to allow transmission of new message in every hop. With this scheme, it is demonstrated that the bandwidth efficiency penalty can be kept low even for networks with large number of hops. Detailed analysis on the above two issues are provided in Section 4.2 and Section 4.3 respectively, and the results are summarised in Section 4.4

4.2 Role of Relay and Power Allocation in 3-Node Network

With the increasing popularity of cooperative relay network, it is becoming more and more important to understand the role of relay node in terms of how much performance improvement it can provide. This section is motivated to shed light on this problem. It addresses the question whether relaying can indeed improve link performance; and if it does, to what extend and what is the criteria of optimality. It is in this context that this section discusses different systems including simple decode-and-forward system, and a more complex Distributed Space Time Block Coding (DSTBC) cooperative system.

4.2.1 System Model

A three-node network consisting of a Source Node (SN), Destination Node (DN), and Relay Node (RN) as depicted in Figure 4.1 is considered. The SN and DN are separated by distance

d, and one RN is located between them. Although three node line network is considered, where RN is assumed to be located in the straight line between SN and DN, the results and discussions presented here are also valid for a more general case where RN is located at any point in the area between SN and DN. Normalised distance r is defined as a ratio between the distance from SN to RN and the distance from SN to DN.

The scalar multiplicative channel between SN to RN, SN to DN, and RN to DN are denoted as h_{SR}, h_{SD}, and h_{RD} respectively. Here, a discrete time memoryless channel is assumed, where for all node pair, h represents combined response of transmit pulse shaping filter, channel transfer function, and receiving filter (sampled optimally at Nyquist rate). Therefore h can be modeled as random process whose samples are distributed according to $\mathcal{CN}(0, \frac{1}{\lambda})$, a complex normal distribution with variance $\frac{1}{\lambda}$. Equivalently, the channel power $x = |h|^2$ is distributed according to exponential distribution with parameter λ, whose probability density function (PDF) can be expressed as:

$$f_x(x) = \lambda \, exp\,(-\lambda \, x) \tag{4.1}$$

In the above equations, corresponding subscripts for h and λ can be similarly applied depending on which pair of nodes are being considered. Parameter λ is determined by the distance between the two nodes under consideration, as well as path loss exponent α. For example, in the case of channel between SN and DN, the channel parameter λ_{SD} can be calculated through the path loss equation as follows [165, Ch. 15.2.1]:

$$L_p = 10 \log\,(\lambda_{SD}) = C_1 \; + \; 10 \, \alpha \log\,(d) \; + \; \chi \tag{4.2}$$

where L_p is the path loss measured in decibel, α and d are the path loss exponent (typically ranges from 3 to 5 depending on the propagation condition) and source destination distance separation measured in kilometre respectively. Constant C_1 determines path loss at reference distance (normally measured at 1 km for outdoor channels or 1 m for indoor channels [165]),

and χ is the log-normal random value which depends on system parameters including transmitter and receiver antenna height, carrier frequency, and terrain type. Parameter λ_{SR} and λ_{RD} can be found by replacing d with rd and $(1-r)d$ respectively. For simplicity of exposition, the effect of shadow fading is integrated into the path loss formula, and the channel is mainly governed by large scale path loss and small scale Rayleigh fast fading effect. Here, a path loss constant of -32.45dB (typical urban terrain [165]) is used throughout the analysis.

It is assumed that the receiver can accurately measure the realised fading coefficient in their received signals, while transmitter either does not posses or does not exploit knowledge of the realised fading coefficient. For a fair comparison, all systems under consideration employ BPSK (Binary Phase Shift Keying) signaling with coherent detection, and total power available in the system is normalised to unity. Here, ρ denotes the SNR, which is defined as the ratio between system total power and noise variance N_0. Since the total power is unity, SNR is related to noise variance as $\rho = \frac{1}{N_0}$.

4.2.2 Transmission Protocol and Numerical Results

Four different transmission protocols are considered in the following subsections. Throughout the simulation, the source destination distance d is set to 10 km (typical cell radius), while the path loss exponent α is set to 3.

Direct Transmission

In this protocol, SN transmits its message to DN without any help of RN. The instantaneous probability of error for this transmission can be calculated as [165]:

$$P_e = \mathcal{Q}\left(\sqrt{2\rho\left|h_{SD}\right|^2}\right) \tag{4.3}$$

Here, $\mathcal{Q}(x)$ is the right tail probability of unit normal distribution:

$$\mathcal{Q}(x) = \int_x^\infty \frac{1}{\sqrt{2\pi}} exp\left(-\frac{t^2}{2}\right) dt \tag{4.4}$$

By integrating P_e in equation (4.3) over the distribution of channel realisation, and applying Chernoff standard approximation of Q-function [166] to the integration, the average error probability ($\overline{P_e}$) can be calculated as follows:

$$\begin{aligned} \overline{P_e} &\leq \int_0^\infty \frac{1}{2}\, exp\left(-\rho\, s\right) \lambda_{SD}\, exp\left(-\lambda_{SD}\, s\right)\, ds \\ &\approx \frac{1}{2\left(1+\frac{1}{\lambda_{SD}}\,\rho\right)} \end{aligned} \tag{4.5}$$

Note that in the above calculation, parameter $|h_{SD}|^2$ is substituted with s for better readability. The average error probability curve for this protocol as calculated using equation (4.5) is shown in the straight (—) line curves in Figure 4.2, 4.4, and 4.6 and acts as a reference.

Decode and Forward Relaying

Transmission of a message using this protocol takes two time slots. Within the first time slot, SN transmits its message to RN. After decoding the message, RN will then re-encode and transmit it on the following time slot to DN. Here, to satisfy the total power constraint, power has to be distributed among SN and RN. Denote γ as the portion of total power used by SN. The instantaneous probability of decoding error at SN-RN link and RN-DN link can then be calculated as follows [165]:

$$\begin{aligned} P_e^{(1)} &= \mathcal{Q}\left(\sqrt{2\gamma\rho\,|h_{SR}|^2}\right) \\ P_e^{(2)} &= \mathcal{Q}\left(\sqrt{2(1-\gamma)\rho\,|h_{RD}|^2}\right) \end{aligned} \tag{4.6}$$

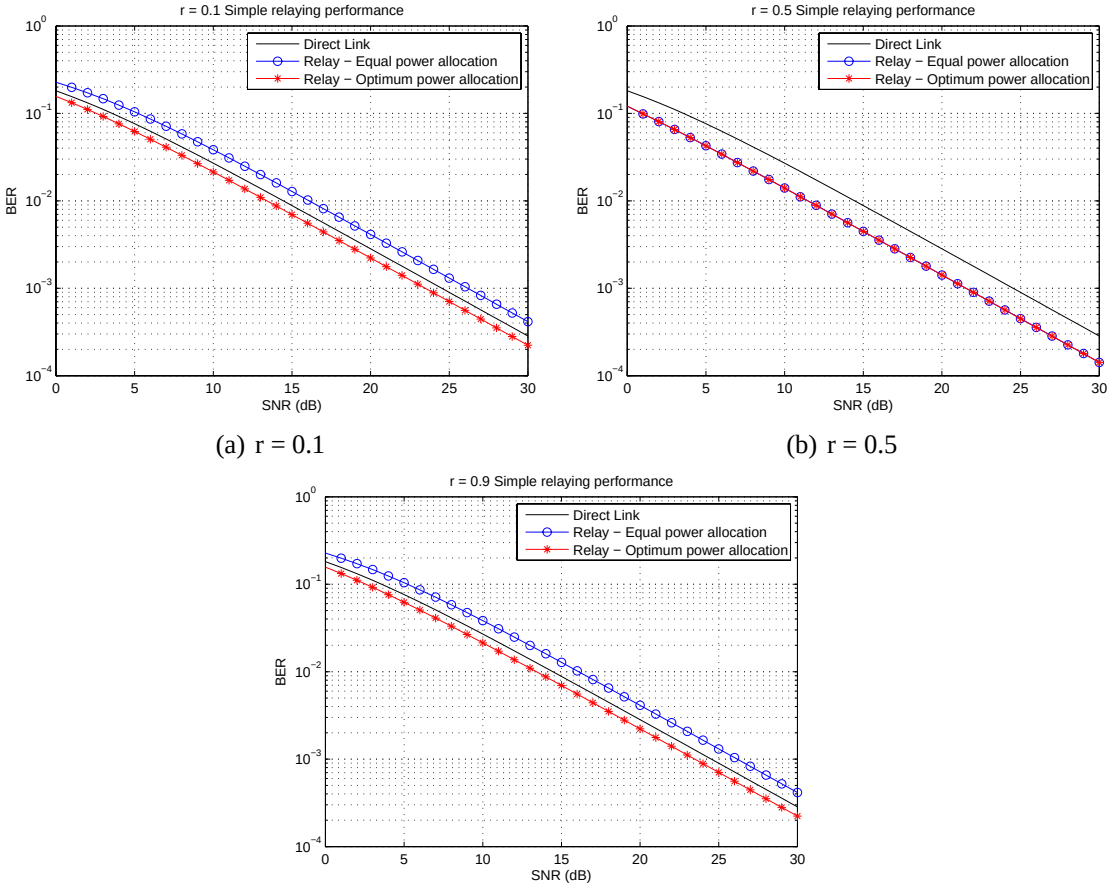

(a) r = 0.1 (b) r = 0.5

(c) r = 0.9

Figure 4.2: Decode and Forward Relaying Performances for Three Different Relay Locations (Normalised Distances)

Considering that the message will be received correctly at DN when transmission of both slots are correct, the end to end error probability can be found using:

$$P_e^{e-e} = 1 - ((1 - P_e^{(1)}) \times (1 - P_e^{(2)})) \tag{4.7}$$

Note that the above equation neglects the fact that error in both first and second time slot may result in double bit flipping, which end up with correct decision at DN. However, for simplicity, this work only considers condition as used in equation (4.7) as the correct decoding criteria at DN.

By integrating equation (4.7) with respect to the distribution of its random terms, the average probability of error can be calculated as:

$$\overline{P_e^{e-e}} \approx \frac{1}{2\left(1+\frac{\gamma\rho}{\lambda_{SR}}\right)} + \frac{1}{2\left(1+\frac{(1-\gamma)\rho}{\lambda_{RD}}\right)} - \frac{1}{4\left(1+\frac{\gamma\rho}{\lambda_{SR}}\right)\left(1+\frac{(1-\gamma)\rho}{\lambda_{RD}}\right)} \tag{4.8}$$

The average probability of error curve for the above formula assuming equal power distribution between SN and RN (i.e. $\gamma = 0.5$) is depicted in the circled (-o-) line curves in Figure 4.2 for three different relay locations.

It can be seen that the average error performance is very much dependent on the normalised distance r (the location of RN). When RN is too close or too far from SN, the performance of Decode and Forward system with equal power allocation is actually worse than direct transmission (as shown in Figure 4.2a and c). With optimum power allocation, however, this can be prevented. From equation (4.8), optimum power allocation can be found by taking the first derivation and equate it to zero. This will result in polynomial degree 2 in the form of $a\gamma^2 + b\gamma + c = 0$, where:

$$\begin{aligned} a &= (\lambda_{RD} - \lambda_{SR})\,\rho^2 \\ b &= 3\lambda_{SR}\lambda_{RD}\rho + 2\lambda_{SR}\rho^2 \\ c &= 0.5\lambda_{SR}\lambda_{RD}\,(\lambda_{SR} - \lambda_{RD}) - 1.5\lambda_{SR}\lambda_{RD}\rho - \lambda_{SR}\rho^2 \end{aligned} \tag{4.9}$$

Solving the above second degree polynomial, optimum power allocation is obtained as the positive real root which lies between zero and one. Average BER performance of decode and forward using optimal power control is shown as the crossed (-*-) line curves of Figure 4.2 for three different r settings. Unlike equal power distribution, optimal power control scheme allows this protocol to perform strictly better than direct link, regardless of RN position.

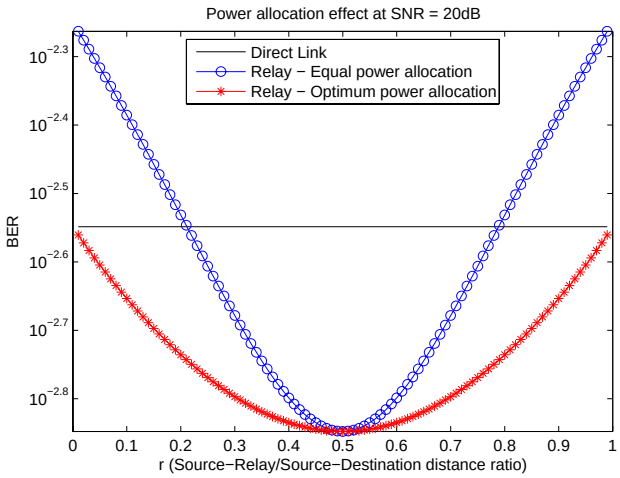

Figure 4.3: Performance Comparisons of Decode and Forward Relaying with and without Optimum Power Allocation for Different Relay Locations

Figure 4.3 shows the difference in BER value of Decode and Forward system with and without optimum power control evaluated at $SNR = 20$dB, and r varies from 0.01 to 0.99. It is observed that Decode and Forward can improve the performance, especially when RN is located in the middle between SN and DN. However, when RN is away from center point, performance will degrade.

Ideal DSTBC

DSTBC protocol considered in this work uses Alamouti codes [26] for transmission. The word *Ideal* here means that the channel quality from SN to RN is very good, and perfect channel estimation is available at RN such that it is able to decode the message perfectly. Similarly, since in this protocol both SN and RN are involved in message transmission, power needs to be allocated among them to maintain the total power constraint. Denoting γ as the portion of total power used by SN, instantaneous probability of error can be expressed as follows [36]:

$$P_e = \mathcal{Q}\left(\sqrt{2\rho(\gamma\left|h_{SD}\right|^2 + (1-\gamma)\left|h_{RD}\right|^2)}\right) \tag{4.10}$$

Average probability of error can then be calculated by integrating (4.10) with respect to the

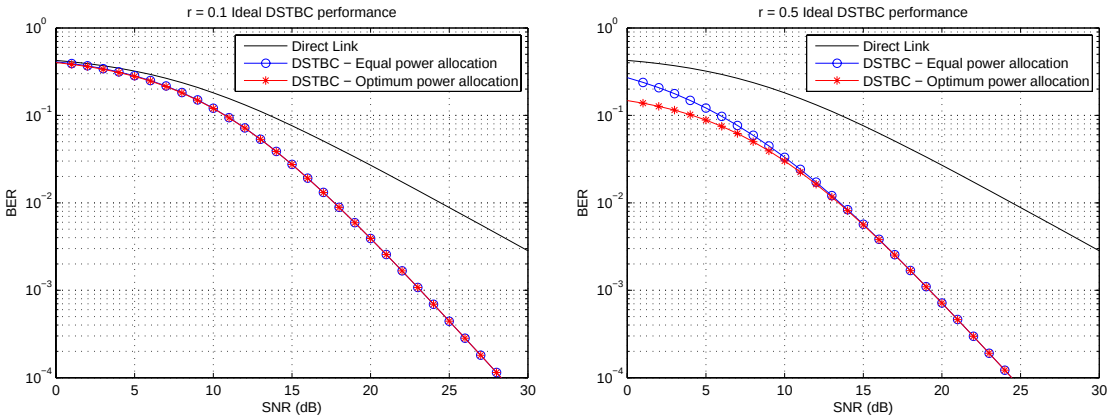

(a) r = 0.1

(b) r = 0.5

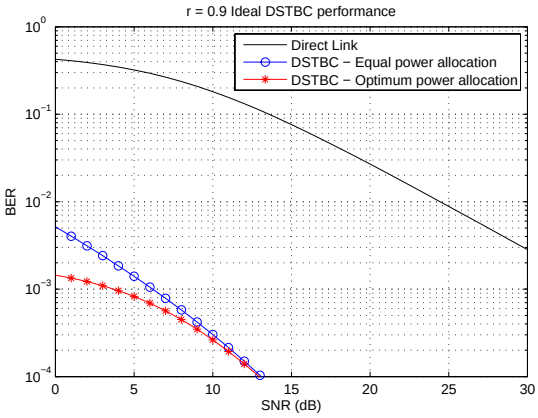

(c) r = 0.9

Figure 4.4: Cooperative Distributed Space Time Block Coding Performances for Three Different Relay Locations (Normalised Distances)

distribution of random terms, which will give the following expression:

$$\overline{P_e} \approx \frac{1}{2\left(1+\frac{\rho\gamma}{\lambda_{SD}}\right)\left(1+\frac{\rho(1-\gamma)}{\lambda_{RD}}\right)} \tag{4.11}$$

Without power control, the total power would be equally distributed among SN and RN (i.e. $\gamma = 0.5$). The circled (-o-) line curves in Figure 4.4 shows the performance of ideal DSTBC under equal power allocation as calculated using equation (4.11) above, with three different values of r (RN locations). It can be seen that this method outperforms direct transmission in all cases, and diversity gain is observed from the steeper slope at high SNR regime.

Another interesting observation from Figure 4.4 is that as the value of r increases (RN is moving closer toward DN), the BER curve is moving toward lower value. This is a consequence of the *Ideal* assumption, where the channel from SN to RN is very good, and perfect channel estimation is available at RN such that perfect decoding is possible. By assigning non zero power to RN, and putting RN arbitrarily close to DN, the BER can be made arbitrarily low, as the superior channel quality between RN and DN dominates the overall system performance.

Optimum power allocation in this protocol can be performed by taking the first derivation of equation (4.11) and equate it to zero. Again, the solution of optimum γ has to lie between zero and one, and it can be expressed by the following equation:

$$\gamma_{opt} = 0.5 \times \left(\frac{\lambda_{SD} - \lambda_{RD}}{\rho} + 1 \right) \tag{4.12}$$

Substituting the value of γ_{opt} back into equation (4.11), optimum average probability of error is obtained as follows:

$$\overline{P_e^{opt}} \approx \frac{2\lambda_{SD}\lambda_{RD}}{(\lambda_{SD} + \lambda_{RD} + \rho)^2} \tag{4.13}$$

The BER corresponding to the above optimum average probability of error is depicted by the crossed (-*-) line curves in Figure 4.4. It is observed that optimum power allocation for Ideal DSTBC protocol is only effective in low SNR regime. Moreover, as the RN moves further away from DN (smaller value of r), the curves with and without power allocation coincides. Figure 4.5 shows the difference in BER performance between equal and optimum power allocation, evaluated at $SNR = 5$dB with r from 0.01 to 0.99.

Practical DSTBC

In practical implementation of DSTBC, instead of assuming that RN has perfect knowledge on what SN wants to transmit, SN has to convey the information, and hence two time slots are allocated for message transmission. In the first time slot, SN transmits its message to RN.

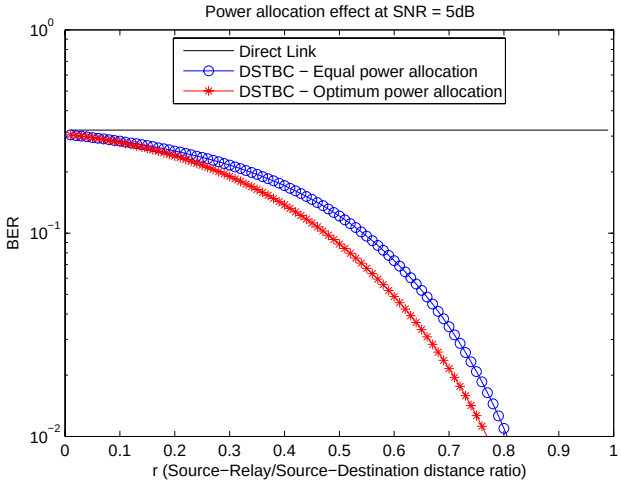

Figure 4.5: Performance Comparisons of Distributed Space Time Block Coding with and without Optimum Power Allocation for Different Relay Locations

After decoding the message, both SN and RN cooperate to perform DSTBC transmission in the subsequent time slot.

Power allocation problem here consists of two parts. The first part is to distribute total power among first slot and second slot transmission, while the second part is to distribute power between SN and RN for DSTBC transmission. It can be seen that the power allocation problem for these two parts can be completely decoupled. Therefore, the solution found in the previous subsection (equation (4.12)) can be directly applied for second part, leaving us with only first part of the problem.

Denoting η as the portion of total power used in the first slot, instantaneous probability of error for the first and second slot transmission can be expressed as follows [36], [165]:

$$\begin{aligned} P_e^{(1)} &= \mathcal{Q}\left(\sqrt{2\rho\eta\left|h_{SR}\right|^2}\right) \\ P_e^{(2)} &= \mathcal{Q}\left(\sqrt{2\rho(1-\eta)\left(\gamma_{opt}\left|h_{SD}\right|^2+(1-\gamma_{opt})\left|h_{RD}\right|^2\right)}\right) \end{aligned} \tag{4.14}$$

where γ_{opt} is the solution of optimum power allocation in the second slot, and it is expressed as in equation (4.12). The end-to-end error probability can be calculated by substituting $P_e^{(1)}$

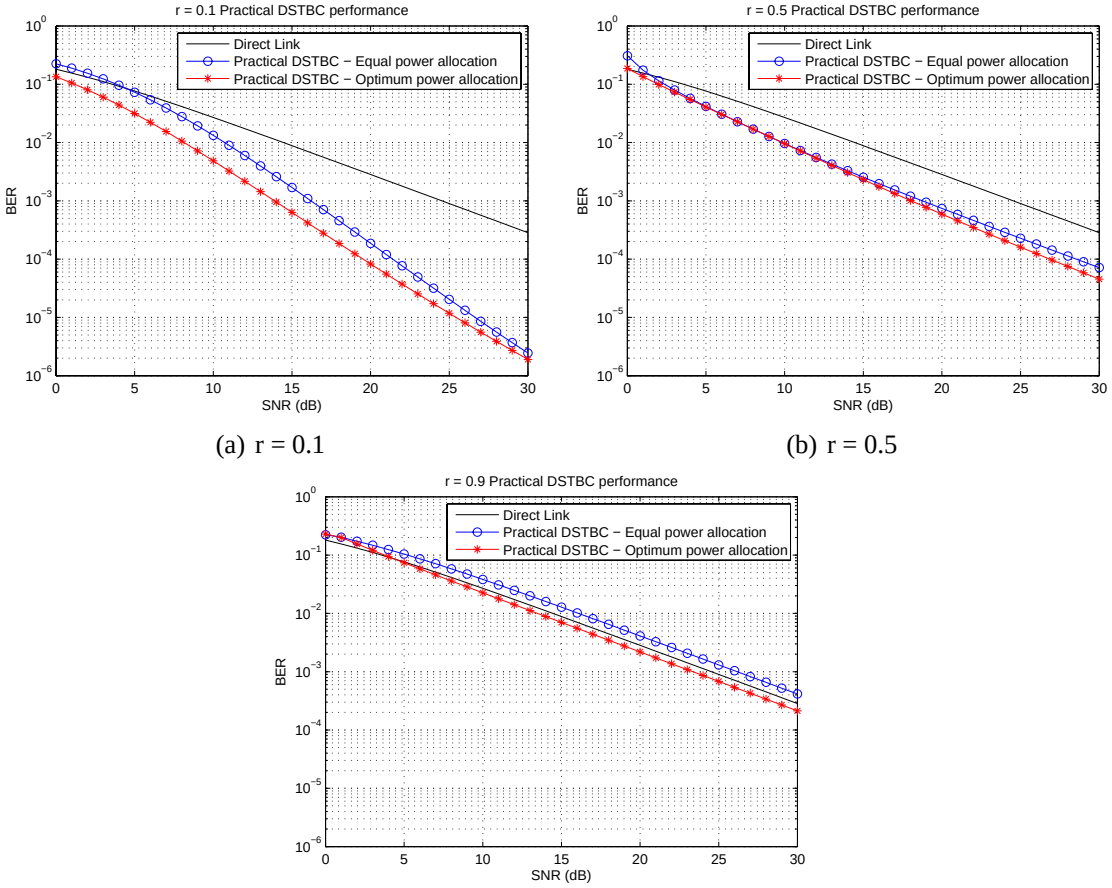

(a) r = 0.1 (b) r = 0.5

(c) r = 0.9

Figure 4.6: Practical DSTBC Performances for Three Different Relay Locations

and $P_e^{(2)}$ above into equation (4.7). By integrating end-to-end error probability expression with respect to the distribution of random terms, average end-to-end probability of error is obtained, which is expressed as follows:

$$\overline{P_e^{e-e}} \approx \frac{1}{2\left(1+\frac{\eta\rho}{\lambda_{SR}}\right)} + \frac{2}{\left(3+\frac{(1-\eta)\rho}{\lambda_{SD}}-\frac{\lambda_{RD}}{\lambda_{SD}}\right)\left(3+\frac{(1-\eta)\rho}{\lambda_{RD}}-\frac{\lambda_{SD}}{\lambda_{RD}}\right)} - \frac{1}{\left(1+\frac{\eta\rho}{\lambda_{SR}}\right)\left(3+\frac{(1-\eta)\rho}{\lambda_{SD}}-\frac{\lambda_{RD}}{\lambda_{SD}}\right)\left(3+\frac{(1-\eta)\rho}{\lambda_{RD}}-\frac{\lambda_{SD}}{\lambda_{RD}}\right)} \tag{4.15}$$

Without power allocation strategy, the total power will be equally distributed among first and second slot transmission ($\eta = 0.5$). The circled (-o-) line curves in Figure 4.6 shows the

BER performance of the system under equal power allocation as calculated using equation (4.15) for three different values of r. It can be seen that when RN is close to SN ($r = 0.1$), this system performs very good, especially at high SNR range due to diversity gain at the second slot transmission. However, as RN moves away from SN, the performance degrades up to the point where it is worse than direct transmission (as shown in Figure 4.6c when r = 0.9).

By using the same technique, optimum power allocation can be found from equation (4.15). Taking the first derivation and equate it to zero, the optimisation problem translates into solving quartic polynomial $a\eta^4+b\eta^3+c\eta^2+d\eta+e = 0$, where the coefficients are expressed as follows:

$$
\begin{aligned}
a &= \frac{\rho^4}{\lambda_{SD}^2\lambda_{RD}^2} \\
b &= \frac{8\rho^3}{\lambda_{SR}\lambda_{SD}\lambda_{RD}} - \frac{4\rho^3}{\lambda_{SD}\lambda_{RD}^2} - \frac{4\rho^3}{\lambda_{SD}^2\lambda_{RD}} - \frac{4\rho^4}{\lambda_{SD}^2\lambda_{RD}^2} \\
c &= \frac{38\rho^2}{\lambda_{SD}\lambda_{RD}} - \frac{8\rho^2}{\lambda_{SR}\lambda_{SD}} - \frac{8\rho^2}{\lambda_{SR}\lambda_{RD}} - \frac{2\rho^2}{\lambda_{SD}^2} - \frac{2\rho^2}{\lambda_{RD}^2} + \frac{12\rho^3}{\lambda_{SD}\lambda_{RD}^2} + \frac{12\rho^3}{\lambda_{SD}^2\lambda_{RD}} - \\
&\quad \frac{8\rho^3}{\lambda_{SR}\lambda_{SD}\lambda_{RD}} + \frac{6\rho^4}{\lambda_{SD}^2\lambda_{RD}^2} \\
d &= \frac{4\rho\lambda_{SR}}{\lambda_{SD}\lambda_{RD}} + \frac{12\rho\lambda_{SD}}{\lambda_{RD}^2} + \frac{12\rho\lambda_{RD}}{\lambda_{SD}^2} - \frac{36\rho}{\lambda_{RD}} - \frac{36\rho}{\lambda_{SD}} + \frac{4\rho^2}{\lambda_{SD}^2} + \frac{4\rho^2}{\lambda_{RD}^2} - \frac{64\rho^2}{\lambda_{SD}\lambda_{RD}} \\
&\quad - \frac{12\rho^3}{\lambda_{SD}\lambda_{RD}^2} - \frac{12\rho^3}{\lambda_{SD}^2\lambda_{RD}} - \frac{4\rho^4}{\lambda_{SD}^2\lambda_{RD}^2} \\
e &= 98 - \frac{54\lambda_{SD}}{\lambda_{RD}} - \frac{54\lambda_{RD}}{\lambda_{SD}} - \frac{4\lambda_{SR}}{\lambda_{SD}} - \frac{4\lambda_{SR}}{\lambda_{RD}} + \frac{9\lambda_{SD}^2}{\lambda_{RD}^2} + \frac{9\lambda_{RD}^2}{\lambda_{SD}^2} + \frac{24\rho}{\lambda_{SD}} + \frac{24\rho}{\lambda_{RD}} - \frac{12\rho\lambda_{SD}}{\lambda_{RD}^2} \\
&\quad - \frac{12\rho\lambda_{RD}}{\lambda_{SD}^2} - \frac{4\rho\lambda_{SR}}{\lambda_{SD}\lambda_{RD}} - \frac{2\rho^2}{\lambda_{SD}^2} - \frac{2\rho^2}{\lambda_{RD}^2} + \frac{26\rho^2}{\lambda_{SD}\lambda_{RD}} + \frac{4\rho^3}{\lambda_{SD}\lambda_{RD}^2} + \frac{4\rho^3}{\lambda_{SD}^2\lambda_{RD}} + \frac{\rho^4}{\lambda_{SD}^2\lambda_{RD}^2}
\end{aligned}
\tag{4.16}
$$

Optimum η value is chosen as the positive real root which falls between zero and one. BER performance of this scheme is shown by the crossed (-*-) line curves in Figure 4.6.

It is interesting to see that even with optimum power allocation, degradation in performance is still observed as r increases. This signifies the importance of SN-RN link quality (hence the correctness of message at RN) in cooperative DSTBC system. Difference in BER performance

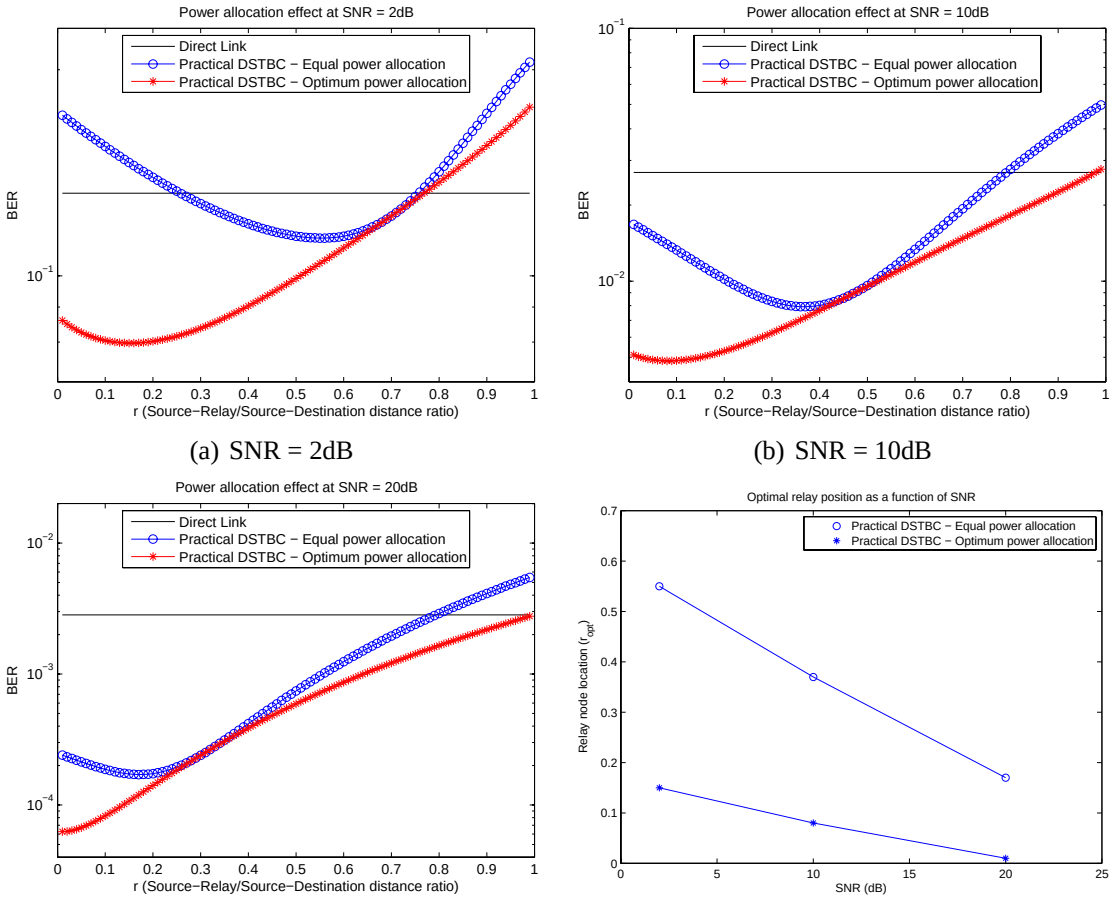

(a) SNR = 2dB (b) SNR = 10dB

(c) SNR = 20dB (d) Optimal relay position

Figure 4.7: Performance Comparisons of Practical DSTBC for Different SNR values and the optimal relay node locations

of this system under low, medium, and high SNR, as r changes from 0.01 to 0.99 is shown in Figure 4.7a, 4.7b, and 4.7c respectively. With optimum power allocation, the lowest BER is achieved when $r \approx 0.1$; whereas with equal power allocation, optimum r changes from 0.6 at low SNR to 0.2 at high SNR. Figure 4.7d shows the value of optimal r as SNR changes. When RN is located far away from SN, direct transmission is preferred, especially at low SNR.

From the numerical results obtained for different cooperative schemes in three node line network, it is apparent that the addition of relay node can indeed improve the overall system performance. However, it has to be used in conjunction with a proper power allocation strategy. Otherwise, adding relay node could even bring an adverse effect to system performance.

4.3 Inter-node Interference in Multi-hop Transmission

In some cases, when the source and destination are separated by long distances, message transmission needs to go through several hops before reaching its destination. One major drawback of multi hop relaying is the requirement of orthogonal channel during relay slots, which can significantly affect the overall bandwidth efficiency. Different approaches have been discussed to alleviate this, such as using space-time coding techniques across relay terminals [108]-[109], or combining TDMA (Time Division Multiple Access) with consolidation of relay slots [167]. However, none of these approaches is able to completely eliminate the penalty on bandwidth efficiency, since they still require (although a shorter period of) relay slot.

Dirty paper coding (DPC) [2] is an exciting transmission technique which allows transmitter to send information in the presence of known interference at the rate equal to capacity of interference free channel. By applying this property on each stage of the relay transmission (thus the name Successive Dirty Paper Coding/SDPC), it will be shown that it is possible to achieve higher bandwidth efficiency in relay network.

The potential of DPC scheme to improve transmission rate in single-hop transmission has been studied in [85], and its application in relay networks has been considered in [96]. However, they only consider dual hop case, where DPC technique is used on the first relaying phase. In this chapter, performances of different cooperative relay networks are analysed for multi-hop scenario. The proposed SDPC scheme is then studied, and its underlying concept to apply dirty paper coding scheme on each relay stage is explained. Its performance is then analysed and compared to the existing relay schemes in terms of network outage probability.

4.3.1 System Model

A uniformly distributed ad-hoc network is considered. Each node can transmit its message to any other node in the network either through direct transmission or via relaying, depending on the distance of the destination node. If the distance is within a certain radius r, direct transmis-

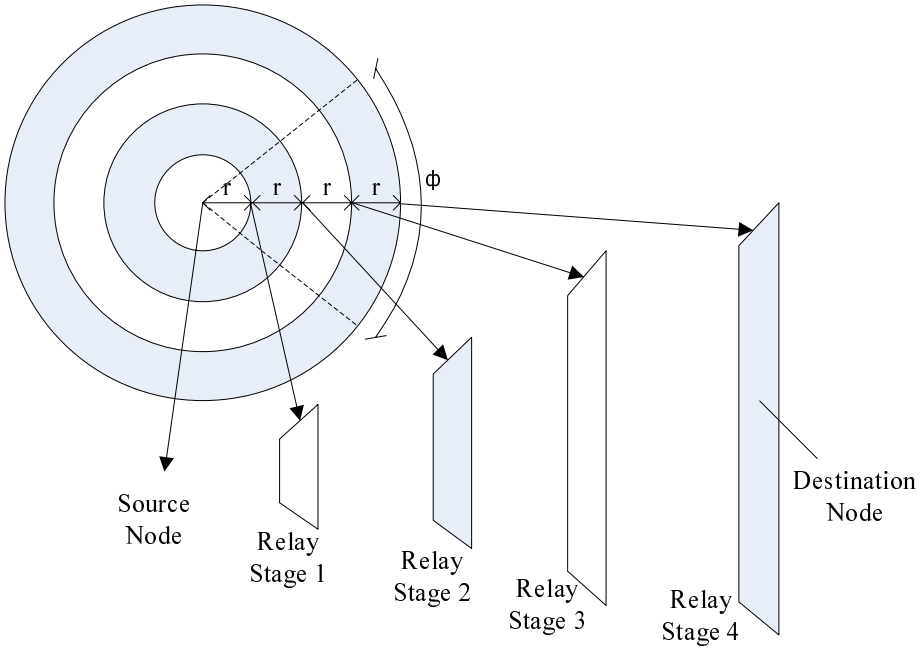

Figure 4.8: Multiple Hops Cooperative Relay Network

sion is used; otherwise relaying has to be employed. Figure 4.8 shows the illustration of relay grouping for a network with 4 relay stages (RSs). Here, nodes are grouped into different RSs. RS 1 consists of nodes which are within radius r from the source node, RS 2 consists of those which are of radius r to $2r$ apart from the source node. Subsequent RSs are similarly defined. Note that only nodes which are located between the source and destination (within an angle ϕ denoted by dashed line in Figure 4.8) are joined into the RS group. In the actual system, the maximum allowable number of RSs to reach the furthest node is defined as g_{max}, and its value is set according to the desired coverage of the network.

Here, the area of circle with radius r is normalized to unity. A system parameter called *normalized density* $\mathcal{T}$ is then defined as the total number of nodes contained within a unit area. It is important to note that as the RS gets further away from the source, the area (hence the number of relay nodes) becomes larger.

To simplify the analysis, system bandwidth is set to $1Hz$, and each node has equal transmit power constraint of P_{tot}. Moreover, it is assumed that each node has only one antenna; hence

no broadcasting strategy can be employed (since there is only a single communication stream). Nodes are assumed to operate in half-duplex mode, where no simultaneous transmission and reception is allowed at the same channel. In any RS i, the received signal observed by a particular node due to transmission of a single node from the previous RS, can be expressed as:

$$y_i[n] = h_{i-1,i}\, x_{i-1}[n] + z_i[n] \tag{4.17}$$

where $x_{i-1}[n]$ is the transmitted symbol ($x_0[n]$ being the symbol transmitted by the source node), $h_{i-1,i}$ is the complex channel gain between the node at RS $i-1$ and the node at RS i, and $z_i[n]$ is the additive noise. Here, $h_{i-1,i}$ captures the effects of path loss, shadowing, and frequency non-selective fading. Statistically, $h_{i-1,i}$ is modelled as zero-mean, independent, circularly symmetric complex Gaussian random variables with unit variance, so that the magnitudes $|h_{i-1,i}|$ are Rayleigh distributed ($|h_{i-1,i}|^2$ are exponentially distributed, or equivalently Chi-square distributed with 2 degree of freedom [168, Page 42]) and the phases $\angle h_{i-1,i}$ are uniformly distributed in $[0, 2\pi)$. Furthermore, $z_i[n]$ is modelled as zero-mean mutually independent, circularly symmetric complex Gaussian random sequences with variance N_0.

In a relay transmission, message has to traverse through RSs to reach its destination. Therefore, the end-to-end capacity of such channel is equal to the minimum capacity of each RSs involved:

$$C(g) = \min_{i\,=\,1..g} \left[\frac{1}{g} \times C_{<.>\_i}\right] \tag{4.18}$$

Here, g is the RS where the ultimate destination is located, and $C_{<.>\_i}$ is the capacity of the link between RS $i-1$ and i (RS 0 being the source node), and its value depends on the relaying strategy used. The subscript $_{<.>}$ is used to differentiate link capacities between RS $i-1$ and i under different relaying schemes. The division by g in equation (4.18) is due to the fact that g time slots are required for the message to reach its destination. A large g would bring down the end-to-end capacity, which signifies the bandwidth efficiency penalty of relay process.

Assuming that each node in the network is equally probable to be the ultimate destination, and using the fact that different RS contains different number of nodes proportional to its area, the overall capacity of the network can be expressed as:

$$\begin{aligned} C &= \sum_{g=1}^{g_{max}} Pr(\text{Destination Stage} = g) \times C(g) = \sum_{g=1}^{g_{max}} \frac{\text{Area of RS } g}{\text{Area of the network}} \times C(g) \\ &= \sum_{g=1}^{g_{max}} \frac{\pi\left(g\,r\right)^2 - \pi\left(\left(g-1\right)r\right)^2}{\pi\left(g_{max}\,r\right)^2} \times C(g) = \sum_{g=1}^{g_{max}} \frac{(2g-1)}{g_{max}^2} \times C(g) \end{aligned} \tag{4.19}$$

Here, the simplification is valid for the system model used, where RSs have constant linear increase in the radius, such that the ratio of their areas forms an odd-number series (Area of RS1 : RS2 : ... : RSg = πr^2 : ($\pi(2r)^2$ - πr^2) : ... : ($\pi(gr)^2$ - $\pi(gr-r)^2$) = 1 : 3 : ... : $(2g-1)$).

In the following subsections, three different relaying strategies are analysed. Namely Pure Relaying, Repetition Coding Decode and Forward, and Space Time Coded Relaying. Most of the derivations shown here provide extension to the work presented in [108] into multi-hop case.

4.3.2 No Cooperation, Pure Relaying

This is the simplest scenario where only one node in each RS is involved in the relay process. As emphasized earlier, the relay process has to be performed in an orthogonal channel, therefore during this period, no other node may transmit their message on the same channel. Under this scheme, capacity of the link between RS $(i-1)$ and i is expressed as:

$$\begin{aligned} C_{NC\_i} &= log_2\left(1 + SNR_i\right) \\ &= log_2\left(1 + \left|h_{i-1,i}\right|^2 \frac{P_{tot}}{N_0}\right) \end{aligned} \tag{4.20}$$

which is just a basic expression for point-to-point Shannon's capacity in the presence of channel fading.

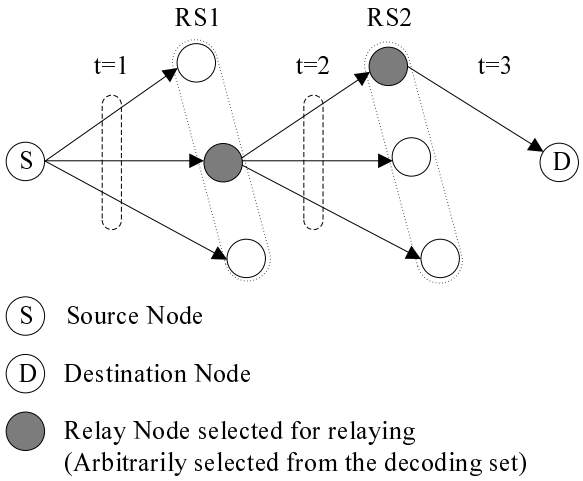

Figure 4.9: Pure Relaying System Diagram

Figure 4.9 shows the system diagram of three-hops relay network with Pure Relaying scheme. As shown in the figure, although there might be more than one relay nodes which are able to decode the message from the previous RS, only one of them is allowed to relay the message to the next RS on the following time slot.

4.3.3 Repetition Coding Decode and Forward

This scheme can be described as follows. Initially, the source node transmits its message to the RS 1. Then, using the same notation as in [108], a decoding set $\mathcal{D}_1(s)$ is defined, containing all nodes in RS 1 that can successfully decode the message.

Within the following time slot, each of these nodes in the $\mathcal{D}_1(s)$ will sequentially repeat their decoded message to the next RS. Then, similarly on the RS 2, a decoding set $\mathcal{D}_2(s)$ is defined, containing all nodes in RS 2 that can successfully decode the message from RS 1. This process is continued until finally the message reaches its ultimate destination. The system diagram of Repetition Coded relay network is illustrated in Figure 4.10.

Since capacity of the link between RS $i-1$ and i depends on the decoding set $\mathcal{D}_{i-1}(s)$, on

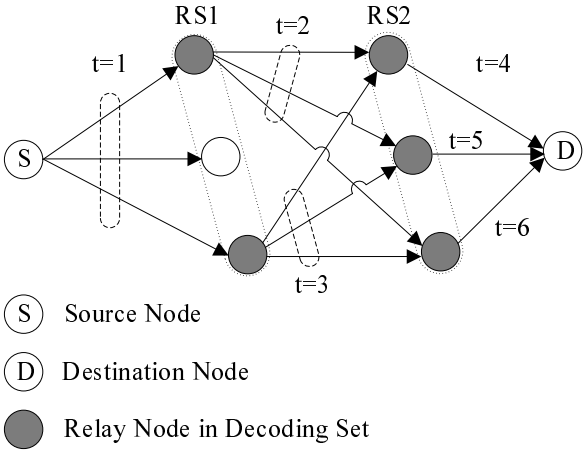

Figure 4.10: Repetition Coded Relaying System Diagram

average, this capacity can be expressed as:

$$C_{RC\_i} = \sum_{\mathcal{D}_{i-1}(s)} Pr_{RC}\left[\mathcal{D}_{i-1}(s)\right] \times C_{RC\_i}(\mathcal{D}_{i-1}(s)) \tag{4.21}$$

where the summation is performed over all possible values of $\mathcal{D}_{i-1}(s)$. Here, $Pr_{RC}\left[\mathcal{D}_{i-1}(s)\right]$ and $C_{RC\_i}(\mathcal{D}_{i-1}(s))$ are the probability of decoding set $\mathcal{D}_{i-1}(s)$ and link capacity between RS $i-1$ to i given the decoding set $\mathcal{D}_{i-1}(s)$, respectively.

For this particular relaying scheme, the conditional link capacity between RS $i-1$ and i is:

$$\begin{aligned} C_{RC\_i}(\mathcal{D}_{i-1}(s)) &= \frac{1}{|\mathcal{D}_{i-1}(s)|} \times log_2\left(1 + \sum_{m\in\mathcal{D}_{i-1}(s)} SNR_i(m)\right) \\ &= \frac{1}{|\mathcal{D}_{i-1}(s)|} \times log_2\left(1 + \frac{P_{tot}}{N_0} \sum_{m\in\mathcal{D}_{i-1}(s)} |h_{i-1,i}(m)|^2\right) \end{aligned} \tag{4.22}$$

The division by $|\mathcal{D}_{i-1}(s)|$ is due to the number of time slots required to relay the message, as each relay node sequentially repeats to the subsequent relay stage. Except for $\mathcal{D}_0(s)$, in which case the set contains only source node, the decoding set $\mathcal{D}_i(s)$ is a random set, whose elements depend on the transmission between RS $i-1$ and i. For any node n in RS i, the capacity

between RS $i-1$ and i is given as:

$$C_{i-1,i}^{(n)} = \frac{1}{|\mathcal{D}_{i-1}(s)|} \times log_2 \left(1 + \frac{P_{tot}}{N_0} \sum_{m \in \mathcal{D}_{i-1}(s)} |h_{i-1,i}(m,n)|^2\right)$$

The probability that node n in RS i is included to the decoding set $D_i(s)$, is equal to the probability that the capacity exceeds a certain rate R.

$$\begin{aligned} Pr_{RC}[n \in \mathcal{D}_i(s)] &= Pr\left[\sum_{m \in \mathcal{D}_{i-1}(s)} |h_{i-1,i}(m,n)|^2 > \frac{2^{R|\mathcal{D}_{i-1}(s)|}-1}{P_{tot}/N_0}\right] \\ &= \left(\frac{\gamma\left(|\mathcal{D}_{i-1}(s)|, \frac{2^{R|\mathcal{D}_{i-1}(s)|}-1}{2P_{tot}/N_0}\right)}{\Gamma(|\mathcal{D}_{i-1}(s)|)}\right) \end{aligned} \tag{4.23}$$

where $\gamma(.)$ and $\Gamma(.)$ are the incomplete and complete Gamma functions respectively [169]. The above equation is derived using the fact that the sum of K squared magnitude of complex Gaussian random variables is a Gamma distributed random variable (which in this case can also be represented as Chi-squared distribution with $2K$ degree of freedom, where K is the total number of elements being added [168, page 42]).

Since different nodes are independent to each other, and the fading coefficients are drawn from independent distribution, the probability of decoding set $\mathcal{D}_i(s)$ can be expressed as follows:

$$\begin{aligned} Pr_{RC}\left[\mathcal{D}_i(s)\right] &= \prod_{n \in \mathcal{D}_i(s)} \frac{\gamma\left(|\mathcal{D}_{i-1}(s)|, \frac{2^{R|\mathcal{D}_{i-1}(s)|}-1}{2P_{tot}/N_0}\right)}{\Gamma(|\mathcal{D}_{i-1}(s)|)} \\ &\quad \times \prod_{n \notin \mathcal{D}_i(s)} \left(1 - \frac{\gamma\left(|\mathcal{D}_{i-1}(s)|, \frac{2^{R|\mathcal{D}_{i-1}(s)|}-1}{2P_{tot}/N_0}\right)}{\Gamma(|\mathcal{D}_{i-1}(s)|)}\right) \end{aligned} \tag{4.24}$$

Substituting equations (4.24) and (4.22) into equation (4.21), the link capacity between RS $i-1$ and i is obtained.

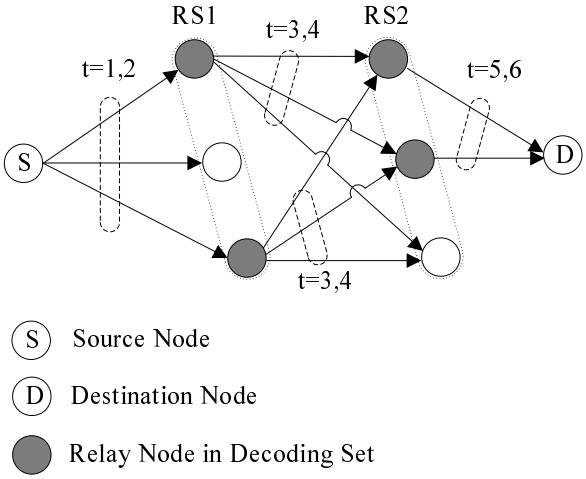

Figure 4.11: Space Time Coded Relay Network System Diagram

4.3.4 Space Time Coded Relaying

This scheme is very similar to the repetition coding decode and forward, where a decoding set $\mathcal{D}_i(s)$ is defined for each RS containing all nodes which can successfully decode the transmitted message from the previous RS. However, instead of sequentially repeating the decoded message, all nodes in the decoding set cooperate with each other, and simultaneously transmit the space-time-coded version of the message to the subsequent RS. Figure 4.11 illustrates the system diagram of three-hop Space Time Coded relay network.

Here, RS 1 waited for two consecutive messages transmitted during the first and second time slot in order to perform space time coding on the following two time slots. In a real system implementation, the number of messages that RS has to wait depends on the number of nodes in the decoding set. Using the same argument as the one used in equation (4.21), average link capacity is expressed as:

$$C_{STC\_i} = \sum_{\mathcal{D}_{i-1}(s)} Pr_{STC}\left[\mathcal{D}_{i-1}(s)\right] \times C_{STC\_i}(\mathcal{D}_{i-1}(s)) \tag{4.25}$$

Note that the only difference is on the subscript, where STC is used to indicate space time coded relaying scheme.

In this case, the link capacity between RS $i-1$ and i given decoding set $\mathcal{D}_{i-1}(s)$ is:

$$\begin{aligned} C_{STC\_i}(\mathcal{D}_{i-1}(s)) &= log_2\left(1+\frac{1}{|\mathcal{D}_{i-1}(s)|}\sum_{m\in\mathcal{D}_{i-1}(s)} SNR_i(m)\right) \\ &= log_2\left(1+\frac{P_{tot}}{N_0\ |\mathcal{D}_{i-1}(s)|}\sum_{m\in\mathcal{D}_{i-1}(s)} |h_{i-1,i}(m)|^2\right) \end{aligned} \quad (4.26)$$

As compared to equation (4.22), the division by $|\mathcal{D}_{i-1}(s)|$ is moved into the logarithmic argument. This division is necessary to maintain equal total energy consumption on each time slot, so that fair comparisons across different schemes can be made. It shows that this scheme uses one time slot to relay message from one RS to the next RS, where the use of orthogonal space-time code design (with sum power constraint of P) is assumed. Similarly, $\mathcal{D}_i(s)$ is a random set, and the probability that node n in RS i is joined to $\mathcal{D}_i(s)$ can be calculated as:

$$\begin{aligned} Pr_{STC}[n\in\mathcal{D}_i(s)] &= Pr\left[\sum_{m\in\mathcal{D}_{i-1}(s)} |g_{i-1,i}(m,n)|^2 > \frac{2^R-1}{P_{tot}/N_0}\,|\mathcal{D}_{i-1}(s)|\right] \\ &= \left(\frac{\gamma\left(|\mathcal{D}_{i-1}(s)|\,,\frac{2^R-1}{2P_{tot}/N_0}\,|\mathcal{D}_{i-1}(s)|\right)}{\Gamma(|\mathcal{D}_{i-1}(s)|)}\right) \end{aligned} \quad (4.27)$$

and the probability of decoding set $\mathcal{D}_i(s)$ is:

$$\begin{aligned} Pr_{STC}\left[\mathcal{D}_i(s)\right] &= \prod_{n\in\mathcal{D}_i(s)} \frac{\gamma\left(|\mathcal{D}_{i-1}(s)|\,,\frac{2^R-1}{2P_{tot}/N_0}\,|\mathcal{D}_{i-1}(s)|\right)}{\Gamma(|\mathcal{D}_{i-1}(s)|)} \\ &\quad\times\prod_{n\notin\mathcal{D}_i(s)}\left(1-\frac{\gamma\left(|\mathcal{D}_{i-1}(s)|\,,\frac{2^R-1}{2P_{tot}/N_0}\,|\mathcal{D}_{i-1}(s)|\right)}{\Gamma(|\mathcal{D}_{i-1}(s)|)}\right) \end{aligned} \quad (4.28)$$

The link capacity between RS $i-1$ and i can be obtained by substituting equations (4.28) and (4.26) into equation (4.25).

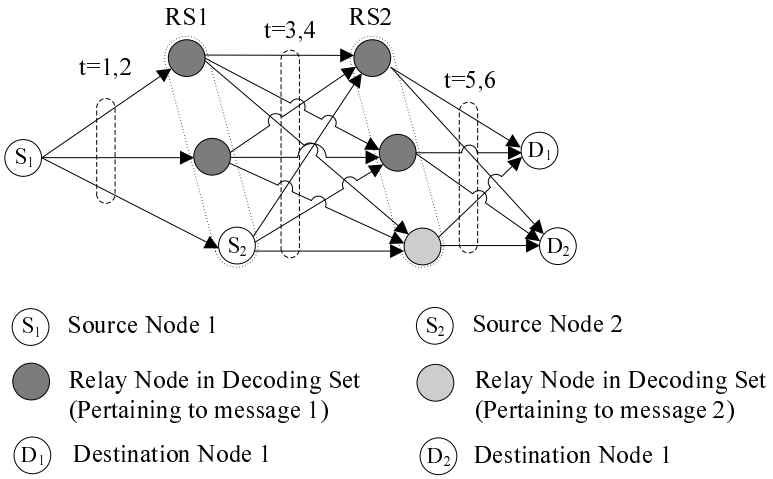

Figure 4.12: Successive Dirty Paper Coded Relay Network System Diagram

4.3.5 A Novel Strategy for Cooperative Relaying

It was shown that the presence of interference can be prevented from reducing channel capacity, as long as the interference (and the global channel knowledge for the case of fading channel) is fully known at the transmitter. This concept is known as Dirty Paper Coding and was initially proposed by Costa [2]. Exploiting this property into relay transmission case, a Successive Dirty Paper Coding scheme is proposed as a part of the present work.

The scheme can be described as follows. Initially, source node transmits its message to the first RS, and decoding set $\mathcal{D}_1(s)$ is defined, containing all nodes in RS 1 that can decode the message. Among these nodes in $\mathcal{D}_1(s)$, one node is allowed to opt from relaying the message, and transmit its own information instead.

On the next time slot, this node acts as a new source node, and transmits its message to the next RS. During this time slot, other nodes in $\mathcal{D}_1(s)$ also relay their decoded message to the subsequent RS as per normal. However, since the new source node knows exactly the message that the other nodes are going to transmit as well as the global channel state information, this scenario reduces to the case of transmitting message in a channel with known interference, and it has been proven that using dirty paper coding scheme, the capacity is equal to the capacity when the interference is not present [2]. This relaying process is illustrated in Figure 4.12.

It is important to note that this process has a consequence to the other relaying nodes in the decoding set. Firstly, the number of relaying nodes is reduced by one at each stage. Secondly, since the other relaying nodes does not have the knowledge of the information transmitted by the new source node, interference will be introduced.

From the above argument, one new source node can transmit its message in every RS, hence creating a new relay stream. Since each node is equally probable to be the ultimate destination, the average number of independent messages being relayed can be calculated as:

$$M = \sum_{g=1}^{g_{max}} g \times \frac{(2g-1)}{(g_{max})^2} = \frac{4\,(g_{max})^2 + 3\,g_{max} - 1}{6\,g_{max}}$$

where g_{max} is the maximum number of relay stages a message can go through to reach destination. Moreover, since the capacity between RS $i-1$ and i depends on the decoding set $\mathcal{D}_{i-1}(s)$, using the same argument as the one used in equations (4.21) and (4.25), and considering the average number of independent relayed messages calculated earlier, the link capacity can be expressed as:

$$C_{SDPC\_i} = M \times \sum_{\mathcal{D}_{i-1}(s)} \left(Pr_{SDPC}\left[\mathcal{D}_{i-1}(s)\right] \times C_{SDPC\_i}(\mathcal{D}_{i-1}(s))\right) \tag{4.29}$$

where subscript SDPC is used to indicate Successive Dirty Paper Coding scheme.

Under this scheme, the capacity between RS $i-1$ and i given decoding set $\mathcal{D}_{i-1}(s)$ is:

$$C_{SDPC\_i}(\mathcal{D}_{i-1}(s)) \;=\; log_2\left(1 + \frac{P_{tot} \times \sum_{\substack{m\in\mathcal{D}_{i-1}(s)\\ m\neq s'}} |h_{i-1,i}(m)|^2}{N_0\;(|\mathcal{D}_{i-1}(s)|-1) + P_{tot}\;|h_{i-1,i}(s')|^2}\right) \tag{4.30}$$

The above expression is a direct consequence that one node from the decoding set $\mathcal{D}_{i-1}(s)$ (denoted as s') transmits its own message, hence introduces interference rather than relays the previously decoded message. Again, the use of orthogonal space-time code design is assumed in this case.

The derivation of the probability that a node n in RS i is joined to $\mathcal{D}_i(s)$ is not straightforward in this scenario, due to the existence of two random variables in the numerator and denominator of the logarithmic argument. However, it can be shown (Appendix C) that the probability is expressed as:

$$Pr_{SDPC}[n \in \mathcal{D}_i(s)] = \begin{cases} \gamma\left(1, \frac{2^R-1}{2P_{tot}/N_0}\right), & i = 1 \\ 1 - \frac{(2^R-1)\times\left(exp\left[\frac{(|D_{i-1}(s)|-1)}{2P_{tot}/N_0}\right]-1\right)}{\left(2+\frac{1}{(2^R-1)}\right)^{|D_{i-1}(s)|-1}}, & i > 1 \end{cases} \tag{4.31}$$

Here, when $i = 1$, the probability is identical to equation (4.27) with only one node in the decoding set (the original source node itself); whereas for $i > 1$, interference from the new source node in the decoding set is introduced, therefore the capacity is different. It is worth noting that for the case when $i = 1$, there may be other message being relayed to its destination. However, since that message is known by the source node, using DPC property, its capacity expression is identical to the interference free case given in equation (4.27).

The probability of decoding set $\mathcal{D}_i(s)$ can then be expressed as:

$$\begin{aligned} Pr_{SDPC}\left[\mathcal{D}_i(s)\right] = & \prod_{n \in \mathcal{D}_i(s)} Pr[n \in \mathcal{D}_i(s)] \\ & \times \prod_{n \notin \mathcal{D}_i(s)} \left(1 - Pr[n \in \mathcal{D}_i(s)]\right) \end{aligned} \tag{4.32}$$

where $Pr[n \in \mathcal{D}_i(s)]$ is as defined in equation (4.31). Finally, link capacity between RS $i-1$ and i is obtained by substituting equations (4.32) and (4.30) into equation (4.29).

4.3.6 Performance Comparisons

In this section, the performance of different relaying schemes is compared. For simplicity of exposition, the system is considered for $R = 1$ bit/sec/Hz transmission rate, and density of 2 nodes per unit area. More generally, the results can be readily updated to incorporate different

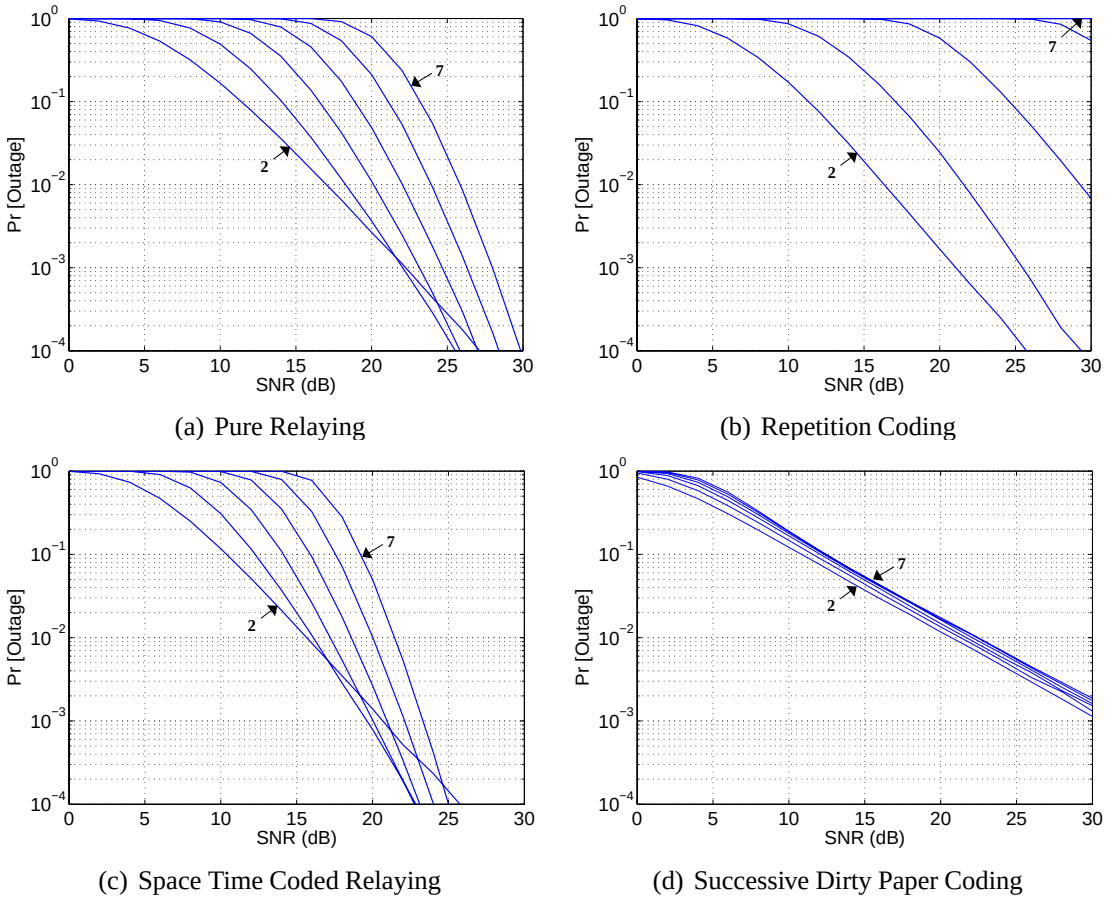

(a) Pure Relaying (b) Repetition Coding

(c) Space Time Coded Relaying (d) Successive Dirty Paper Coding

Figure 4.13: Outage probabilities of different relaying schemes

network conditions. Figure 4.13 shows the outage probability curves of different schemes described earlier. In order to analyse the outage probability, the capacity of different relaying schemes are calculated according to equation (4.19), with the link capacity from RS $i-1$ to i calculated using equation (4.20), (4.21), (4.25), or (4.29), depending whether Pure Relaying, Repetition Coding Decode and Forward Relaying, Space Time Coded Relaying, or Successive Dirty Paper Coded Relaying is used respectively. By calculating the capacity for different random channel realisations, and analysing the percentage of times that the capacity is less than the target rate (which in this case is equal to 1 bit/sec/Hz), the outage probability can be obtained accordingly. Different maximum relaying stages ranging from 2 to 7 are considered, and the performance is evaluated from $SNR = 0$ to 30dB.

As a baseline of comparison, let's first consider the pure relaying case depicted in Figure 4.13(a). It is evident that as the relay stage increases, higher SNR is required for reliable transmission, which is observed from the right-shift in outage curve as the number of maximum relay stage is increased. This is due to bandwidth efficiency penalty of relaying, as more time slots are required for a message to reach its destination.

Under repetition code relaying, a number of nodes in the decoding set on each RS sequentially repeat the message to the next RS. On one hand, this will provide better signal quality for the subsequent RS as a form of diversity, where multiple copies of the same message is received at different time slots. On the other hand, this process further reduces bandwidth efficiency as more time slots are required to relay message from one RS to the next RS. From Figure 4.13(b), it is observed that the penalty outweighs the diversity advantage, which is depicted by a larger right-shift in outage curve as the maximum relay stage is increased.

Space time coded relaying exploits spatial diversity across different relay nodes to gain advantage while eliminating the need for multiple relay slots. This is achieved via cooperation and joint decoding among relay nodes in the decoding set. As shown in Figure 4.13(c), this scheme is able to reduce bandwidth efficiency penalty as compared to the non-cooperation case. However, the shift on the outage curve is still observed as the maximum relay stage is increased.

Figure 4.13(d) shows the outage probabilities of the SDPC scheme. In contrast to Figure 4.13(a-c), the curves are far less sensitive to the maximum relay stage parameter. This signifies the robustness of the scheme to be implemented in a network with large relay stages/coverage. However, the complexity of SDPC is much higher than that of the other three schemes. Figure 4.14 shows different outage probability performances evaluated at 15dB SNR level, and it is observed that for relay stage larger than 4, successive dirty paper coding outperforms the other relaying schemes.

Despite the advantage, Figure 4.13(d) shows that the gradient/slope of the outage probabil-

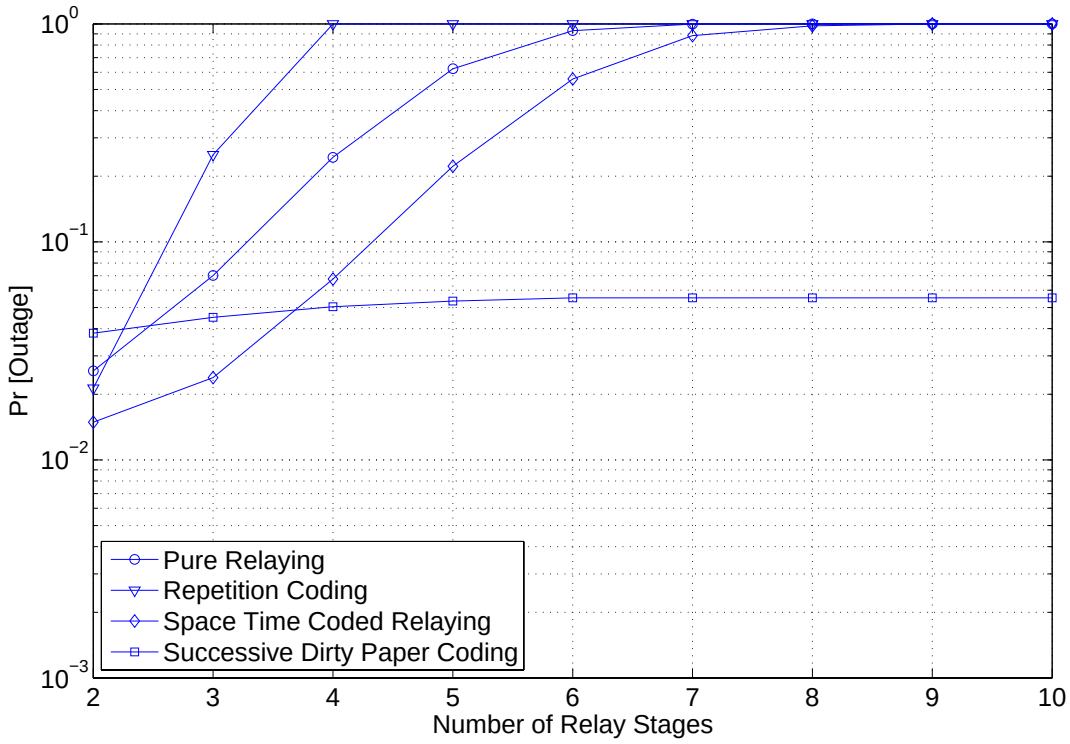

Figure 4.14: Outage probabilities at 15dB SNR

ity curve is not as good as the others. This is due to interference introduced by the new source node on every RS, which prevent the capacity from increasing with respect to SNR. Therefore, although equation (4.29) seems to be superior due to the multiplication factor M, the resultant capacity is not as good due to the interference term in equation (4.30).

4.4 Summary

In this chapter, two issues pertaining to cooperative relay networks are addressed. First, the role of relay node in improving end to end performance is studied. It is shown that adding relay node alone does not guarantee better performance. Appropriate power allocation method has to be used in conjunction to the additional relay node, and it is a necessary condition to ensure end to end performance improvement. Optimal power allocation method is then proposed, which minimises average probability of error at the destination. The scheme makes use of

a relatively slow varying second order statistics of the channel, hence its implementation in practical systems can be justified.

By using simple decode and forward relaying with optimal power allocation, one can obtain up to 2.5 dB performance gain. The ideal RN location using this scheme is at the middle point between SN and DN. When RN is moved away from middle point between SN and DN, the gain diminishes to approximately 1 dB. For *ideal* DSTBC scheme, up to 6 dB gain is observed at 10^{-2} BER level. This is mainly contributed from higher diversity order achieved. Moreover, BER can be made arbitrarily low by moving RN closer to DN, which is possible due to *ideal* assumption that the channel quality from SN to RN is very good, and perfect channel estimation is available at RN such that it is able to decode the message perfectly. In practical DSTBC scheme, significant performance gain is only available when RN is close to SN, in which case the same diversity order as the ideal scenario is achieved. Here, optimum power allocation can bring about additional 2 dB gain. However, as RN moves away from SN, the SN-RN link quality degrades, and therefore bring the overall performance down.

The second issue addressed in this chapter is the inherent problem of interference in multi hop transmission. To eliminate interference, only one message is allowed to be transmitted at every time slot, which severely degrade the bandwidth efficiency of the system. A novel relaying scheme called Successive Dirty Paper Coding is proposed to address this issue, and its performance is evaluated. For comparison, the study of other existing schemes including pure relaying, repetition coding decode and forward, and space time coded relaying are extended into multiple hops scenario. The average end to end capacities of different schemes are derived and compared. It is shown that significant improvement in outage behavior can be achieved with the proposed scheme, especially when the maximum relay stage (which affects the total number of relay stages required for message transmission) is large.

Chapter 5

Extending Cooperative Communication for Multiple Relays

5.1 Introduction

The discussion on cooperative relaying so far considers the case where source and destination node are fixed and known a priori. Although it is useful in giving a figure on how much performance improvement can be expected out of cooperation in point to point transmission, it does not capture the overall gain when network performance is the metric of interest. In practice, every node in the network is a potential relay as well as a destination node. Moreover, the number of nodes that are able to act as relays is likely to be greater than one. Therefore, even though the network is static and nodes are not mobile, the distances between source, relay, and destination are not fixed. Since different distances would incur different path losses, average performance calculation needs to consider all possible relay and destination node locations in the network.

In this chapter, a generalisation of cooperative relay network is considered. Section 5.2 discusses a scenario of multiple relay nodes to help transmission together with the performance analysis in terms of average outage probability. Then, the situation where the destination node

is not known a priori while the remaining nodes are potential relays is considered in Section 5.3. In the analysis, the network is assumed to be fixed and take a particular structure (the most general case when the network is random and every node can be either the source, relay, or destination node is a subject of discussion in Chapter 6). It can be seen that when a certain traffic pattern is imposed, for example when each node is restricted to communicate only with its immediate neighbour, the average path loss is expected to be smaller. As such, it is apparent that there is a relation between traffic pattern and overall system performance. In addition, the number of potential relay nodes is also affected by the source location, hence traffic origin also plays a significant role in the transmission quality. Performance analysis of cooperative networks in the presence of the above mentioned factors will be studied in Section 5.3. Finally, Section 5.4 ends this chapter with a summary on the results and concluding remarks.

5.2 Outage Probability Analysis of Multiple Relay Cooperative Networks

The existence of relay node can help to improve transmission quality by providing extra diversity gain at the destination. Therefore, as the number of available relay nodes increases, it is expected that the end to end performance also improves. However, compared to the diversity gain in MISO and MIMO systems, the number of diversity branches in cooperative relay network depends largely on the channel quality. This is due to the fact that only relay nodes which can reliably decode the source message are able to forward it further to destination. In this section, the relationship between the number of available relay nodes, channel quality, and the overall performance is characterised. For this purpose, exact outage probability expression of the system is derived, and the corresponding numerical results are presented.

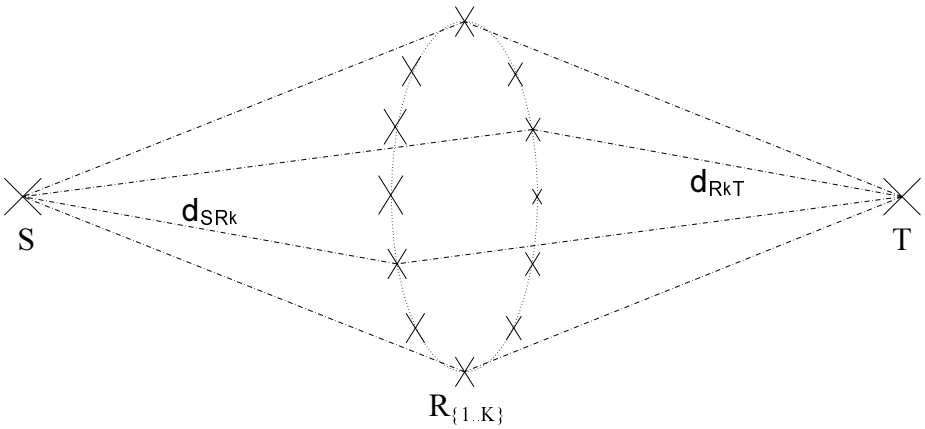

Figure 5.1: Point To Point Network

5.2.1 System Model

Here, source node S and destination node T are assumed to be fixed. K relay nodes (denoted as $R_k, k \in \{1..K\}$) are then positioned between S and T, such that $d_{SR_k} = d_{SR}, d_{R_kT} = d_{RT}, \forall k$. Figure 5.1 shows one possible relay configuration that satisfies this. The purpose of this idealistic setting is to show that even in this simplified scenario, the statistical situation can be quite complex as the number of relay nodes who actually help transmission is random. Moreover, the technique used to derive average outage expression under this setting can be viewed as the basis for deriving the average outage expression of other types of network.

In point to point network, transmission from S to T is performed in two time slots. In the first time slot, S broadcasts its message to all other nodes. At the following slot, relay nodes which are successful in decoding the message (denoted as decoding set $\mathcal{D}$) transmit the decoded message to T. At the destination, message from both slots are combined and passed through decision device to recover the message from S.

Channel gain between S to R_k and between R_k to T are denoted as h_{SR_k} and h_{R_kT}; and they are modelled as flat Rayleigh fading with variance $\sigma^2_{SR} \leq 1$ and $\sigma^2_{RT} \leq 1$ respectively. This constraint on channel variance implies that the channel could not introduce additional energy, which is true in practice as path loss phenomena would cause the received signal's power to

be always less than the transmitted power. The actual value of fading variance is determined by the separation distance through the path loss equation as expressed in equation (4.2) and reproduced in the following for clarity:

$$L_p = 10 \log \left(1/\sigma^2\right) = C_1 \ + \ 10\,\alpha \log\left(d\right) \ + \ \chi \tag{5.1}$$

where C_1, α, d, and χ are the path loss at reference distance, path loss exponent, separation distance, and shadow fading as defined in the previous chapter.

5.2.2 Outage Probability Calculation

According to Shannon's theorem of reliable communication, transmission from S to R_k is successful if the transmission rate satisfies $2R = R' < \log\left(1 + \rho|h_{SR_k}|^2\right)$. Here, ρ is the transmitter Signal to Noise Ratio (SNR), R denotes effective end-to-end rate, while R' is the required per-hop rate to maintain R. The factor of two multiplication above is to ensure a fair comparison with direct transmission case. Since the transmission scheme under consideration is performed in two stages, the per-hop rate has to be twice as large to achieve the same level of end-to-end rate as that in direct transmission. Using the same approach as in [108], the number of relay nodes that are able to decode successfully is random and follows binomial distribution. The probability that there are precisely k relay nodes in the correctly decoding set is expressed as:

$$Pr(|\mathcal{D}| = k) = C_k^K \left[e^{\left(-\frac{2^{2R}-1}{\sigma_{SR}^2\rho}\right)}\right]^k \left[1 - e^{\left(-\frac{2^{2R}-1}{\sigma_{SR}^2\rho}\right)}\right]^{K-k} \tag{5.2}$$

where $|.|$ and C_k^K denotes cardinality (not to be confused with the absolute operation used in channel gain) and combination operation respectively. The above expression follows directly from the fact that $|h_{SR_k}|^2$ is exponentially distributed with variance σ_{SR}^2.

At the second slot, T combines the signal from S and all nodes in $\mathcal{D}$. Using match filter

bound, the maximum channel capacity is:

$$C(\mathcal{D}) \leq \log\left(1+\rho\left(|h_{ST}|^2+\sum_{R_k\in\mathcal{D}}|h_{R_kT}|^2\right)\right) \tag{5.3}$$

and the point to point (p2p) outage probability $P_{out}^{(p2p)}(\mathcal{D})$ at T is:

$$P_{out}^{(p2p)}(\mathcal{D}) = Pr\left(|h_{ST}|^2+\sum_{R_k\in\mathcal{D}}|h_{R_kT}|^2 \leq (2^{2R}-1)/\rho\right) \tag{5.4}$$

From the above, it can be seen that the first term $|h_{ST}|^2$ is exponentially distributed with variance σ_{ST}^2. Assuming that channel variances of all relay nodes are identical, the second term $\sum_{R_k\in\mathcal{D}}|h_{R_kT}|^2$ is chi square distributed with $2|\mathcal{D}|$ degree of freedom and variance $\sigma_{RT}^2/2$, whose cumulative distribution function (CDF) is in the form of regularised gamma function $\gamma(x/\sigma_{RT}^2,|\mathcal{D}|)/\Gamma(|\mathcal{D}|)$.

Since $|\mathcal{D}|$ always takes integer value, the CDF can be rewritten as:

$$Pr\left(\sum_{R_k\in\mathcal{D}}|h_{R_kT}|^2 \leq x\right) = 1-\sum_{i=0}^{|\mathcal{D}|-1}\frac{x^i}{i!(\sigma_{RT}^2)^i}e^{-x/\sigma_{RT}^2} \tag{5.5}$$

The joint CDF of the first and second term can then be found using standard procedure by integrating conditional CDF of the second term with respect to the distribution of the first over a valid range. Denoting $U=\frac{(2^{2R}-1)}{\rho}$ and $V=\frac{(\sigma_{RT}^2-\sigma_{ST}^2)}{(\sigma_{ST}^2\sigma_{RT}^2)}$, equation (5.4) reduces to:

$$\begin{aligned}P_{out}^{(p2p)}(\mathcal{D}) = {} & 1-e^{-U/\sigma_{ST}^2} \\ & -\sum_{i=0}^{|\mathcal{D}|-1}\frac{e^{-U/\sigma_{RT}^2}}{i!\sigma_{ST}^2(\sigma_{RT}^2)^i}\sum_{l=0}^{i}\frac{C_l^i(-1)^l U^{i-l}l!}{V^{l+1}}\left[1-\sum_{m=0}^{l}e^{-UV}\,(UV)^m/m!\right]\end{aligned} \tag{5.6}$$

The above formula has an interesting interpretation. The first two terms $1-e^{-U/\sigma_{ST}^2}$ is nothing but the outage probability of the direct link, while the third one is the improvement that relay

nodes contribute. Finally, the unconditional outage probability is:

$$P_{out}^{(p2p)} = \sum_{k=0}^{K} Pr(|\mathcal{D}| = k) P_{out}^{(p2p)}(\mathcal{D}) \tag{5.7}$$

which can be calculated using equations (5.2) and (5.6).

5.2.3 Numerical Results

Throughout the analysis, the largest channel variance between any given two nodes is normalised to unity. Following the system model considered for the analysis, the relay nodes are located at the middle section between source and destination, such that source destination distance is twice as large as the source-relay or relay-destination distance. As far as the path loss model is concerned, path loss exponent of 3 is assumed, and the path loss measured at reference distance is set to -32.45dB, which is a typical value for urban terrain [165]. The log normal shadow fading variance is set to 3dB, and the target end-to-end spectral efficiency is 1 b/s/Hz. Equivalently, the required per-hop spectral efficiency is 2 b/s/Hz.

Figure 5.2 shows the outage performance in point to point network calculated using equation (5.7) for total number of relay nodes $K = 0$ to $K = 30$ with 5 increment. As expected, the outage performance improves as the number of relay nodes increases due to higher diversity order. Similar to MIMO systems, diversity gain diminishes as the number of relay nodes becomes too large. This suggests that deploying too many relay nodes may not be required since most of the improvement is achieved by the first few increments on available relay nodes.

From the figure, significant improvement is observed when the number of relay nodes is increased from 0 (direct transmission) to 5. Further improvement is still observed when the number of relay nodes is increased to 10, and any further addition only gives marginal improvements. Hence, in practical scenario, deploying not more than 10 relay nodes is more likely to find acceptance.

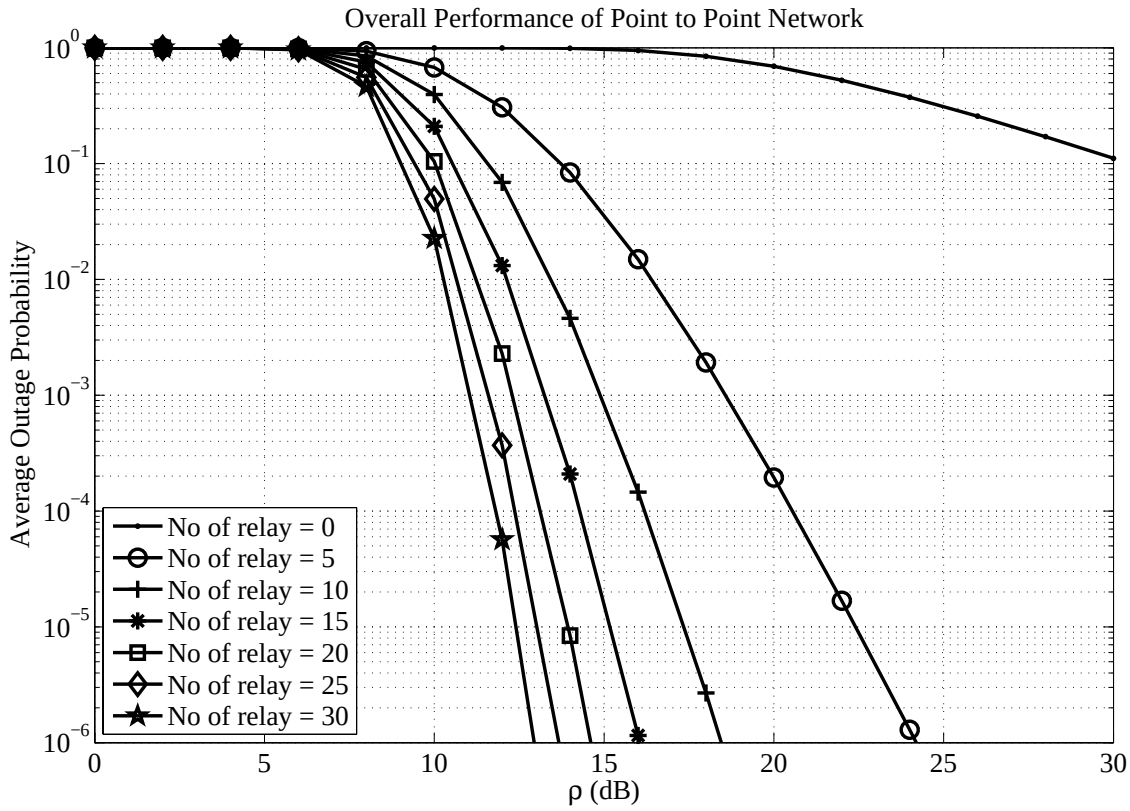

Figure 5.2: Outage Performance of Cooperative Relay Network with Multiple Relays

5.3 Generalisation when Destination Node is Not Known A Priori

In a more realistic scenario, different nodes are located in a planar area. Therefore the assumption that all relays are located at equal distance with respect to either source or destination node can no longer be used. Moreover, every other node except the source has equal probability to be the destination of any transmission. Hence performance evaluation must be averaged across all possible destination locations. In the present analysis, a network with regular structure whereby nodes are located at lattice points is considered. This will simplify the distance calculation between any given two nodes, which is necessary to characterise the path loss attenuation. At the same time, the relationship between lattice parameters and the overall performance can be analysed.

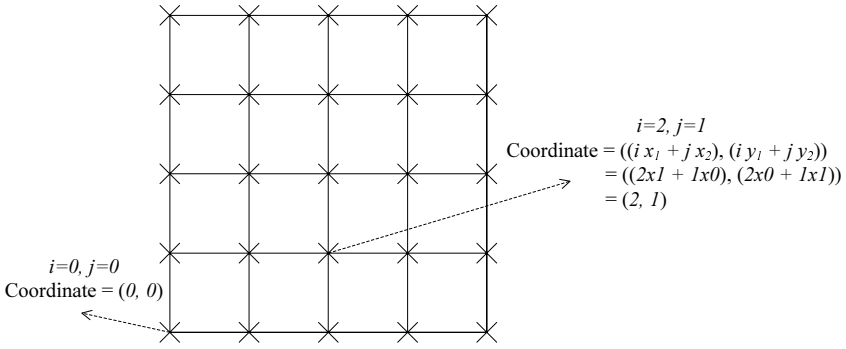

Figure 5.3: Example of (1,0), (0,1), 5 Lattice Network

5.3.1 System Model

A lattice is characterised by three parameters, namely (x_1, y_1), (x_2, y_2), and N. Any point location in the lattice can be decomposed into $((i\,x_1 + j\,x_2),\ (i\,y_1 + j\,y_2))$, where integer $i, j \in 0..N-1$. An example of lattice network with $(x_1, y_1) = (1, 0)$, $(x_2, y_2) = (0, 1)$, and $N = 5$ is shown in Figure 5.3.

There are two reasons why lattice is used in the present analysis to model a planar network. Firstly, there are situations in practical scenarios where lattice comes as a natural model that best approximate node placements in the network, such as cooperative robotics in the factory sites that are placed in a regular grid, or sensor nodes that are deployed in the field to monitor soil condition in different patches of a farm. Secondly, the regular structure of lattice greatly simplifies the calculation of path loss, since the distance d_{PQ} between any given two points (denoted as P and Q) in a lattice, which is located at $((P_i\,x_1 + P_j\,x_2),\ (P_i\,y_1 + P_j\,y_2))$ and $((Q_i\,x_1 + Q_j\,x_2),\ (Q_i\,y_1 + Q_j\,y_2))$ respectively, can be easily calculated as follows:

$$d_{PQ} = \sqrt{\left(\delta_i^{PQ} x_1 + \delta_j^{PQ} x_2\right)^2 + \left(\delta_i^{PQ} y_1 + \delta_j^{PQ} y_2\right)^2} \tag{5.8}$$

where $\delta_i^{PQ} = (Q_i - P_i)$ and $\delta_j^{PQ} = (Q_j - P_j)$. The corresponding variance can then be calculated using path loss equation in (5.1).

Without loss of generality, it is assumed that the variance of channel gain between two

closest lattice points is normalised to unity, therefore the constraint $\sigma^2_{PQ} \leq 1$ is valid for all P and Q. This is due to the fact that path loss will degrade signal power, such that the received power is always less than the transmitted power (as a consequence, the channel variance is always less than unity).

5.3.2 Outage Probability Calculation

As argued earlier, the point to point model considers fixed source and destination, therefore traffic pattern is irrelevant in such setting. Moreover, due to the idealistic assumption that all relay nodes are located equidistance with respect to both source and destination node, the channel variances are identical. As such, the conditional outage probability only depends on the size of $\mathcal{D}$ rather than its composition.

A more practical and realistic model is a planar network with nodes placed in regular lattice points. Let nodes be indexed as $P^{(k)}$ (where $k \in 1..N^2$) with arbitrary ordering, and let the union be $\mathcal{P}$. Given source S, there are $N^2 - 2$ potential relay nodes in the network (all except S and T). The probability that a subset $\mathcal{D} \subset \mathcal{P} - \{S, T\}$ are able to decode the source message is given by:

$$Pr(\mathcal{D}) = \prod_{P^{(k)} \in \mathcal{D}} e^{-\frac{2^{2R}-1}{\sigma^2_{SP^{(k)}}\rho}} \times \prod_{P^{(k)} \in \mathcal{P}-\{\mathcal{D},S,T\}} 1 - e^{-\frac{2^{2R}-1}{\sigma^2_{SP^{(k)}}\rho}} \tag{5.9}$$

where $\sigma^2_{SP^{(k)}}$ is determined by path loss pertaining to the distance from $P^{(k)}$ to S, which can be calculated by equations (5.1) and (5.8).

Generally, destination T can be located anywhere in the network. However, in some cases such as very large networks, it might be desirable to impose certain constraint where source node S is allowed to send message only to those nodes which are within its vicinity. This type of constraint is better known as traffic locality. In mathematical terms, it can be stated that S is only allowed to send message to T where $max(\delta_i^{ST}, \delta_j^{ST}) \leq l$, and $1 \leq l \leq N$.

It can be seen that $l = N$ means that there is no traffic locality imposed, as all other nodes

in the network can become the destination. On the other extreme, when $l = 1$, source node can only send message to its immediate neighbour. It has been previously shown in [170] that in interference limited network where several nodes simultaneously transmitting, the optimal strategy is for each node to transmit to only its immediate neighbour. However, no cooperation strategy is considered in their work. This work is motivated to analyse whether the same trend is observed in planar lattice network with cooperation between nodes.

Using the same approach as in point to point case, after two slot transmissions, T combines the message from S and $\mathcal{D}$. The resulting channel capacity and outage probability is then similar to that in equations (5.3) and (5.4) respectively, with an exception that channel variance $\sigma^2_{P^{(k)}T}$ are distinct for different k (due to different distances and considering log normal shadow fading).

The governing conditional outage probability is then characterised by CDF of a sum of exponential random variables with distinct variances. Denoting again $U = (2^{2R} - 1)/\rho$, it can be shown that the outage probability $P^{(Lat)}_{out}(\mathcal{D}, T)$ is expressed as:

$$P^{(Lat)}_{out}(\mathcal{D}, T) = \sum_{k:P^{(k)} \in \{\mathcal{D}, S\}} (1 - e^{-U/\sigma^2_{P^{(k)}T}}) \prod_{\substack{j\,:\,P^{(j)} \in \{\mathcal{D}, S\} \\ j \neq k}} \frac{\sigma^2_{P^{(k)}T}}{(\sigma^2_{P^{(k)}T} - \sigma^2_{P^{(j)}T})} \tag{5.10}$$

It can be seen from the above that given empty set $\mathcal{D}$, conditional outage probability reduces to $1 - e^{-U/\sigma^2_{ST}}$, which is the performance of direct transmission.

Defining $\mathcal{B}_l = \{T : max(\delta^{ST}_i, \delta^{ST}_j) \leq l\}$ as a set of nodes to which S is allowed to communicate, the unconditional outage probability can be expressed as:

$$P^{(Lat)}_{out} = \sum_{T \in \mathcal{B}_l} \frac{1}{|\mathcal{B}_l|} \sum_{\mathcal{D}} Pr(\mathcal{D}) P^{(Lat)}_{out}(\mathcal{D}, T) \tag{5.11}$$

which can be calculated using equations (5.9) and (5.10).

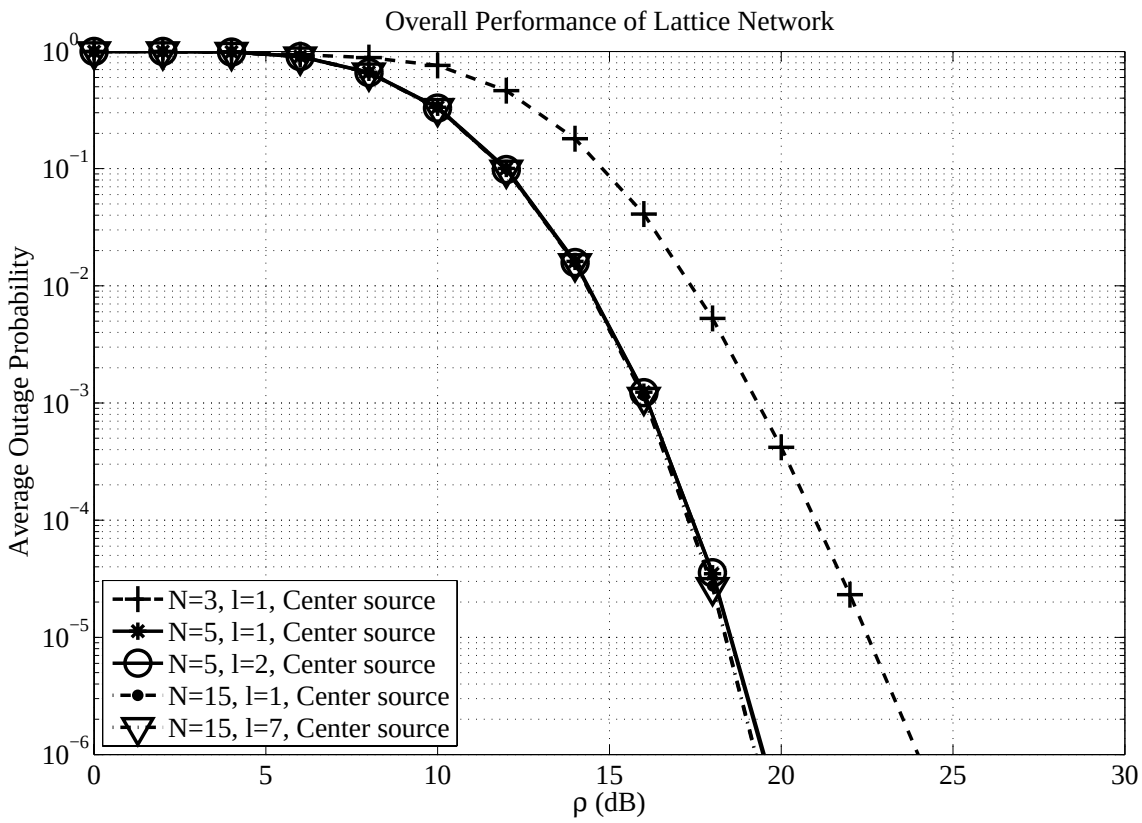

Figure 5.4: Effect of traffic locality in Lattice Networks (N=lattice size, l=traffic locality)

5.3.3 Numerical Results

In lattice network, there are more degrees of freedom which influence system performance. Figure 5.4 shows the average outage probability of lattice network calculated using equation (5.11) for different lattice sizes when source is located at the centre. It is observed that increasing network size (number of nodes) can be beneficial, especially when N is small. However, this quickly saturates as N grows, which again attributed from diversity behaviour. It can be seen from the figure that approximately 5dB improvement at 10^{-6} outage level is attained when network size is increased from $N = 3$ to $N = 5$; and further increasing the network size does not bring any improvement.

Comparing Figure 5.4 and Figure 5.2, it is interesting to see that the performance of lattice network for $N = 3$ is close to that in point to point network for $K = 5$, even though the

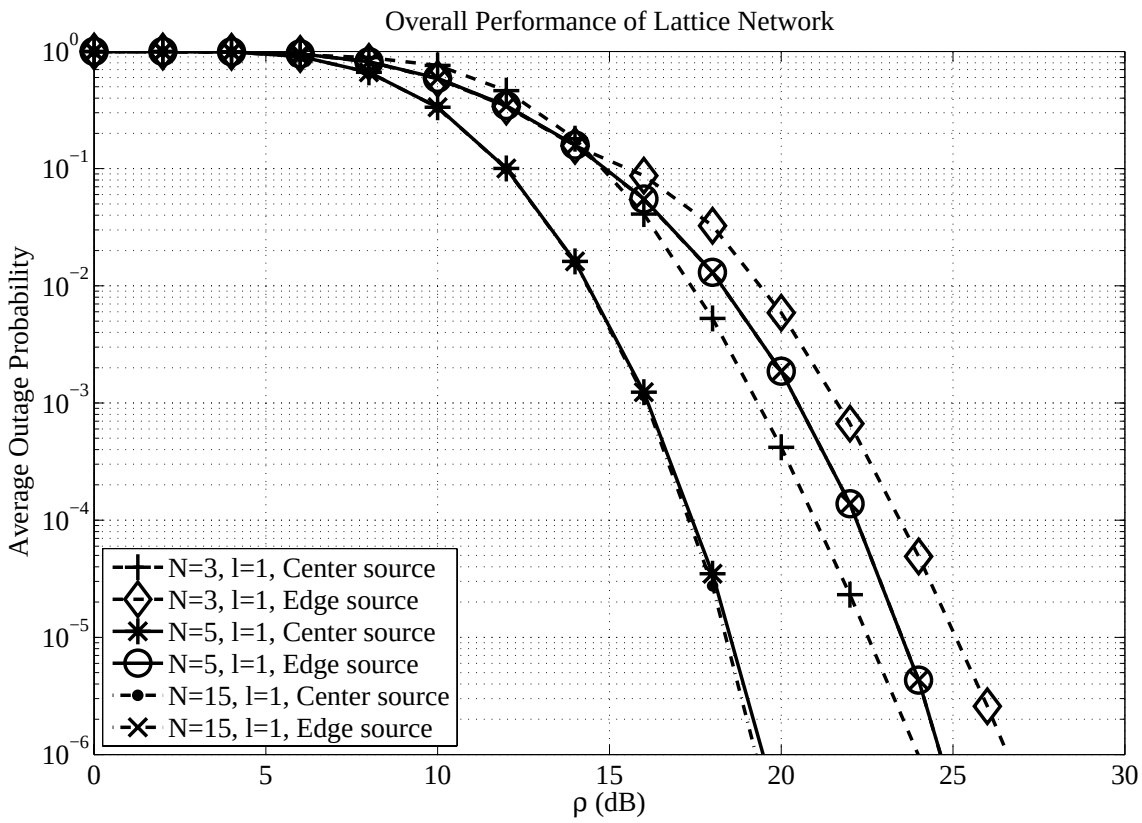

Figure 5.5: Effect of traffic origins in Lattice Networks

number of potential relay nodes in lattice network is larger ($N^2 - 2 = 7$ nodes). This is due to the structure of lattice network, such that some of the relay nodes are further away from destination; hence their contribution towards overall performance is limited. Similar result is observed for larger lattice networks with $N \geq 5$, which exhibit the same performance as point to point network with $K = 10$. This signifies the fact that only certain portion of potential relay nodes is important in improving the overall performance, and this number converges to a constant value as network size grows.

Figure 5.4 also shows the influence of traffic locality, whereby $l = 1$ and $l = 2$ is considered for $N = 5$; while $l = 1$ and $l = 7$ is considered for $N = 15$ (l denotes the maximum hops away a destination is allowed from the source). As opposed to the interference limited networks considered in [170], traffic locality does not have any influence towards system performance in cooperative lattice network.

Another traffic pattern considered in this study is traffic origins. Since the network is co-operative network, the number of nodes in the vicinity of source node plays significant role in determining the number of potential helper nodes. Hence, it is expected that traffic origins affect the overall performance.

Figure 5.5 shows the average outage probability for different network sizes. Two extreme scenarios of traffic origins are considered, namely when the source node is located at the lattice centre, and when it is located at the lattice corner. Approximately 3dB degradation for lattice size of $N = 3$ is observed when traffic origin is set to lattice corner as compared to the case when it is located at the centre. Larger degradation (up to 5dB) is observed for larger lattice sizes ($N \geq 5$), which conforms to the earlier analysis that the number of potential helper nodes surrounding source node plays an important role in the overall performance.

5.4 Summary

In this chapter, a closed form expression of average outage probability in cooperative network is derived for point to point network and planar lattice network. In point to point scenario, it is demonstrated that the performance is solely determined by the number of relay nodes, whereby more relay nodes results in better performance. It is also shown that performance improvement diminishes as the number of relay increases, whereby no further improvement is observed when N is increased beyond 5. This is due to the saturated diversity gain as the number of diversity branches (contributed from different relay nodes) increases.

For planar lattice network, the effect of traffic pattern, namely traffic locality and traffic origins, are studied. It is demonstrated that traffic locality does not have any significant impact towards overall performance. Meanwhile, traffic origins play an important role, in which source nodes at the network edge exhibit worse performance. This shows that the diversity gain is more influential than path loss in average outage probability. Since less nodes are available when the source is located at the edges, the performance degradation is inevitable.

Chapter 6

Cooperative Communication in Random Networks

6.1 Introduction

In the most general case where cooperative network is not bound to have any particular structure, each node can be randomly placed within the network. This scenario is found in typical sensor networks, where multiple sensor nodes are randomly placed in a certain area to collect site specific data. Another possible application where the network is best modelled as random network is ad-hoc network. In certain cases of ad-hoc networks, it is necessary to impose mission-specific constraints on node design. For example, in ad-hoc networks for disaster recovery purposes or military applications, low power consumption and small form factor is a desirable feature. In such cases, deploying multiple antennas in a single node introduces many practical constraints, and single-antenna node is a more preferable choice. Cooperative communication is attractive in such networks, as it allows the network to exploit the available diversity gain despite the resource limitation on their individual nodes.

Practically, every node in the network is identical, and they have equal probability to be the source, relay, or destination of any transmission. This, together with the fact that each node

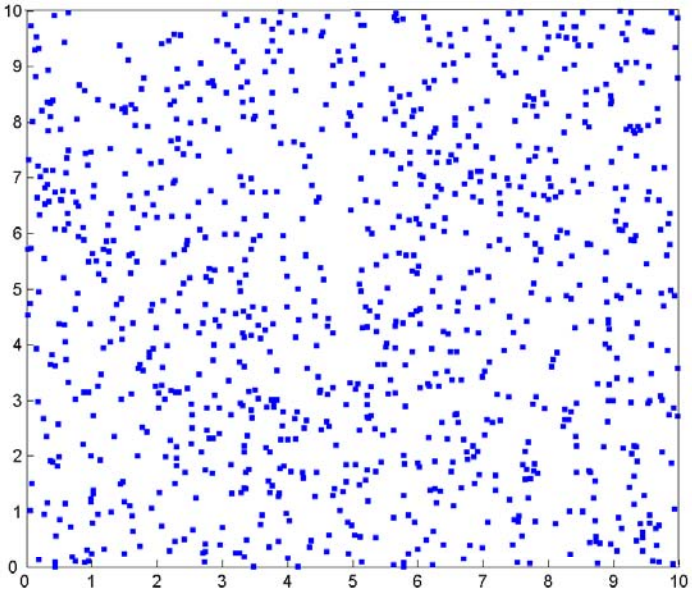

Figure 6.1: Example for Network Topology of a square network with $L = 10$ km $M = 1000$ nodes

can be located anywhere within the network, makes performance analysis difficult. The performance analysis has to be averaged across all possible source, relay, and destination location within the network. In this chapter, a scheme to analyse the average performance of cooperative random network is developed. Different transmission schemes are considered, and their performances are compared. The influence of network parameters towards overall performance are also studied.

6.2 System Description

A wireless ad-hoc network covering a rectangular geographic area of size L by L is considered. The total number of M single-antenna half-duplex nodes are randomly distributed within the area as shown in Figure 6.1. The network topology in Figure 6.1 leads to the formation of a *random network*, which is defined as a set of nodes uniformly and randomly distributed in a

Figure 6.2: Medium Access Control Structure

planar region of given area. The transmission between two nodes is modelled using discrete time signal model $y = hx + z$, where x and y are the transmitted symbol from source node and the received symbol at destination node respectively. z is the Additive White Gaussian Noise (AWGN) with zero mean and variance N_0, and h is the Rayleigh flat fading gain distributed according to $\mathcal{CN}(0, \frac{1}{\lambda})$, a complex normal distribution with variance $\frac{1}{\lambda}$. The parameter λ captures the path loss effect and macroscopic fading, and it is calculated through the path loss equation as defined earlier.

In the present system, at any one time only one message is allowed to be transmitted. Before transmitting a message, a node should sense the network to check the presence of transmission. This can be done by using collision avoidance technique such as CSMA-CA (Carrier Sense Multiple Access - Collision Avoidance). A node can transmit its message only when there is no transmission taking place, otherwise it will back off and retry after a certain time out. More details on this collision avoidance algorithm is available at [171]. For simplicity, it is assumed that all nodes in the network are able to listen to any transmission going on in the network.

Meanwhile, to guarantee that any message transmission will last for two time slots, one bit indicator is used to differentiate between the first and second slot transmission. This indicator is included in the Medium Access Control header together with the destination address as illustrated in Figure 6.2. When the source transmit a message, bit indicator is set to zero. Whenever a node received a message, the destination address of the message is checked whether it matches with its own address. If it matches, the message is kept for future combining with different copies from potential relay nodes. Otherwise, the receiving node will check the value of bit indicator. If the bit indicator is equal to 0 (which indicates that the message comes directly from the source node), it will try to decode the message. Otherwise the message will

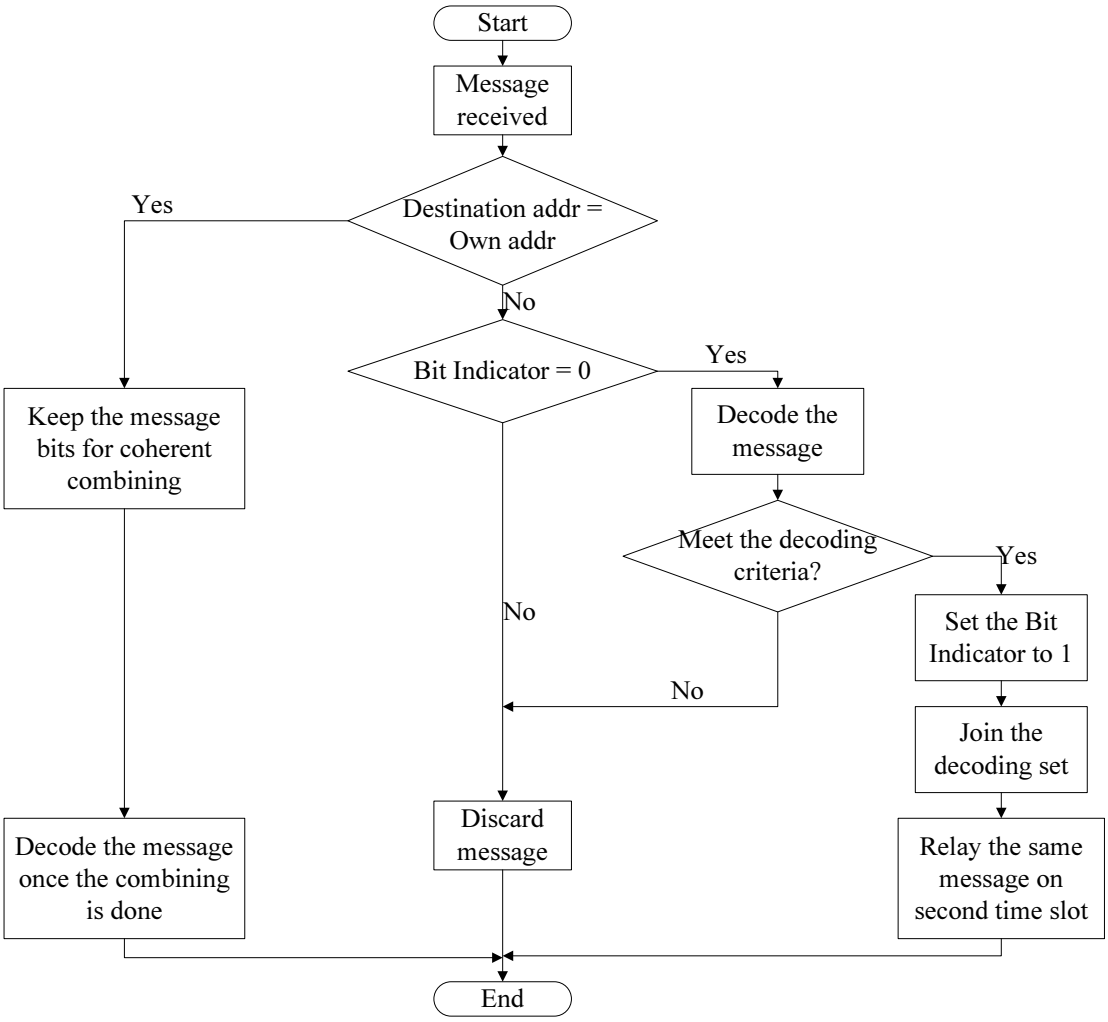

Figure 6.3: Nodes Behaviour Flowchart

be simply discarded. When the decoding process is successful, the receiving node will set the bit indicator to 1, and then join the decoding set which will then forward the message on the next slot. The flowchart illustrating the node behaviour as it receives a message is depicted in Figure 6.3.

6.3 Cooperative Transmission Protocols

Different cooperative schemes considered in the analysis are described in the following sub-sections.

6.3.1 Direct Transmission

As a baseline of comparison, direct transmission is considered, whereby source node transmits its message to its corresponding destination without any help from other nodes. Under direct transmission, destination node employs coherent detection based on the message it received from source node. The instantaneous error probability in this case can then be expressed as: $P_e = \mathcal{Q}\left(\sqrt{\mathcal{R}\frac{\mathcal{E}_s}{N_0}\left|h_{sd}\right|^2}\right)$, where constant $\mathcal{R}$ is determined by the euclidean distance between constellation points, which depends on the modulation order used [171] ($\mathcal{R} = 2$ for BPSK, $\mathcal{R} = 1$ for QPSK, $\mathcal{R} \approx 0.2$ for 16QAM, and so on). Since $\mathcal{Q}(x)$ is a monotonically decreasing function of x, there exists one and only value of $\left|h_{sd}\right|^2 = \varphi$ to achieve a certain threshold value of $P_e^{(thld)}$. Throughout this work, finite alphabet symbol constellation is used, hence the outage probability is defined as the probability that $P_e \geq P_e^{(thld)}$, which is equal to:

$$P_{\text{out}}^{(\text{direct})} = 1 - e^{-\lambda_{sd}\varphi} \tag{6.1}$$

where λ_{sd} is the path loss parameter of source-destination channel. The same approach of outage probability analysis has also been adopted in [172], whereby the distribution of effective received SNR is derived and used to characterise the average error probability (and its upper bound).

6.3.2 Amplify-and-Forward

For amplify-and-forward relaying, the transmission of one message requires two time slots. On the first time slot, source node broadcasts its message, and both relay and destination nodes listen. The received symbol at relay and destination node can be expressed as follows:

$$\begin{aligned} y_r &= h_{sr}\, x_s + z_r \\ y_d^{(1)} &= h_{sd}\, x_s + z_d^{(1)} \end{aligned} \tag{6.2}$$

Here, h_{sr} and h_{sd} are the channel gain from source to relay and from source to destination respectively, and they are distributed according to parameter λ_{sr} and λ_{sd}, which are in turn determined by source, relay, and destination separation. Upon receiving a message from the source, relay node will forward whatever it received to the destination. In order to satisfy the power constraint, normalisation is performed as follows:

$$x_r = \frac{y_r \sqrt{\mathcal{E}_s}}{\sqrt{E\left[|y_r|^2\right]}} = \frac{y_r}{\sqrt{|h_{sr}|^2 + \frac{N_0}{\mathcal{E}_s}}} \tag{6.3}$$

On the second time slot, relay node forward the scaled message x_r to the destination, and the received symbol at destination can be expressed as:

$$\begin{aligned} y_d^{(2)} &= h_{rd}\, x_r + z_d^{(2)} = h_{rd} \frac{y_r}{\sqrt{|h_{sr}|^2 + \frac{N_0}{\mathcal{E}_s}}} + z_d^{(2)} \\ &= \frac{h_{sr}\, h_{rd}\, x_s}{\sqrt{|h_{sr}|^2 + \frac{N_0}{\mathcal{E}_s}}} + \frac{h_{rd}\, z_r}{\sqrt{|h_{sr}|^2 + \frac{N_0}{\mathcal{E}_s}}} + z_d^{(2)} \end{aligned} \tag{6.4}$$

Upon receiving both $y_d^{(1)}$ and $y_d^{(2)}$, destination node performs Maximum Receive Ratio Combining (MRRC) and decodes the message. It can be shown that the effective SNR after MRRC is given as:

$$\rho_{\text{eff}}^{(\text{AnF})} = \frac{\mathcal{E}_s}{N_0} \left(|h_{sd}|^2 + \frac{|h_{sr}|^2\, |h_{rd}|^2}{|h_{sr}|^2 + |h_{rd}|^2 + \frac{N_0}{\mathcal{E}_s}} \right) \tag{6.5}$$

Coherent detection is then performed on the combined message. The probability of error at the destination can be calculated as $P_e = \mathcal{Q}\left(\sqrt{\mathcal{R}\, \rho_{\text{eff}}^{(\text{AnF})}}\right)$. Note that error probability analysis of two-hop AnF transmission with multiple relay nodes has been done in the past, both under Nakagami-m fading [173] as well as Gaussian fading channel [174].

Finding the outage probability under AnF scheme is not straightforward, due to the difficulty in finding CDF of $\rho_{\text{eff}}^{(\text{AnF})}$. The probability that instantaneous P_e is greater than $P_e^{(thld)}$ is equal to the probability that $\rho_{\text{eff}}^{(\text{AnF})}$ falls below a certain value φ, where φ is the exact value

of $\rho_{\text{eff}}^{(\text{AnF})}$ which make instantaneous P_e equal to $P_e^{(thld)}$. Letting $\rho^* = \frac{\rho_{\text{eff}}^{(\text{AnF})}}{\mathcal{E}_s/N_0}$, its CDF can be expressed as follows (See Appendix D for detailed derivation):

$$F_{\rho^*}(v) = \int_0^v \left(1 - e^{-(\lambda_{sr}+\lambda_{rd})(v-q)} 2\sqrt{\lambda_{sr}\lambda_{rd}(v-q)(v-q+\frac{N_0}{\mathcal{E}_s})} K_1\left(2\sqrt{\lambda_{sr}\lambda_{rd}(v-q)(v-q+\frac{N_0}{\mathcal{E}_s})}\right)\right) \lambda_{sd} e^{-\lambda_{sd} q} dq \quad (6.6)$$

Using the above expression, outage probability can be calculated as:

$$P_{\text{out}}^{(\text{AnF})} = Pr\left[\rho_{\text{eff}}^{(\text{AnF})} \leq \varphi\right] = F_{\rho^*}(\varphi^*) \quad (6.7)$$

where $\varphi^* = \frac{\varphi}{\mathcal{E}_s/N_0}$, and φ is as defined earlier.

It is important to note that under this scheme, the effective throughput is half as much as direct transmission case. Denoting $\mathcal{A}$ as the constellation alphabet, the effective throughput can be expressed as $\frac{log_2(|\mathcal{A}|)}{2}$ bits/symbol duration (i.e. 1 for QPSK and 2 for 16QAM). As a fair comparison between transmission methods, equal throughput or 2 b/s/Hz is always considered. Hence, QPSK is used for direct transmission and 16QAM for all other 2-hop relaying schemes (AnF, D-TxMRC, and DSTBC) is assumed for comparisons, unless otherwise mentioned.

6.3.3 Distributed Transmitter Maximum Ratio Combining (D-TxMRC)

This scheme applies Maximum Ratio Transmission technique [175] for point to point MIMO system into distributed scenario. Since channel powers relative to the destination now vary across different cooperating nodes, modification to the analysis in [175] is needed.

When source node broadcasts its message on the first time slot, received signal at node k can be expressed as:

$$y_k = h_{sk} x_s + z_k \qquad k \in \{1..M\}, k \neq s \quad (6.8)$$

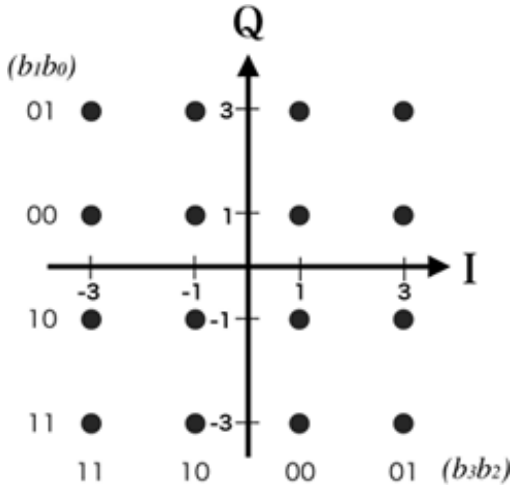

Figure 6.4: 16QAM constellation

where h_{sk} is the channel gain from source s to node indexed k, while x_s and z_k are transmitted symbol from source s with $E[|x_s|^2] = \mathcal{E}_s$, and AWGN at node k respectively. Out of these nodes, some of them would be able to decode the message with high reliability; and for such nodes, the average probability of error is less than a pre-specified threshold value $P_e^{(thld)}$. All such nodes together form a decoding set $\mathcal{D}$. Note that the same concept of decoding set has been used in [108] to indicate potential relay nodes.

The average bit error probability at node k when using 16QAM can then be calculated as:

$$\overline{P_e} = \frac{3}{8}\left[1 - \sqrt{\frac{\rho}{\rho + (10\lambda_{sk})}}\right] + \frac{1}{4}\left[1 - \sqrt{\frac{\rho}{\rho + (\frac{10}{9}\lambda_{sk})}}\right] - \frac{1}{8}\left[1 - \sqrt{\frac{\rho}{\rho + (\frac{2}{5}\lambda_{sk})}}\right] \quad (6.9)$$

where ρ is defined as SNR without fading measured at transmitter ($\rho = \mathcal{E}_s/N_0$). The derivation of equation (6.9) can be explained as follows. 16QAM modulation as depicted in Figure 6.4 is used in the transmission (2 b/s/Hz effective spectral efficiency), and coherent detection is used at the receiver. Since the average symbol energy satisfies $E[|x_s|^2] = \mathcal{E}_s$, the received signal energy can be represented as [171]:

$$E[|y_k|^2] = |h_{sk}|^2 \, \mathcal{E}_s \; + \; N_0 \quad (6.10)$$

Note that in order to maintain an average symbol energy of $\mathcal{E}_s$, each symbol in 16QAM constellation has to use an average amplitude of $\sqrt{\mathcal{E}_s/10}$. From Figure 6.4, it is apparent that bit b_3 and b_2 are only affected by the real part of the noise term, while bit b_1 and b_0 are affected by the imaginary part of the noise for a coherent detection. Moreover, since the real and imaginary parts of the noise are identically distributed, the bit error probability of bit b_3 and b_1 are equal, and they can be expressed as:

$$P_e^{b_1} = P_e^{b_3} = \frac{1}{2}\,\mathcal{Q}\left(\sqrt{\frac{9\,\mathcal{E}_s\,|h_{sk}|^2}{5\,N_0}}\right) + \frac{1}{2}\,\mathcal{Q}\left(\sqrt{\frac{\mathcal{E}_s\,|h_{sk}|^2}{5\,N_0}}\right) \tag{6.11}$$

Similarly, the bit error probability of bit b_2 and b_0 are equal, and they can be expressed as:

$$P_e^{b_0} = P_e^{b_2} = \frac{1}{2}\left(\mathcal{Q}\left(\sqrt{\frac{\mathcal{E}_s|h_{sk}|^2}{5\,N_0}}\right) - \mathcal{Q}\left(\sqrt{\frac{5\mathcal{E}_s|h_{sk}|^2}{N_0}}\right)\right) + \frac{1}{2}\left(\mathcal{Q}\left(\sqrt{\frac{\mathcal{E}_s|h_{sk}|^2}{5\,N_0}}\right) + \mathcal{Q}\left(\sqrt{\frac{9\mathcal{E}_s|h_{sk}|^2}{5\,N_0}}\right)\right) \tag{6.12}$$

The above two equations are direct implication of AWGN noise, in which the probability that the particular bit is in error is equal to the probability that the noise (in a particular dimension) is larger than the distance of the constellation to the decision boundary. Since the noise is normally distributed, this probability can be calculated using right tail probability integral as follows:

$$Pr[z \geq c] = \int_c^{\infty} \frac{1}{\sqrt{\pi\,N_0}}\, e^{\frac{-t^2}{N_0}}\, dt = \mathcal{Q}\left(\frac{c}{\sqrt{N_0/2}}\right) \tag{6.13}$$

The instantaneous bit error probability can then be calculated by averaging the error probability for bit b_3, b_2, b_1, and b_0, resulting in the following expression:

$$P_e = \frac{3}{4}\,\mathcal{Q}\left(\sqrt{\frac{\mathcal{E}_s\,|h_{sk}|^2}{5\,N_0}}\right) + \frac{1}{2}\,\mathcal{Q}\left(\sqrt{\frac{9\,\mathcal{E}_s\,|h_{sk}|^2}{5\,N_0}}\right) - \frac{1}{4}\,\mathcal{Q}\left(\sqrt{\frac{5\,\mathcal{E}_s\,|h_{sk}|^2}{N_0}}\right) \tag{6.14}$$

Now, the remaining task is to integrate the above expression with respect to the distribution of the channel gain. For simplicity, consider integrating a Q-function as follows (note that $|h_{sk}|^2$

is exponentially distributed, and its distribution function can be expressed as $\lambda_{sk}\, e^{-\lambda_{sk}\,|h_{sk}|^2}$):

$$\int_0^\infty \mathcal{Q}\left(\sqrt{\frac{A\,\mathcal{E}_s\,|h_{sk}|^2}{N_0/2}}\right)\,\lambda_{sk}\,e^{-\lambda_{sk}\,|h_{sk}|^2}\,d\left(|h_{sk}|^2\right) \tag{6.15}$$

The constant A can be varied according to the requirement. Denoting and expanding the Q-function, the integration can be performed as follows:

$$\begin{aligned}
\overline{P_e} &= \int_0^\infty \int_{\sqrt{A\,\mathcal{E}_s}}^\infty \sqrt{\frac{s}{\pi\,N_0}} e^{\frac{-\,t^2\,s}{N_0}}\,\lambda\,e^{-\lambda\,s}\,dt\,ds && (6.16)\\
&= \int_{\sqrt{A\,\mathcal{E}_s}}^\infty \frac{\lambda}{\sqrt{\pi\,N_0}} \int_0^\infty \sqrt{s}\,e^{-\left(\lambda+\frac{t^2}{N_0}\right)\,s}\,ds\,dt && (6.17)\\
&= \frac{0.5}{\sqrt{N_0\,\lambda}} \int_{\sqrt{A\,\mathcal{E}_s}}^\infty \frac{1}{(1+\frac{t^2}{N_0\,\lambda})^{3/2}}\,dt && (6.18)\\
&= 0.5\left[1-\sqrt{\frac{1}{1+\frac{N_0\,\lambda}{\mathcal{E}_s\,A}}}\right] && (6.19)\\
&= 0.5\left[1-\sqrt{\frac{\rho}{\rho+\lambda/A}}\right] && (6.20)
\end{aligned}$$

where substitution $\rho = \mathcal{E}_s/N_0$ has been used. Using the same technique for all the three terms in the instantaneous bit error probability of equation (6.14), the average bit error probability as expressed in equation (6.9) is obtained.

The condition that average bit error probability is smaller than $P_e^{(thld)}$ can be found by calculating equation (6.9) for different path loss values λ_{sk}. Denote λ^* as the value of path loss which satisfies $\overline{P_e} = P_e^{(thld)}$. Since equation (6.9) is an increasing function of λ_{sk}, all nodes in $\mathcal{D}$ would have $\lambda_{sk} \leq \lambda^*$. However, since path loss is random (due to macroscopic fading), it is necessary to associate a probabilistic measure to the above condition. The decoding set is then defined as a set of nodes having path loss $\lambda_{sk} \leq \lambda^*$ with sufficiently high probability. Throughout this work, 99% probability is used as the threshold. It can be seen that this definition would ensure the set $\mathcal{D}$ contains all nodes who can reliably decode the message satisfying $\overline{P_e} \leq P_e^{(thld)}$ with near certainty. The remaining task is now to translate this condition into

the geometric structure of $\mathcal{D}$. Define $L_p^* = 10\ log(\lambda^*)$ as the path loss threshold measured in logarithmic scale. Since path loss is distributed according to $\mathcal{N}(C_1 + 10\ \alpha\ log(l), \sigma_s^2)$, the following relation holds:

$$Pr\left[L_p \leq L_p^*\right] = 1 - \mathcal{Q}\left(\frac{L_p^* - (C_1 + 10\ \alpha\ log(l_{sk}))}{\sqrt{\sigma_s^2}}\right) \tag{6.21}$$

Using Chernoff standard approximation for Q-function, it can be shown that the above relation translates to the condition $l_{sk} \leq l^*$, where $l^* = \sqrt[\alpha]{10^{0.1(L_p^* - C_1 - 2.797\ \sigma_s)}}$ is the maximum distance from the source node to any relay node in $\mathcal{D}$.

In the second time slot, all nodes in $\mathcal{D}$ simultaneously transmit a weighted version of the decoded message, and destination d receives a superposition from all the nodes as follows:

$$y_d = \sum_{k \in \mathcal{D}} h_{kd} w_k x_s + z_d \tag{6.22}$$

The weight w_k depends on the channel realisation as well as the total number of nodes in $\mathcal{D}$, and it is chosen to maximise received SNR at destination. As a fair comparison, the total transmit energy used by all nodes in $\mathcal{D}$ is constrained to be $\sum_{k \in \mathcal{D}} E[|w_k x_s|^2] = \mathcal{E}_s$. Using the same derivation as in [175], it can be shown that the optimal w_k which maximises the received SNR is $w_k = \frac{h_{kd}^*}{\sqrt{\sum_{j \in \mathcal{D}} |h_{jd}|^2}}$. This implies that the global CSI is required for every node in $\mathcal{D}$, which causes considerable complexity for practical implementation. However, their analysis assumes the existence of an effective method to disseminate CSI. With optimal w_k, received SNR in the second time slot can be calculated as $\frac{\mathcal{E}_s}{N_0} \sum_{k \in \mathcal{D}} |h_{kd}|^2$. Combining the received signal at the first and second time slot following MRRC technique, the overall SNR is expressed as:

$$\rho_{\text{eff}}^{\text{(D-TxMRC)}} = \frac{\mathcal{E}_s}{N_0}\left(|h_{sd}|^2 + \sum_{k \in \mathcal{D}} |h_{kd}|^2\right) \tag{6.23}$$

The exact instantaneous bit error probability can then be calculated by substituting $\frac{\mathcal{E}_s\ |h_{sk}|^2}{N_0}$

terms in equation (6.14) with the above effective SNR value as follows:

$$P_e = \frac{3}{4}\,\mathcal{Q}\left(\sqrt{\frac{\rho_{\text{eff}}^{\text{(D-TxMRC)}}}{5}}\right) + \frac{1}{2}\,\mathcal{Q}\left(\sqrt{\frac{9\,\rho_{\text{eff}}^{\text{(D-TxMRC)}}}{5}}\right) - \frac{1}{4}\,\mathcal{Q}\left(\sqrt{5\,\rho_{\text{eff}}^{\text{(D-TxMRC)}}}\right) \quad (6.24)$$

Denote φ to be the value of $\rho_{\text{eff}}^{\text{(D-TxMRC)}}$ which make $P_e = P_e^{\text{(thld)}}$. Following earlier definition, the outage probability can then be calculated as $P_{\text{out}}^{\text{(D-TxMRC)}} = Pr\left[\rho_{\text{eff}}^{\text{(D-TxMRC)}} \leq \varphi\right]$. Removing the constant terms and defining normalised $\rho^* = \frac{\varphi}{\mathcal{E}_s/N_0}$, outage probability expression can be rewritten as:

$$P_{\text{out}}^{(D-TxMRC)} = P_r\left[\left(|h_{sd}|^2 + \sum_{k\in\mathcal{D}}|h_{kd}|^2\right) \leq \rho^*\right] \quad (6.25)$$

In the following, different types of gain available in D-TxMRC scheme are analysed, namely array gain and diversity gain. No analysis is given on multiplexing gain, as constant spectral efficiency of 2 b/s/Hz is assumed as stated earlier.

Array/Antenna Gain

Array gain is defined as the increase in average received SNR due to coherent combining at the destination. From equation (6.23), it can be seen that effective SNR is a function of channel gain from s to d, as well as channel gain from all nodes in decoding set $\mathcal{D}$ to d. Calculating the average received SNR requires an averaging with respect to all squared channel gain, each of which are distributed according to exponential distribution with different parameters. Since these parameters depend on the distances between each node with respect to destination, the average SNR is determined by the exact location of nodes in $\mathcal{D}$, which lies within a circular region of radius l^* from source node. The average SNR can then be calculated as:

$$\begin{aligned} E\left[\rho_{\text{eff}}^{\text{(D-TxMRC)}}\right] &= \frac{\mathcal{E}_s}{N_0}\left(E\left[|h_{sd}|^2\right] + \sum_{k\in\mathcal{D}}E\left[|h_{kd}|^2\right]\right) = \frac{\mathcal{E}_s}{N_0}\left(\frac{1}{\lambda_{sd}} + \sum_{k\in\mathcal{D}}\frac{1}{\lambda_{kd}}\right) \\ &= \frac{\mathcal{E}_s}{N_0\,10^{0.1\,C_1}}\left(\frac{1}{(l_{sd})^{\alpha}\,10^{0.1\,\chi_{sd}}} + \sum_{k\in\mathcal{D}}\frac{1}{(l_{kd})^{\alpha}\,10^{0.1\,\chi_{kd}}}\right) \end{aligned} \quad (6.26)$$

where substitution with the path loss equation has been used. To further simplify the analysis, the upper and lower bound of the performance is used. Using the fact that the lower distance with respect to destination will result in better average SNR, the upper bound on the performance occurs when all nodes in $\mathcal{D}$ are located at the circle boundary of distance l^* from source node in the direction of destination node. On the contrary, lower bound on the performance occurs when all nodes are located at the circle boundary away from destination node. Additionally, due to macroscopic fading variables χ_{kd} for all k which are independent and identically distributed according to $\mathcal{N}(0, \sigma_S^2)$, the upper bound is obtained by setting $\chi_{kd} = \underline{\chi} = \min_{k \in \mathcal{D}} \chi_{kd}$. Correspondingly, the lower bound is obtained by setting $\chi_{kd} = \overline{\chi} = \max_{k \in \mathcal{D}} \chi_{kd}$. Therefore, the average SNR can be bounded as follows:

$$\frac{\mathcal{E}_s}{N_0\, 10^{0.1\, C_1}} \left(\frac{1}{(l_{sd})^{\alpha}\, 10^{0.1\, \chi_{sd}}} + \sum_{k \in \mathcal{D}} \frac{1}{(l_{sd} + l^*)^{\alpha}\, 10^{0.1\, \overline{\chi}}} \right) \leq E\left[\rho_{\text{eff}}^{\text{(D-TxMRC)}}\right] \leq \frac{\mathcal{E}_s}{N_0\, 10^{0.1\, C_1}} \left(\frac{1}{(l_{sd})^{\alpha}\, 10^{0.1\, \chi_{sd}}} + \sum_{k \in \mathcal{D}} \frac{1}{(l_{sd} - l^*)^{\alpha}\, 10^{0.1\, \underline{\chi}}} \right) \quad (6.27)$$

Defining direct link average SNR as $E\left[\rho_{\text{eff}}^{\text{(direct)}}\right] = \frac{\mathcal{E}_s}{N_0\, 10^{0.1\, C_1}} \frac{1}{(l_{sd})^{\alpha}\, 10^{0.1\, \chi_{sd}}}$, the bound reduces to:

$$E\left[\rho_{\text{eff}}^{\text{(direct)}}\right] \left(1 + |\mathcal{D}| \frac{l_{sd}^{\alpha} 10^{0.1(\chi_{sd} - \overline{\chi})}}{(l_{sd} + l^*)^{\alpha}}\right) \leq E\left[\rho_{\text{eff}}^{\text{(D-TxMRC)}}\right] \leq E\left[\rho_{\text{eff}}^{\text{(direct)}}\right] \left(1 + |\mathcal{D}| \frac{l_{sd}^{\alpha} 10^{0.1(\chi_{sd} - \underline{\chi})}}{(l_{sd} - l^*)^{\alpha}}\right) \quad (6.28)$$

Hence, the array gain γ_{arr} can be bounded as follows:

$$1 + |\mathcal{D}| \frac{10^{0.1(\chi_{sd} - \overline{\chi})}}{\left(1 + \frac{l^*}{l_{sd}}\right)^{\alpha}} \leq \gamma_{arr} \leq 1 + |\mathcal{D}| \frac{10^{0.1(\chi_{sd} - \underline{\chi})}}{\left(1 - \frac{l^*}{l_{sd}}\right)^{\alpha}} \quad (6.29)$$

The actual value of the array gain achieved is dependent on system parameters as well as the values of shadow fading from all relay nodes with respect to destination node. The distribution

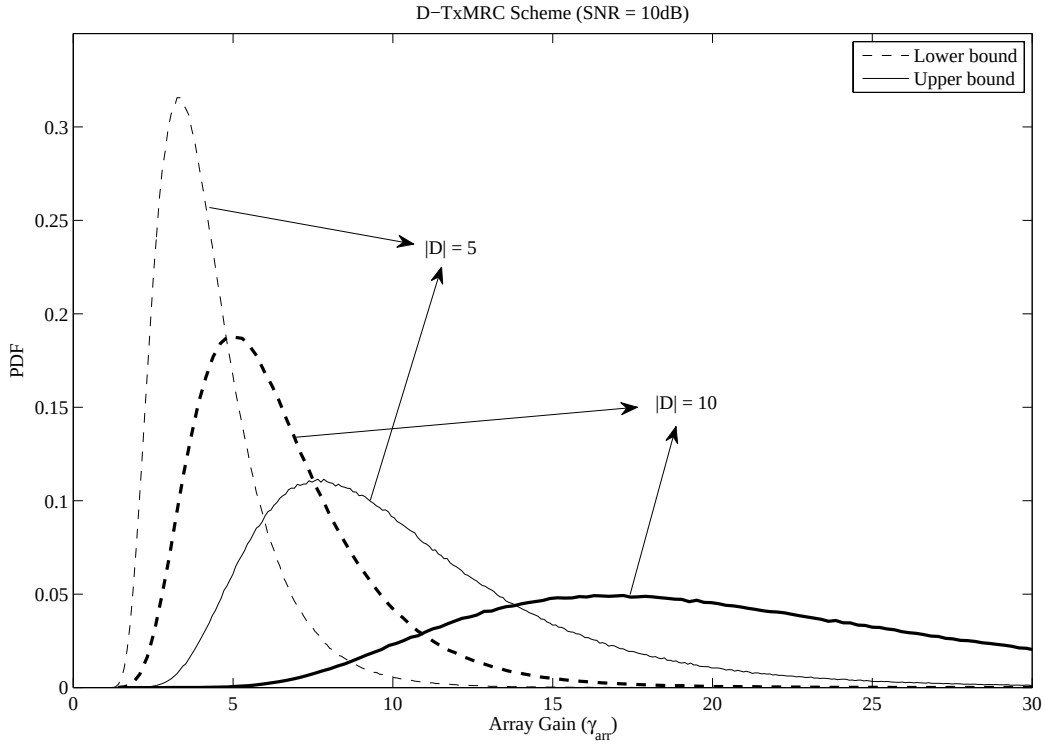

Figure 6.5: Probability Density Function of achievable array gain in typical D-TxMRC setting ($\rho = 10$dB, $\sigma_s^2 = 3$dB, $l_{sd} = 6$ km, $P_e^{(thld)} = 10^{-6}$, α = 3)

of this gain under typical system settings are shown in Figure 6.5.

Diversity Gain

Diversity gain is characterised by the gradient of average symbol error probability curve or outage probability curve at high SNR regime. Using the effective SNR derived earlier in equation (6.23), the symbol error probability assuming maximum likelihood (ML) detection at the receiver can be approximated as [36, Ch. 5.2]:

$$P_e \approx \overline{N_e}\, \mathcal{Q}\left(\sqrt{\frac{\rho_{\text{eff}}^{\text{(D-TxMRC)}}\, d_{min}^2}{2}}\right) \tag{6.30}$$

where $\overline{N_e}$ is the average number of nearest neighbours in the constellation, and d_{min}^2 is the minimum Euclidean distance separation between two constellation points. For 16QAM con-

stellation, the parameter $\overline{N_e}$ and d_{min}^2 are equal to 3 and 0.4 respectively. Applying Chernoff bound, $\mathcal{Q}(x) \leq e^{-\frac{x^2}{2}}$ and substituting $\rho_{\text{eff}}^{\text{(D-TxMRC)}}$ expression in equation (6.23), the symbol error probability expression can be written as:

$$P_e \leq \overline{N_e}\, e^{-\frac{\mathcal{E}_s\, d_{min}^2}{4\, N_0}\left(|h_{sd}|^2 + \sum_{k\in\mathcal{D}} |h_{kd}|^2\right)} \tag{6.31}$$

When channel gains from different cooperating nodes are independent, the average symbol error probability can be calculated accordingly. Denoting $|h_{sd}|^2$ and $|h_{kd}|^2$ as x and x_k respectively, and letting $\frac{\mathcal{E}_s\, d_{min}^2}{4\, N_0} = A$, the calculation can be performed as follows:

$$\begin{aligned}
\overline{P_e} &= \int_0^\infty \int_0^\infty \cdots \int_0^\infty P_e\, f(x)\, dx \prod_{k\in\mathcal{D}} f(x_k)\, dx_k && (6.32)\\
&\leq \overline{N_e} \int_0^\infty \int_0^\infty \cdots \int_0^\infty e^{-A\, x}\, f(x)\, dx\, e^{-A\, \sum_{k\in\mathcal{D}} x_k} \prod_{k\in\mathcal{D}} f(x_k)\, dx_k && (6.33)\\
&= \overline{N_e}\, \lambda_{sd} \int_0^\infty e^{-(A+\lambda_{sd})\, x}\, dx \prod_{k\in\mathcal{D}} \lambda_{kd} \int_0^\infty e^{-(A+\lambda_{kd})x_k}\, dx_k && (6.34)\\
&= \overline{N_e} \frac{1}{1+\frac{\mathcal{E}_s\, d_{min}^2}{4\, N_0\, \lambda_{sd}}} \prod_{k\in\mathcal{D}} \frac{1}{1+\frac{\mathcal{E}_s\, d_{min}^2}{4\, N_0\, \lambda_{kd}}} && (6.35)
\end{aligned}$$

In the high SNR regime, $\frac{\mathcal{E}_s}{N_0} >> 1$, the average error probability expression can be further simplified as:

$$\begin{aligned}
\overline{P_e} &\leq \overline{N_e} \frac{4\, N_0\, \lambda_{sd}}{\mathcal{E}_s\, d_{min}^2} \prod_{k\in\mathcal{D}} \frac{4\, N_0\, \lambda_{kd}}{\mathcal{E}_s\, d_{min}^2}\\
&\approx \overline{N_e} \left(\frac{\mathcal{E}_s\, d_{min}^2}{4\, N_0}\right)^{-(|\mathcal{D}|+1)} \prod_{k\in\{s,\mathcal{D}\}} \lambda_{kd} && (6.36)
\end{aligned}$$

which shows that D-TxMRC is able to achieve diversity in the order of total number of cooperating nodes.

When different cooperating nodes are located closely to each other (which is likely to occur when $|\mathcal{D}|$ is large), the independent fading assumption can no longer be used. In this case, it

is necessary to consider the channel correlation from different cooperating nodes. To perform the analysis, let k_i be the i^{th} node in $\mathcal{D}$, and $\tilde{\boldsymbol{h}} = [h_{sd}, h_{k_1 d}, h_{k_2 d}, ..., h_{k_{|\mathcal{D}|} d}]^T$ be the channel vector between all cooperating nodes (including the source) to destination. Here, $[.]^T$ denotes transpose operation. Correlation matrix is then defined as $\boldsymbol{R} = E\left[\tilde{\boldsymbol{h}}\,\tilde{\boldsymbol{h}}^H\right]$, where $[.]^H$ denotes Hermitian (conjugate transpose) operation. $\boldsymbol{R}$ is a symmetric matrix whose diagonal elements are composed of the channel powers $diag\{\frac{1}{\lambda_{sd}}, \frac{1}{\lambda_{k_1 d}}, \frac{1}{\lambda_{k_2 d}}, ..., \frac{1}{\lambda_{k_{|\mathcal{D}|} d}}\}$, and its off-diagonal elements are composed of the correlation measure between two channels indicated by its row and column position. Using this notation, the symbol error probability in equation (6.31) can be rewritten as [36, Ch. 5.2]:

$$P_e \leq \overline{N_e}\, e^{-\frac{\mathcal{E}_s\, d_{min}^2 \|\tilde{h}\|_F^2}{4\, N_0}} \tag{6.37}$$

where $\left\|\tilde{\boldsymbol{h}}\right\|_F^2$ is the squared Frobenius norm of $\tilde{\boldsymbol{h}}$. Since $\tilde{\boldsymbol{h}}$ is a column matrix, this norm is equal to $\tilde{\boldsymbol{h}}^H \tilde{\boldsymbol{h}}$, which is random with Moment Generating Function (MGF) expressed as:

$$\Psi_{\|\tilde{h}\|_F^2}(v) = \prod_{i=1}^{|\mathcal{D}|+1} \frac{1}{1 + v\, \theta_i(\boldsymbol{R})} \tag{6.38}$$

Here, $\theta_i(\boldsymbol{R})$ is the i^{th} eigenvalue of $\boldsymbol{R}$. Using similar technique as [36, Ch. 5.6.1] to average symbol error probability in equation (6.37) with the above MGF, the following expression is obtained:

$$\overline{P_e} \leq \overline{N_e} \prod_{i=1}^{|\mathcal{D}|+1} \frac{1}{1 + \frac{\mathcal{E}_s\, d_{min}^2}{4\, N_0}\, \theta_i(\boldsymbol{R})} \tag{6.39}$$

Denoting $r(\boldsymbol{R})$ to be the rank of correlation matrix $\boldsymbol{R}$ (the total number of its non-zero eigenvalues), in high SNR regime ($\frac{\mathcal{E}_s}{N_0} >> 1$) the average error probability can be further simplified as:

$$\overline{P_e} \;\leq\; \overline{N_e} \left(\frac{\mathcal{E}_s\, d_{min}^2}{4\, N_0}\right)^{-r(\boldsymbol{R})} \prod_{i=1}^{r(\boldsymbol{R})} (\theta_i(\boldsymbol{R}))^{-1} \tag{6.40}$$

It is apparent from the above equation that the diversity order is limited by the rank of correla-

tion matrix. As opposed to the independent case, the achievable diversity order in the presence of correlation is smaller.

6.3.4 Distributed Space Time Block Coding (DSTBC)

This scheme also requires two time slots for message transmission. The first slot of DSTBC is identical to that of D-TxMRC case. The main difference lies in the way cooperating nodes forward the message. In DSTBC, instead of symbol-by-symbol forwarding, cooperating nodes operate on a sequence of symbols. This requirement is due to the underlying space-time coding (STC) matrix used. In this case, each node in the decoding set is required to transmit a certain row in STC matrix, which contains a transformed and re-ordered version of the symbol sequence. The number of symbols in the sequence is therefore determined by the size of STC matrix used, which is an important design parameter.

Unlike D-TxMRC, DSTBC scheme does not require global CSI on cooperating nodes, and this makes DSTBC more appealing for practical use. However, unlike D-TxMRC scheme which can operate optimally on any number of cooperating nodes, DSTBC performance is dependent on the STC matrix used. Designing an efficient STC matrix is a major research topic in itself, and there are many challenges associated with it. Further details on these issues are not covered within the scope of the present analysis. Interested readers are referred to [143]-[147], [176], and the reference therein for solutions dealing with the above problems. Let $\mathcal{W}(\boldsymbol{x_s})$ denote the $N \times N$ STC matrix corresponding to the received symbol sequence in the first slot $[x_s(1)\ x_s(2)\ ...\ x_s(N)]^T = \boldsymbol{x_s}$, and $[\mathcal{W}]_{k,n}$ denotes an element in k^{th} row and n^{th} column of the matrix $\mathcal{W}$. In the second slot, the k^{th} node in $\mathcal{D}$ transmits the symbol sequence in the k^{th} row of $\mathcal{W}$. The received signal at destination node during second slot transmission can be expressed as:

$$y_d(n) = \sum_{k \in \mathcal{D}} h_{kd} \left[\mathcal{W}(\boldsymbol{x_s})\right]_{k,n} + z_d(n) \quad for\ n = 1..N \tag{6.41}$$

Note that this is equivalent as what the receiver would have received when the message is transmitted from multiple-antenna transmitter, therefore conventional MIMO equalisation can be performed. Again, as a fair comparison, the total power consumed during one symbol duration is normalised to $\mathcal{E}_s$. Therefore, each column in STC matrix is normalised such that $\sum_{k=1}^{N} E\left[\left|[\mathcal{W}(\boldsymbol{x_s})]_{k,n}\right|^2\right] = \mathcal{E}_s$ for all n.

Upon receiving the whole message sequence on the second slot and performing equalisation, destination will recover the individual message. As long as the underlying STC matrix adopts orthogonal design principle [27], it can be shown that the signal to noise ratio in the second slot is given as:

$$\rho'' = \frac{\mathcal{E}_s}{N_0} \frac{1}{\min(N, |\mathcal{D}|)} \sum_{k \in \mathcal{D}_1^N} |h_{kd}|^2 \tag{6.42}$$

where $\mathcal{D}_1^N$ is used to denote the first N elements of set $\mathcal{D}$. After combining the received signal from the first and second time slots, the effective SNR is expressed as:

$$\rho_{\text{eff}}^{(\text{DSTBC})} = \frac{\mathcal{E}_s}{N_0} \left(|h_{sd}|^2 + \frac{1}{\min(N, |\mathcal{D}|)} \sum_{k \in \mathcal{D}_1^N} |h_{kd}|^2 \right) \tag{6.43}$$

Given that the STC matrix size is large ($N >> 1$), the effective SNR can be simplified as follows:

$$\rho_{\text{eff}}^{(\text{DSTBC})} = \frac{\mathcal{E}_s}{N_0} \left(|h_{sd}|^2 + \frac{1}{|\mathcal{D}|} \sum_{k \in \mathcal{D}} |h_{kd}|^2 \right) \tag{6.44}$$

The analysis on the overall performance with DSTBC scheme is identical to those in D-TxMRC case. The only difference is the effective SNR, in which equation (6.44) is used instead of (6.23). Therefore, the outage probability expression can be written as:

$$P_{\text{out}}^{(DSTBC)} = P_r \left[\left(|h_{sd}|^2 + \frac{1}{|\mathcal{D}|} \sum_{k \in \mathcal{D}} |h_{kd}|^2 \right) \leq \rho^* \right] \tag{6.45}$$

Note that for complex constellation, full rate STC matrix only exists when the size $N \leq 2$. For

STC matrix with larger dimension, the rate is strictly less than one. This rate loss needs to be taken into consideration when calculating the threshold ρ^*, which is defined as the normalised SNR required to achieve transmission at target rate such that the error probability is less than $P_e^{(\text{thld})}$. The array and diversity gain of DSTBC scheme can then be analysed as follows.

Array/Antenna Gain

Using the same technique as the one in D-TxMRC, the average received SNR can be calculated as follows:

$$\begin{aligned} E\left[\rho_{\text{eff}}^{(\text{DSTBC})}\right] &= \frac{\mathcal{E}_s}{N_0}\left(E\left[|h_{sd}|^2\right] + \frac{1}{|\mathcal{D}|}\sum_{k\in\mathcal{D}} E\left[|h_{kd}|^2\right]\right) = \frac{\mathcal{E}_s}{N_0}\left(\frac{1}{\lambda_{sd}} + \frac{1}{|\mathcal{D}|}\sum_{k\in\mathcal{D}}\frac{1}{\lambda_{kd}}\right) \\ &= \frac{\mathcal{E}_s}{N_0\, 10^{0.1\, C_1}}\left(\frac{1}{(l_{sd})^{\alpha}\, 10^{0.1\,\chi_{sd}}} + \frac{1}{|\mathcal{D}|}\sum_{k\in\mathcal{D}}\frac{1}{(l_{kd})^{\alpha}\, 10^{0.1\,\chi_{kd}}}\right) \end{aligned} \tag{6.46}$$

Bounding above and below the average SNR, the following inequality is obtained:

$$\begin{aligned} \frac{\mathcal{E}_s}{N_0\, 10^{0.1\, C_1}}\left(\frac{1}{(l_{sd})^{\alpha}\, 10^{0.1\,\chi_{sd}}} + \frac{1}{|\mathcal{D}|}\sum_{k\in\mathcal{D}}\frac{1}{(l_{sd}+l^*)^{\alpha}\, 10^{0.1\,\overline{\chi}}}\right) \;\le\; E\left[\rho_{\text{eff}}^{(\text{DSTBC})}\right] \;\le \\ \frac{\mathcal{E}_s}{N_0\, 10^{0.1\, C_1}}\left(\frac{1}{(l_{sd})^{\alpha}\, 10^{0.1\,\chi_{sd}}} + \frac{1}{|\mathcal{D}|}\sum_{k\in\mathcal{D}}\frac{1}{(l_{sd}-l^*)^{\alpha}\, 10^{0.1\,\underline{\chi}}}\right) \end{aligned} \tag{6.47}$$

Correspondingly, the array gain γ_{arr} can be bounded as follows:

$$1 + \frac{10^{0.1(\chi_{sd}-\overline{\chi})}}{\left(1+\frac{l^*}{l_{sd}}\right)^{\alpha}} \;\le\; \gamma_{arr} \;\le\; 1 + \frac{10^{0.1(\chi_{sd}-\underline{\chi})}}{\left(1-\frac{l^*}{l_{sd}}\right)^{\alpha}} \tag{6.48}$$

which again depends on the system parameters and shadow fading values. The distribution of this gain under typical system settings are shown in Figure 6.6. It is observed that the array gain in DSTBC is generally smaller than D-TxMRC. Moreover, increasing decoding set size does not increase array gain, as opposed to D-TxMRC case which shows larger right shift on the distribution for larger value of $|\mathcal{D}|$.

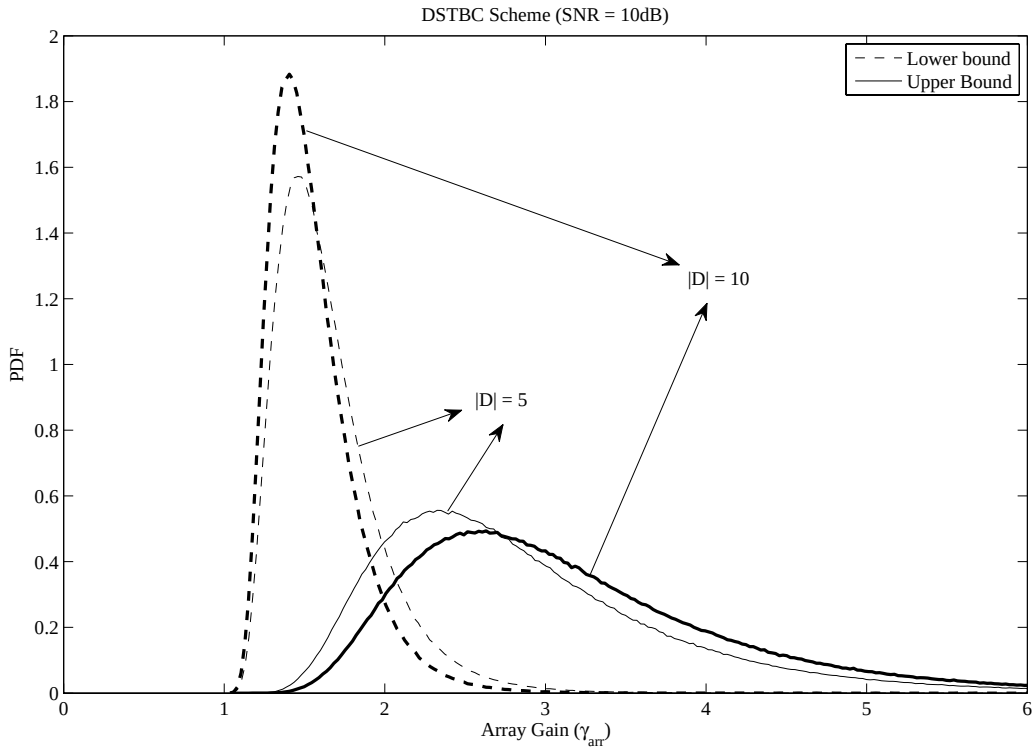

Figure 6.6: Probability Density Function of achievable array gain in typical DSTBC setting ($\rho = 10$dB, $\sigma_s^2 = 3$dB, $l_{sd} = 6$ km, $P_e^{(thld)} = 10^{-6}$, α = 3)

Diversity Gain

Here, the same approximation on symbol error probability is used:

$$P_e \approx \overline{N_e}\, \mathcal{Q}\left(\sqrt{\frac{\rho_{\text{eff}}^{(\text{DSTBC})}\, d_{min}^2}{2}}\right) \tag{6.49}$$

After applying Chernoff bound and substituting SNR_{eff} with the value in equation (6.44):

$$P_e \;\leq\; \overline{N_e}\, e^{-\frac{\mathcal{E}_s\, d_{min}^2}{4\, N_0}\left(|h_{sd}|^2 + \frac{1}{|\mathcal{D}|}\, \sum_{k\in\mathcal{D}} |h_{kd}|^2\right)} \tag{6.50}$$

When different channel gains are independent, $\overline{P_e}$ can be simplified for high SNR regime into:

$$\overline{P_e} \;\leq\; \overline{N_e}\, |\mathcal{D}|^{|\mathcal{D}|} \left(\frac{\mathcal{E}_s\, d_{min}^2}{4\, N_0}\right)^{-(|\mathcal{D}|+1)} \prod_{k\in\{s,\mathcal{D}\}} \lambda_{kd} \tag{6.51}$$

Hence, under uncorrelated fading, like D-TxMRC, DSTBC scheme achieves $|\mathcal{D}|+1$ diversity order. When independent assumption between channel gains is not applicable, it is necessary to incorporate channel correlation into the analysis. Define $\tilde{\boldsymbol{h}} = [\sqrt{|\mathcal{D}|}h_{sd}, h_{k_1 d}, h_{k_2 d}, ..., h_{k_{|\mathcal{D}|}d}]^T$ as the scaled channel vector between cooperating nodes to destination. Similarly, correlation matrix is defined as $\boldsymbol{R} = E\left[\tilde{\boldsymbol{h}}\,\tilde{\boldsymbol{h}}^H\right]$. The symbol error probability in equation (6.50) can then be rewritten as:

$$P_e \leq \overline{N_e}\, e^{-\frac{\mathcal{E}_s\, d_{min}^2 \|\tilde{h}\|_F^2}{4\, N_0\, |\mathcal{D}|}} \tag{6.52}$$

Using MGF of scaled channel vector Frobenius norm, average symbol error probability can be calculated, which exhibits the following characteristic at high SNR regime:

$$\overline{P_e} \;\leq\; \overline{N_e} \left(\frac{\mathcal{E}_s\, d_{min}^2}{4\, N_0\, |\mathcal{D}|}\right)^{-r(\boldsymbol{R})} \prod_{i=1}^{r(\boldsymbol{R})} (\theta_i(\boldsymbol{R}))^{-1} \tag{6.53}$$

It can be seen from the above equation that the same trend is observed as in D-TxMRC, whereby diversity order is limited to the rank of correlation matrix (which is $\leq |\mathcal{D}|+1$) in the presence of channel correlation.

6.4 Geometry Specific Issue in Random Network

The analysis so far provides a method to calculate the performance of different cooperative transmission schemes given a particular node position. As highlighted earlier, in random network, nodes can be located anywhere; therefore performance evaluation must take into consideration all possible node locations. However, doing so would impose some geometry specific issues. This section describes some of these issues pertaining to different cooperative scheme used. An efficient technique to handle the corresponding issue is then developed and used for network performance analysis, which is described in the next section.

6.4.1 Distance Distribution Function

The immediate impact of randomness in node locations is the randomness in source destination distance. Regardless of the cooperative scheme used, network performance must be averaged across all possible source destination node locations. For this purpose, given any two arbitrary nodes, the distance distribution is required.

Using the fact that the network considered is a rectangular network of size $L \times L$, and all nodes are uniformly distributed within the region, the PDF of the squared distance between two nodes selected randomly from the network can be expressed as (See Appendix E):

$$f_{l_{sd}^2}(z) = \begin{cases} \frac{\pi}{L^2} - \frac{4\sqrt{z}}{L^3} + \frac{z}{L^4} & \text{if } 0 \leq z < L^2 \\ \frac{4}{L^2}\ \text{arcSin}\left(\frac{L}{\sqrt{z}}\right) - \frac{(\pi+2)}{L^2} + \frac{4\sqrt{z-L^2}}{L^3} - \frac{z}{L^4} & \text{if } L^2 \leq z < 2L^2 \\ 0 & \text{elsewhere} \end{cases} \tag{6.54}$$

Note that the above distribution is for the squared distance instead of the conventional distance. The advantage of using squared distance is two folds. Firstly, the distribution function is easier to derive and can be expressed in a closed form. Secondly, it can be applied directly when evaluating network performance, since path loss is just a polynomial function of distance.

6.4.2 Relay Node Position in Amplify-and-Forward

Calculating network performance under AnF relaying scheme is more complicated than for direct transmission, due to the dependence of relay node position. It can be seen that the effective SNR expression in equation (6.5) is a function of three channel parameters namely h_{sr}, h_{rd}, as well as h_{sd}, and therefore averaging across distribution of source-destination distance alone is not sufficient. In order to average across all three channels, a new dimension has to be introduced, which is termed as relay node position.

A *region of interest* (RoI), illustrated in Figure 6.7, is defined as a collection of points

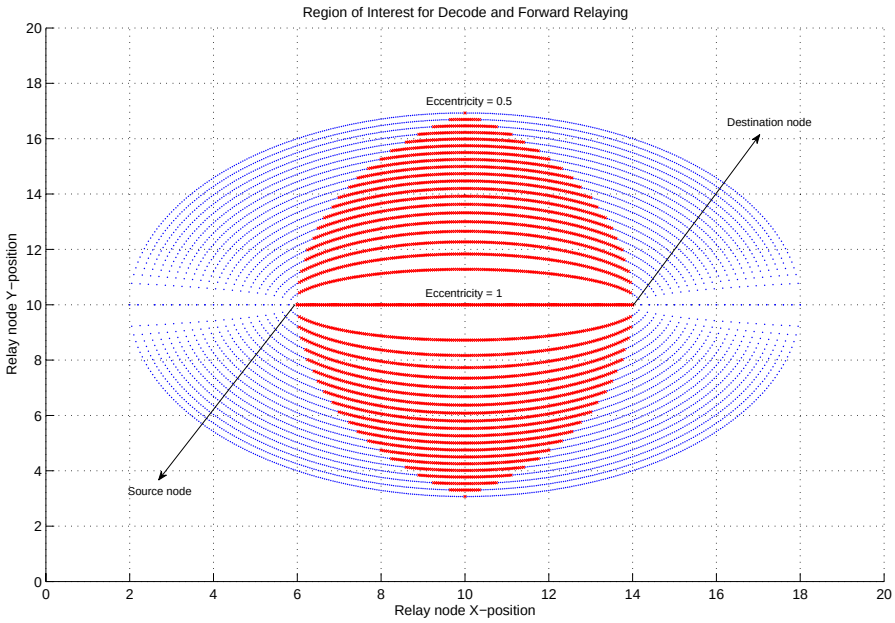

Figure 6.7: Region of Interest for Relay Node Position: An illustration

which is not further away from source-destination distance (measured from both source and destination). The intuition behind this definition of RoI is that when relay node is further away (either from source or destination) than source destination distance, then direct transmission is preferred. Ideally, outage calculation must consider all possible relay node position within the RoI. To simplify the averaging process, ellipses are drawn with source and destination nodes as their foci. The *eccentricity* (ratio of source-destination distance and the major axis) ranges from 1 to 0.5, and anything beyond that does not contain any RoI (see Figure 6.7). Furthermore, parts of the ellipse which have *ratio* (distance from one of the foci over the sum distance to both foci) ranging from (1 - eccentricity) to eccentricity of the ellipse are well contained within the RoI. Two parameters δ_e and δ_r are then defined as the step sizes of eccentricity and ratio respectively. Given a particular value of eccentricity and ratio, the source-relay and relay-destination distances can be found. The channel variances and outage probability can then be calculated accordingly. Network performance evaluation can now be approximated by averaging with respect to all values within the valid range of eccentricity and ratio with step

size δ_e and δ_r. It can be seen that in the infinitesimal of the step sizes, this approach converges into integration within RoI, which is equal to the exact calculation considering all possible relay node position within the RoI.

It is noted that the above process is equivalent to breaking the RoI into cells, each of which is centered along the line of the ellipses which is within the region of interest. Since nodes are uniformly distributed, the number of nodes in any given region Θ follows Poisson Point Process [177]. Defining $|\Theta|$ as the area of Θ, the probability of exactly n nodes in Θ (denoted as $\Phi(|\Theta|)$) is:

$$Pr\left[\Phi\left(|\Theta|\right)=n\right]=e^{-\frac{M}{L^2}|\Theta|}\frac{\left(\frac{M}{L^2}\ |\Theta|\right)^n}{n!} \tag{6.55}$$

The averaging process can then be performed via weighted sum operation with the above probability as the scaling factor.

6.4.3 Relay Nodes Cardinality and Positions in D-TxMRC and DSTBC

Due to the nature of how D-TxMRC and DSTBC transmission works, there are two challenges in evaluating overall performance of cooperative network under such schemes. Firstly, the shape of decoding set area given a source node location has to be found. When the network is unbounded (infinite in size), the decoding set area can be assumed to be in circular shape. However, this is unrealistic, and intersection with network boundary (known as *edge effect*) has to be considered. Secondly, given decoding set area, the number and position of cooperating nodes need to be approximated. Here, a novel technique to handle these two problems is proposed. The present analysis in this direction assumes the following conventions:

1. The angular measurements are taken in a counter clockwise direction.

2. Every point in the circle is identified by its relative angular measurement (in radians) from positive x axis centered at circle center. Upper case letter are used to denote a point, while the respective lower case letter represents its measurement. For example,

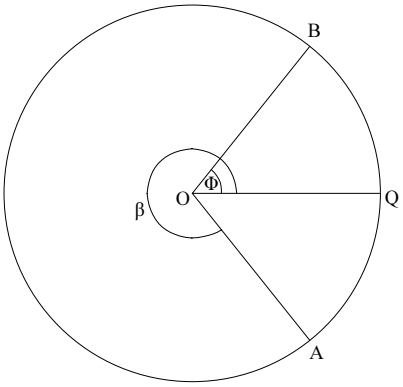

Figure 6.8: Notational convention for points in a circle and their corresponding measurements

in Figure 6.8, point Q lies in the positive x axis, therefore its value $q = 0$. Similarly, point B and A have their values of $b = \phi$ and $a = \beta$ respectively, indicating that they are located at ϕ and β radians in counter clockwise direction relative to positive x axis.

3. A location in the network is measured relative to the bottom left corner as $(0, 0)$ coordinate. Therefore, any point in the network can be identified by its position which ranges from $(0, 0)$ to (L, L).

4. The network size L is assumed to be greater than the diameter of decoding set area $\mathcal{D}$, therefore, intersection with network boundary can only happen with at most two sides of the network.

From the first two conventions, given two points A and B in a circle, it is possible to check if another point C is inside the arc spanning from A to B (in positive direction). Normalising all points with respect to the starting point A, this is equivalent as checking whether or not $(c - a)_{2\pi} < (b - a)_{2\pi}$, where $(.)_{2\pi}$ represents circular modulo operation of its argument (e.g. $(3\pi)_{2\pi} = \pi$ and $\left(-\frac{\pi}{2}\right)_{2\pi} = \frac{3\pi}{2}$).

Due to edge effect, special measure needs to be taken when source node is located near network edge, in which case the decoding set area is no longer a complete circle. As illustrated in Figure 6.9, depending on which network edge the source node is located, different truncation

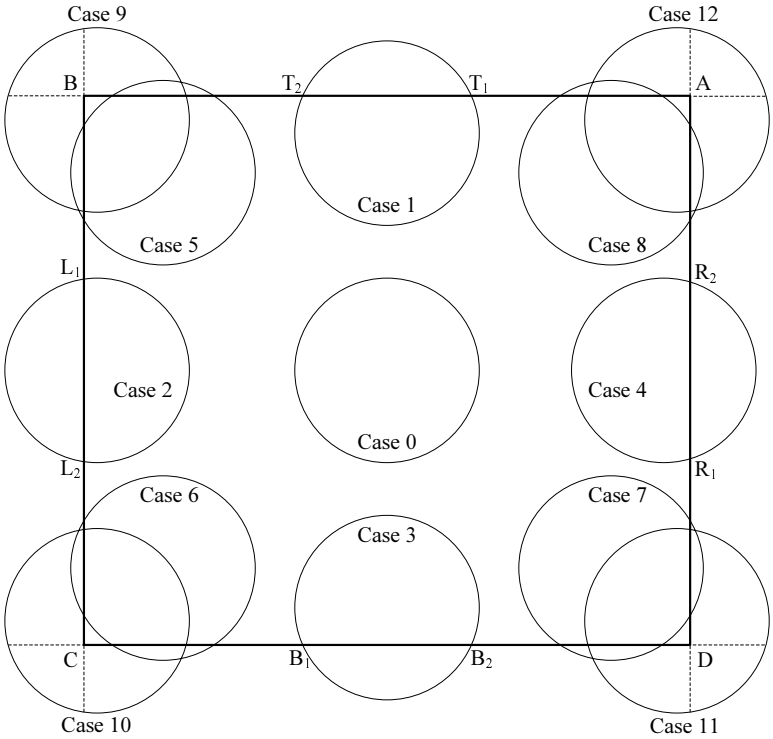

Figure 6.9: Illustration of different possible cases of decoding set area based on different location of source node

region is formed as part of the circle which lies outside network $ABCD$. When calculating decoding set area, this truncation has to be deducted from the circle area. In general, the truncation region forms a segment (or overlapping segments) inside the circular area. Since the size of this truncation region is inversely proportional to the distance of source node to network edge (which can be derived from its position), it is possible to find a closed form solution to calculate decoding set area given the source node location.

Given two points A and B on the circumference of radius r, the area of segment enclosed in an arc spanning from A to B (shaded region in Figure 6.10) can be calculated as:

$$\begin{aligned} 2\left(\int\int_{BOQ} - \int\int_{BOP}\right) disc_r(x,y)\,dxdy &= 2\left(\frac{\angle BOQ}{2\pi}\pi r^2 - (r-l)\,0.5\,r\,\sin(\angle BOQ)\right) \\ &= \frac{r^2}{2}(b-a)_{2\pi} - \frac{r^2}{2}\sin((b-a)_{2\pi}) \end{aligned} \tag{6.56}$$

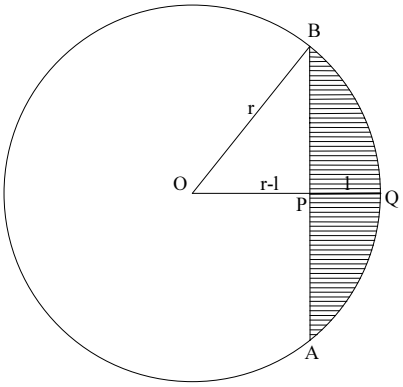

Figure 6.10: Calculation of segment area of distance l from circle circumference (the shaded region)

Noting the relationship between a, b, and the distance l of a line creating the segment with respect to circle interior, the area of a segment created from a line of distance l from circle interior with radius r can be calculated as:

$$S_2(l,r) = r^2 \operatorname{acos}\frac{r-l}{r} \; - \; (r-l)\sqrt{r^2-(r-l)^2} \tag{6.57}$$

which can be obtained by substitution of $l = r\left(1-\cos\frac{(b-a)_{2\pi}}{2}\right)$ into equation (6.56).

In some cases, when calculating decoding set area, the overlapping region of two segments needs to be found. Given two segments enclosed in an arc spanning from $A1$ to $A2$ and from $B1$ to $B2$ within a circle of radius r (shaded region in Figure 6.11), the overlapping region of the two can be calculated as:

$$\begin{aligned} S_3(a1,a2,b1,b2,r) = {} & 0.5\left[r^2\frac{(a2-a1)_{2\pi}}{2} - \frac{r}{2}\sin\left((a2-a1)_{2\pi}\right)\right] \; - \\ & 0.5\left[r^2\left(\frac{a1+a2}{2}-b2\right) - \frac{r}{2}\sin(a1+a2-2b2)\right] \; - \\ & 0.5\left[r\left(\cos\left(\frac{a1+a2}{2}-b2\right) - \cos\left(\frac{(a2-a1)_{2\pi}}{2}\right)\right)\right] \times \\ & r\left(\cos\left(\frac{a1+a2}{2}-b2\right) - \cos\left(\frac{(a2-a1)_{2\pi}}{2}\right)\right)\tan\left(\frac{\pi}{2} - \frac{a1+a2}{2} + \frac{b1+b2}{2}\right) + \\ & 2r\sin\left(\frac{a1+a2}{2}-b2\right) \end{aligned} \tag{6.58}$$

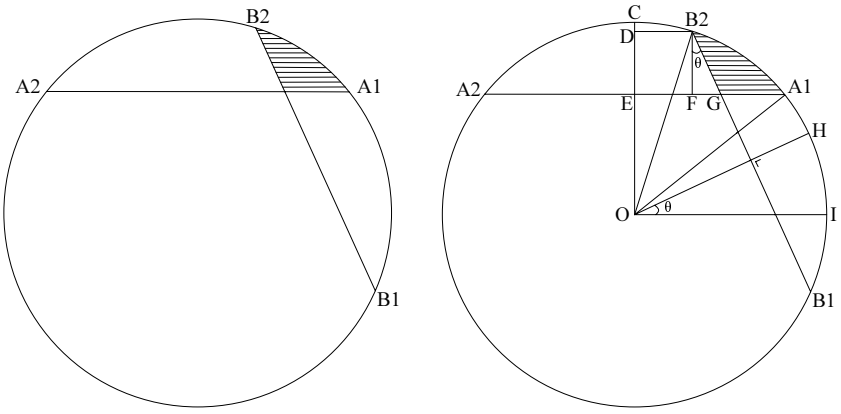

Figure 6.11: Calculation of intersection area between two segments spanning from point $A1$ to $A2$ and from point $B1$ to $B2$

The derivation of the above is made clearer by observing Figure 6.11b, where it is apparent that the area of shaded region can be decomposed as follows:

$$\begin{aligned}\iint_{A1GB2} disc_r(x,y)\,dxdy &= \left(\iint_{A1CE} - \iint_{B2CEG}\right) disc_r(x,y)\,dxdy \\ &= \left(\iint_{A1CE} - \iint_{B2CD} - \iint_{B2DEG}\right) disc_r(x,y)\,dxdy \quad (6.59)\end{aligned}$$

Noting that point C and H are in the middle of $A1$, $A2$ and $B1$, $B2$; their values can be calculated as $c = \frac{a1+a2}{2}$ and $h = \frac{b1+b2}{2}$ respectively. Denoting l_{AB} to be the length of a line from A to B, the following lengths can be calculated:

$$l_{CD} = r\,(1 - \cos\angle B2OC) = r\left(1 - \cos\left(\frac{a1+a2}{2} - b2\right)\right) \quad (6.60)$$

$$l_{DE} = l_{CE} - l_{CD} = r\left(1 - \cos\frac{a2-a1}{2}\right) - r\left(1 - \cos\left(\frac{a1+a2}{2} - b2\right)\right) \quad (6.61)$$

$$l_{DB2} = r\sin\angle B2OC = r\sin\left(\frac{a1+a2}{2} - b2\right) \quad (6.62)$$

$$\begin{aligned}l_{FG} &= l_{DE}\tan\angle IOH = l_{DE}\tan\left(\frac{\pi}{2} - (c-h)\right) \\ &= r\left[\cos\left(\frac{a1+a2}{2} - b2\right) - \cos\frac{a2-a1}{2}\right]\tan\left(\frac{\pi}{2} - \frac{a1+a2}{2} + \frac{b1+b2}{2}\right) \quad (6.63)\end{aligned}$$

Each component of (6.59) can now be calculated individually. First, $\int\int_{A1CE} disc_r(x,y)\,dxdy$ is equal to half of segment area enclosed in an arc spanning point $A1$ and $A2$, therefore it can be calculated as $0.5\ S_1(a1,a2,r)$ using equation (6.56). Similarly, $\int\int_{B2CD} disc_r(x,y)\,dxdy$ is equal to half of segment area created by a line of distance l_{CD} from circle interior, therefore it can be calculated as $S_2(l_{CD},r)$ according to equation (6.57), where l_{CD} is given in equation (6.60). Finally, the last term $\int\int_{B2DEG} disc_r(x,y)\,dxdy$ is an area of a trapezium, and it can be calculated as $0.5\,(2\,l_{DB2}+l_{FG})\,l_{DE}$. Substituting all the values of l_{DE}, l_{DB2}, and l_{FG} obtained from the expressions given in equations (6.61), (6.62), and (6.63) respectively, the overlapping region can be calculated using equation (6.58). Using equations (6.56) and (6.58) above, let $ABCD$ be a square network of size L by L, and $Disc_r(x,y)$ be a circle of radius r centered at (x,y). The circle area which overlaps with $ABCD$ (decoding set area) can be expressed as:

$$\int\int_{ABCD} Disc_r(x,y)\,dx\,dy =$$

$$\begin{cases}
\pi r^2 & \text{if } r \le x \le L-r \text{ and } r \le y \le L-r, \\
\pi r^2 - S_2\,(r-(L-y),r) & \text{if } r \le x \le L-r \text{ and } y > L-r \\
\pi r^2 - S_2\,(r-x,r) & \text{if } x < r \text{ and } r \le y \le L-r \\
\pi r^2 - S_2\,(r-y,r) & \text{if } r \le x \le L-r \text{ and } y < r \\
\pi r^2 - S_2\,(r-(L-x),r) & \text{if } x > L-r \text{ and } r \le y \le L-r \\
\pi r^2 - S_2\,(r-x,r) - S_2\,(r-(L-y),r) & \text{if } x < r,\ y > L-r, \text{ and } \sqrt{x^2+(L-y)^2} \ge r \\
\pi r^2 - S_2\,(r-x,r) - S_2\,(r-y,r) & \text{if } x < r,\ y < r, \text{ and } \sqrt{x^2+y^2} \ge r \\
\pi r^2 - S_2\,(r-(L-x),r) - S_2\,(r-y,r) & \text{if } x > L-r,\ y < r, \text{ and } \sqrt{(L-x)^2+y^2} \ge r \\
\pi r^2 - S_2\,(r-(L-x),r) - S_2\,(r-(L-y),r) & \text{if } x > L-r,\ y > L-r, \text{ and } \sqrt{(L-x)^2+(L-y)^2} \ge r \\
\pi r^2 - S_2\,(r-x,r) - S_2\,(r-(L-y),r) & \\
\quad +S_3\,(l_1,l_2,t_1,t_2,r) & \text{if } x < r,\ y > L-r, \text{ and } \sqrt{x^2+(L-y)^2} < r \\
\pi r^2 - S_2\,(r-x,r) - S_2\,(r-y,r) & \\
\quad +S_3\,(b_1,b_2,l_1,l_2,r) & \text{if } x < r,\ y < r, \text{ and } \sqrt{x^2+y^2} < r \\
\pi r^2 - S_2\,(r-(L-x),r) - S_2\,(r-y,r) & \\
\quad +S_3\,(r_1,r_2,b_1,b_2,r) & \text{if } x > L-r,\ y < r, \text{ and } \sqrt{(L-x)^2+y^2} < r \\
\pi r^2 - S_2\,(r-(L-x),r) - S_2\,(r-(L-y),r) & \\
\quad +S_3\,(t_1,t_2,r_1,r_2,r) & \text{if } x > L-r,\ y > L-r, \text{ and } \sqrt{(L-x)^2+(L-y)^2} < r
\end{cases} \tag{6.64}$$

where $S_2(.)$ and $S_3(.)$ are given in equations (6.57) and (6.58); and $T_1, T_2, L_1, L_2, B_1, B_2, R_1,$ and R_2 are the intersection points of $Disc_r(x, y)$ with top, left, bottom and right side of $ABCD$ respectively, whose values are calculated as:

$$t_1 = \pi/2 - \text{acos}((L-y)/r) \qquad t_2 = \pi/2 + \text{acos}((L-y)/r) \tag{6.65}$$

$$l_1 = \pi - \text{acos}(x/r) \qquad l_2 = \pi + \text{acos}(x/r) \tag{6.66}$$

$$b_1 = 3\pi/2 - \text{acos}(y/r) \qquad b_2 = 3\pi/2 + \text{acos}(y/r) \tag{6.67}$$

$$r_1 = 2\pi - \text{acos}((L-x)/r) \qquad r_2 = \text{acos}((L-x)/r) \tag{6.68}$$

The proof of the above calculation requires consideration of different cases individually. Equation (6.64) consists of 13 different cases of area calculation denoted as case 0 to case 12 in the order of appearance in the equation. Each of these cases corresponds to different shape of overlapping region of $Disc_r(x, y)$ and $ABCD$ as shown in Figure 6.9. When $r \leq x \leq L - r$ and $r \leq y \leq L - r$ (case 0), the $Disc_r(x, y)$ is contained inside $ABCD$, therefore the overlapping area is equal to the area of $Disc_r(x, y)$, and is given as πr^2.

The proofs of case 1, 2, 3 and 4 are identical. For these cases, the $Disc_r(x, y)$ intersects with only one side of $ABCD$. Consider case 1 where the intersection is with the top side of $ABCD$. It is apparent that the overlapping region equals the area of $Disc_r(x, y)$ minus the part that is outside $ABCD$ (which is equal to segment area created from a line of distance $r-(L-y)$ from circle interior). Using equation (6.57), the overlapping region can be calculated as $\pi r^2 - S_2\,(r - (L - y), r)$.

The proofs of case 5, 6, 7, and 8 are also identical. For these cases, the $Disc_r(x, y)$ intersects with two sides of $ABCD$, and the segments created by these intersections do not overlap each other. Consider case 5 where the intersection is with the top and left side of $ABCD$. Following the proof for case 1, the overlapping region can be calculated as $\pi r^2 - S_2\,(r - x, r) - S_2\,(r - (L - y), r)$.

Finally, the proof of case 9, 10, 11, and 12 are also identical. These cases are equivalent to the earlier cases, with the exception that the two segments created by the intersection overlaps one another. To prevent double reduction when subtracting with both segment areas, the region of overlapping segments need to be computed. Assuming case 9, the four points (T_1, T_2, and L_1, L_2) corresponding to the intersection points with the top and left side of $ABCD$ can be calculated using equations (6.65) and (6.66) respectively. Using equation (6.58), the region of overlapping segments can be calculated as $S_3\left(l_1, l_2, t_1, t_2, r\right)$. Adding this term into area calculation, the final expression is obtained.

Combining all the above cases for all possible source node locations, equation (6.64) is obtained. Once the decoding set area is obtained through equation (6.64), its cardinality can be obtained using Poisson point process [177] as expressed in equation (6.55).

At this point, decoding set area and its cardinality given source node location is available, hence the problem is left with estimating the location of these nodes within $\mathcal{D}$. Denote the distance between node $d \in \mathcal{D}$ and target node t as l_{dt}. In order to simplify the analysis, l_{dt} is broken into two parts, namely the distance in the direction of a straight line from s to t (denoted as $l_{dt}^{\parallel}$), and the distance perpendicular to the direction from s to t (denoted as $l_{dt}^{\perp}$). These three parameters are related through trigonometry relation $l_{dt} = \sqrt{\left(l_{dt}^{\parallel}\right)^2 + \left(l_{dt}^{\perp}\right)^2}$. The following two subsections discuss each of these distance components separately.

Direct Distance $l_{dt}^{\parallel}$ Estimation

To find $l_{dt}^{\parallel}$ for all $d \in \mathcal{D}$, a straight line from s to t is drawn. Then, another line perpendicular to it is drawn and slided across the decoding set area as depicted in Figure 6.12a. Assuming that the decoding set area is a full circle, the shaded area created as the line is swept across the circle is shown in Figure 6.12b. It can be seen that the area of shaded region forms a cumulative-distribution-like curve, starting from 0 (when the line is still outside the circle) and reaches maximum at the whole decoding set area (when the line has completely swept through

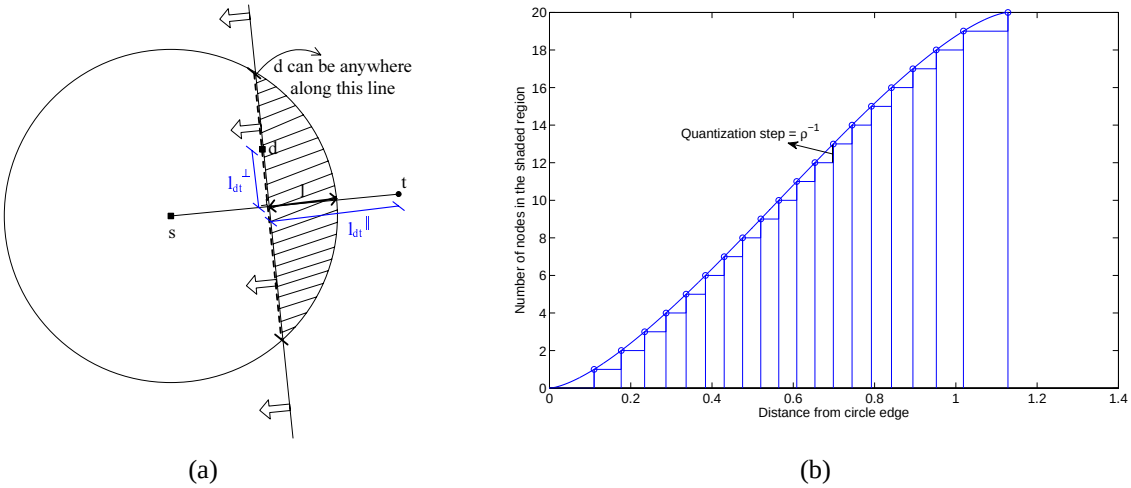

(a) (b)

Figure 6.12: Quantisation process of decoding set area to estimate the location of $|\mathcal{D}|$ nodes within the region

the circle).

In the figure, the horizontal axis represents the distance of the sweeper line from circle interior. Using continuous approximation theorem, the probable area within which the presence of exactly one node is equal to the inverse of node density within $\mathcal{D}$, which is given as $\rho^{-1} = \frac{A}{n}$. Here, A is the area of $\mathcal{D}$ calculated using (6.64), and n is the total number of nodes currently considered in $\mathcal{D}$. In line with this assumption, the curve is then quantised at ρ^{-1} step size. The abscissas of resulting quantisation points will then give the estimate distances (from circle interior) of decoding set nodes. Correspondingly, $l_{dt}^{\parallel}$ for all $d \in \mathcal{D}$ can be calculated by adding the obtained values with the distance of target node t to the circle circumference, which is equal to $\sqrt{(x_t - x_s)^2 + (y_t - y_s)^2} - r$. Note that this way of estimation would give a worse case scenario, in which direct distance is measured from the furthest line of an area containing each decoding set node, hence the performance obtained would serve as lower bound.

The analysis so far considers the case when there is no intersection between decoding set area with network boundaries, hence the shape of $\mathcal{D}$ is a full circle. In order to apply this technique for arbitrary source node location, a formula to calculate portion of decoding set

area which overlap with a segment of distance l from circle interior (in the direction from t to s) has to be derived.

Let different sides of network be indexed as $i = \{1, 2, 3, 4\}$; representing the Top, Left, Bottom, and Right side respectively. Denote $f_i(x, y)$ to be the overlapping area between a segment created by a line of distance l from circle interior (in the direction from t to s) with the segment created by intersection of $Disc_r(x, y)$ with the corresponding side of network boundaries. Then,

$$\int\int f_i(x,y)dxdy = \begin{cases} S_3\left(z_1(i),\ z_2(i),\ \text{atan}\frac{y_t-y_s}{x_t-x_s} - \text{acos}\frac{r-l}{r},\ \text{atan}\frac{y_t-y_s}{x_t-x_s} + \text{acos}\frac{r-l}{r},\ r\right) & \text{if overlap} \\ 0 & \text{if disjoint} \end{cases} \tag{6.69}$$

where $S_3(.)$ can be calculated using equation (6.58). Here, $z_1 = \{t_1, l_1, b_1, r_1\}$ and $z_2 = \{t_2, l_2, b_2, r_2\}$ denotes two different sets, where the index i represents the i^{th} element of the corresponding set whose values can be calculated using equations (6.65), (6.66), (6.67), and (6.68) respectively. Note that the range of integration in equation (6.69) is understood from the context, and therefore not stated explicitly.

The derivation of the above equation is identical for different cases of i. Without loss of generality, let $i = 1$ and the decoding set area intersects with top side of network boundary. Given source and target node location, the direction of t relative to s can be calculated as $atan\frac{y_t-y_s}{x_t-x_s}$. A segment created by a line of distance l from circle interior in the direction from t to s would be enclosed in an arc spanning from point $atan\frac{y_t-y_s}{x_t-x_s} - acos\frac{r-l}{r}$ to point $atan\frac{y_t-y_s}{x_t-x_s} + acos\frac{r-l}{r}$. To calculate the overlapping area of this segment with the one created from intersection with top side of network boundary, one must identify whether or not they are disjoint. From equation (6.65), two points (T_1 and T_2) representing the segment at network boundary can be calculated. Recall from earlier conventions that given two points in a circle, it

is possible to check if a third point is inside the arc spanning across the two. By checking the relative position of the two points representing a segment with respect to an arc spanning from T_1 to T_2, one can determine whether or not they overlap each other. If they are disjoint, there will be no overlap and the area is 0. Otherwise, the area of overlapping region can be found following equation (6.58) as $S_3\left(t_1,\ t_2,\ atan\frac{y_t-y_s}{x_t-x_s}-acos\frac{r-l}{r},\ atan\frac{y_t-y_s}{x_t-x_s}+acos\frac{r-l}{r},\ r\right)$. Combining the discussions for all cases of i results in equation (6.69).

In certain cases when there are intersection with two sides of network boundaries (in which the two created segments overlap one another), a common area covered by both segments and another segment of distance l from circle interior (in the direction from t to s) needs to be calculated.

Let $i = \{1, 2, 3, 4\}$ be an index representing the Top, Left, Bottom, and Right side of network respectively. Denote $g_i(x, y)$ to be the common area between a segment created by a line of distance l from circle interior (in the direction from t to s) with the overlapping area of two segments created by intersection of $Disc_r(x, y)$ with side i and side $(i)_4 + 1$ of network boundaries. Then,

$$\int\int g_i(x,y)dxdy = S_3\left(z_1(i),\ z_2(i),\ z_1\left((i)_4+1\right),\ z_2\left((i)_4+1\right),\ r\right) \bigcap S_1\left(\text{atan}\frac{y_t-y_s}{x_t-x_s}-\text{acos}\frac{r-l}{r},\ \text{atan}\frac{y_t-y_s}{x_t-x_s}+\text{acos}\frac{r-l}{r},\ r\right) \quad (6.70)$$

where $S_1(.)$ and $S_3(.)$ can be calculated using equations (6.56) and (6.58) respectively, and z_1 and z_2 are the sets similarly defined in equation (6.69). Again, the derivation of the above equation is identical for different cases of i, therefore without loss of generality, $i = 1$ is considered. Following the derivation of equation (6.69), the direction of target node t relative to s can be calculated as $atan\frac{y_t-y_s}{x_t-x_s}$. Two points representing a segment created by a line of distance l from circle interior in the direction from t to s can then be calculated as $atan\frac{y_t-y_s}{x_t-x_s}-acos\frac{r-l}{r}$ and $atan\frac{y_t-y_s}{x_t-x_s}+acos\frac{r-l}{r}$. Using equation (6.56), the area of a segment within an arc spanning

from both points can be calculated as $S_1\left(atan\frac{y_t-y_s}{x_t-x_s}-acos\frac{r-l}{r},\ atan\frac{y_t-y_s}{x_t-x_s}+acos\frac{r-l}{r},\ r\right)$.

Then, four points representing two segments created by intersection with top and left side of network boundaries can be calculated using equations (6.65) and (6.66) respectively. Using equation (6.58), the overlapping area between the two segments can be calculated as $S_3\left(l_1,l_2,t_1,t_2,r\right)$. Finally, the common area between a segment created by a line of distance l from circle interior (in the direction from t to s) with the overlapping area of two segments created by intersection of $Disc_r(x,y)$ with network boundaries can be calculated by performing cut set operation to the two areas obtained, resulting in equation (6.70).

Using equations (6.69) and (6.70), the segment calculation taking into consideration all cases of edge effects can be performed. Let $ABCD$ be a square network of size L by L, and $Disc_r(x,y)$ be a circle of radius r centered at (x,y). Denote $Segment_l(x,y)$ to be a segment in $Disc_r(x,y)$ created from a line of distance l from disc interior (in the direction from node s to t). Then:

$$\int\int_{ABCD} Segment_l(x,y)\,dxdy = S_2(l,r) - \sum_{i=1}^{4}\int\int f_i(x,y)\,dxdy + \sum_{i=1}^{4}\int\int g_i(x,y)\,dxdy \tag{6.71}$$

where $S_2(.)$ is given in equation (6.57), and function $f_i(x,y)$ and $g_i(x,y)$ are as defined in equations (6.69) and (6.70) respectively.

To proof the correctness of equation (6.71), different cases are considered. Denote these cases as case 0 to case 12 following definition in equation (6.64). When decoding set area are enclosed in $ABCD$ (case 0), there will be no intersection with any of network boundaries, therefore both $f_i(x,y)$ and $g_i(x,y)$ are zero. The area of $Segment_l(x,y)$ is then equal to $S_2(l,r)$, which is in line with equation (6.57).

When decoding set area intersects with one side or two sides of $ABCD$ with no overlap (case 1 to 8), the function $g_i(x,y)$ would return zero. Meanwhile, the second term of equation (6.71) calculates the area of portion of the segment that is outside the four boundaries of

$ABCD$. Hence, by subtracting this value from $S_2(l, r)$, the area of $Segment_l(x, y)$ that lies inside $ABCD$ is obtained as desired.

When decoding set area intersects with two sides of $ABCD$ and the segments are overlapping (case 9 to 12), the area calculation is similar as the earlier case. However, since the segments created with network boundaries overlap, there will be double reduction on the common area between the overlapping region and $Segment_l(x, y)$. Adding all the common areas at four corners of $ABCD$ (which is calculated using $g_i(x, y)$ according to equation (6.70)), the last term of equation (6.71) is obtained. Hence, equation (6.71) is valid for all possible cases of source node location (with different shapes of decoding set area).

Using equation (6.71), the proposed technique to find $l_{dt}^{\parallel}$ for all $d \in \mathcal{D}$ by quantising the curve representing sub area of $\mathcal{D}$ as explained earlier can be applied for all possible source node locations. Therefore, given an arbitrary decoding set and location of s and t, the direct distance $l_{dt}^{\parallel}$ for all $d \in \mathcal{D}$ can be obtained.

Perpendicular Distance $l_{dt}^{\perp}$ Estimation

In Figure 6.12a, it can be seen that knowing $l_{dt}^{\parallel}$ alone is not sufficient to describe a location of decoding set node, as the node can be anywhere along the dashed line. Since nodes are uniformly distributed in the network, it can be assumed that the decoding set node is positioned in the dashed line with uniform probability.

Denote u_l and u_r to be the left and right range of possible decoding set node location. Then $l_{dt}^{\perp}$ can be approximated as $\mathcal{U}(u_l, u_r)$. It is also noted that the values of u_l and u_r depends on the shape of decoding set area. Moreover, the distance l from circle interior from which the decoding set node is located also determines the values of u_l and u_r. The following derivations are required to estimate perpendicular distances $l_{dt}^{\perp}$ of decoding set nodes d for all $d \in \mathcal{D}$.

Given four points $A1$, $A2$, $B1$, and $B2$ in a circle of radius r, let (x_p, y_p) be the coordinates (relative to circle center) of intersection point between a line passing through points $A1$, $A2$,

and another line passing through points $B1$, $B2$. Then, it can be shown that the coordinates of intersection point can be calculated using the following formula:

$$x_p(a1,a2,b1,b2,r) = \frac{r}{M_a - M_b}\left[\sin(b1) - \sin(a1) + M_a\cos(a1) - M_b\cos(b1)\right] \quad (6.72)$$

$$y_p(a1,a2,b1,b2,r) = \frac{r}{M_a^{-1} - M_b^{-1}}\left[\cos(b1) - \cos(a1) + M_a^{-1}\sin(a1) - M_b^{-1}\sin(b1)\right] \quad (6.73)$$

where $M_a = \frac{sin(a2)-sin(a1)}{cos(a2)-cos(a1)}$ and $M_b = \frac{sin(b2)-sin(b1)}{cos(b2)-cos(b1)}$, representing the gradient of a line passing through $A1$, $A2$, and a line passing through $B1$, $B2$ respectively.

Now, given two coordinates $(x1, y1)$ and $(x2, y2)$ relative to circle center, denote v_l and v_r as the distance from a point of intersection (between a line passing through both coordinates with a perpendicular line passing through circle center) to point $(x1, y1)$ and $(x2, y2)$ respectively. Then:

$$v_l(x1,y1,x2,y2) = \left[\left(x1 - \frac{M_o^2\,x1}{M_o^2+1} + \frac{M_o\,y1}{M_o^2+1}\right)^2 + \left(y1 - \frac{y1}{M_o^2+1} + \frac{M_o\,x1}{M_o^2+1}\right)^2\right]^{0.5} \quad (6.74)$$

$$v_r(x1,y1,x2,y2) = \left[\left(x2 - \frac{M_o^2\,x1}{M_o^2+1} + \frac{M_o\,y1}{M_o^2+1}\right)^2 + \left(y2 - \frac{y1}{M_o^2+1} + \frac{M_o\,x1}{M_o^2+1}\right)^2\right]^{0.5} \quad (6.75)$$

where $M_o = \frac{y2-y1}{x2-x1}$ represents the gradient of a straight line passing through $(x1, y1)$ and $(x2, y2)$.

Using equations (6.72), (6.73) and (6.74), (6.75), the range of perpendicular distance can be calculated. Let $ABCD$ be a square network of size L by L, and $Disc_r(x, y)$ be a circle of radius r centered at (x, y). Index $i = 1, 2, 3, 4$ represents the Top, Left, Bottom, and Right side of $ABCD$ respectively. Given a line of distance l from disc interior (in the direction from s to t), an arc is created spanning from point $P1$ to $P2$, where:

$$\begin{aligned} p1 &= \text{atan}\frac{y_t - y_s}{x_t - x_s} - \text{acos}\frac{r-l}{r} \\ p2 &= \text{atan}\frac{y_t - y_s}{x_t - x_s} + \text{acos}\frac{r-l}{r} \end{aligned}$$

Let u_l and u_r be the length of left and right portion of the line measured from its intersection point (with a straight line from s to t). Then, the parameters u_l and u_r are dependent on three basic scenarios, namely:

a. The line does not cross any of network boundaries

b. The line crosses side i of the network, and point $p2$ is inside $ABCD$

c. The line crosses two sides of network denoted as side i and side $(i)_4 + 1$

where notation $(.)_4$ is used to indicate circular modulo 4 operation. Based on the above scenarios, the values of u_l and u_r can be calculated as:

$$u_l = \begin{cases} -\sqrt{r^2 - (r-l)^2} & \text{case a} \\ v_l\left[r\cos(p2), r\sin(p2), x_p(z_1(i), z_2(i), p1, p2, r), y_p(z_1(i), z_2(i), p1, p2, r))\right] & \text{case b} \\ v_l[x_p(z_1(i), z_2(i), p1, p2, r), y_p(z_1(i), z_2(i), p1, p2, r), x_p(z_1\left((i)_4 + 1\right), & \\ z_2\left((i)_4 + 1\right), p1, p2, r), y_p\left(z_1\left((i)_4 + 1\right), z_2\left((i)_4 + 1\right), p1, p2, r\right)] & \text{case c} \end{cases} \tag{6.76}$$

$$u_r = \begin{cases} \sqrt{r^2 - (r-l)^2} & \text{case a} \\ v_r\left[r\cos(p2), r\sin(p2), x_p(z_1(i), z_2(i), p1, p2, r), y_p(z_1(i), z_2(i), p1, p2, r))\right] & \text{case b} \\ v_r[x_p(z_1(i), z_2(i), p1, p2, r), y_p(z_1(i), z_2(i), p1, p2, r), x_p(z_1\left((i)_4 + 1\right), & \\ z_2\left((i)_4 + 1\right), p1, p2, r), y_p\left(z_1\left((i)_4 + 1\right), z_2\left((i)_4 + 1\right), p1, p2, r\right)] & \text{case c} \end{cases} \tag{6.77}$$

Here, $x_p(.)$, $y_p(.)$ are as defined in equations (6.72) and (6.73), $v_l[.]$, $v_r[.]$ are as defined in equations (6.74) and (6.75), while z_1 and z_2 are the sets defined in equation (6.69).

The derivation of the above for different cases will be handled separately. First, when the line does not cross any of network boundaries, both $P1$ and $P2$ are located at circle circumference inside $ABCD$, therefore the intersection point with a straight line from s to t will divide

the line equally. The length of a line of distance l from circle interior of radius r can be calculated as $2\,r\,\sin\left(\text{acos}\frac{r-l}{r}\right)$. Since the intersection point divide the line equally, u_l and u_r would have opposite sign but the same magnitude, given as $r\,\sin\left(\text{acos}\frac{r-l}{r}\right)$. After some modifications using trigonometric identity, the expression in the first case of equations (6.76) and (6.77) are obtained.

When the line crosses one side of network boundary, either $P1$ or $P2$ are not located at circle circumference, but at the boundary itself. Without loss of generality, let the intersection be with the top side of $ABCD$, and let $P2$ be the one inside $ABCD$. The coordinate of $P2$ relative to circle center can be calculated as $(x_{p2}, y_{p2}) = (r\,cos(p2), r\,sin(p2))$. Similarly, the coordinate of $P1$ can be calculated using equations (6.72) and (6.73) as $(x_{p1}, y_{p1}) = (x_p(t_1, t_2, p1, p2, r), y_p(t_1, t_2, p1, p2, r))$. Then, the parameters u_l and u_r can be calculated using equations (6.74) and (6.75) as $v_l(x_{p2}, y_{p2}, x_{p1}, y_{p1})$ and $v_r(x_{p2}, y_{p2}, x_{p1}, y_{p1})$ respectively, which gives the expression in the second case of equations (6.76) and (6.77).

The last case corresponds to scenario when the line crosses two sides of network boundaries. Due to the assumption that network size L is greater than the diameter of decoding set $\mathcal{D}$, the line can only cross two sides that is adjacent to each other. Without loss of generality, let $P1$ and $P2$ be the points at the left and top side of $ABCD$ respectively. The coordinate of $P1$ can be calculated as $(x_{p1}, y_{p1}) = (x_p(l_1, l_2, p1, p2, r), y_p(l_1, l_2, p1, p2, r))$ using equations (6.72) and (6.73). With the same approach, $P2$ can be calculated as $(x_{p2}, y_{p2}) = (x_p(t_1, t_2, p1, p2, r), y_p(t_1, t_2, p1, p2, r))$. The values of u_l and u_r can then be calculated using equations (6.74) and (6.75) as $v_l(x_{p2}, y_{p2}, x_{p1}, y_{p1})$ and $v_r(x_{p2}, y_{p2}, x_{p1}, y_{p1})$ respectively, which gives the expression in the last case of equations (6.76) and (6.77).

Using the above systematic method to calculate the decoding set area, its cardinality, and to approximate the locations of relay nodes within the decoding set, average network performance under D-TxMRC and DSTBC scheme can be found via numerical integration. Detailed discussion on network performance analysis is given in the next section.

6.5 Performance Analysis and Effect of Network Parameters

As explained earlier, in random networks, performance analysis needs to consider all possible node locations. Throughout this work, network outage probability is used as the performance metric. The word 'network' is used to emphasise that outage is measured from network perspective considering all possible source destination pairs as well as relay locations; in contrast to the conventional outage probability used for point to point communication link. The system parameters as described in Section 6.2 is used for the simulation model, and the system is evaluated for 2 b/s/Hz bandwidth efficiency at 10^{-6} error rate. Different network parameters including total number of nodes, network size, path loss exponent, edge effect, and how those parameters affect the overall performance are studied.

6.5.1 Direct Transmission

In direct transmission, the randomness of point to point outage probability in equation (6.1) is solely determined by the randomness of parameter λ_{sd}. Therefore, to calculate the network outage probability, equation (6.1) is averaged across the distribution of λ_{sd}. And since λ_{sd} is related to source destination distance through path loss equation, this averaging process can be done via integration with respect to distance distribution as given in equation (6.54).

It is apparent that total number of nodes does not have any impact to the network outage probability when direct transmission is used. Moreover, since no relay node is involved in the transmission, edge effect is irrelevant to the performance evaluation. Figure 6.13 shows the network outage probability of direct transmission, and how network size as well as path loss exponent affect the overall performance. The figure shows an approximate performance loss of $9 - 10$dB when the network size is increased by a factor of 4 while fixing the path loss exponent to 3. The same amount of performance degradation is observed when path loss

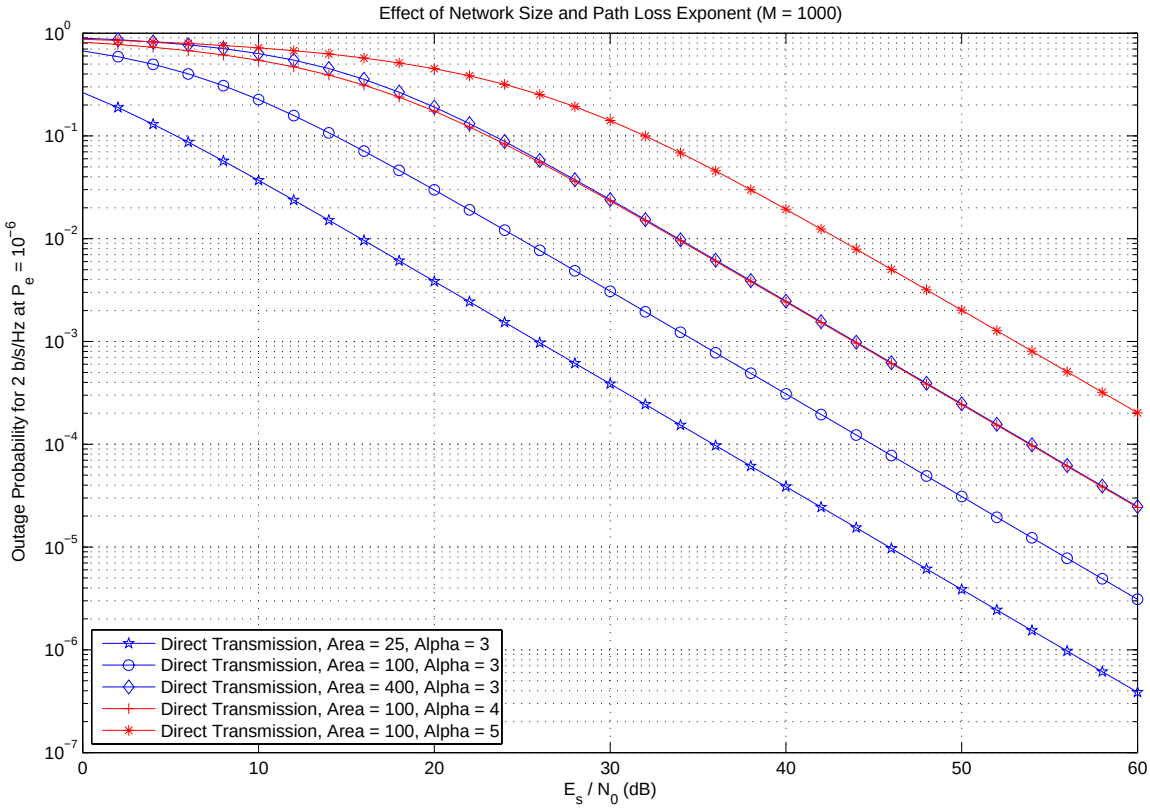

Figure 6.13: Effect of Total Number of Nodes and Edge Effect in Direct Transmission

exponent is varied from 3 to 5 while keeping the network area unchanged.

6.5.2 Amplify and Forward

The situation is more complex when Amplify and Forward (AnF) is used as the transmission protocol. From the point to point outage probability expressed in equation (6.7), it can be seen that all λ_{sd}, λ_{sr}, and λ_{rd} (which is related to source-destination, source-relay, and relay-destination distance respectively) affect the performance. As such, calculating network outage probability involves integrating the point to point performance with respect to the distribution of all the three factors. Following the argument in Subsection 6.4.2, the source-relay and relay-destination distance must include all possible relay locations within the Region of Interest (RoI), while the source-destination distance must consider all possible node placements in the network. In that subsection, a method to break down RoI into cells was also discussed as an

efficient method to simplify the integration process. The process can be explained as follows.

First, let the cells be numbered, and let Θ_{c_x} denotes cell x ($x \in (1..T)$, where T is the total number of cells in the region of interest). $|\Theta_{c_x}|$ is the area of Θ_{c_x}, and $\Phi\left(|\Theta_{c_x}|\right)$ denotes the number of nodes inside Θ_{c_x}. The network outage probability can be calculated by adding conditional outage probabilities for all possible relay node locations and the outage probability when the region of interest is empty (in which the transmission has to fall back to direct transmission) as follows:

$$\begin{aligned} P_{\text{out}} &= \sum_{t=1}^{T}\left(\prod_{s=1}^{t-1} Pr\left[\Phi\left(|\Theta_{c_s}|\right)=0\right]\right)\left(1 - Pr\left[\Phi\left(|\Theta_{c_t}|\right)=0\right]\right) P_{\text{out}}^{(\text{AnF})}\left(c_t\right) \\ &\quad + \prod_{s=1}^{T} Pr\left[\Phi\left(|\Theta_{c_s}|\right)=0\right] P_{\text{out}}^{(\text{direct})} \end{aligned} \tag{6.78}$$

where $P_{\text{out}}^{(\text{AnF})}\left(c_t\right)$ is the outage probability of AnF relaying with relay node located at the center of t^{th} cell, which is calculated through equation (6.7), and $P_{\text{out}}^{(\text{direct})}$ is the outage probability of direct transmission as given in equation (6.1).

It is evident that the outage probability is affected by how the cells are numbered. From equation (6.78), it can be seen that the optimum numbering is to allocate the smallest number to the cell which result in the lowest outage probability. In practical implementation, this optimum numbering corresponds to relay node selection, in which the best relay node always gets selected first. The network outage probability is then calculated by averaging equation (6.78) with respect to the distribution of source-destination distance according to equation (6.54). In the following, network outage probability under AnF transmission scheme is analysed for different network settings.

Total Number of Nodes

In AnF scheme, the total number of nodes affects the likeliness of relay node existence. Figure 6.14 shows network outage probability when the number of nodes in the network M is

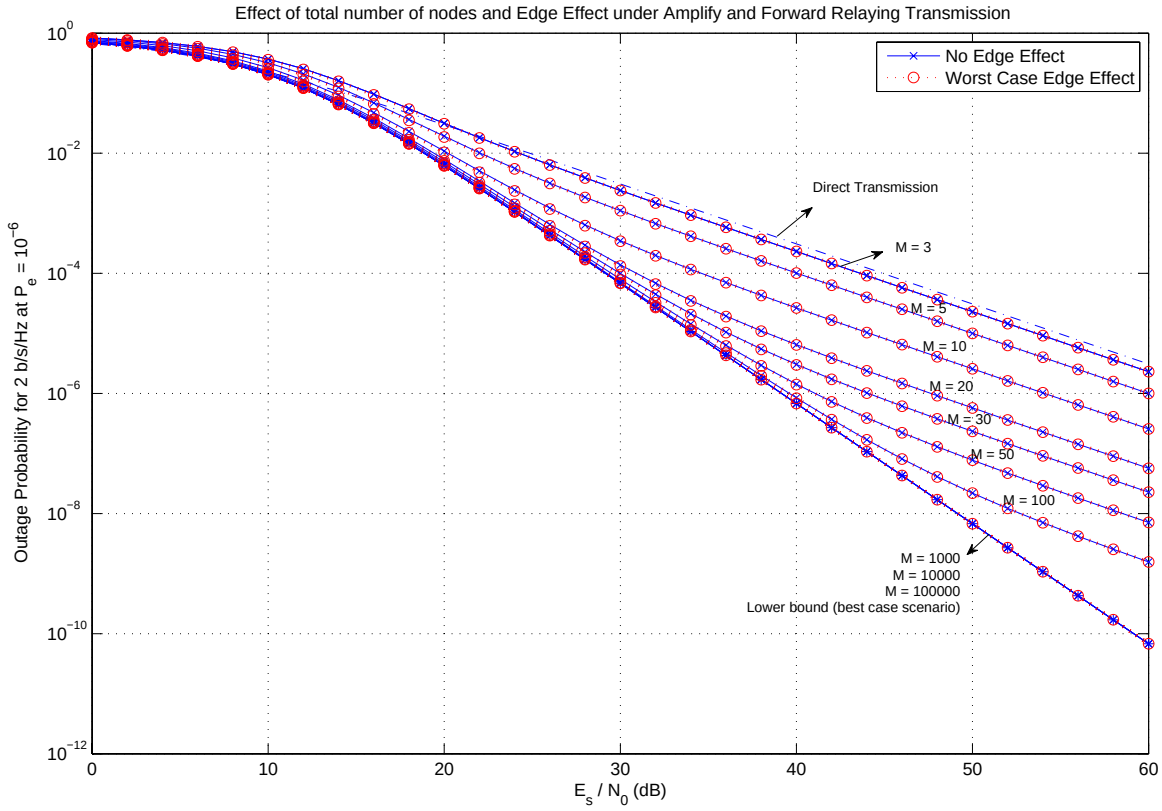

Figure 6.14: Effect of Total Number of Nodes and Edge Effect in AnF Relaying

varied from 3 to 100000 (where optimum selection between relay nodes is adopted). Several conclusions can be deduced from Figure 6.14.

First of all, the number of nodes affects the performance by providing different diversity gains. When the number of nodes is too small, for example when $M = 3$, there is only one potential relay node in the network apart from source and destination. And the probability that this node is located within the region of interest is also small. Therefore the performance of AnF relaying collapses to direct transmission case.

Secondly, it is also observed that as the number of nodes increases, the performance is improved. However, it is important to note that the gap between outage probability curves for different number of nodes differs at different SNR ranges. For example, it is noted that the performance for $M = 20$ and above are very close when SNR $\leq$ 20dB. As the SNR increases, the gap between $M = 20$ and $M = 30$ is widening, and then the gap remains constant for

SNR $\geq$ 40dB. The same trend is true for other M values but with different SNR ranges. This shows that operating SNR has a significant role in deciding optimum number of nodes to be deployed in the network.

Finally, it is observed that as the number of nodes in the network gets very large ($M = 1000$ or more), the performance converges to the best case scenario, in which the relay node is located right in the middle of source and destination. This again gives an insight that deploying too many nodes would be a waste of resources, because no performance improvement can be achieved out of it. However, this is valid only for AnF scheme with single relay. When a more complex technique is adopted (such as distributed space-time coding [108] or cooperative spatial multiplexing [178]), and more than one relay nodes are deployed for message transmission, the network outage performance is expected to improve. This is achieved by exploiting multi-antenna technique with different relay nodes acting as virtual antenna. Since capacity of multiple antenna systems is higher in point-to-point link ([3]-[4]), the same trend is expected in networked scenario.

Edge Effect

When both source and destination nodes are located near the same side of network boundary, the region of interest would be truncated and the number of potential relay nodes would be decreased. Edge Effect happened due to truncation of region of interest. The worst case Edge Effect happens when both source and destination nodes are located right in the same side of network edge. In this case, the region of interest is half the size of the normal case. Since the probability of relay node existence is proportional to the area of this region, the number of potential relay nodes would be decreased.

To completely analyse this effect, one needs to consider all possible shapes of region of interest for the given position of source and destination. The network outage probability has to be calculated considering different possible areas of this region. This task is too complex

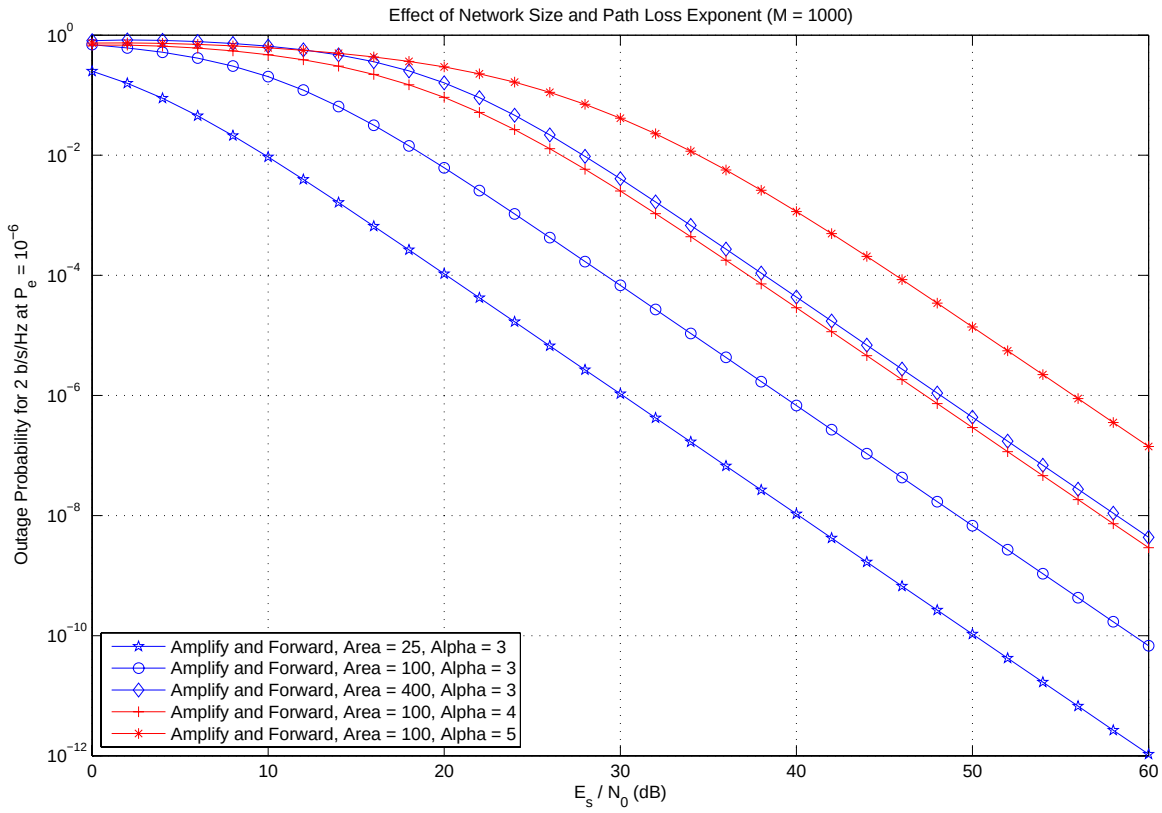

Figure 6.15: Effect of Network Size and Path Loss Explonent in AnF Relaying

to evaluate, and therefore the present analysis resorts to consider the worst case scenario, regardless of the source and destination location. Although this approach does not result in exact performance, it is useful in giving the lower bound of network outage probability.

Figure 6.14 shows the network outage probability performance without edge effect and with worst case edge effect for different total number of nodes. It is observed that regardless of the number of nodes, edge effect does not cause any significant degradation in performance (both the crossed solid curves and the circled dashed curves in Figure 6.14 coincide with one another).

Network Size

The average distance between source and destination increases with the network size, resulting in poorer performance. Figure 6.15 signifies this effect by showing network outage perfor-

mance under AnF scheme with different network sizes. It is observed that under AnF scheme, approximately $8-9$dB performance loss occurs when the network size is increased by a factor of 4, which is slightly better than direct transmission scheme whereby a larger loss of $9-10$dB is observed for the same scaling factor.

Path Loss Exponent

Figure 6.15 also shows the network outage probability under AnF scheme for three different path loss exponent values (ranging from 3 to 5). It is observed that 8dB loss in outage performance occurs in AnF scheme when path loss exponent is increased by 1 point, which again smaller than direct transmission, where the performance loss is around 10dB.

6.5.3 Distributed Transmitter Maximum Ratio Combining (D-TxMRC)

Looking at the point to point outage probability expression for D-TxMRC scheme in equation (6.25), it is observed that the outage probability itself is a random variable, and is dependent on the source destination distance, as well as the number of cooperative nodes in $\mathcal{D}$.

For the source destination distance, the squared distance distribution derived earlier in equation (6.54) can be readily used. As for the size of $\mathcal{D}$, it is first assumed that the area of radius l^* from source node is contained within the network. A discussion on the edge effect and how it affects the performance will be given in later part of this subsection. Since all nodes are uniformly distributed in the network, the number of nodes within a circle of radius $r = l^*$ from source s obeys Binomial Distribution [179], hence the probability that there are i nodes in $\mathcal{D}$ is:

$$Pr[|\mathcal{D}| = i] = \begin{pmatrix} M-1 \\ i \end{pmatrix} \left(\frac{\pi r^2}{L^2}\right)^i \left(1 - \frac{\pi r^2}{L^2}\right)^{M-i-1} \tag{6.79}$$

Finally, considering all factors of randomness, the network outage probability under D-

TxMRC scheme can be calculated as:

$$\overline{P_{out}^{(D-TxMRC)}} = \int_0^{L^2} \left[\sum_{i=0}^{M-2} Pr[|\mathcal{D}| = i] \;\; P_r \left[\left(|h_{sd}|^2 \; + \; \sum_{k \in \mathcal{D}} |h_{kd}|^2 \right) \leq \rho^* \right] \;\; PDF_{l_{sd}^2}(z) \right] dz \tag{6.80}$$

Note that the upper limit of the summation above is set to $M-2$, which is the number of all nodes except the source and destination node. It is apparent that there are two main terms affecting the network outage probability, namely $Pr[|\mathcal{D}| = i]$ (the probability that the decoding set contains i nodes) and $P_r\left[\left(|h_{sd}|^2 \; + \; \sum_{k \in \mathcal{D}} |h_{kd}|^2\right) \leq \rho^*\right]$ (the probability that the combined channel effect is less than a given threshold). These two terms are affected by the relay nodes cardinality and positions as discussed in Subsection 6.4.3. Firstly, the decoding set area is dependent to the source node location, which is given by the relation in equation (6.64). Then, given that the decoding set area is equal to A, the probability mass function of the relay nodes cardinality $Pr[|\mathcal{D}| = i]$ is given by equation (6.79), with the term πr^2 replaced by A as follows:

$$Pr[|\mathcal{D}| = i] = \begin{pmatrix} M-1 \\ i \end{pmatrix} \left(\frac{A}{L^2}\right)^i \left(1 - \frac{A}{L^2}\right)^{M-i-1} \tag{6.81}$$

Secondly, given a source (and destination) node location and the corresponding area of the decoding set, the position of the relay nodes has to be estimated. The direct distance $l_{dt}^{\parallel}$ needs to be obtained by quantising the function given in equation (6.71). This is followed by the perpendicular distance $l_{dt}^{\perp}$ calculation, which can be approximated as uniform distribution $\mathcal{U}(u_l, u_r)$, with both parameters calculated according to equation (6.76) and (6.77) respectively. Then, the distances from each relay to destination can be calculated as $\sqrt{\left(l_{dt}^{\parallel}\right)^2 + \left(l_{dt}^{\perp}\right)^2}$. The distance from the relay to destination affects the distribution of the respective channel gain $|h_{kd}|^2$ (in particular its mean and variance), which is attributed from the amount of path loss (as governed by the path loss model in equation (4.2)). This in turn affects the outage probability through the value of $P_r\left[\left(|h_{sd}|^2 \; + \; \sum_{k \in \mathcal{D}} |h_{kd}|^2\right) \leq \rho^*\right]$.

In order to find the network outage probability, all possible placements of nodes within $\mathcal{D}$ have to be taken into consideration. To simplify the analysis, upper and lower bound on the performance are considered instead. Noting that the decoding set is contained in a circle of radius l^* from source node, for all $k \in \mathcal{D}$, λ_{kd} are bounded as:

$$\underbrace{10^{0.1C_1}\ (l_{sd}+l^*)^{\alpha}\ 10^{0.1\overline{\chi}}}_{\lambda^{(l)}} \ \geq\ \lambda_{kd}\ \geq\ \underbrace{10^{0.1C_1}\ (l_{sd}-l^*)^{\alpha}\ 10^{0.1\underline{\chi}}}_{\lambda^{(u)}} \tag{6.82}$$

where $\overline{\chi}$ and $\underline{\chi}$ are the largest and smallest values of macroscopic fading respectively. Using the above approximations, the term $P_r\left[\left(|h_{sd}|^2\ +\ \sum_{k\in\mathcal{D}}|h_{kd}|^2\right) \leq \rho^*\right]$ in equation (6.80) can be calculated as follows. First, note that the distribution of different channel gains may be dependent to one another. In this case, it is difficult to analyse the outage probability as it involves the derivation of CDF of a sum of correlated random variables. To deal with this scenario, the present analysis resorts to Monte Carlo simulation. On the other hand, when different channel gains are independent, closed form solution can be obtained. First, note that $\sum_{k\in\mathcal{D}}|h_{kd}|^2$ now becomes a chi-squared distributed random variable with $2|\mathcal{D}|$ degree of freedom with parameter $\lambda^{(.)}$ (the superscript $\lambda^{(u)}$ or $\lambda^{(l)}$ is used depending whether upper or lower bound is considered). Its CDF can be expressed as $\frac{\gamma\left(x\lambda^{(.)},|\mathcal{D}|\right)}{\Gamma(|\mathcal{D}|)}$, where $\gamma(.)$ and $\Gamma(.)$ represent incomplete and complete gamma function respectively. By conditioning the CDF with respect to $|h_{sd}|^2$ and integrating it within a range of interest, the following relation is obtained:

$$P_r\left[\left(|h_{sd}|^2\ +\ \sum_{k\in\mathcal{D}}|h_{kd}|^2\right) \leq \rho^*\right] = \int_0^{\rho^*} \frac{\gamma\left((\rho^*-t)\lambda^{(.)},|\mathcal{D}|\right)}{\Gamma(|\mathcal{D}|)}\ \lambda_{sd}\ e^{-\lambda_{sd}t}\ dt \tag{6.83}$$

Substituting equations (6.54), (6.79), and (6.83) into equation (6.80), the network outage probability can be calculated numerically.

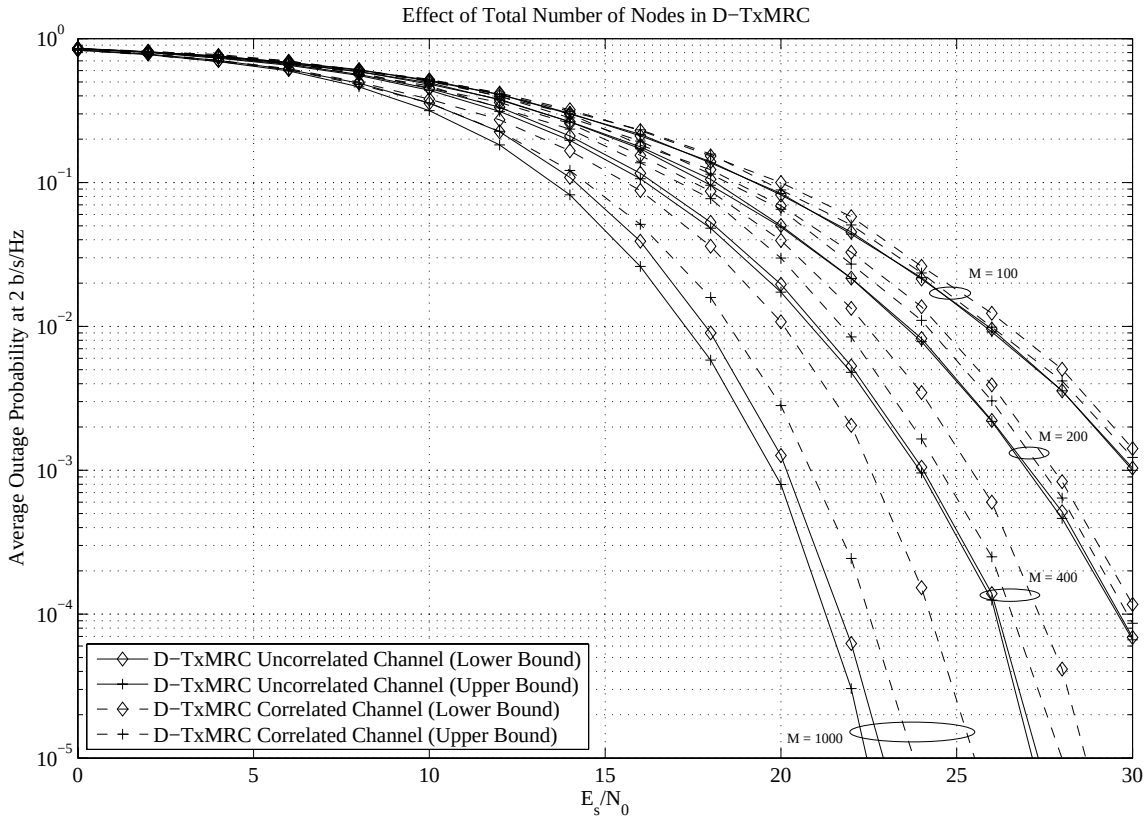

Figure 6.16: Effect of Total Number of Nodes in D-TxMRC Scheme ($L = 10$ km, α = 3, $\sigma_s^2 = 3$dB)

Total Number of Nodes

Total number of nodes in the network will affect the size of decoding set $\mathcal{D}$. In probabilistic terms, this corresponds to the right shift on the mode of $|\mathcal{D}|$ (according to equation (6.79)). Therefore, large values of i in $Pr\left[|\mathcal{D}| = i\right]$ will dominate the network outage calculation in equation (6.80). Since the achievable gain is linearly related to $|\mathcal{D}|$, the overall performance will improve as the number of nodes increases. The network outage probability of the system for different total number of nodes is shown in Figure 6.16.

In the figure, when lower bound performance is considered, macroscopic fading $\overline{\chi}$ is taken to be the largest value among all relay nodes, while all nodes are assumed to be located in the distance ($l_{sd} + l^*$) away from destination node. An interesting observation from Figure 6.16 is that the bound on network outage probability is tighter for lower values of M. This can

be explained by analysing equation (6.83), which computes cumulative distribution function of normalised SNR. The upper and lower bound is obtained by substituting $\lambda^{(.)}$ with $\lambda^{(u)}$ and $\lambda^{(l)}$ respectively. It is noted that the gradient of incomplete gamma function $\gamma(.,.)$ is inversely proportional to the parameter in the second argument. Hence, as the value of $|\mathcal{D}|$ increases, changes in the first argument (caused by the difference between $\lambda^{(u)}$ and $\lambda^{(l)}$) will result in negligible variation, which explain why the bound is tighter in higher values of M.

As far as the effect of channel correlation is concerned, the dashed curves in Figure 6.16 shows the network outage probability for different M. Throughout the simulation, all relay nodes in decoding set are assumed to be mutually correlated to each other with correlation coefficient 0.9. From the figure, it is apparent that the presence of channel correlation generally degrades overall performance, especially for large values of M. Since larger $|\mathcal{D}|$ (which is likely to occur when total number of nodes is large) implies more channels are correlated, performance degradation is more severe for large M.

Edge Effect

In a geometrically bounded network, edge effect is known to have significant impact in network performance. In D-TxMRC scheme, edge effect happens when source node is located near to the network boundary. When this happens, the area of $\mathcal{D}$ will be in the form of truncated circle, which will then affect the probability of total number of helper nodes $Pr\left[|\mathcal{D}| = i\right]$. The truncation of $\mathcal{D}$ will also change the lower bound analysis, since a point of distance l^* from source node (in the opposite direction of destination node) may not be in the network. In order to do an exact analysis on edge effect, the equation (6.80) has to be modified to include the truncation phenomena. This means that the integration can not be performed solely with respect to separation distance, but rather on the location of source and destination node. Correspondingly, the calculation of the CDF has to be replaced with the conditional CDF, in which the conditioning variable is the source node location. Only then the truncation of $\mathcal{D}$ can

be incorporated into the network outage calculation.

Here, the edge effect is analysed as the lower bound of the performance. Note that the lower bound due to edge effect consideration is different from the bounding due to node location in decoding set. For a square network, it is not difficult to see that the worst case edge effect occurs when the source node is located at the corner of the network. In this case, the decoding set area is in the form of quarter of a circle, reducing the area of $\mathcal{D}$ by a factor of 4. As such, the probability that there are i nodes in the decoding set can be calculated using equation (6.79), with πr^2 replaced with $\pi r^2/4$ as follows:

$$Pr[|\mathcal{D}| = i] = \begin{pmatrix} M-1 \\ i \end{pmatrix} \left(\frac{\pi r^2}{4\,L^2}\right)^i \left(1 - \frac{\pi r^2}{4\,L^2}\right)^{M-i-1} \tag{6.84}$$

Additionally, since the decoding set area is only a quarter of a circle, the largest relay destination distance can be shown to be equal to $\sqrt{l_{sd}^2 + r^2}$, which happens when the destination is located at the network edge. This would result in the worse case scenario, as the channel gain would have the smallest variance and mean value.

By assuming that the decoding set area is always one quarter of a circle area regardless of the source node position, and that all relay destination distances always take the largest possible value, a worst case edge effect can be analysed.

Figure 6.17 shows the performance of both D-TxMRC scheme with and without worst case edge effect. It can be observed that edge effect has the potential to severely degrade overall performance. Approximately 8dB degradation at 10^{-5} outage probability is observed. In the presence of channel correlation, further degradation is observed as shown by the dashed curves in Figure 6.17. Under worst case edge effect, the extra degradation is not as severe. This again follows from the mutual correlation assumption. Since edge effect reduces the size of $\mathcal{D}$ (and therefore the number of relay nodes), the effect of channel correlation is also reduced.

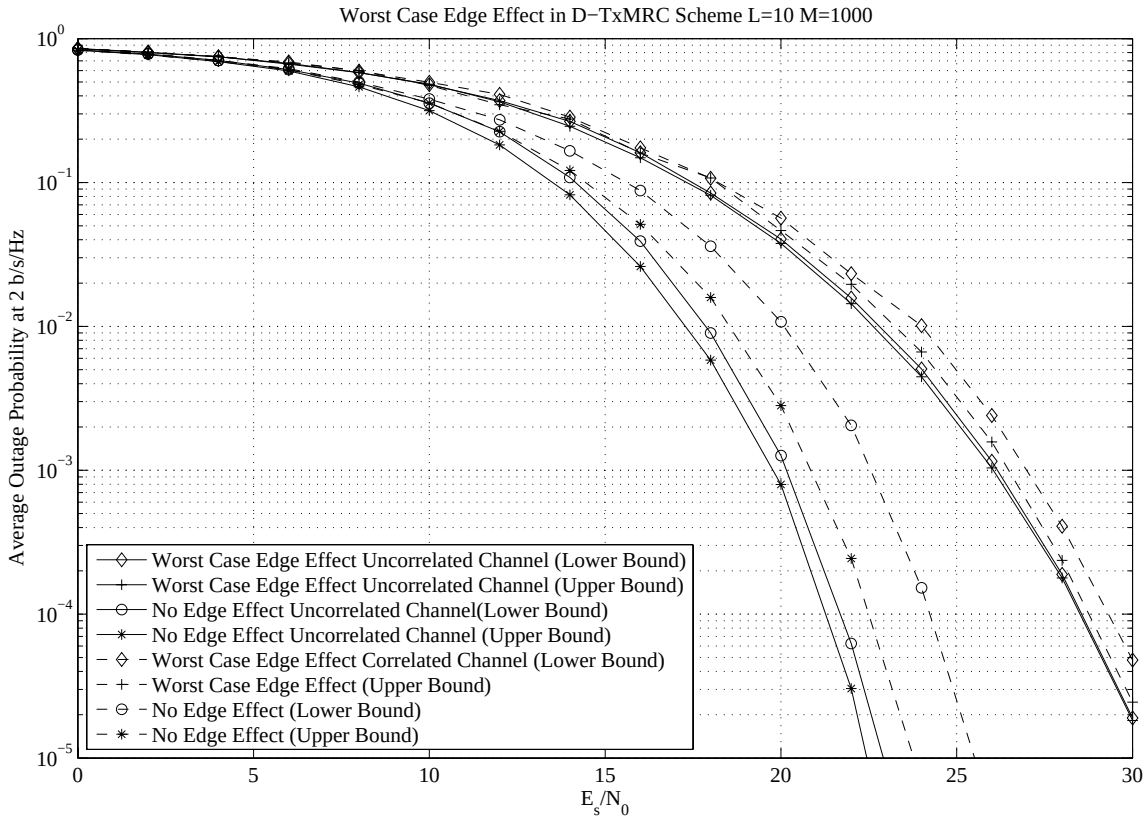

Figure 6.17: Influence of Edge Effect in D-TxMRC Scheme ($M = 1000$ nodes, $L = 10$ km, α = 3, $\sigma_s^2 = 3$dB)

Network Size

Network size affects the overall performance in two ways. Firstly, for the same total number of nodes, larger network size implies lower node density, which decreases the likely number of nodes in decoding set through equation (6.79). Since the overall performance is directly related to the number of nodes in decoding set, larger network size (and correspondingly lower node density) will degrade the overall performance.

Secondly, larger network size will increase the separation distance between source and destination. Due to larger path loss, this will also degrade overall performance (as reflected by the larger integration range in equation (6.80)). However, it is not yet clear which one of these two factors is the major contributor to the performance loss. Figure 6.18 shows the network outage probability performance for different network sizes.

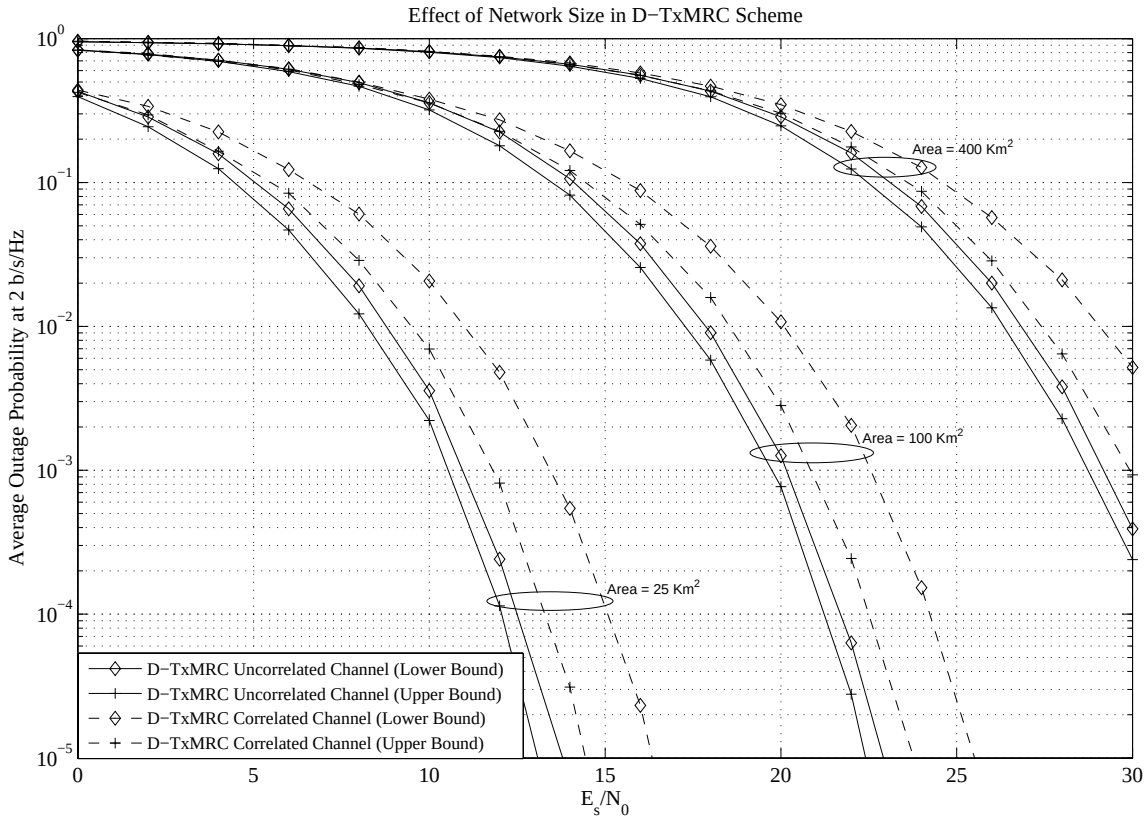

Figure 6.18: Effect of Network Size in D-TxMRC Scheme ($M = 1000$ nodes, α = 3, $\sigma_s^2 = 3$dB)

It is observed that a loss of approximately 8dB at 10^{-5} outage rate for every factor-of-four increase in the network area is incurred. It is also observed that increasing network size does not change the diversity order achieved, which can be seen from equal gradient on all the curves in Figure 6.18. This signifies the dominance of the second factor as the main cause in performance degradation. In other words, the performance loss caused by a decrease in the number of nodes in decoding set is negligible compared to the one caused by the increase in path loss effect.

For completeness, the overall performance in the presence of channel correlation is also analysed for different network sizes. It is observed that irrespective of channel correlation, the same degradation occurs in the overall network outage performance.

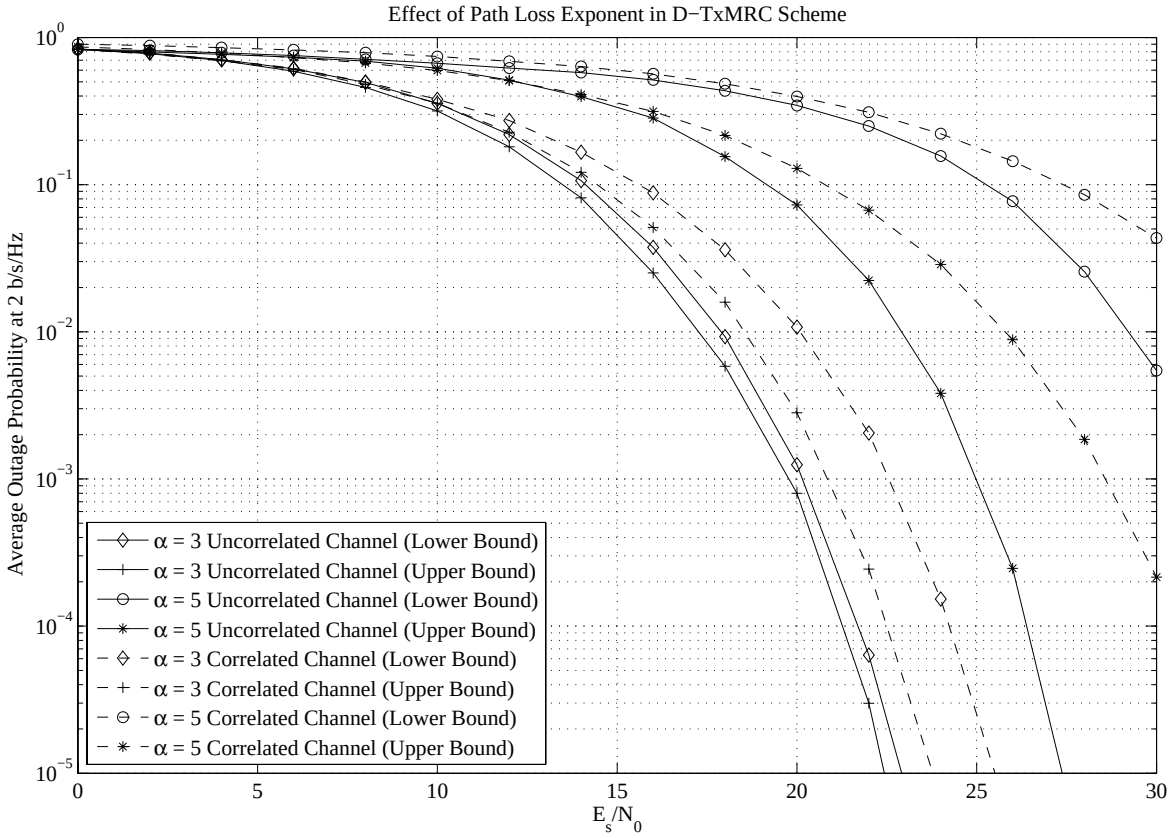

Figure 6.19: Effect of Path Loss Exponent in D-TxMRC Scheme ($M = 1000$ nodes, $L = 10$ km, $\sigma_s^2 = 3$dB)

Path Loss Exponent

The effect of path loss exponent is reflected through the path loss given in equation (4.2). Higher path loss exponent results in larger λ, which in turn affects the distribution of the channel gain. Since channel gain is exponentially distributed, its CDF can be expressed as $1 - e^{-\lambda x}$. Therefore, higher value of λ will increase the likelihood of smaller channel gain. Similarly, higher λ will increase the gradient of the compound channel CDF, hence reducing the overall system performance.

Figure 6.19 shows the network outage probability for different values of α. It can be seen that increasing path loss exponent parameter will greatly degrade system performance. Approximately 12dB loss at 10^{-2} outage rate is observed when α is increased from 3 to 5.

Another interesting observation from Figure 6.19 is that higher α will increase the gap between upper and lower bound of the performance. This can be observed directly from equation (6.82), in which higher α will increase the difference between $\lambda^{(l)}$ and $\lambda^{(u)}$. Hence, when applied to equation (6.83), the difference between upper bound and lower bound network outage probability (as calculated in equation (6.80)) will also be larger.

Similar trend is observed when channel correlation is taken into consideration. From the dashed curves in the Figure 6.19, it is apparent that channel correlation causes larger degradation when path loss exponent is higher. This is because larger path loss exponent induces smaller eigenvalues in the channel correlation matrix, such that the average probability of error as expressed in equation (6.40) is higher. As such, the overall performance in the presence of channel correlation is worse off when path loss exponent is large.

6.5.4 Distributed Space Time Block Coding (DSTBC)

The analysis in DSTBC scheme is very much similar to that in D-TxMRC scheme. This can also be observed through the point to point outage probability expression in equation (6.45) which resemblance the one for D-TxMRC scheme in equation (6.25). Under independence assumption, it can be shown that $\frac{1}{|\mathcal{D}|}\ \sum_{k\in\mathcal{D}}|h_{kd}|^2$ is also a chi-squared distributed random variable with $2|\mathcal{D}|$ degree of freedom. However, the parameter of the chi-squared random variable will now become $\lambda^{(.)}|\mathcal{D}|$, resulting in a CDF of the form $\frac{\gamma\left(x|\mathcal{D}|\lambda^{(.)},|\mathcal{D}|\right)}{\Gamma(|\mathcal{D}|)}$. After conditioning the CDF with respect to variable $|h_{sd}|^2$ and integrating it in the range of interest, the following relation is obtained.

$$P_r\left[\left(|h_{sd}|^2\ +\ \frac{1}{|\mathcal{D}|}\sum_{k\in\mathcal{D}}|h_{kd}|^2\right)\leq\rho^*\right]=\int_0^{\rho^*}\frac{\gamma\left((\rho^*-t)|\mathcal{D}|\lambda^{(.)},|\mathcal{D}|\right)}{\Gamma(|\mathcal{D}|)}\,\lambda_{sd}\,e^{-\lambda_{sd}t}\,dt \tag{6.85}$$

Finally, the network outage probability can be found using the same equation as that in D-TxMRC scheme, as follows:

$$\overline{P_{out}^{(DSTBC)}} = \int_0^{L^2} \left[\sum_{i=0}^{M-2} Pr[|\mathcal{D}| = i] \; P_r \left[\left(|h_{sd}|^2 \; + \; \frac{1}{|\mathcal{D}|} \sum_{k \in \mathcal{D}} |h_{kd}|^2 \right) \leq \rho^* \right] \; PDF_{l_{sd}^2}(z) \right] dz \tag{6.86}$$

Substituting equations (6.54), (6.79), and (6.85) into the above equation, the overall performance of the scheme can be numerically calculated.

The same argument as that in D-TxMRC also applies in this case, whereby the network outage probability is affected by two main terms; namely the probability that the decoding set contains i nodes $Pr[|\mathcal{D}| = i]$, and the probability that the combined channel effect is less than a certain threshold $P_r \left[\left(|h_{sd}|^2 \; + \; \frac{1}{|\mathcal{D}|} \sum_{k \in \mathcal{D}} |h_{kd}|^2 \right) \leq \rho^* \right]$. Similarly, the first term depends on the decoding set area through equation (6.81) and (6.64), while the second one depends on the channel gain distribution (which indirectly depends on the relay node locations through path loss equation (4.2) and relay destination distances calculated using equation (6.71), (6.76), and (6.77)).

Total Number of Nodes

As explained eariler, total number of nodes in the network will affect the size of decoding set $\mathcal{D}$. Larger number of nodes in the network would increase the size of $|\mathcal{D}|$, which will in turn improve the overall performance. The network outage probability of the system for different total number of nodes (both in the presence and absence of channel correlation case) is shown in Figure 6.20.

Comparing Figure 6.20 with Figure 6.16 for D-TxMRC scheme, it is observed that for large M, D-TxMRC outperforms DSTBC scheme, while the performances of the two schemes are comparable for low values of M. It is also observed that the performance degradation of DSTBC is more prominent in the lower bound case, whereby up to 4dB difference is observed

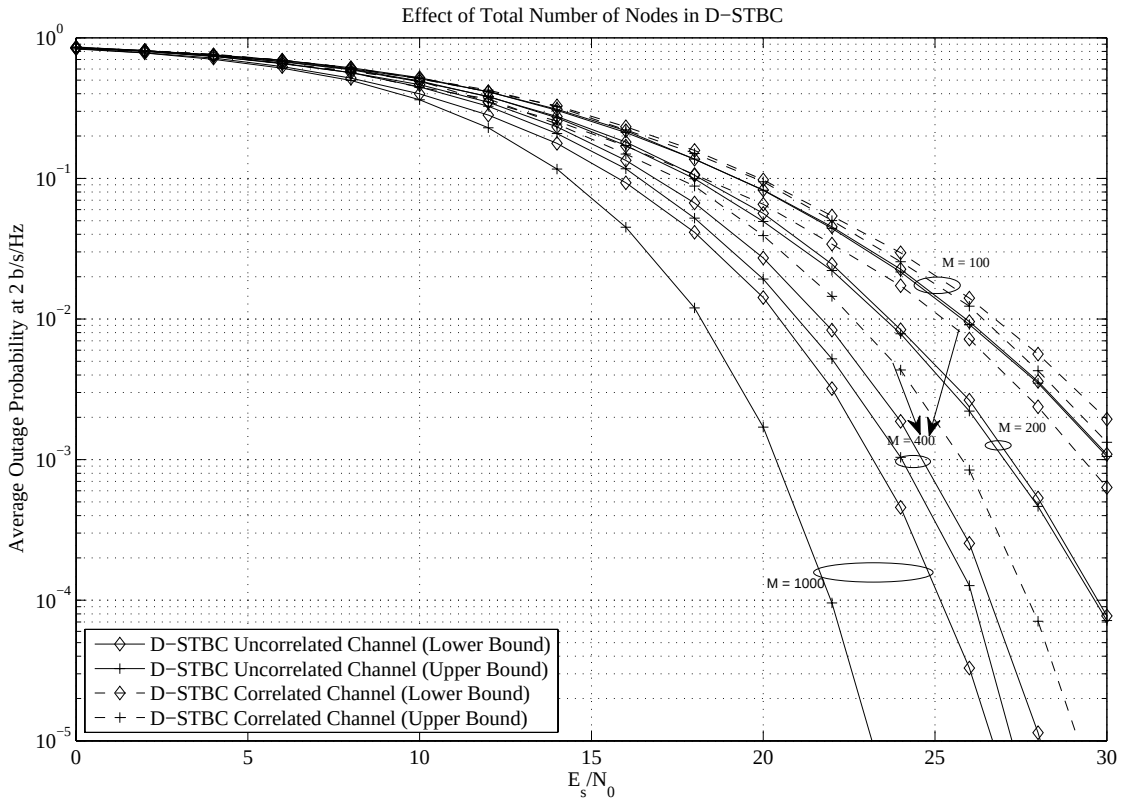

Figure 6.20: Effect of Total Number of Nodes in DSTBC Scheme ($L = 10$ km, α = 3, $\sigma_s^2 =$ 3dB)

at 10^{-5} outage rate. This is related to the behaviour of the array gain distribution in equations (6.29) and (6.48) for D-TxMRC and DSTBC scheme respectively. When lower bound performance is considered, macroscopic fading $\overline{\chi}$ is taken to be the largest value among all relay nodes, while all nodes are assumed to be located in the distance ($l_{sd}+l^*$) away from destination node. This causes larger increase in the mean array gain for D-TxMRC compared to DSTBC scheme, hence larger gap between the two performances are evident. When M is small, the value of $|\mathcal{D}|$ is also likely to be small. Since array gain is proportional to $|\mathcal{D}|$, the performance gap between the two schemes will also decrease.

From Figure 6.20, it is observed that the bound on network outage probability is tighter for lower values of M. The same behaviour is also observed in D-TxMRC scheme, which demonstrates the influence of $|\mathcal{D}|$ to the value of gamma function $\gamma(.,.)$ in equations (6.83)

and (6.85). As larger $|\mathcal{D}|$ would reduce the sensitivity of gamma function with respect to changes in λ, the tighter bound is evident.

Similarly, the same trend is observed for channel correlation effect, whereby degradation in overall performance is incurred (especially for large M) as depicted in the dashed curves in Figure 6.20. As compared to D-TxMRC scheme, it is observed that DSTBC scheme is more sensitive to channel correlation. This is because DSTBC heavily relies on diversity gain, and only limited array gain is available. Since channel correlation affects the diversity performance, severe degradation in DSTBC is evident.

Edge Effect

Edge effect influences the performance of DSTBC scheme in very much the same way as in D-TxMRC scheme. Edge effect happens when source node is located near to the network boundary, reducing the size of decoding set area. Following the same argument as the edge effect analysis in D-TxMRC, the worst case edge effect occurs when the source node is located at the corner of the network, in which the decoding set area is in the form of quarter of a circle. In this case, the probability mass function of the decoding set cardinality $Pr[|\mathcal{D}| = i]$ is expressed as in equation (6.84). Additionally, as explained earlier, the largest possible relay destination distance happens when the destination is located at network edge, in which the distance can be calculated as $\sqrt{l_{sd}^2 + r^2}$. By assuming that the decoding set is always one quarter of a circle, and the relay destination distance always takes its largest value, the worst case edge effect can be analysed.

Figure 6.21 shows the performance of DSTBC scheme with and without worst case edge effect. Similar to D-TxMRC scheme, edge effect has the potential to severely degrade overall performance. Approximately $4 - 7$dB degradation at 10^{-5} outage probability is observed in DSTBC scheme (depending whether upper or lower bound performance is considered). As compared to D-TxMRC performance in Figure 6.17, D-TxMRC scheme suffers more loss

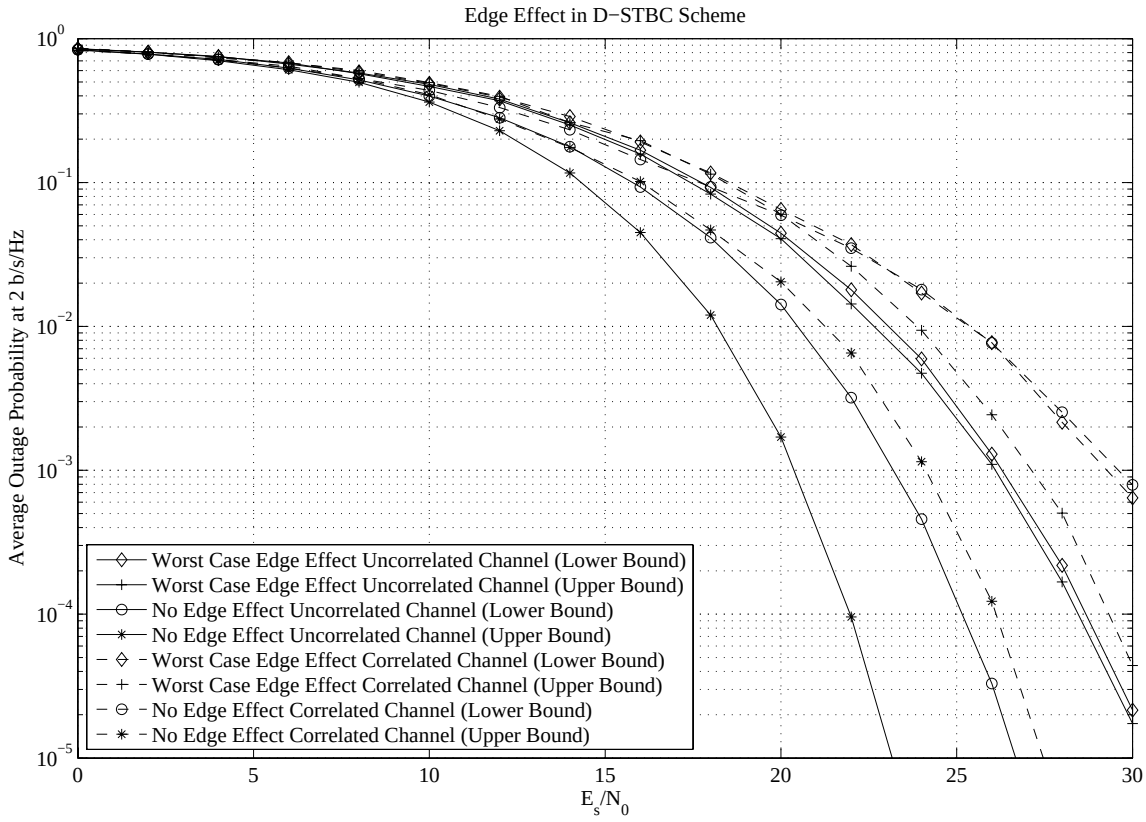

Figure 6.21: Influence of Edge Effect in DSTBC Scheme ($M = 1000$ nodes, $L = 10$ km, α = 3, $\sigma_s^2 = 3$dB)

compared to DSTBC. This is because in D-TxMRC scheme, both array and diversity gain are degraded; while in DSTBC scheme, only diversity gain is degraded, and the array gain remain constant. In the presence of channel correlation, further degradation is also observed as shown by the dashed curves in Figure 6.21.

Network Size

Following the same argument used in D-TxMRC scheme, larger network size will generally degrade overall performance due to larger path loss. Figure 6.22 shows the network outage probability of DSTBC scheme for different network sizes.

An approximately 8dB performance degradation is observed at 10^{-5} outage rate for every factor-of-four increase in the network area. It is also observed that the diversity order achieved

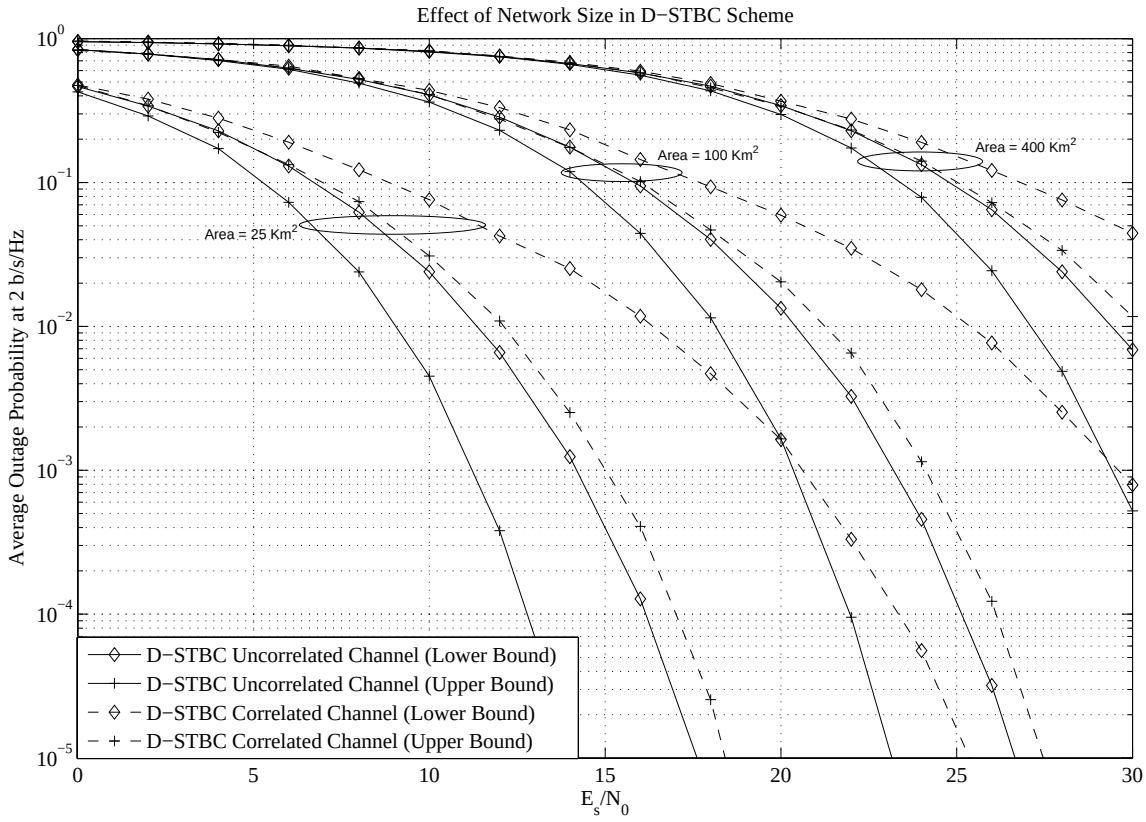

Figure 6.22: Effect of Network Size ($M = 1000$ nodes, α = 3, $\sigma_s^2 = 3$dB)

is independent from network size. The overall performance in the presence of channel correlation is also analysed for different network sizes. It is observed that irrespective to channel correlation, the same degradation occurs in the network outage performance. The presence of channel correlation, however, introduces more severe degradation. Comparing to the performance of D-TxMRC in Figure 6.18, performance loss due to channel correlation is more severe in DSTBC scheme, which is reflected by the larger gap relative to the uncorrelated case.

Path Loss Exponent

As higher path loss exponent causes larger λ, degradation in network outage probability is expected. Figure 6.23 shows the network outage probability for different values of α. It can be seen that increasing path loss exponent parameter will greatly degrade system performance. Up to 13dB loss at 10^{-2} outage rate is observed in DSTBC scheme when α is increased from

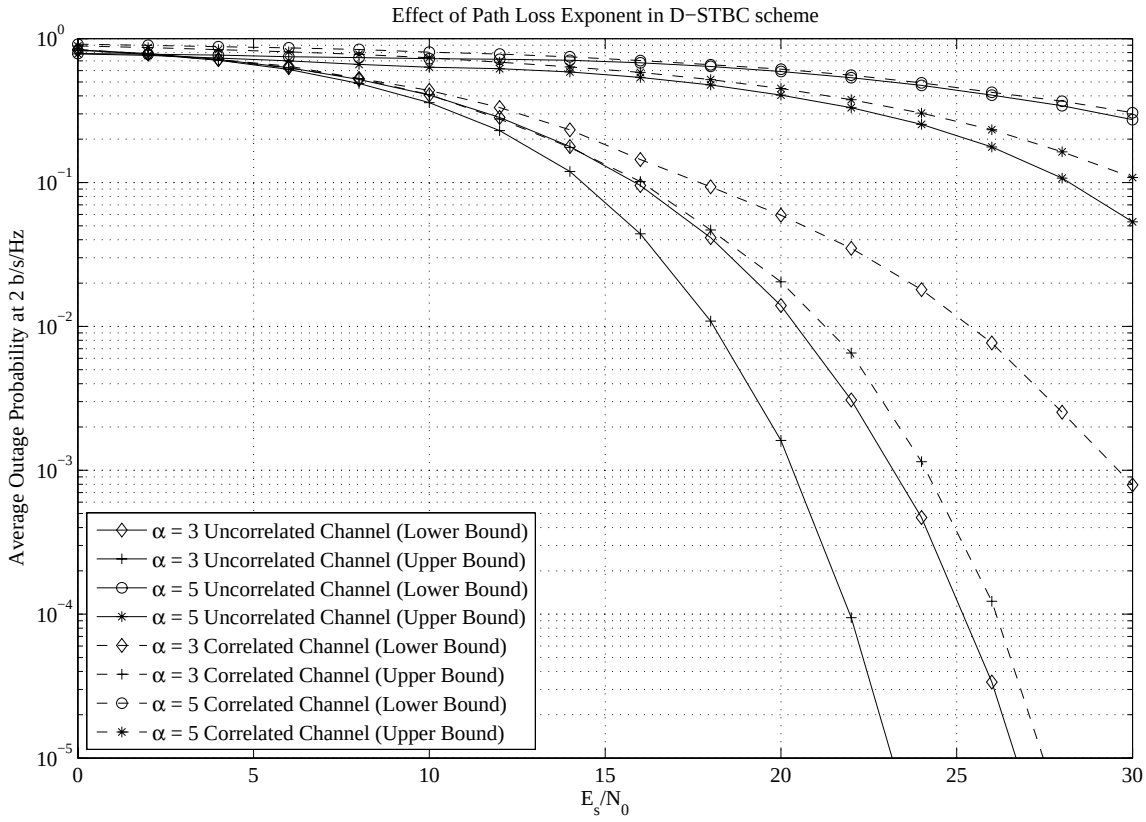

Figure 6.23: Effect of Path Loss Exponent in DSTBC ($M = 1000$ nodes, $L = 10$ km, $\sigma_s^2 = 3$dB)

3 to 5, which is more severe than D-TxMRC scheme. The reason why DSTBC suffers larger loss than D-TxMRC can be observed through equations (6.83) and (6.85). A multiplication factor of $|\mathcal{D}|$ in the first argument of incomplete gamma function for equation (6.85) will cause larger change in CDF for the same amount of change in λ, the path loss value. Since incomplete gamma function is a monotonically increasing function of the first argument, larger degradation in outage probability for DSTBC scheme is evident. This analysis also implies that the absence of array gain causes DSTBC to be more vulnerable to the path loss exponent.

Other trends observed from Figure 6.23 are similar to the D-TxMRC case, whereby higher α will increase the gap between upper and lower bound of the performance, and that channel correlation causes larger degradation when path loss exponent is higher.

6.6 Summary

In this chapter, the analysis of cooperative relay communication is generalised for random networks. Different cooperative relaying schemes are studied, including direct transmission, single relay AnF scheme, D-TxMRC scheme, and DSTBC schemes. Performance comparison between different schemes are then conducted using average outage probability as the performance criteria.

First, the outage probability of different cooperative schemes given a particular source, relay, and destination locations are analysed. Under direct transmission, the conventional point to point outage analysis can be readily applied. While for the other schemes, the expression of effective received SNR is first developed. The outage probability is then found by calculating the probability that the effective SNR falls below a certain threshold. In addition, the array gain and diversity gain of D-TxMRC and DSTBC schemes are studied. It is shown that under independent fading assumption, both schemes are able to extract full diversity gain in the order of total number of cooperating nodes, which scales according to $|\mathcal{D}| + 1$. However, when the channel from different relay nodes to destination node are correlated to one another, the diversity gain is limited by the rank of the correlation matrix. It is also shown that the D-TxMRC scheme is superior as it is able to extract larger array gain compared to the D-STBC scheme. This limitation of the D-STBC scheme is mainly due to the absence of global CSI in the cooperative nodes, hence preventing them to perform coherent combining. Although D-TxMRC is better than D-STBC, this superiority comes at the price of higher complexity and global CSI knowledge requirement, making it difficult to be implemented in practice. Furthermore, when the large-scale/macroscopic fading is considered, the actual amount of array gain achieved by the scheme is random, and it is characterised by its distribution.

Several geometry specific issues pertaining to different cooperative schemes, which are necessary for network performance evaluation, are addressed. Distance distribution between any given two nodes are derived. For AnF scheme, the location of potential relay nodes within

the region of interest is estimated using ellipses with different eccentricity. The associated probability mass function is then calculated using Poisson point process. As for the D-TxMRC and DSTBC scheme, a systematic method to calculate the circular area from a given position in the network is developed. This area is necessary to find the distribution of number of relay nodes who join the decoding set. A technique to estimate the position of different relay nodes within the decoding set area (considering all possible intersections with the network boundaries) is then developed.

Finally, the network outage probability of different schemes when applied to cooperative random network are analysed. By integrating the outage probability with respect to all possible source and destination locations as well as all possible number of cooperating nodes, the network outage probability is obtained. The effects of network parameters (including total number of nodes, network size, edge effect, and path loss exponent) toward system performance are also analysed. For direct transmission scheme, the diversity gain is absent since no relay node is involved in the transmission. The performance is also independent on node density and edge effect. Using AnF scheme, diversity order of 2 can be achieved, provided that the number of nodes in the network is sufficiently large. Effect of different network parameters on AnF performance is studied. As for the other two schemes, it is shown that in all cases, D-TxMRC always performs better than D-STBC especially for large number of nodes, confirming the earlier analysis on the available gain for each scheme. How the different factors such as an increase in network size, path loss exponent, and edge effect could degrade the system performance are studied through analytical formulation and supported by simulation results.

Chapter 7

Conclusions and Future Work

7.1 Contribution to Research

The present research addresses various aspects of cooperative communication, both in cooperative broadcasting and cooperative relaying scenario. The results and contributions of this work to the research on cooperative communication are summarised in the following.

Under cooperative broadcast communication, antenna selection scheme is proposed for multi antenna BC systems; which addresses the issue on hardware cost and space limitation inherent to any multi antenna systems. The scheme segregates the selection process for the transmit and receive antenna separately, and exploit the duality between BC and MAC in order to bring down the overall complexity. It is demonstrated that the scheme is able to benefit from most of the selection gain available, while using only a fraction of the complexity in brute force scheme. The selection algorithm is also extended for frequency selective channel, where the propagation is characterised by multipath fading, and optimal selection must consider different subcarriers jointly. The applicability of antenna selection to broadband wireless access such as IEEE 802.16 based system is also analysed.

The issue of power allocation in three-node cooperative network in the absence of direct source to target link is addressed. It is shown that additional relay node does not necessarily

result in better performance, and optimal power allocation is a necessary condition for performance improvement. Using the information of the second order statistics of the channel, power allocation scheme which minimises average error probability is proposed. It is shown that for decode and forward relaying, the optimal power allocation can be found by solving for the positive real root of a quadratic equation. For a more complex distributed space time coded relaying, the optimal power allocation can be found by solving for the positive real root of a quartic equation. The analysis provided maintains equal total power constraint and equal end-to-end throughput for fair comparison, and it is shown that as long as appropriate power allocation strategy is used, additional relay node will always result in better performance.

For multi-hop cooperative links, a novel relaying scheme called Successive Dirty Paper Coding (SDPC) is proposed. The scheme applies dirty paper encoding strategy on each relay stage, such that a new message can be transmitted at every relay slot while maintaining the interference to the existing transmission low. The performance of this relay strategy is then analysed and compared to other existing relay schemes. It is demonstrated that SDPC is superior to the other schemes by providing higher bandwidth efficiency, especially when the number of hops is large.

For multiple-relay cooperation case, exact expression for outage probability is developed. First, an ideal case where all relay nodes are located equidistant from source and target nodes is considered. In this scenario, the average outage probability is only affected by relay nodes cardinality. Extending the analysis for cases where destination node is not known a priori, a planar network where nodes are positioned in the lattice points is considered. It is shown that in this scenario, traffic pattern has an influence towards average outage performance. In particular, traffic locality and traffic origins are studied, and how they affect the overall performance are analysed.

In the most general setting of random network, where every node can take any position within the network boundary, a framework for performance evaluation is developed. Since

node location is random, network performance evaluation must take into consideration all possible source, relay, and destination positions. In addition, several geometry specific issues including distance distribution, edge effect, relay nodes cardinality and position estimation are addressed. Four different transmission schemes, namely direct transmission, AnF relaying, D-TxMRC, and DSTBC are studied. The conditional outage probability given a particular node positions are derived. Squared distance distribution function is then developed and used to integrate the conditional outage probability. For AnF relaying, a technique to consider different relay node positions within the region of interest is developed; while for D-TxMRC and DSTBC scheme, a systematic approach to calculate decoding set area and to approximate the cardinality as well as position of relay nodes is developed. Finally, the average outage performance of different cooperative schemes are analysed, in which different types of gain associated with different schemes are studied. The effect of network parameters and their influence to the average outage probability are also evaluated.

7.2 Future Works

In the following, some of the possible extensions to the work presented so far, which serves as future research direction are described.

7.2.1 Analysis of Feedback Delay and Inaccurate Feedback

The antenna selection algorithm proposed for MIMO-BC systems assumed that perfect feedback channel is available. In practice, the feedback channel might introduce error due to channel fading or excessive noise and interference. Since antenna selection performance relies on the quality of feedback information from all users, it is apparent that feedback error will degrade the effectiveness of this scheme. Moreover, when the channel coherence time is not sufficiently large (especially when the communicating terminal is mobile), the feedback received

from the users might get outdated before it can be used by the antenna selection process. In this case, it is also expected that performance degradation would occur. Therefore, the effect of feedback delay and an effective method to overcome the problem need to be analysed further.

7.2.2 Precoder Design for Dirty Paper Encoder

The Successive Dirty Paper Coding (SDPC) scheme proposed for multiple hop relay communication makes use of the property of DPC, in which transmission in the presence of interference can be performed as if the interference is not present, as long as it is known non-causally at the transmitter. Although this property is very useful in allowing new message to be transmitted in every relay slot, its practical realisation requires a complex encoder design. The current solution of DPC encoder makes use of nested lattice [180] and coset dilution strategy [181], which involves large computational complexity. A sub optimal alternative of DPC encoder design is to use low complexity Tomlinson-Harashima precoder [182]-[183]. However, some reductions in the performance is expected from this scheme, due to imperfections such as modulo loss, power loss, and shaping loss, which are inherent to any Tomlinson-Harashima precoder [184]. In order to implement SDPC scheme efficiently, a precoding strategy which provide close to optimal DPC property, while requiring a relatively low computational complexity is required. Further research on the development of this kind of precoder design is necessary.

7.2.3 Theoretical Analysis for Network Capacity with Cooperation

The network performance analysis conducted so far have shown that cooperation is able to improve the overall performance. However, due to the unavailability of the definitive bound on how far the performance can be improved, no conclusion can be made regarding the optimality of different cooperative schemes. In point to point communication, Shannon's capacity has become a well accepted limit on the achievable transmission rate. Unfortunately, the same limit is not directly applicable to multiuser communication channel. Attempts to characterise

the capacity of wireless network have been made in the past, such as reference [170] for direct transmission case and reference [185] for the relay case. Although it gives an idea on how fast the network capacity can scale, their work does not consider node cooperation. When different nodes are allowed to cooperate, the transmission quality can be improved, hence the network capacity will also increase. Consideration of other factors such as mobility (which has been shown to improve network capacity in [186]) and the use of different performance metric like transport capacity as proposed in [187] also need to be included. Once the limiting capacity of wireless network with cooperation is available, the development of a new cooperative strategy which achieves or performs close to this limit will naturally follow.

7.2.4 Generalisation into Arbitrary Ad-hoc Networks

In a general ad-hoc network, the area covered by the network can take any shape. The distance distribution between nodes depends on the geometry of the network. Therefore, since the network outage probability involves an integration with respect to the distance distribution of the nodes, it is apparent that different network shapes would result in different performances. Analysis on how network geometry affects the network outage probability is necessary, especially for networks that are not constrained to a particular shape. Furthermore, when the network is large and the nodes are mobile, the distance between source and destination can be very large. In such scenario, issues related to mobile multihop relaying will complicate the analysis. Synchronisation between nodes in such highly time-varying channel will also emerge as a challenge which requires special attention. On the other hand, when the network is very large, nodes which are well separated can be considered as free from mutual interference and can transmit at the same time. In that case, the spatial reuse of the network can potentially increase the network capacity. However, the issue with their influence towards the other message being relayed will also complicate the analysis. The method on how to control which set of nodes are to be allowed to transmit at any one time, which has to be performed in a distributed

manner as there is no centralised controller, must be carefully considered before any claim can be made on their performance.

7.2.5 On-Chip Implementation and System Level Simulation

Having analysed the theoretical performance of cooperative communication in wireless networks, it is essential to apply them in real hardware. For this, system on-chip implementation of cooperative nodes needs to be developed. Several challenges associated with this implementation must also be addressed, such as the cooperative Medium Access Control design to support the adaptive nature of the transmission, cross layer communication, carrier frequency offset estimation as well as phase noise cancellation. Apart from that, other issues pertaining to the resource allocation such as scheduling, bandwidth allocation, and power control mechanism should be addressed. With the developed cooperative nodes, it is expected that system level simulation can be performed to study the network performance. Comparative study with their analytical results will then follow. Similar study can be found in [188], where ad-hoc network using IEEE 802.11 wireless LAN (Local Area Network) devices is used to analyse network capacity, and then compared to the theoretical result. The analysis of cooperative network is more challenging as there is no commercially available cooperative node in the market to date. Hence, the development of a prototype model for cooperative node must precede any further analysis.

Appendix A

WiMax Systems: An Overview of IEEE 802.16 Based Systems

The development of IEEE 802.16 standards was driven by the strong demand for broadband services. This is coupled with user demand for wireless connectivity, and the high cost of laying wired infrastructure to deliver broadband service to end users.

802.16 working group was formed in the early 1999 [189] with an attempt to standardise the technology. Soon after it is formed, the first standard was published in April 2002 [190]. The initial standard focused on the 10 to 66 GHz band of operation using single carrier method under Line of Sight (LOS) condition. Further amendment to the standard is to include the licensed and license-exempt band of 2 to 11 GHz operation under NLOS (Non-Line of Sight) condition, which is standardised under 802.16a [191], and was published in April 2003. In this standard, three additional physical specifications are defined, namely WirelessMAN-SCa (Single Carrier based system), WirelessMAN-OFDM (Multi-carrier 256 points OFDM based system), and WirelessMAN-OFDMA (Multi-carrier 2048 points OFDMA based system). The most recently approved stand on Fixed Broadband Wireless Access Systems, which is a revision on the 802.16a standard, is called 802.16REVd. It was approved as 802.16-2004 [162] in June 2004. This project focuses on the OFDMA mode of operation.

All the above mentioned standards are for fixed BWA, which only support static and nomadic users. The need to support mobile user moving at vehicular speed has led to the development of 802.16e [163], which supports a combined fixed and mobile BWA operation. Operating in mobile operation, 802.16e is faced with the challenges of some propagation impairments, such as fast fading and Doppler effects. This necessitates better channel sounding capability to keep track of the instantaneous channel response of each user. Multiple-antenna configuration is also included as optional feature in 802.16 standards to maintain system performance. The block diagram of 802.16 with two-antenna configuration is shown in Figure A.1.

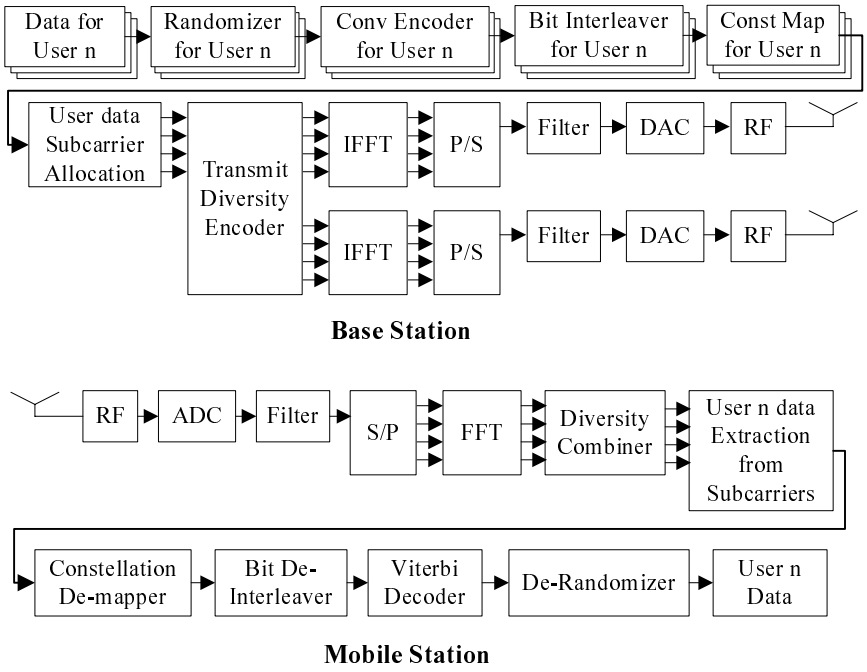

Figure A.1: 802.16 transceiver block diagram

The following are brief description on each individual block:

- *Randomizer*

  The main purpose of this module is to provide some form of security by translating a series of bits into another form carrying the same message. This module consists of shift

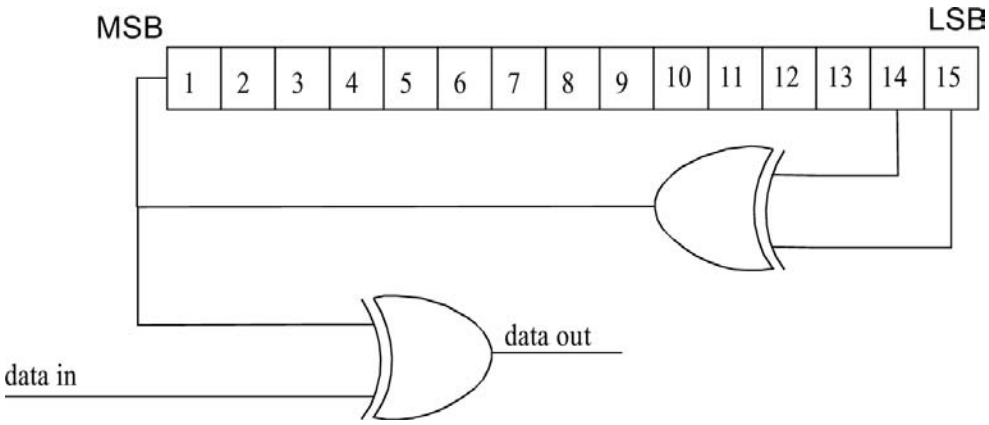

Figure A.2: Randomiser

registers and two exclusive-or gate as depicted in Figure A.2.

The content of the shift registers shall be initialised with 10 LSB (Least Significant Bit) of OFDMA symbol offset and 5 LSB of Subchannel offset.

- *Convolutional Encoder*

  The standard channel coding used is half-rate convolutional encoder with constraint length = 7 and generator polynomial of $G_1 = 171_{oct}$ and $G_2 = 133_{oct}$ respectively (Figure A.3). Tail biting type is used where the shift registers are initialised with the last 7 bits of the message block. Different coding rates are also supported by using the appropriate puncturing mechanism.

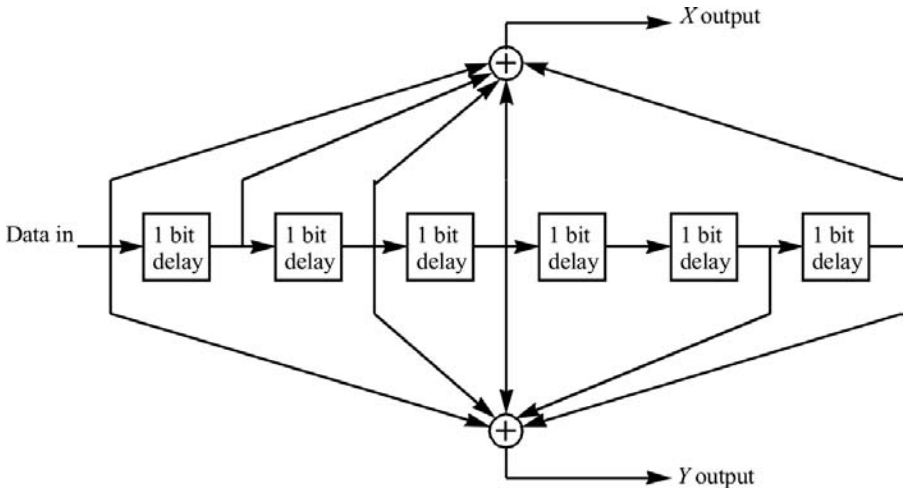

Figure A.3: Convolutional Encoder

- *Bit Interleaver*

  The main purpose of this module is to prevent burst error by relocating adjacent symbols as far apart as possible. The following formula is used to translate bit location to its new location.

$$
\begin{aligned}
m_k &= (N_{cbps}/16) \times k_{mod(16)} + floor(k/16) \\
J_k &= s.floor(m_k/s) + (m_k + N_{cbps} - floor(16 \times m_k/N_{cbps}))_{mod(s)}
\end{aligned}
$$

  Where N_{cbps} is the block size, k is the bit index within the block, J_k is the new bit index, and s is a parameter related to the constellation used, which is set to half of the number of bits per symbol.

- *Constellation Mapper*

  Complex Quadrature Amplitude Modulation (QAM) is used, ranging from QPSK (Quadrature Phase Shift Keying), 16-QAM, and 64-QAM. Normalisation is performed on the constellation points so that the average transmit power is equal to unity. Figure A.4

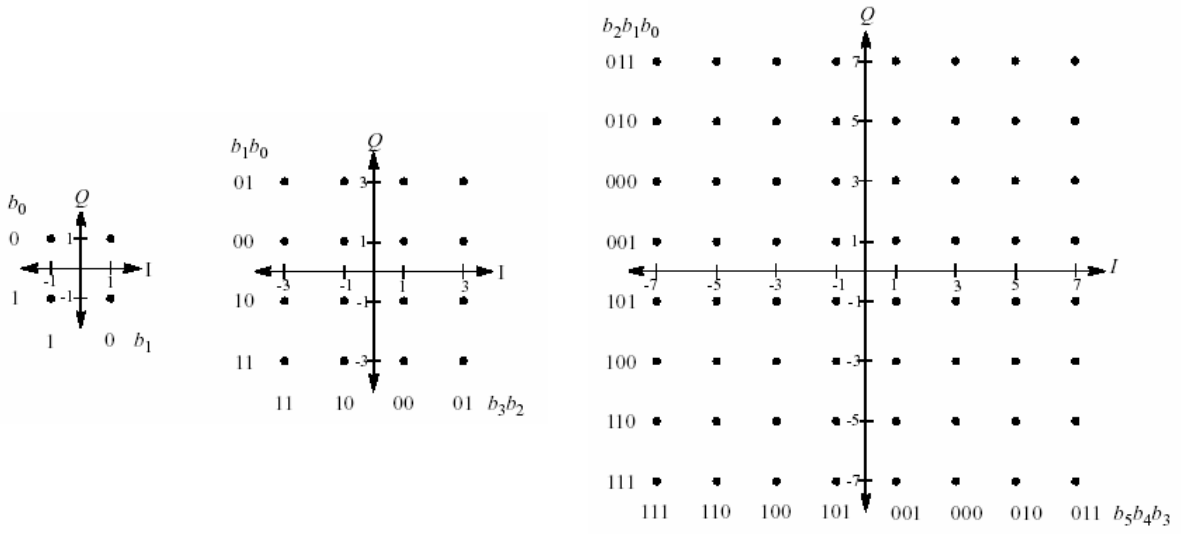

Figure A.4: Constellation Diagram

- *User data Subcarrier Allocation*

  This module is used to allocate symbols to the appropriate subcarriers according to their allocation scheme. There are different subcarrier allocation schemes defined in the 802.16 standard, namely PUSC (Partial Use of Sub Channels), FUSC (Full Use of Sub Channels), Optional FUSC, AMC (Adaptive Modulation and Coding) adjacent permutation scheme, TUSC 1 (Tile Use of Sub Channels type 1), and TUSC 2 (Tile Use of Sub Channels type 2). PUSC is defined as the mandatory subcarrier allocation method. Every frame transmission shall start with PUSC permutation scheme, while others may appear in the middle of the frame according to permutation zone information given in the MAC messages. For this reason, this work focuses on PUSC permutation scheme. Some parameters related to PUSC permutation are listed in Table A.1.

Table A.1: OFDMA PUSC allocation parameters

Parameter	Value	Comments
No of DC subcarriers	1	Index 1024
Guard subcarriers, Left	184	
Guard subcarriers, Right	183	
No of used subcarriers	1681	Number of all subcarriers used in a symbol, including pilots and DC carriers
No of subcarriers per cluster	14	
No of clusters	120	
Renumbering sequence	1	6, 108, 37, 81, 31, 100, 42, 116, 32, 107, 30, 93, 54, 78, 10, 75, 50, 111, 58, 106, 23, 105, 16, 117, 39, 95, 7, 115, 25, 119, 53, 71, 22, 98, 28, 79, 17, 63, 27, 72, 29, 86, 5, 101, 49, 104, 9, 68, 1, 73, 36, 74, 43, 62, 20, 84, 52, 64, 34, 60, 66, 48, 97, 21, 91, 40, 102, 56, 92, 47, 90, 33, 114, 18, 70, 15, 110, 51, 118, 46, 83, 45, 76, 57, 99, 35, 67, 55, 85, 59, 113, 11, 82, 38, 88, 19, 77, 3, 87, 12, 89, 26, 65, 41, 109, 44, 69, 8, 61, 13, 96, 14, 103, 2,80, 24, 112, 4, 94, 0
No of data subcarriers in each symbol per Subchannel	24	
Number of subchannels	60	

In brief, the allocation of data into subcarriers can be described as follows. OFDMA subcarriers are first divided into 120 physical clusters, each consisting of 14 adjacent subcarriers. These clusters are then reordered with a specific renumbering sequence, which will translate the physical cluster number to logical cluster number. From these logical clusters, six groups are formed, each consisting of 24 clusters (for even numbered

group) or 16 clusters (for odd numbered group) with continuous logical cluster number. Finally, segments are assigned a set of cluster groups, which will then be used to allocate data symbols. In PUSC, pilot symbols are first assigned in each cluster according to Figure A.5, and then the remaining subcarriers are assigned with data symbols.

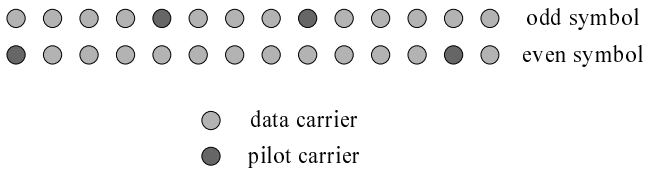

Figure A.5: PUSC cluster structure

- *Transmit Diversity Encoder*

  The space time encoding is implemented using Alamouti technique on a cluster base (Figure A.6). In this setting, the placement of the pilot symbols needs to be modified in order to perform channel estimation on all antennas.

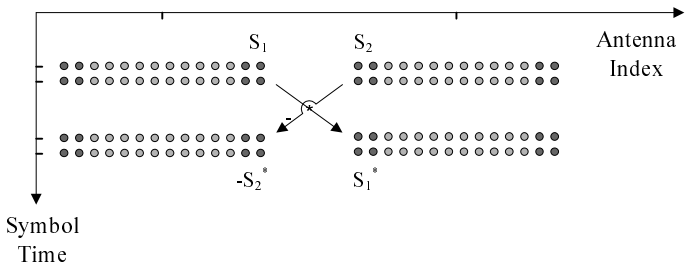

Figure A.6: Cluster based Alamouti space time encoding

- *Diversity Combiner*

  This module is used to combine the signal strength of redundant messages provided by Transmit Diversity Encoder. Zero Forcing (ZF) base diversity combiner is employed for its simplicity.

- *User n data Extraction from Subcarriers*

  Here, the allocation message in MAC layer is used to determine which portion of the

data to be extracted out. It makes sure that only data that is destined to the respective user is further processed, while the rest are discarded.

- *Constellation De-mapper*

  This is the reverse operation of Constellation Mapper, where symbols are translated back to bit stream. Same constellation diagram is used as the one used in Constellation Mapper module (Figure A.4).

- *Bit De-Interleaver*

  This module performs the inverse operation of Bit Interleaver. The following formula is used to relocate bit position back to its original place.

$$\begin{aligned} m_j &= s \times floor(j/s) + (j + floor(16 \times j/N_{cbps}))_{mod(s)} \\ k_j &= 16 \times m_j - (N_{cbps} - 1) \times floor(16 \times m_j/N_{cbps}) \end{aligned}$$

  Where N_{cbps} is the block size, j is the bit index within the block, k_j is the original bit index, and s is a parameter related to the constellation used, which is set to half of the number of bits per symbol.

- *Viterbi Decoder*

  This module is used to perform channel decoding to the received bit stream according to the channel coding technique used at the transmitter.

Appendix B

Standard Channel Model for WiMax Systems

Table B.1: SUI type-1 channel parameters

	Tap 1	Tap 2	Tap 3	Units
Delay	0	0.4	0.9	μs
Power (omni)	0	-15	-20	dB
K Factor (omni)	4	0	0	dB
Doppler	0.4	0.3	0.5	Hz
Gain Reduction Factor: 0 dB			Terrain Type: C	
Normalization Factor: -0.1771 dB			RMS delay: 0.111 μs	

Table B.2: SUI type-2 channel parameters

	Tap 1	Tap 2	Tap 3	Units
Delay	0	0.4	1.1	μs
Power (omni)	0	-12	-15	dB
K Factor (omni)	2	0	0	dB
Doppler	0.2	0.15	0.25	Hz
Gain Reduction Factor: 2 dB			Terrain Type: C	
Normalization Factor: -0.3930 dB			RMS delay: 0.202 μs	

Table B.3: SUI type-3 channel parameters

	Tap 1	**Tap 2**	**Tap 3**	**Units**
Delay	0	0.4	0.9	µs
Power (omni)	0	-5	-10	dB
K Factor (omni)	1	0	0	dB
Doppler	0.4	0.3	0.5	Hz
Gain Reduction Factor: 3 dB			Terrain Type: B	
Normalization Factor: -1.5113 dB			RMS delay: 0.264 µs	

Table B.4: SUI type-4 channel parameters

	Tap 1	**Tap 2**	**Tap 3**	**Units**
Delay	0	1.5	4	µs
Power (omni)	0	-4	-8	dB
K Factor (omni)	0	0	0	dB
Doppler	0.2	0.15	0.25	Hz
Gain Reduction Factor: 4 dB			Terrain Type: B	
Normalization Factor: -1.9218 dB			RMS delay: 1.257 µs	

Table B.5: SUI type-5 channel parameters

	Tap 1	**Tap 2**	**Tap 3**	**Units**
Delay	0	4	10	µs
Power (omni)	0	-5	-10	dB
K Factor (omni)	0	0	0	dB
Doppler	2	1.5	2.5	Hz
Gain Reduction Factor: 4 dB			Terrain Type: A	
Normalization Factor: -1.5113 dB			RMS delay: 2.842 µs	

Table B.6: SUI type-6 channel parameters

	Tap 1	**Tap 2**	**Tap 3**	**Units**
Delay	0	14	20	µs
Power (omni)	0	-10	-14	dB
K Factor (omni)	0	0	0	dB
Doppler	0.4	0.3	0.5	Hz
Gain Reduction Factor: 4 dB			Terrain Type: A	
Normalization Factor: -0.5683 dB			RMS delay: 5.240 µs	

Appendix C

Probability Analysis for SDPC Relay Nodes in Decoding Set

To calculate the probability that a node n in RS i is joined to $\mathcal{D}_{i-1}$, lets rewrite the following capacity expression:

$$C_{SDPC\_i}(\mathcal{D}_{i-1}(s)) \;=\; log_2\left(1+\frac{P_{tot}\times\sum_{\substack{m\in\mathcal{D}_{i-1}(s)\\ m\neq s'}}|a_{i-1,i}(m)|^2}{N_0\;(|\mathcal{D}_{i-1}(s)|-1)+P_{tot}\;|a_{i-1,i}(s')|^2}\right) \tag{C.1}$$

Any rate R less than the capacity can be achieved with arbitrarily small probability of error. Hence, a node n is joined to $\mathcal{D}_{i-1}$ if the rate is smaller than the capacity.

$$R < log_2\left(1+\frac{P_{tot}\times\sum_{\substack{m\in\mathcal{D}_{i-1}(s)\\ m\neq s'}}|a_{i-1,i}(m)|^2}{N_0\;(|\mathcal{D}_{i-1}(s)|-1)+P_{tot}\;|a_{i-1,i}(s')|^2}\right) \tag{C.2}$$

$$\sum_{\substack{m\in\mathcal{D}_{i-1}(s)\\ m\neq s'}}|a_{i-1,i}(m)|^2 > \left(2^R-1\right)\frac{N_0}{P_{tot}}\left(|D_{i-1}(s)|-1\right)+\left(2^R-1\right)|a_{i-1,i}(s')|^2 \tag{C.3}$$

$$\left(2^R-1\right)\frac{N_0}{P_{tot}}\left(|D_{i-1}(s)|-1\right) < \underbrace{\sum_{\substack{m\in\mathcal{D}_{i-1}(s)\\ m\neq s'}}|a_{i-1,i}(m)|^2}_{let=x} - \underbrace{\left(2^R-1\right)|a_{i-1,i}(s')|^2}_{let=y} \tag{C.4}$$

From the above equation, right hand side contains all the random variables, while left hand side contains deterministic variables. It can be seen that x is a chi-square distributed random variables with $2|D_{i-1}(s)| - 2$ degree of freedom, and each of its components has zero mean and unit variance. It can also be seen that y is chi-square distributed random variable with 2 degree of freedom, and each of its components has zero mean and variance equal to $2^R - 1$. Hence, we have the following probability density functions:

$$pdf_x(x) = \frac{x^{|D_{i-1}(s)|-2} exp(-x)}{(|D_{i-1}(s)| - 2)! \times 2^{|D_{i-1}(s)|-1}} \tag{C.5}$$

$$pdf_y(y) = \frac{exp(-\frac{y}{2(2^R-1)})}{2} \tag{C.6}$$

Now, defining:

$$z = x - y \tag{C.7}$$

a new random variable is obtained. The probability density function of z can be calculated as follows:

$$pdf_z(z) = \int_{-\infty}^{\infty} pdf_x(z+y) pdf_y(y) dy \tag{C.8}$$

$$= \int_{-\infty}^{\infty} \frac{(z+y)^{|D_{i-1}(s)|-2}\, exp(-(z+y))}{(|D_{i-1}(s)| - 2)!\, 2^{|D_{i-1}(s)|-1}} \times \frac{exp(-\frac{y}{2(2^R-1)})}{2} dy \tag{C.9}$$

letting:

$$k = z + y\ ;\ dk = dy\ ;\ y = k - z \tag{C.10}$$

the pdf of z can be written as:

$$\begin{aligned} pdf_z(z) &= \int_{-\infty}^{\infty} \frac{k^{|D_{i-1}(s)|-2}\, exp(-z)\, exp(-(1+\frac{1}{2(2^R-1)})(k-z))}{(|D_{i-1}(s)|-2)!\, 2^{|D_{i-1}(s)|}} dk \\ &= \frac{exp(-z)\, exp((1+\frac{1}{2(2^R-1)})z)}{(|D_{i-1}(s)|-2)!\, 2^{|D_{i-1}(s)|}} \int_{-\infty}^{\infty} k^{|D_{i-1}(s)|-2}\, exp\left(-(1+\frac{1}{2(2^R-1)})k\right) dk \\ &= \frac{exp((\frac{1}{2(2^R-1)})z)}{(|D_{i-1}(s)|-2)!\, 2^{|D_{i-1}(s)|}} \underbrace{\int_{-\infty}^{\infty} k^{|D_{i-1}(s)|-2}\, exp\left(-(1+\frac{1}{2(2^R-1)})k\right) dk}_{\text{Integration term}} \end{aligned} \tag{C.11}$$

Evaluating the integration term:

$$\begin{aligned} &\int_{-\infty}^{\infty} k^{|D_{i-1}(s)|-2}\, exp\left(-(1+\frac{1}{2(2^R-1)})k\right) dk \\ &= \int_{-\infty}^{\infty} \frac{(1+\frac{1}{2(2^R-1)})}{(1+\frac{1}{2(2^R-1)})} k^{|D_{i-1}(s)|-2}\, exp\left(-(1+\frac{1}{2(2^R-1)})k\right) dk \\ &= \frac{1}{(1+\frac{1}{2(2^R-1)})} \int_{-\infty}^{\infty} (1+\frac{1}{2(2^R-1)}) k^{|D_{i-1}(s)|-2}\, exp\left(-(1+\frac{1}{2(2^R-1)})k\right) dk \end{aligned} \tag{C.12}$$

Using the property of exponential distribution:

$$\int_{-\infty}^{\infty} \lambda exp(-\lambda x) dx = 1 \tag{C.13}$$

$$\int_{-\infty}^{\infty} x^n\, \lambda\, exp(-\lambda x) dx = \frac{n!}{\lambda^n} \tag{C.14}$$

Setting $n = |D_{i-1}(s)| - 2$ and $\lambda = (1 + \frac{1}{2(2^R-1)})$, the integration term C.12 can be solved as the following:

$$\begin{aligned}\int_{-\infty}^{\infty} k^{|D_{i-1}(s)|-2}\, exp\left(-(1+\frac{1}{2(2^R-1)})k\right)\, dk \\ &= \frac{1}{(1+\frac{1}{2(2^R-1)})^{|D_{i-1}(s)|-2}} \times \frac{(|D_{i-1}(s)|-2)!}{(1+\frac{1}{2(2^R-1)})} \\ &= \frac{(|D_{i-1}(s)|-2)!}{(1+\frac{1}{2(2^R-1)})^{|D_{i-1}(s)|-1}}\end{aligned} \tag{C.15}$$

Substituting the integration term back into equation (C.11):

$$pdf_z(z) = \frac{exp((\frac{1}{2(2^R-1)})z)}{(|D_{i-1}(s)|-2)!\ 2^{|D_{i-1}(s)|}} \frac{(|D_{i-1}(s)|-2)!}{(1+\frac{1}{2(2^R-1)})^{|D_{i-1}(s)|-1}} \tag{C.16}$$

$$= \frac{exp((\frac{1}{2(2^R-1)})z)}{2^{|D_{i-1}(s)|}\ \left(1+\frac{1}{2(2^R-1)}\right)^{|D_{i-1}(s)|-1}} \tag{C.17}$$

The cumulative density function of random variable z can then be found by performing indefinite integration to the above probability density function as follows:

$$\begin{aligned}cdf_z(z) &= \int_0^z pdf_z(z)dz \\ &= \int_0^z \frac{1}{2^{|D_{i-1}(s)|}\ \left(1+\frac{1}{2(2^R-1)}\right)^{|D_{i-1}(s)|-1}}\, exp((\frac{1}{2(2^R-1)})z)dz \\ &= \frac{(2(2^R-1))}{2^{|D_{i-1}(s)|}\ \left(1+\frac{1}{2(2^R-1)}\right)^{|D_{i-1}(s)|-1}} \times \left(exp((\frac{1}{2(2^R-1)})z) - 1\right)\end{aligned} \tag{C.18}$$

Now, going back to equation (C.4), to calculate the probability that such condition occurs, the concept of complementary cumulative distribution function can be readily used. Replacing the

right hand side equation into a new variable z as derived earlier, the probability that:

$$\left(2^R-1\right)\frac{N_0}{P_{tot}}\left(|D_{i-1}(s)|-1\right)<z \tag{C.19}$$

occurs is equal to $ccdf_z\left(\left(2^R-1\right)\frac{N_0}{P_{tot}}\left(|D_{i-1}(s)|-1\right)\right)$, which can be calculated as follows:

$$\begin{aligned}
&ccdf_z\left(\left(2^R-1\right)\frac{N_0}{P_{tot}}\left(|D_{i-1}(s)|-1\right)\right)=1-cdf_z\left(\left(2^R-1\right)\frac{N_0}{P_{tot}}\left(|D_{i-1}(s)|-1\right)\right)\\
&=1-\left[\frac{(2(2^R-1))}{2^{|D_{i-1}(s)|}\left(1+\frac{1}{2(2^R-1)}\right)^{|D_{i-1}(s)|-1}}\left(exp\left(\frac{(2^R-1)\frac{N_0}{P_{tot}}(|D_{i-1}(s)|-1)}{2(2^R-1)}\right)-1\right)\right]\\
&=1-\left[\frac{(2^R-1)}{2^{|D_{i-1}(s)|-1}\left(1+\frac{1}{2(2^R-1)}\right)^{|D_{i-1}(s)|-1}}\left(exp\left(\frac{(|D_{i-1}(s)|-1)}{2P_{tot}/N_0}\right)-1\right)\right]\\
&=1-\frac{(2^R-1)\times\left(exp\left(\frac{|D_{i-1}(s)|-1}{2P_{tot}/N_0}\right)-1\right)}{\left(2+\frac{1}{(2^R-1)}\right)^{|D_{i-1}(s)|-1}}
\end{aligned} \tag{C.20}$$

Appendix D

Derivation of Composite Channel CDF

The CDF of ρ_{eff} is required to find the outage probability of AnF scheme. Focusing only on the random term, a normalised SNR $\rho^* = \frac{\rho_{eff}}{\mathcal{E}_s/N_0}$ can be expressed as follows:

$$\rho^* = |h_{sd}|^2 + \frac{|h_{sr}|^2 |h_{rd}|^2}{|h_{sr}|^2 + |h_{rd}|^2 + \frac{N_0}{\mathcal{E}_s}} \tag{D.1}$$

where $|h_{sd}|^2$, $|h_{sr}|^2$, and $|h_{rd}|^2$ are independent exponential distributed random variables with parameter λ_{sd}, λ_{sr}, and λ_{rd} respectively. To simplify the CDF derivation of ρ^*, the two terms in the summation are considered separately. Lets first consider the second term by letting $X = |h_{sr}|^2$ and $Y = |h_{rd}|^2$. Now let:

$$Z = \frac{X\,Y}{X + Y + \frac{N_0}{\mathcal{E}_s}} \tag{D.2}$$

and its CDF can be written as follows:

$$\begin{aligned} Pr[Z \leq z] &= Pr\left[\frac{X\,Y}{X + Y + \frac{N_0}{\mathcal{E}_s}} \leq z\right] \\ &= Pr\left[X(Y - z) \leq Yz + \frac{N_0}{\mathcal{E}_s}z\right] \end{aligned} \tag{D.3}$$

Fixing $Y = y$, the conditional CDF of Z can be written as follows:

$$F_{Z|Y}(z) = \begin{cases} Pr\left[X \geq \frac{yz+\frac{N_0}{\mathcal{E}_s}z}{y-z}\right] & \text{if } y < z, \\ Pr\left[X \leq \frac{yz+\frac{N_0}{\mathcal{E}_s}z}{y-z}\right] & \text{if } y \geq z \end{cases} \tag{D.4}$$

Unconditioning with respect to variable Y, the CDF of Z can be obtained as follows:

$$\begin{aligned} & F_Z(z) \\ = & \int_{-\infty}^{\infty} F_{Z|Y}(z)\, f_Y(y)\, dy \\ = & \int_0^z Pr\left[X \geq \frac{yz+\frac{N_0}{\mathcal{E}_s}z}{y-z}\right] f_Y(y)\, dy \;+\; \int_z^{\infty} Pr\left[X \leq \frac{yz+\frac{N_0}{\mathcal{E}_s}z}{y-z}\right] f_Y(y)\, dy \\ = & \int_0^z 1\, f_Y(y)\, dy \;+\; \int_z^{\infty} \left(1 - exp\left[-\lambda_{sr}\frac{yz+\frac{N_0}{\mathcal{E}_s}z}{y-z}\right]\right) f_Y(y)\, dy \\ = & \int_0^z \lambda_{rd} e^{-\lambda_{rd}\, y} dy \;+\; \int_z^{\infty} \lambda_{rd} e^{-\lambda_{rd}\, y} dy \;-\; \lambda_{rd} \int_z^{\infty} exp\left[-\lambda_{sr}\frac{yz+\frac{N_0}{\mathcal{E}_s}z}{y-z} \;-\; \lambda_{rd}\, y\right] dy \\ = & \; 1 - e^{-\lambda_{rd}\, z} \;+\; e^{-\lambda_{rd}\, z} \;-\; \lambda_{rd} e^{-(\lambda_{sr}+\lambda_{rd})z} \int_0^{\infty} exp\left[-\frac{\lambda_{sr}\, z\left(z+\frac{N_0}{\mathcal{E}_s}\right)}{p} \;-\; \lambda_{rd} p\right] dp \\ = & \; 1 - e^{-(\lambda_{sr}+\lambda_{rd})\, z}\; 2\sqrt{\lambda_{sr}\lambda_{rd}\, z\left(z+\frac{N_0}{\mathcal{E}_s}\right)}\; K_1\left(2\sqrt{\lambda_{sr}\lambda_{rd}\, z\left(z+\frac{N_0}{\mathcal{E}_s}\right)}\right) \end{aligned} \tag{D.5}$$

where change of variable $p = y - z$ is used. Here, $K_1(.)$ denotes the first order modified Bessel function of the second kind. The above derivation makes use of the following integration property [192]:

$$\int_0^{\infty} exp\left[-\frac{a}{x} - b\, x\right]\, dx = 2\sqrt{\frac{a}{b}}\, K_1\left(2\sqrt{a\, b}\right) \tag{D.6}$$

Finally, denoting the first term of summation in ρ^* expression as $Q = |h_{sd}|^2$, the conditional

CDF of ρ^* fixing $Q = q$ can be written as follows:

$$\begin{aligned} F_{\rho^*|Q=q}(v) &= Pr\left[\rho^* \leq v | Q = q\right] = Pr\left[q + Z \leq v\right] = Pr\left[Z \leq v - q\right] \\ &= \begin{cases} 0 & \text{if } q > v \\ F_Z(v-q) & \text{if } q \leq v \end{cases} \end{aligned} \tag{D.7}$$

Unconditioning with respect to Q (which is exponentially distributed with parameter λ_{sd}), the CDF of ρ^* can be calculated as:

$$\begin{aligned} F_{\rho^*}(v) &= \int_0^v F_Z(v-q)\, f_Q(q)\, dq \\ &= \int_0^v (1 - exp\left[-(\lambda_{sr} + \lambda_{rd})(v-q)\right] 2\sqrt{\lambda_{sr}\lambda_{rd}(v-q)(v-q+\frac{N_0}{\mathcal{E}_s})} \\ &\qquad K_1\left(2\sqrt{\lambda_{sr}\lambda_{rd}(v-q)(v-q+\frac{N_0}{\mathcal{E}_s})}\right)\lambda_{sd} exp\left[-\lambda_{sd} q\right] dq \end{aligned} \tag{D.8}$$

Appendix E

Derivation of squared distance density function

Denote L as the length of the network edge covering a rectangular area of L^2, and let (S_x, S_y), (D_x, D_y) be the coordinate of the source and destination node (relative to the lower left corner of the network) respectively. Since all nodes are uniformly distributed within the network, $S_x, S_y, D_x,$ and D_y are i.i.d. with the following PDF and CDF:

$$f_{S_x}(l) = f_{S_y}(l) = f_{D_x}(l) = f_{D_y}(l) = U[0, 1/L] = \begin{cases} \frac{1}{L} & \text{if } 0 \leq l < L \\ 0 & \text{elsewhere} \end{cases} \tag{E.1}$$

$$F_{S_x}(l) = F_{S_y}(l) = F_{D_x}(l) = F_{D_y}(l) = \begin{cases} 0 & \text{if } l < 0, \\ \frac{l}{L} & \text{if } 0 \leq l < L \\ 1 & \text{if } l \geq L \end{cases} \tag{E.2}$$

Denoting the squared distance between source to destination as Z, the following relation follows from trigonometry property:

$$Z = (D_y - S_y)^2 + (D_x - S_x)^2 \tag{E.3}$$

Since $S_x, S_y, D_x,$ and D_y are i.i.d., $(D_y - S_y)$ and $(D_x - S_x)$ will also be i.i.d.; and their PDF can be calculated by performing convolution on the PDF of its elements, resulting in the following PDF:

$$f_{(D_x-S_x)}(l) = f_{(D_y-S_y)}(l) = \begin{cases} \frac{1}{L} + \frac{l}{L^2} & \text{if } -L \leq l < 0 \\ \frac{1}{L} - \frac{l}{L^2} & \text{if } 0 \leq l < L \\ 0 & \text{elsewhere} \end{cases} \tag{E.4}$$

By integration, the following CDF can be obtained:

$$F_{(D_x-S_x)}(l) = F_{(D_y-S_y)}(l) = \begin{cases} 0 & \text{if } l < -L, \\ \frac{1}{2}\left(1 + \frac{l}{L}\right)^2 & \text{if } -L \leq l < 0 \\ 1 - \frac{1}{2}\left(1 - \frac{l}{L}\right)^2 & \text{if } 0 \leq l < L \\ 1 & \text{if } l \geq L \end{cases} \tag{E.5}$$

The next step is to find the distribution of $(D_y - S_y)^2$ and $(D_x - S_x)^2$, which can be found using the following technique of change of variables:

$$F_{X^2}(x) = Pr[X^2 \leq x] = Pr[X \leq \sqrt{x}] - Pr[X \leq -\sqrt{x}] = F_X(\sqrt{x}) - F_X(-\sqrt{x})$$

which results in the following:

$$F_{(D_x-S_x)^2}(l) = F_{(D_y-S_y)^2}(l) = \begin{cases} 0 & \text{if } l < 0, \\ 2\frac{\sqrt{l}}{L} - \frac{l}{L^2} & \text{if } 0 \leq l < L^2 \\ 1 & \text{if } l \geq L^2 \end{cases} \tag{E.6}$$

Taking the first derivation of the above CDF, the corresponding PDF is obtained as follows:

$$f_{(D_x-S_x)^2}(l) = f_{(D_y-S_y)^2}(l) = \begin{cases} \frac{1}{L\sqrt{l}} - \frac{1}{L^2} & \text{if } 0 \leq l < L^2 \\ 0 & \text{elsewhere} \end{cases} \tag{E.7}$$

Finally, the PDF of squared distance Z can be calculated by performing convolution of two PDFs:

$$\begin{aligned} f_Z(z) &= \int_{-\infty}^{\infty} f_{(D_y-S_y)^2}(l) f_{(D_x-S_x)^2}(z-l)dl \\ &= \begin{cases} 0 & \text{if } z < 0, \\ \frac{\pi}{L^2} - \frac{4\sqrt{z}}{L^3} + \frac{z}{L^4} & \text{if } 0 \leq z < L^2 \\ \frac{4}{L^2}\ arcSin\left(\frac{L}{\sqrt{z}}\right) - \frac{(\pi+2)}{L^2} + \frac{4\sqrt{(z-L^2)}}{L^3} - \frac{z}{L^4} & \text{if } L^2 \leq z < 2L^2 \\ 0 & \text{if } z \geq 2L^2 \end{cases} \end{aligned} \tag{E.8}$$

Bibliography

[1] P. P. Bergmans and T. M. Cover, ”Cooperative Broadcasting,” *IEEE Trans. on Inform. Theory*, vol. IT-20, pp. 317-324, May 1974

[2] M. Costa, ”Writing on Dirty Paper,” *IEEE Trans. on Inform. Theory*, vol. IT-29, pp. 439-441, May 1983

[3] E. Teletar, ”Capacity of Multi-Antenna Gaussian Channels,” *AT&T-Bell Labs Internal Tech. Memo*, June 1995

[4] G. J. Foschini and M. J. Gans, ”On Limits of Wireless Communications in a Fading Environment when Using Multiple Antennas,” *Wireless Pers. Commun.*, vol. 6, pp. 311-335, March 1998

[5] S. Vishwanath, N. Jindal, and A. Goldsmith, ”Duality, Achievable Rates, and Sum-Rate Capacity of Gaussian MIMO Broadcast Channels,” *IEEE Trans. on Inform. Theory*, vol.49, pp.2658-2668, Oct. 2003

[6] A. Sendonaris, E. Erkip, and B. Aazhang, ”User Cooperation Diversity - Part I: System Description,” *IEEE Trans. on Commun.*, vol. 51, pp. 1927-1938 Nov. 2003

[7] A. Sendonaris, E. Erkip, and B. Aazhang, ”User Cooperation Diversiy - Part II: Implementation Aspects and Performance Analysis,” *IEEE Trans. on Commun.*, vol. 51, pp. 1939-1948, Nov. 2003

[8] T. M. Cover, ”Broadcast Channels,” *IEEE Trans. on Inform. Theory*, vol. IT-18, pp. 2-14, Jan. 1972

[9] A. E. Gamal and T. M. Cover, ”Multiple User Information Theory,” *Proceedings of the IEEE*, vol. 68, pp. 1466-1483, Dec. 1980

[10] P. P. Bergmans, ”Random Coding Theorem for Broadcast Channels with Degraded Components,” *IEEE Trans. on Inform. Theory*, vol. IT-19, pp. 197-207, March 1979

[11] P. P. Bergmans, ”A Simple Converse for Broadcast Channels with Additive White Gaussian Noise,” *IEEE Trans. on Inform. Theory*, vol. IT-20, pp. 279-280, March 1974

[12] R. G. Gallager, ”Capacity and Coding for Degraded Broadcast Channels,” *Probl. Pered. Inform.*, vol. 10, pp. 3-14, July-Sept. 1974; translated in *Probl. of Inform. Transm.*, pp. 185-193, July-Sept. 1974

[13] T. M. Cover, ”Comments on Broadcast Channels,” *IEEE Trans. on Inform. Theory*, vol. 44, pp. 2524-2530, Oct. 1998

[14] S. I. Gelfand, ”Capacity of One Broadcast Channel,” *Probl. Pered. Inform.*, vol. 13, pp. 106-108, July-Sept. 1977; translated in *Probl. of Inform. Transm.*, pp. 240-242, July-Sept. 1977

[15] K. Marton, ”The Capacity Region of Deterministic Broadcast Channels,” *Proceedings of IEEE Int. Symp. on Inform. Theory*, pp. 243-248, June 1977

[16] M. S. Pinsker, ”Capacity of Noiseless Broadcast Channels,” *Probl. Pered. Inform.*, vol. 14, pp. 28-34, April-June 1978; translated in *Probl. of Inform. Transm.*, pp. 97-102, April-June 1978

[17] D. Slepian and J. K. Wolf, ”Noiseless Coding of Correlated Information Sources,” *IEEE Trans. on Inform. Theory*, vol. IT-19, pp. 471-480, July 1973

[18] E. van der Meulen, ”Random Coding Theorems for the General Discrete Memoryless Broadcast Channel,” *IEEE Trans. on Inform. Theory*, vol. IT-21, pp. 180-190, March 1975

[19] T. M. Cover, ”An Achievable Rate Region for the Broadcast Channel,” *IEEE Trans. on Inform. Theory*, vol. IT-21, pp. 399-404, July 1975

[20] K. Marton, ”A Coding Theorem for the Discrete Memoryless Broadcast Channel,” *IEEE Trans. on Inform. Theory*, vol. IT-25, pp. 306-311, May 1979

[21] D. G. Brennan, ”Linear Diversity Combining Techniques,” *Proceedings of the IRE*, vol. 47, pp. 1075-1102, June 1959

[22] T. K. Y. Lo, ”Maximum Ratio Transmission,” *IEEE Trans. on Commun.*, vol. 47, pp. 1458-1461, Oct. 1999

[23] S. Zhou and G. B. Giannakis, ”Optimal Transmitter Eigen-Beamforming and Space-Time Block Coding Based on Channel Mean Feedback,” *IEEE Trans. on Signal Processing*, vol. 50, pp. 2599-2613, Oct. 2002

[24] S. Zhou and G. B. Giannakis, ”Optimal Transmitter Eigen-Beamforming and Space-Time Block Coding Based on Channel Correlations,” *IEEE Trans. on Inform. Theory*, vol. 49, pp. 1673-1690, July 2003

[25] L. Zheng and D. N. C. Tse, ”Diversity and Multiplexing: A Fundamental Tradeoff in Multiple-Antenna Channels,” *IEEE Trans. on Inf. Theory*, vol. 49, pp. 1073-1096, May 2003

[26] S. M. Alamouti, ”A Simple Transmit Diversity Technique for Wireless Communications,” *IEEE J. on Select. Areas Commun.*, vol. 16, pp. 14511458, Oct. 1998

[27] V. Tarokh, H. Jafarkhani, and A. R. Calderbank, ”Space-Time Block Codes from Orthogonal Designs,” *IEEE Trans. on Inform. Theory*, vol. 45, pp. 1456-1467, July 1999

[28] V. Tarokh, N. Seshadari, and A. R. Calderbank, ”Space-Time Codes for High Data Rate Wireless Communication: Performance Criterion and Code Construction,” *IEEE Trans. on Inform. Theory*, vol. 44, pp. 744-765, March 1998

[29] V. Tarokh, N. Seshadari, and A. R. Calderbank, ”Space-Time Codes for High Data Rate Wireless Communication: Performance Results,” *IEEE Journal on Selected Area in Commun.*, vol. 17, pp. 451-460, March 1999

[30] V. Tarokh, A. Naguib, N. Seshadari, and A. R. Calderbank, ”Space-Time Codes for High Data Rate Wireless Communication: Performance Criteria in the Presence of Channel Estimation Errors, Mobility, and Multiple Paths,” *IEEE Trans. on Commun.*, vol. 47, pp. 199-207, Feb. 1999

[31] G. J. Foschini, ”Layered Space-Time Architecture for Wireless Communication in a Fading Environment When Using Multi-Element Antennas,” *Bell Labs Technical Journal*, pp.41-59, Autumn 1996

[32] P. W. Wolniansky, G. J. Foschini, G. D. Golden, and R. A. Valenzuela, ”V-BLAST: An Architecture for Realizing Very High Data Rates Over the Rich-Scattering Wireless Channel,” *URSI International Symposium on Signal, Systems, and Electronics*, pp. 295-300, Sept-Oct. 1998

[33] G. J. Foschini, G. D. Golden, R. A. Valenzuela, and P. W. Wolniansky, ”Simplified Processing for High Spectral Efficiency Wireless Communication Employing Multi-Element Arrays,” *IEEE Journal on Selected Area in Commun.*, vol. 17, pp. 1841-1852, Nov. 1999

[34] A. Sezgin, E. A. Jorswieck, and V. Jungnickel, ”Maximum Diversity Detection for Layered Space-Time Codes,” *IEEE Vehicular Technology Conference*, vol. 2, pp. 833-837, April 2003

[35] D. Gesbert, M. Shafi, D. Shiu, P. J. Smith, and A. Naguib, ”From Theory to Practice: An Overview of MIMO Space-Time Coded Wireless Systems,” *IEEE Journal on Selected Area in Commun.*, vol. 21, pp. 281-302, April 2003

[36] A. Paulraj, R. Nabar, and D. Gore *Introduction to Space-Time Wireless Communications*,Cambridge University Press, 2003

[37] A. Paulraj and C. B. Papadias, ”Space-Time Processing for Wireless Communications,” *IEEE Signal Processing Magazine*, vol. 14, pp. 49-83, Nov. 1997

[38] A. Paulraj and B. C. Ng, ”Space-Time Modems for Wireless Personal Communications,” *IEEE Pers. Commun.*, vol. 5, pp. 36-48, Feb. 1998

[39] M. A. Khalighi, J. M. Brossier, G. V. Jourdain, and K. Raoof, ”Water Filling Capacity of Rayleigh MIMO Channels,” *IEEE 12th Int. Symp. on Personal, Indoor and Mobile Radio Communication*, pp. A155-A158, Sept.-Oct. 2001

[40] W. Yu and J. M. Cioffi, ”Constant-Power Waterfilling: Performance Bound and Low-Complexity Implementation,” *IEEE Trans. on Commun.*, vol. 54, pp. 23-28, Jan. 2006

[41] H. Shin and J. H. Lee, ”Exact Symbol Error Probability of Orthogonal Space-Time Block Codes,” *IEEE Global Telecom. Conf.*, pp. 1197-1201, Nov. 2002

[42] R. V. Nee, A. V. Zelst, and G. Awater, ”Maximum Likelihood Decoding in a Space Division Multiplexing System,” *IEEE 51st Vehicular Technology Conf.*, pp. 6-10, May 2000

[43] X. Zhu and R. D. Murch, ”Performance Analysis of Maximum Likelihood Detection in a MIMO Antenna System,” *IEEE Trans. on Commun.*, vol. 50, pp. 187-191, Feb. 2002

[44] B. A. Bjerke and J. G. Proakis, ”Multiple-Antenna Diversity Techniques for Transmission over Fading Channels,” *IEEE Wireless Commun. and Networking Conf.*, pp. 1038-1042, Sept. 1999

[45] G. H. Golub and C. F. Van Loan, *Matrix Computations*, The Johns Hopkins University Press, Baltimore and London, 1996

[46] Y. Li, J. C. Chuang, and N. R. Sollenberger, "Transmitter Diversity for OFDM Systems and Its Impact on High-Rate Data Wireless Networks," *IEEE Journal on Selected Areas in Commun.*, vol. 17, pp. 1233-1243, July 1999

[47] T. Himsoon, W. Su, and K. J. R. liu, "Single-Block Differential Transmit Scheme for Frequency Selective MIMO-OFDM Systems," *IEEE Wireless Commun. and Networking Conf.*, pp. 532-537, March 2005

[48] H. Shi, T. Abe, and H. Suda, "An Iterative Transmission Power Allocation Scheme for MIMO-OFDM Systems," *IEEE Vehicular Technology Conf.*, pp. 4828-4832, Sept. 2004

[49] Y. H. Pan, K. B. Letaief, and Z. Cao, "Dynamic Spatial Subchannel Allocation with Adaptive Beamforming for MIMO/OFDM Systems," *IEEE Trans. on Wireless Commun.*, vol. 3, pp. 2097-2107, Nov. 2004

[50] K. W. Park and Y. S. Cho, "An MIMO-OFDM Technique for High-Speed Mobile Channels," *IEEE Commun. Letters*, vol. 9, pp. 604-606, July 2005

[51] W. G. Jeon, K. H. Chang, and Y. S. Cho, "An Equalization Technique for Orthogonal Frequency-Division Multiplexing Systems in Time-Variant Multipath Channels," *IEEE Trans. on Commun.*, vol. 47, pp. 27-32, Jan. 1999

[52] A. Correia, A. Hottinen, and R. Wichman, "Space-Time Transmitter Diversity Schemes for Wideband CDMA," *IEEE Vehicular Technology Conf.*, pp. 313-317, May 2000

[53] L. U. Choi and R. D. Murch, "A Pre-BLAST DFE Technique for the Downlink of Frequency-Selective Fading MIMO Channels," *IEEE Trans. on Commun.*, vol. 52, pp. 737-743, May 2004

[54] D. S. Shiu, G. J. Foschini, M. J. Gans, and J. M. Kahn, ”Fading Correlation and Its Effect on the Capacity of Multielement Antenna Systems,” *IEEE Trans. on Commun.*, vol. 48, pp. 502-513, March 2000

[55] G. Gritsch, H. Weinrichter, and M. Rupp, ”A Union Bound of the Bit Error Ratio for Data Transmission over Correlated Wireless MIMO Channels,” *IEEE Int. Conf. on Acoustics, Speech, and Signal Processing*, pp. iv405-iv408, May 2004

[56] D. A. Gore and A. Paulraj, ”MIMO Antenna Subset Selection with Space-Time Coding,” *IEEE Trans. On Signal Processing*, vol. 50, pp. 2580-2588, Oct. 2002

[57] D. A. Gore and A. Paulraj, ”Space-Time Block Coding with Optimal Antenna Selection,” *IEEE Int. Conf. on Acoustics, Speech, and Signal Processing*, pp. 2441-2444, May 2001

[58] D. A. Gore, R. Heath, and A. Paulraj, ”Statistical Antenna Selection for Spatial Multiplexing Systems,” *IEEE Int. Conf. on Commun.*, pp. 450-454, April-May 2002

[59] D. A. Gore, A. Gorokhov, and A. Paulraj, ”Joint MMSE Versus V-BLAST and Antenna Selection,” *Asilomar Conf. on Signals, Systems, and Computers*, pp. 505-509, Nov. 2002

[60] D. A. Gore, R. U. Nabar, and A. Paulraj, ”Selecting an Optimal Set of Transmit Antennas for a Low Rank Matrix Channel,” *IEEE Int. Conf. on Acoustics, Speech, and Signal Processing*, pp. 2785-2788, June 2000

[61] D. A. Gore, R. W. Heath, and A. Paulraj, ”Transmit Selection in Spatial Multiplexing Systems,” *IEEE Commun. Letters*, vol. 6, pp.491-493, Nov. 2002

[62] R. W. Heath, S. Sandhu, and A. Paulraj, ”Antenna Selection for Spatial Multiplexing Systems with Linear Receivers,” *IEEE Commun. Letters*, vol. 5, pp. 142-144, April 2001

[63] M. A. Jensen and M. L. Morris, ”Efficient Capacity-Based Antenna Selection for MIMO Systems,” *IEEE Trans. on Vehicular Technology*, vol. 54, pp. 110-116, Jan. 2005

[64] A. Gorokhov, ”Antenna Selection Algorithms for MEA Transmission Systems,” *IEEE Int. Conf. on Acoustics, Speech, and Signal Processing*, pp. III 2857-III 2860, May 2002

[65] A. Gorokhov, D. A. Gore, and A. Paulraj, ”Receive Antenna Selection for MIMO Spatial Multiplexing: Theory and Algorithms,” *IEEE Trans. on Signal Processing*, vol. 51, pp. 2796-2807, Nov. 2003

[66] A. Gorokhov, D. A. Gore, and A. Paulraj, ”Receive Antenna Selection for MIMO Flat-Fading Channels: Theory and Algorithms,” *IEEE Trans. on Inform. Theory*, vol. 49, pp. 2687-2696, Oct. 2003

[67] A. F. Molisch, M. Z. Win, Y. S. Choi, and J. H. Winters, ”Capacity of MIMO Systems with Antenna Selection,” *IEEE Trans. on Wireless Commun.*, vol. 4, pp. 1759-1772, July 2005

[68] I. Bahceci, T. M. Duman, and Y. Altunbasak, ”Performance of MIMO Antenna Selection for Space-Time Coded OFDM Systems,” *IEEE Wireless Commun. and Networking Conf.*, pp. 987-992, March 2004

[69] X. Shao, J. Yuan, and P. Rapajic, ”Antenna Selection for MIMO-OFDM Spatial Multiplexing System,” *IEEE Int. Symp. on Inform. Theory*, pp. 90, June-July 2003

[70] S. Sandhu and M. Ho, ”Analog Combining of Multiple Receive Antennas with OFDM,” *IEEE Int. Conf. on Commun.*, pp. 3428-3432, May 2003

[71] E. Kurniawan, A. S. Madhukumar, and Francois Chin, ”Sub Optimal Antenna Selection Method for MIMO-OFDM Systems,” *IEEE Vehicular Technology Conference*, pp. 435-439, April 2007

[72] E. Kurniawan, A. S. Madhukumar, and Francois Chin, ”Antenna selection technique for MIMO-OFDM systems over frequency selective Rayleigh fading channel,” *IET Communications*, vol. 1, pp. 458 - 463, June 2007

[73] H. Shi, M. Katayama, T. Yamazato, H. Okada, and A. Ogawa, "An Adaptive Antenna Selection Scheme for Transmit Diversity in OFDM Systems," *IEEE Vehicular Technology Conf.*, pp. 2168-2172, Oct. 2001

[74] Y. Qiu, Y.H. Pan, Z. Cao, and K. B. Letaief, "Constant Rate Adaptive Modulation with Selection Transmit Diversity for Broadband OFDM Systems," *IEEE 14th Int. Symp. on Personal, Indoor and Mobile Radio Communication*, pp. 722-726, Sept. 2003

[75] M. Torabi and M. R. Soleymani, "Variable-Rate OFDM Systems with Selective Antenna Diversity and Adaptive Modulation," *IEEE Vehicular Technology Conf.*, pp. 562-566, April 2003

[76] M. Torabi and M. R. Soleymani, "Adaptive Bit Allocation for Space-Time Block Coded OFDM System," *IEEE Int. Conf. on Acoustics, Speech, and Signal Processing*, pp. IV 409-IV 412, April 2003

[77] G. Caire and S. Shamai, "On the Achievable Throughput of a Multiantenna Gaussian Broadcast Channel," *IEEE Trans. on Inform. Theory*, vol. 49, pp. 1691-1706, July 2003

[78] H. Sato, "An Outer Bound to the Capacity Region of Broadcast Channels," *IEEE Trans. on Inform. Theory*, vol. IT-24, pp. 374-377, May 1978

[79] W. Yu and J. Cioffi, "Sum Capacity of Gaussian Vector Broadcast Channels," *IEEE Trans. on Inform. Theory*, vol. 50, pp. 1875-1892, Sept. 2004

[80] N. Jindal, S. Vishwanath, and A. Goldsmith, "On the Duality of Gaussian Multiple-Access and Broadcast Channels," *IEEE Trans. on Inform. Theory*, vol. 50, pp. 768-783, May 2004

[81] S. Vishwanath, N. Jindal, and A. Goldsmith, "On the Capacity of Multiple Input Multiple Output Broadcast Channels," *IEEE Int. Conf. on Commun.*, pp. 1444-1450, April-May 2002

[82] P. Viswanath and D. N. C. Tse, "Sum Capacity of the Vector Gaussian Broadcast Channel and Uplink-Downlink Duality," *IEEE Trans. on Inform. Theory*, vol. 49, pp. 1912-1921, Aug. 2003

[83] R. Agarwal and J. Cioffi, "Achieving Sum-Capacity of the MIMO BC with Large Transmit Array using One-Shot Scalable Feedback Protocol," *IEEE Vehicular Technology Conf.*, pp. 2038-2042, April 2007

[84] M. Sharif and B. Hassibi, "On the Capacity of MIMO Broadcast Channels with Partial Side Information," *IEEE Trans. on Inform. Theory*, vol. 51, pp. 506-522, Feb. 2005

[85] N. Jindal and A. Goldsmith, "Dirty-Paper Coding Versus TDMA for MIMO Broadcast Channels," *IEEE Trans. on Inform. Theory*, vol. 51, pp. 1783-1794, May 2005

[86] Z. Shen, R. Chen, J. G. Andrews, R. W. Heath, and B. L. Evans, "Sum Capacity of Multiuser MIMO Broadcast Channels with Block Diagonalization," *IEEE Trans. on Wireless Commun.*, vol. 6, pp. 2040-2045, June 2007

[87] A. Nosratinia, T. E. Hunter, and A. Hedayat, "Cooperative Communication in Wireless Networks," *IEEE Commun. Magazine*, vol. 42, pp. 74-80, Oct. 2004

[88] A. Stefanov and E. Erkip, "Cooperative Coding for Wireless Networks," *IEEE Trans. on Commun.*, vol. 52, pp. 1470-1476, Sept 2004

[89] T. E. Hunter and A. Nosratinia, "Diversity through Coded Cooperation," *IEEE Trans. on Commun.*, vol. 5, pp. 1-7, Feb. 2006

[90] T. E. Hunter and A. Nosratinia, "Coded Cooperation under Slow Fading, Fast Fading, and Power Control," *Asilomar Conf. on Signals, Systems and Computers*, pp. 118-122, Nov. 2002

[91] T. E. Hunter and A. Nosratinia, "Performance Analysis of Coded Cooperation Diversity," *IEEE Int. Conf. on Commun.*, pp. 2688-2692, May 2003

[92] J. N. Laneman, D. N. C. Tse, and G. W. Wornell, "Cooperative Diversity in Wireless Networks: Efficient Protocols and Outage Behavior," *IEEE Trans. on Inform. Theory*, vol. 50, pp. 3062-3080, Dec. 2004

[93] J. N. Laneman, G. W. Wornell, "Energy-Efficient Antenna Sharing and Relaying for Wireless Networks," *IEEE Wireless Commun. and Networking Conf.*, pp. 7-12, Sept. 2000

[94] J. N. Laneman, G. W. Wornell, and D. N. C. Tse, "An Efficient Protocol for Realizing Cooperative Diversity in Wireless Networks," *IEEE Int. Symp. on Inform. Theory*, pp. 294, June 2001

[95] R. U. Nabar, H. Boleskei, and F. W. Kneubuhler, "Fading Relay Channels: Performance Limits and Space-Time Signal Design," *IEEE J. on Select. Areas Commun.*, vol. 22, pp. 1099-1109, Aug. 2004

[96] S. Vishwanath, S. Jafar, and S. Sandhu, "Half-Duplex Relays: Cooperative Communication Strategies and Outer Bounds," *IEEE Wireless Commun. and Networking Conf.*, pp. 1455-1459, June 2005

[97] T. M. Cover and A. El. Gamal, "Capacity Theorems for the Relay Channel," *IEEE Trans. on Inform. Theory*, vol. 25, pp. 572-584, Sept. 1979

[98] M. O. Hasna and M. S. Alouini, "Performance Analysis of Two-Hop Relayed Transmissions over Rayleigh Fading Channels," *IEEE Vehicular Technology Conf.*, pp. 1992-1996, Sept. 2002

[99] M. R. Souryal and B. R. Vojcic, "Performance of Amplify-and-Forward and Decode-and-Forward Relaying in Rayleigh Fading with Turbo Codes," *IEEE Int. Conf. on Acoustics, Speech, and Signal Processing*, pp. IV681-IV684, May 2006

[100] V. Emamian, P. Anghel, and M. Kaveh, ”Multi-User Spatial Diversity in a Shadow-Fading Environment,” *IEEE Vehicular Technology Conf.*, pp. 573-576, Sept. 2002

[101] H. Mheidat, M. Uysal, and N. A. Dhahir, ”Equalization Techniques for Distributed Space-Time Block Codes with Amplify-and-Forward Relaying,” *IEEE Trans. on Signal Processing*, vol. 55, pp. 1839-1852, May 2007

[102] E. Lindskog and A. Paulraj, ”A Transmit Diversity Scheme for Channels with Intersymbol Interference,” *IEEE Int. Conf. on Commun.*, pp. 307-311, June 2000

[103] X. Deng and A. M. Haimovich, ”Power Allocation for Cooperative Relaying in Wireless Networks,” *IEEE Commun. Letters*, vol. 9, pp. 994-996, Nov. 2005

[104] C. T. K. Ng and A. J. Goldsmith, ”Capacity and Power Allocation for Transmitter and Receiver Cooperation in Fading Channels,” *IEEE Int. Conf. on Commun.*, pp. 3741 - 3746, June 2006

[105] D. Gunduz and E. Erkip, ”Opportunistic Cooperation by Dynamic Resource Allocation,” *IEEE Trans. on Wireless Commun.*, vol. 6, pp. 1446-1454, April 2007

[106] A. H. Madsen and J. Zhang, ”Ergodic Capacity and Power Allocation in Wireless Relay Channels,” *IEEE Global Telecom. Conf.*, pp. 26 - 30, Dec. 2004

[107] A. H. Madsen and J. Zhang, ”Capacity bounds and power allocation for wireless relay channels,” *IEEE Trans. on Inform. Theory*, vol. 51, pp. 2020-2040, June 2005

[108] J. N. Laneman and G. W. Wornell, ”Distributed Space-Time-Coded Protocols for Exploiting Cooperative Diversity in Wireless Networks,” *IEEE Trans. on Inform. Theory*, vol. 49, pp. 2415-2425, Oct. 2003

[109] J. N. Laneman and G. W. Wornell, "Distributed Space-Time Coded Protocols for Exploiting Cooperative Diversity in Wireless Networks," *IEEE Global Telecom. Conf.*, pp. 77-81, Nov. 2002

[110] J. N. Laneman, "Network Coding Gain of Cooperative Diversity," *IEEE Military Commun. Conf.*, pp. 106-112, Nov. 2004

[111] D. Chen and J. N. Laneman, "Modulation and Demodulation for Cooperative Diversity in Wireless Systems," *IEEE Trans. on Wireless Commun.*, vol. 5, pp. 1785-1794, July 2006

[112] J. N. Laneman, "Limiting Analysis of Outage Probabilities for Diversity Schemes in Fading Channels," *IEEE Global Telecom. Conf.*, pp. 1242-1246, Dec. 2003

[113] T. Unger and A. Klein, "On The Performance of Distributed Space-Time Block Codes in Cooperative Relay Networks," *IEEE Commun. Lettes*, vol. 11, pp. 411-413, May 2007

[114] A. Adinoyi and H. Yanikomeroglu, "Cooperative Relaying in Multi-Antenna Fixed Relay Networks," *IEEE Trans. on Wireless Commun.*, vol. 6, pp. 533-544, Feb. 2007

[115] A. Ribeiro, X. Cai, and G. B. Giannakis, "Symbol Error Probabilities for General Cooperative Links," *IEEE Trans. on Wireless Commun.*, vol. 4, pp. 1264-1273, May 2005

[116] A. K. Sadek, W. Su, and K. J. R. Liu, "Multinode Cooperative Communications in Wireless Networks," *IEEE Trans. on Signal Processing*, vol. 55, pp. 341-355, Jan. 2007

[117] M. Dohler, *Virtual Antenna Arrays*, Ph.D. thesis, King's College London, University of London, 2003

[118] M. Dohler, E. Lefranc, and H. Aghvami, "Virtual Antenna Arrays for Future Wireless Mobile Communication Systems," *Int. Conf. on Telecom.*, Conference CD-ROM, June 2002

[119] M. Dohler, E. Lefranc, and H. Aghvami, "Space-Time Block Codes for Virtual Antenna Arrays," *IEEE Int. Symp. on Personal, Indoor and Mobile Radio Communication*, pp. 414-417, Sept. 2002

[120] M. Dohler, J. Dominguez, H. Aghvami, "Link Capacity Analysis for Virtual Antenna Arrays," *IEEE Vehicular Technology Conf.*, pp. 440-443, Sept. 2002

[121] M. Dohler, B. Rassool, and H. Aghvami, "Performance Evaluation of STTCs for Virtual Antenna Arrays," *IEEE Vehicular Technology Conf.*, pp. 57-60, April 2003

[122] M. Dohler, H. Aghvami, "Distributed PHY-Layer Mesh Networks," *IEEE Int. Symp. on Personal, Indoor and Mobile Radio Communication*, pp. 2543-2547, Sept. 2003

[123] M. Dohler, F. Said, and H. Aghvami, "Higher Order Space-Time Block Codes for Virtual Antenna Arrays," *Int. Conf. on Telecom.*, pp. 198-203, March 2003

[124] M. Dohler, M. Hussain, A. Desai, and H. Aghvami, "Performance of Distributed Space-Time Block Codes," *IEEE Vehicular Technology Conf.*, pp. 742-746, May 2004

[125] S. Yang and J. C. Belfiore, "Towards the Optimal Amplify-and-Forward Cooperative Diversity Scheme," *IEEE Trans. on Inform. Theory*, vol. 53, pp. 3114-3126, Sept. 2007

[126] M. Yuksel and E. Erkip, "Multiple-Antenna Cooperative Wireless Systems: A Diversity-Multiplexing Tradeoff Perspective," *IEEE Trans. on Inform. Theory*, vol. 53, pp. 3371-3393, Oct. 2007

[127] A. Bletsas, H. Shin, and M. Z. Win, "Outage Analysis for Co-operative Communication with Multiple Amplify-and-Forward Relays," *Electronics Letters*, vol. 42, pp. 51-52, March 2007

[128] Y. Zhao, R. Adve, and T. J. Lim, "Outage Probability at Arbitrary SNR with Cooperative Diversity," *IEEE Commun. Letters*, vol. 9, pp. 700-702, Aug. 2005

[129] T. Miyano, H. Murata, and K. Araki, "Cooperative Relaying Scheme with Space Time Code for Multihop Communications among Single Antenna Terminals," *IEEE Global Telecom. Conf.*, pp. 3763-3767, Dec. 2004

[130] M. Dohler, H. Aghvami, Y. Li, and V. Branka, "Stage-by-Stage Detection of Distributed Space-Time Block Encoded Relaying Networks," *IEEE Int. Symp. on Personal, Indoor and Mobile Radio Communication*, pp. 2905-2909, Sept. 2004

[131] M. Dohler, A. Gkelias, and H. Aghvami, "Resource Allocation for FDMA-Based Regenerative Multihop Links," *IEEE Trans. on Wireless Commun.*, vol. 3, pp. 1989-1993, Nov. 2004

[132] M. Dohler, A. Gkelias, and H. Aghvami, "2-hop Distributed MIMO Communication System," *Electronics Letters*, vol. 39, pp. 1350-1351, Sept. 2003

[133] M. Dohler, A. Gkelias, and H. Aghvami, "A Resource Allocation Strategy for Distributed MIMO Multi-hop Communication Systems," *IEEE Commun. Letters*, vol. 8, pp. 99-101, Feb. 2004

[134] M. Dohler, A. Gkelias, and H. Aghvami, "Throughput of Distributed-MIMO Multi-Stage Communication Networks over Non-Ergodic Channels," *IEEE Vehicular Technology Conf.*, pp. 1737-1741, May 2004

[135] R. Annavajjala, P. C. Cosman, and L. B. Milstein, "Statistical Channel Knowledge-Based Optimum Power Allocation for Relaying Protocols in the high SNR Regime," *IEEE J. on Select. Areas Commun.*, vol. 25, pp. 292-305, Feb. 2007

[136] M. Zorzi and R. R. Rao, "Geographic Random Forwarding (GeRaF) for Ad-hoc and Sensor Networks: Multihop Performance," *IEEE Trans. on Mobile Comp.*, vol. 2, pp. 337-348, Oct. 2003

[137] B. Zhao and M. C. Valenti, ”Practical Relay Networks: A Generalization of Hybrid-ARQ,” *IEEE J. on Select. Areas Commun.*, vol. 23, pp. 7-18, Jan. 2005

[138] L. Zhang and L. J. Cimini Jr, ”Hop-by-Hop Routing Strategy for Multihop Decode-and-Forward Cooperative Networks,” *IEEE Wireless Commun. and Networking Conf.*, pp. 576-581, April 2008

[139] V. Mahinthan, L. Cai, J. W. Mark, and X. Shen, ”Maximizing Cooperative Diversity Energy Gain for Wireless Networks,” *IEEE Trans. on Wireless Commun.*, vol. 6, pp. 2530-2539, July 2007

[140] A. Bletsas, A. Khisti, D. P. Reed, and A. Lippman, ”A Simple Cooperative Diversity Method based on Network Path Selection,” *IEEE J. on Select. Areas Commun.*, vol. 24, pp. 659-672, March 2006

[141] A. Bletsas, H. Shin, and M. Z. Win, ”Cooperative Communications with Outage-Optimal Opportunistic Relaying,” *IEEE Trans. on Wireless Commun.*, vol. 6, pp. 3450-3460, Sept. 2007

[142] E. Beres and R. Adve, ”Selection Cooperation in Multi-Source Cooperative Networks,” *IEEE Trans. on Wireless Commun.*, vol. 7, pp. 118-127, Jan. 2008

[143] B. S. Mergen and A. Scaglione, ”Randomized Space-Time Coding for Distributed Cooperative Communication,” *IEEE Trans. on Signal Processing*, vol. 55, pp. 5003-5017, Oct. 2007

[144] B. S. Mergen and A. Scaglione, ”Randomized Space-Time Coding for Distributed Cooperative Communication: Fractional Diversity,” *IEEE Int. Conf. on Acoustics, Speech, and Signal Processing*, pp. IV677-IV680, May 2006

[145] B. S. Mergen and A. Scaglione, ”Randomized Space-Time Coding for Distributed Cooperative Communication,” *IEEE Int. Conf. on Commun.*, pp. 4501-4506, June 2006

[146] A. Hottinen and O. Tirkkonen, "A Randomization Technique for Non-Orthogonal Space-Time Block Codes," *IEEE Vehicular Technology Conf.*, pp. 1479-1482, May 2001

[147] P. Maurer and V. Tarokh, "Transmit Diversity when the Receiver does not know the Number of Transmit Antennas," *Proc. Int. Symp. Wireless Pers. Multimedia Commun.*, Conference CD-ROM, Sept. 2001

[148] Y. Li and X. G. Xia, "A Family of Distributed Space-Time Trellis Codes with Asynchronous Cooperative Diversity," *IEEE Trans. on Commun.*, vol. 55, pp. 790-800, April 2007

[149] S. W. Kim and R. S. Cherukuri, "Adaptive Forwarding and Coding in Cooperative Spatial Multiplexing System," *IEEE Vehicular Technology Conf.*, pp. 2418-2422, Sept. 2005

[150] S. W. Kim, "Cooperative Relaying Architecture for Wireless Video Sensor Networks," *IEEE Global Telecom. Conf.*, pp. 3053-3057, Nov.-Dec. 2005

[151] Y. Zhang, G. Wang, and M. G. Amin, "Cooperative Spatial Multiplexing in Multi-Hop Wireless Networks," *IEEE Int. Conf. on Acoustics, Speech, and Signal Processing*, pp. IV821-IV824, May 2006

[152] N. Jindal, W. Rhee, S. Vishwanath, S. A. Jafar, and A. Goldsmith, "Sum Power Iterative Water-Filling for Multi-Antenna Gaussian Broadcast Channels," *IEEE Trans. on Inform. Theory*, vol. 51, pp.1570-1580, April 2005

[153] W. Yu, "Uplink-Downlink Duality via Minimax Duality," *IEEE Trans. on Inform. Theory*, vol. 52, pp. 361-374, Feb. 2006

[154] R. A. Horn and C. R. Johnson, *Matrix Analysis*, Cambridge University Press, Cambridge, 1985

[155] H. A. David, *Order Statistics*, Wiley, 2003

[156] S. Sanayei and A. Nosratinia, "Asymptotic capacity analysis of transmit antenna selection," *IEEE Int. Symp. on Inform. Theory*, pp. 241, June 2004

[157] Y. Li, J. H. Winters, and N. R. Sollenberger, "MIMO-OFDM for wireless communications, signal detection with enhanced channel estimation," *IEEE Trans. on Commun.*, vol. 50, pp. 1471-1477, Sept. 2002

[158] S. Siwamogsatham and M. P. Fitz, "Robust space-time codes for correlated Rayleigh fading channels," *IEEE Trans. on Signal Processing*, vol. 50, pp. 2408-2416, Oct. 2002.

[159] A. Gorokhov, M. Collados, D. Gore, and A. Paulraj, "Transmit/receive MIMO antenna subset selection," *IEEE Int. Conf. on Acoustics, Speech, and Signal Processing*, pp. 13-16, May 2004

[160] W. C. Jakes, *Microwave Mobile Communications*, Wiley, New York, 1974

[161] M. Hsieh and C. Wei, "Channel estimation for OFDM systems based on comb-type pilot arrangement in frequency selective fading channels," *IEEE Trans. on Consumer Electronics*, vol. 44, pp. 217-225, Feb. 1998

[162] IEEE Std. 802.16-2004, "IEEE Standard for Local and Metropolitan Area Networks Part 16: Air Interface for Fixed Broadband Wireless Access Systems," June 2004, available at *http://standards.ieee.org/getieee802/download/802.16-2004.pdf*

[163] IEEE Std. 802.16e-2005, "Amendment for Physical and Medium Access Control Layers for Combined Fixed and Mobile Operation in Licensed Bands," Feb. 2005, available at *http://standards.ieee.org/getieee802/download/802.16e-2005.pdf*

[164] IEEE 802.16.3c-01/29r4, "Channel Models for Fixed Wireless Applications," July 2001, available at *http://wirelessman.org/tg3/contrib/802163c-01_29r4.pdf*

[165] B. Sklar, *Digial Communications: Fundamentals and Applications*, Prentice Hall, 2002

[166] T. M. Cover and J. A. Thomas, *Elements of Information Theory*, Wiley, New York, 1991

[167] A. Agustin, O. Muhoz, and J. Vidal, "A game theoretic approach for cooperative MIMO schemes with cellular reuse of the relay slot," *IEEE Int. Conf. on Acoustics, Speech, and Signal Processing*, pp. 581-584, May 2004.

[168] J. G. Proakis, *Digital Communications*, McGraw-Hill, New York, 2000

[169] M. Evans, N. Hastings, and J. B. Peacock, *Statistical distributions*, Wiley, 2000.

[170] P. Gupta and P. R. Kumar, "The Capacity of Wireless Networks," *IEEE Trans. on Inform. Theory*, vol. 46, pp. 388-404, March 2000

[171] T. S. Rappaport, *Wireless Communications, Principles and Practice*, Prentice Hall, 2002.

[172] S. S. Ikki and M. H. Ahmed, "Performance of Cooperative Diversity Using Equal Gain Combining (EGC) over Nakagami-m Fading Channels," *IEEE Trans. on Wireless Commun.*, vol. 8, pp. 557-562, Feb. 2009

[173] L. L. Yang and H. H. Chen, "Error Probability of Digital Communications Using Relay Diversity over Nakagmi-m Fading Channels," *IEEE Trans. on Wireless Commun.*, vol. 7, pp. 1806-1811, May 2008

[174] P. A. Anghel and M. Kaveh, "Exact Symbol Error Probability of a Cooperative Network in a Rayleigh-Fading Environment," *IEEE Trans. on Wireless Commun.*, vol. 3, pp. 1416-1421, Sept. 2004

[175] T. K. Y. Lo, "Maximum Ratio Transmission," *IEEE Trans. on Commun.*, vol. 47, pp. 1458-1461, October 1999

[176] M. O. Damen and A. R. Hammons, "Delay-Tolerant Distributed-TAST Codes for Cooperative Diversity," *IEEE Trans. on Inform. Theory*, vol. 53, pp. 3755-3773, Oct. 2007

[177] J. F. Kingman, *Poisson Processes*, Oxford, U.K.:Ford Sci., 1993

[178] Z. Yimin, W. Genyuan, and M. G. Amin, ”Cooperative Spatial Multiplexing in Multi-Hop Wireless Networks,”’ *IEEE Int. Conf. on Acoustics, Speech, and Signal Processing*, pp. 821-824, May 2006

[179] P. Fan, G. Li, K. Cai, and K. B. Letaief, ”On the Geometrical Characteristic of Wireless Ad-Hoc Networks and Its Application in Network Performance Analysis,” *IEEE Trans. on Wireless Commun.*, vol.6, pp.1256-1264, April 2007

[180] R. Zamir, S. Shamai, and U. Erez, ”Nested Linear/Lattice Codes for Structured Multi-terminal Binning,” *IEEE Trans. on Inform. Theory*, vol. 48, pp. 1250-1276, June 2002

[181] S. T. Brink and U. Erez, ”A Close-to-Capacity Dirty Paper Coding Scheme,” *IEEE Int. Symp. on Inform. Theory*, pp. 536, July 2004

[182] M. Tomlinson, ”New Automatic Equalizer Employing Modulo Arithmetic,” *Electron. Lett.*, vol. 7, pp. 138-139, Mar. 1971

[183] H. Harashima and H. Miyakawa, ”Matched-Transmission Technique for Channels with Intersymbol Interference,” *IEEE Trans. on Commun.*, vol. 20, pp. 774-780, Aug. 1972

[184] S. Shamai and R. Laroia, ”The Intersymbol Interference Channel: Lower Bounds on Capacity and Channel Precoding Loss,” *IEEE Trans. on Inform. Theory*, vol. 42, pp. 1388-1404, Sept. 1996

[185] M. Gastpar and M. Vetterli, ”On The Capacity of Wireless Networks: The Relay Case,” *IEEE INFOCOM*, vol. 3, pp. 1577-1586, June 2002

[186] M. Grossglauser and D. N. C. Tse, ”Mobility Increases the Capacity of Ad-hoc Wireless Networks,” *IEEE/ACM Trans. on Networking*, vol. 10, pp. 477-486, August 2002

[187] F. Xue, L. L. Xie, and P. R. Kumar, "The transport capacity of wireless networks over fading channels," *IEEE Trans. of Inform. Theory*, vol. 51, pp. 834-847, March 2005

[188] J. Li, C. Blake, D. S. J. D. Couto, H. I. Lee, and R. Morris, "Capacity of Ad Hoc Wireless Networks," *Int. Conf. on Mobile Computing and Networking*, pp. 61-69, July 2001

[189] R. B. Marks, "The IEEE 802.16 Working Group on Broadband Wireless," IEEE Network, pp. 4-5, March/April 1999.

[190] IEEE Std. 802.16-2001, "Air Interface for Fixed Broadband Wireless Access Systems," April 2002, available at *http://ieeexplore.ieee.org/iel5/7832/21532/00997967.pdf*

[191] IEEE Std. 802.16a-2003, "Amendment 2: Medium Access Control Modification and Additional Physical Layer Specification for 2-11 GHz," April 2003, available at *http://ieeexplore.ieee.org/stamp/stamp.jsp?arnumber=1195640&isnumber=26891*

[192] I. S. Gradshteyn and I. M. Ryzhik, *Table of Integrals, Series, and Products*, 6th ed., New York: Academic Press, 2000